Loughborough University

This item was submitted to Loughborough's Research Repository by the author.
Items in Figshare are protected by copyright, with all rights reserved, unless otherwise indicated.

Application of optimal control to structural load alleviation control systems

PLEASE CITE THE PUBLISHED VERSION

PUBLISHER

© Rudrasena Aditya Prasad

PUBLISHER STATEMENT

This work is made available according to the conditions of the Creative Commons Attribution-NonCommercial-NoDerivatives 4.0 International (CC BY-NC-ND 4.0) licence. Full details of this licence are available at: https://creativecommons.org/licenses/by-nc-nd/4.0/

LICENCE

CC BY-NC-ND 4.0

REPOSITORY RECORD

Prasad, Rudrasena A.. 2015. “Application of Optimal Control to Structural Load Alleviation Control Systems”. figshare. https://hdl.handle.net/2134/17213.

BLL ID NO: D36079/81

LOUGHBOROUGH
UNIVERSITY OF TECHNOLOGY
LIBRARY

AUTHOR/FILING TITLE

PRASAD, R

ACCESSION/COPY NO.

138528/02

VOL. NO. | CLASS MARK

01. JUL 81 | LOAN COPY

-2 FEB 1987

-5 JUL 1987

-2 JUL 1982

- 3 JUL 1992

9 OCT 1992

-1 JUL 1994

013 8528 02

APPLICATION OF OPTIMAL CONTROL TO STRUCTURAL LOAD ALLEVIATION CONTROL SYSTEMS

by

R.A. Prasad, M.Sc.,A.M.R.Ae.S.

A Doctoral Thesis
Submitted in partial fulfilment of the requirements
for the award of
the degree of Ph.D of the Loughborough University of Technology.

November, 1980.

Supervisor: D.McLean, Ph.D.,C.Eng.,F.Inst.M.C.,M.I.E.E.
Department of Transport Technology.

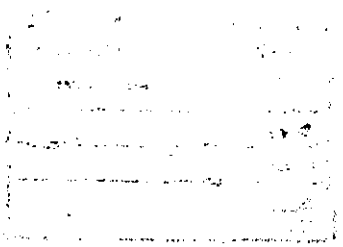
© Rudrasena Aditya Prasad, 1980.

Loughborough University
of Technology Library
Mar 81
Class
Acc. No. 138528/02

PREFACE

This thesis is a report of research carried out by the author in the Department of Transport Technology at Loughborough University of Technology. The thesis is in the main a report of the independent work of the author; the work of others has been referenced where appropriate.

The author would like to express sincere thanks to his supervisor, Dr. D. McLean for his continued guidance and counsel throughout the period of this research. Also special thanks are due to all friends and family for their patience and kind encouragement throughout my stay at Loughborough.



SUMMARY

Feedback laws based upon optimal control theory were derived, and these resulted in a reduction of the structural loads on the wing of a simulated aircraft. Various models of the aircraft dynamics were used, the most complete being of order 79. This model included rigid body motion, structural flexibility effects, unsteady aerodynamics, gust dynamics and actuator dynamics. The structural effects were characterised by the first fifteen bending modes. The subject aircraft studied was considered to employ active ailerons and elevators and was subjected to manoeuvre commands and simulated atmospheric turbulence.

Extensive numerical tests have shown that feedback laws derived from reduced dimension models performed comparably with the feedback law based on the most complete model. Tests were made on feedback laws ranging from order 79 to order 5. It was, however, not possible to reduce the number of feedback variables below five as this then affected the stability of the aircraft. The law based upon five state variable feedback was given the designation 'safety law'.

One of the consequences of operating under the action of the 'safety law' was that the same level of load reduction could not be achieved as was obtained whenever a full state feedback law was employed. In addition, 'safety law' operation was often marked by large transient oscillations of the wing root bending moment and it was considered that this would

subsequently affect the fatigue life of the structure. An observer design was then investigated which reconstructed the complete state vector from a selection of measurements of the sensor signals appropriate to the 'safety law'. Results have shown that it is possible to achieve a practical implementation of such a scheme which will possess all the attendant advantages of full state feedback control.

A consequence of reducing the strength of the wing of the aircraft as a result of employing an active load alleviation scheme is that a considerable degree of reliability of the control system, higher than that of both the basic airframe and its propulsive system, will be required. Because the use of hardware redundancy techniques as a means of providing the required degree of reliability would be expensive, software redundancy techniques suggest an attractive alternative. One example of how software redundancy may be employed is demonstrated in respect of checking the analogue feedback gain controller used in the aircraft to implement linear feedback. It is shown how a microprocessor may be effectively employed to introduce a surrogate gain should one or more of the channels of the controller fail.

CONTENTS

		PAGE
PREFACE		ii
SUMMARY		iii
CONTENTS		v
LIST OF TABLES		viii
LIST OF FIGURES		ix
NOTATION		xi
CHAPTER 1:	GENERAL INTRODUCTION	
	1.1 Problem Description	1
	1.2 Historical Background	4
	1.3 Scope of the Research Investigation	12
CHAPTER 2:	MATHEMATICAL REPRESENTATION OF THE AIRCRAFT	
	2.1 Introduction	16
	2.2 The Subject Aircraft	21
	2.3 State Equation Representation	23
	2.4 The Mathematical Model, ARNE	25
	2.4.1 Rigid Body Motion	25
	2.4.2 Structural Flexibility Equations	26
	2.4.3 Control Surface Actuation	28
	2.4.4 The Küssner Dynamics	29
	2.4.5 Model of Atmospheric Turbulence	34
	2.4.6 The Wagner Dynamics	37
	2.4.7 Output Variables	39
	2.5 Reduced-Order Models	43
CHAPTER 3:	THEORY FOR THE DESIGN OF A SLACS	
	3.1 Introduction	45
	3.2 Optimal Control	47
	3.2.1 General Problem Formulation	47
	3.2.1.1 Solution of the LQP	48
	3.2.1.2 The Linear Quadratic Gaussian (LQG) Problem	50
	3.2.2 Specific Problem Statement - Optimal Output Regulator Solution	55
	3.2.3 Numerical Solution of the Optimal Control Laws	56

3.2.4 Controllability and Stabilisability Requirements 60

3.3 A Scheme to Evaluate the Model's Performance in Simulated Atmospheric Turbulence 62

CHAPTER 4: ASSESSMENT OF VARIOUS SLACS SCHEMES

4.1 Introduction 66

4.2 Derivation of the Optimal Control Laws 68

4.2.1 Selection of Weighting Matrices 68

4.3 Eigenvalue Analysis 72

4.4 Responses 75

4.4.1 Response of the Uncontrolled Aircraft to Deterministic Commands 75

4.4.1a Forcing the Controlled Aircraft 79

4.4.2 Response of the Controlled Aircraft Employing Full-State Feedback 83

4.4.3 Controlled Aircraft Employing Reduced-State Feedback 92

4.4.3a Controllability and Stabilisability 93

4.4.3b Responses 97

4.4.3c Steady-State Checks 101

4.4.3d Servo-Actuator Requirements 106

4.5 Aircraft Response in Atmospheric Turbulence 110

4.5.1 Predicting r.m.s Reductions in Wing Loads 115

CHAPTER 5: OBSERVERS FOR THE SLACS: FULL-ORDER

5.1 Introduction 116

5.2 Theory 119

5.3 Modelling the Observed System 124

5.4 Selection of Observer Weighting Matrices 127

5.5 Time Response Tests 131

CHAPTER 6: OBSERVERS FOR THE SLACS: REDUCED-ORDER

6.1 Introduction 148

6.2 Theory for Optimal Minimal-Order Observers 152

6.2.1 Specifications of the Minimal-Order Observer Design 152

6.2.2 The Optimal Control Problem 155
6.2.3 The Optimal Observer 159
6.3 Modelling the Observed System 166

CHAPTER 7: USE OF A MICROPROCESSOR AS A SELF-REPAIRING CONTROLLER (SRC)
7.1 Introduction 174
7.2 The Micro-Computer System 177
7.3 Self-Repairing Controller 179
7.4 SRC for the SLACS 189

CHAPTER 8: CONCLUSIONS
8.1 Concluding Summary 196
8.2 Recommendations for Further Work 217

REFERENCES 220

APPENDICES
I Composition of the State and Output Vector of each Mathematical Model Considered
II Expressing the Transfer Function of the Dryden Filter in terms of a State Variable Representation
III Some Aspects of Theory Relating to Computer Programs Used
IV Computer Programs
V Micro-computer Programs

LIST OF TABLES

		PAGE
2.1	Main Parameters Associated with Chosen Flight Condition of the Subject Aircraft	21
2.2	Composition of the State Vector of the Model, ARNE	25
2.3	State Variables of ARNE associated with Wagner Dynamics	38
2.4	Dimensions of Mathematical Models Used	43
4.1	Test Situations Employed for Deterministic Case	67
4.2	Test Situations Employed for Atmospheric Turbulence	67
4.3	Eigenvalues of Model CLEMENTI Without and With Feedback Control	73
4.4	Steady-State Values: Rigid Body Motion	83
4.5	Comparison of Feedback Gains Obtained Using Different Models	95
4.6	Comparison of Eigenvalues of the Controlled Model CLEMENTI Using Reduced-Order Feedback	96
4.7	Comparison of Steady-State Bending and Torsional Moments	105
4.8	Percentage Reductions of r.m.s. Values of Bending and Torsional Moments in the Presence of Turbulence Using Full-State Feedback Control	115
5.1	Comparison of Eigenvalues: FAURÉ (FSVF) With Observer	130
7.1	Program Segment Used to compare v_o and $\hat{v}_o$	186

LIST OF FIGURES

		PAGE
2.1	Block Diagram of Küssner dynamics applied to Tail	33
2.2	Block diagram of Küssner dynamics applied to Wing	34
2.3	Block Diagram Representation of the Dryden Filter	35
2.4	Bode Diagram Representations of the Transfer Functions associated with the Wagner Dynamics	40
3.1	Controlled Aircraft with Kalman Filter Incorporated	53
4.1	Response Comparison: Uncontrolled Aircraft: Case A	76
4.2	Response Comparison: Uncontrolled Aircraft: Case B	77
4.3	Response Comparison: Uncontrolled Aircraft: Case C	78
4.4	Simulation Block Structure: Uncontrolled Aircraft	81
4.5	Simulation Block Structure: Controlled Aircraft	81
4.6a	Rigid Body Heave Motion: Case A	82
4.6b	Rigid Body Heave Motion: Case B	82
4.6c	Rigid Body Heave Motion: Case C	82
4.7	Bending Moments at The Wing Root: Law (4.6)	84
4.8	Bending Moments at W.S.3: Law (4.6)	85
4.9	Torsional Moments at the Wing Root: Law (4.6)	87
4.10	Bending Moments at the Wing Root: Law (4.15)	89
4.11	Bending Moments at W.S.3: Law (4.15)	90
4.12	Torsional Moments at the Wing Root: Law (4.15)	91
4.13	Effect of Reduced-Order Feedback on WRBM: Case C	98
4.14	Effect of Reduced-Order Feedback on BM at WS3:Case C	99
4.15	Effect of Reduced-Order Feedback on WRTM: Case C	100
4.16	Control Surface Deflections needed for Load Alleviation	108
4.17	Control Surface Rates needed for Load Alleviation	109
4.18	Simulation of Atmospheric Turbulence	111
4.19	Response to Turbulence: Case D	113
4.20	Response to Turbulence: Case E	114
5.1	Block Diagram of the Observed System	126
5.2	Comparison Response:FSVF with Full-Order Observed System: Case A	132
5.3	Comparison Response:FSVF with Full-Order Observed System: Case B	133
5.4	Comparison Response:FSVF with Full-Order Observed System: Case C	134

5.5	Effect of Mismatch in Initial Conditions on Pitch Rate	136
5.6	Effect of Mismatch in Initial Conditions on Inboard Elevator Deflection	137
5.7	Effect of Mismatch in Initial Conditions on Vertical Velocity	138
5.8	Effect of Mismatch in Initial Conditions on Pitch Rate	140
5.9	Effect of Mismatch in Initial Conditions on Inboard Elevator Deflection	141
5.10	Effect of Mismatch in Initial Conditions on Vertical Velocity	142
5.11	Responses Obtained with a Reconstruction on w and q	145
5.12	Responses obtained with a Reconstruction on $w, q, \delta_A, \delta_{E_i}$.	146
6.1	Comparison Response:FSVF with Reduced-Order Observed System: Case A	170
6.2	Comparison Response:FSVF with Reduced-Order Observed System: Case B	171
6.3	Comparison Response:FSVF with Reduced-Order Observed System: Case C	172
7.1	B & H Micro-Computer Architecture	177
7.2	Self-Repairing Controller	179
7.3	Selection of Correct Output: A Flowchart	180
7.4	Functional Diagram of SRCTU	181
7.5	Self-Repairing Controller Test Unit	182
7.6	PMS-500 MCS and Associated Test Hardware	183
7.7	Plot of Input and Output Signals Associated with Analogue Switches	185
7.8	Plot of Reconstructed Output Signal from PMS-500	185
7.9	Input and Reconstructed Output with 20Hz Sine Wave	187
7.10	Input and Reconstructed Output with 50Hz Sine Wave	187
7.11	A proposed 'safety scheme' for the SLACS	190
7.12	Functional Diagram: SRC for the SLACS	192
7.13a	Signals v_o and v_c Associated with Vertical Velocity	194
7.13b	Signals v_o and v_c Associated with Pitch Rate	194
7.13c	Signals v_o and v_c Associated with Aileron Deflection	195
7.13d	Signals v_o and v_c Associated with Inboard Elevator Deflection	195

NOTATION

b	wing semi-span
$\bar{c}_T$	chord of the tail
$\bar{c}_W$	chord of the wing
h	aircraft height
n	dimension of state vector
n_2	pitch rate normalising factor
m	dimension of control vector
p	dimension of output vector
q	pitch rate
s	Laplace transform variable
t	independent variable, time
t_f	final time
t_o	initial time
v_c	reconstructed signal
v_o	output signal from flight controller
$\hat{v}_o$	estimate of output signal from flight controller
w	vertical velocity
w_g	vertical gust velocity
A_i, B_i, C_i	generalised bending mode coefficients
E	Young's modulus of Elasticity
$G_{w_g}(s)$	transfer function of Dryden filter
H	Hamiltonian
I	moment of inertia
J	performance index
$K, \bar{K}, P$	solution of Riccati equation
$K(c)$	Küssner function
L	wing total lift
$L(c)$	dimensionless lift
L_w	scale length of turbulence
$M_q, M_w, M_{\dot{w}}, M_{\delta_i}$	dimensional pitch stability derivatives
Q_i	generalised force
T	time interval
U_o	equilibrium forward speed of aircraft
$W(c)$	Wagner function
$Z_w, Z_{\dot{w}}, Z_{\delta_i}$	dimensional heave stability derivatives

α	angle of attack
α_0	trim angle of attack
δ_j	deflection of j^{th} control surface
ζ	damping ratio
η, ϵ	white noise
λ_i	bending displacement of i^{th} mode
ρ	density of air
σ_{w_g}	r.m.s. vertical gust velocity
θ	pitch attitude
τ_T	time delay
ω	angular frequency
ξ_k	generalised displacement at wing station (k)
$\mathcal{E}(\cdot)$	expectation operator
$\Phi(\omega)$	power spectral density
Ω	spatial frequency

$A, \hat{A}, \tilde{A}, \bar{A}, A_g, B, \bar{B}, \tilde{B}, B_g,$
$C, C^*, D, \tilde{D}, E, F, F_0, F_1, F_2,$
$G, \hat{G}, \tilde{G}, G_1, G_2, H, H^*,$
$L, M, P, Q, \hat{Q}, \bar{Q}, R, \hat{R}, \bar{R}, S, U,$
$V, W, \Xi, \Theta, \Sigma_0, \Gamma, \Lambda$ — Matrices

$\underline{e}$	error vector
$\underline{q}$	generalised co-ordinates
$\underline{r}$	reference command vector
$\underline{u}$	control vector
$\underline{u}^o$	optimal control vector
$\underline{x}$	state vector
$\underline{\hat{x}}, \underline{x}_e$	reconstructed state vector (full-dimension)
$\underline{y}$	output vector
$\underline{y}_e$	estimate of output vector
$\underline{y}^*$	measured output vector
$\underline{z}$	reconstructed state vector (reduced-dimension)
$\underline{z}_g$	Dryden filter state vector
$\underline{m}$	mean of initial state vector
$\underline{\psi}$	co-state vector

CHAPTER 1: INTRODUCTION

1.1. Problem Description

Current mission and design requirements for modern aircraft are such that the resulting configuration of the vehicle is greatly altered from the familiar earlier designs. These design requirements stem principally from a need to improve one or more of the fuel economy, cruise efficiency or tactical manoeuvrability of the aircraft depending upon its particular role. To achieve these design requirements has resulted in the use of one or more of:

(a) thin lifting surfaces

(b) long slender fuselages

(c) high stress design levels

(d) low load factors.

Inevitably this design trend has produced aircraft which are lighter and as a consequence more flexible. Such aircraft can develop both large amplitude displacements and high accelerations due to flexure, in addition to those due to rigid body motion. These displacements and accelerations may, for instance, in the case of the wing, induce high levels of bending and torsional moments at different locations from root to tip. In addition, large oscillations may occur as a consequence of flying through atmospheric turbulence thereby contributing to the fatigue of the structure. High load levels may also occur as a result of deterministic manoeuvre demands made by the pilot, especially in the case of fighter aircraft, or in having to take sudden and evasive action, in the case of commercial aircraft.

Flexible aircraft pose a new class of flight control problems in which the classical methods of approach to the solution of such problems become hopelessly impractical. However, by the use of optimal control theory, solutions may be obtained quickly although the synthesis of the control laws so derived still tends to pose some difficulty especially if the order of the mathematical models used is high. However, with the availability of very effective airborne digital computers, the synthesis problem may now be solved by relaxing the requirements on state measurements and providing in its place some form of state-estimation. It has thus become possible to consider, practically, the problem of designing a control system to alleviate the loads to which an airframe may be subjected by automatically deflecting active control surfaces. Such systems are variously referred to in the literature as:

(a) Manoeuvre Load Control Systems (MLCS) (Burris & Bender,1969)

(b) Active Load Control Distribution Systems (ALCDS) (Stone C.R. et.al., 1972)

(c) Load Increment Control Systems (LICS) (Van Dierendonck, 1973)

(d) Gust Load Alleviation Systems (GLAS) (Harpur, 1973)

(e) Structural Load Alleviation Control Systems (SLACS) (McLean & Prasad, 1980)

The application of optimal control methods to alleviate structural loads on aircraft was considered in this research. The subject aircraft chosen for the study was the Lockheed C-5A. Both the synthesis and flight integrity aspects of

implementing such control are considered in some detail. Digital simulation was used throughout the study in order to assess the performance of the various control schemes proposed.

1.2 Historical Background.

Structural load alleviation in one form or another has occupied the interest of aircraft designers from the earliest days of aviation. However, with the advent of highly flexible aircraft over the last two decades or so, coupled with the fact that optimal control techniques have expanded to cover a much wider usage, there has been plenty of new interest in the alleviation of structural loads on aircraft by the use of active controls. While early alleviation systems were designed to alleviate loads due to gusts, more recent designs also take into consideration the loads, (which in the case of flexible aircraft can be substantial), due to deterministic control commands.

Real interest in the understanding of the effects of atmospheric turbulence on flight vehicles began when the German aviator Otto Lillienthal was killed in 1896 when his glider became upset as a result of flying through a gusty atmosphere. It appears, however, that the earliest technical reference, (which incidentally was the first NACA report), was not available until 1915 (Hunsaker and Wilson, 1915) although a U.S. patent had already been granted to Sprater (1914) for a "stabilising device to counteract the disturbance (gust) and prevent it from having an injurious effect on the machine." Continued study of atmospheric turbulence resulted in two major contributions which are still often in use today. Von Karman (1937), and more important, Taylor (1937), established the bases

for suitable mathematical representations of atmospheric turbulence. As regards the design and implementation of load alleviation systems, however, the approach has been, in the earlier stages of development of SLACS, to use an open-loop design philosophy, while, in more recent years, closed-loop designs have been more common. The chief reason for adopting an open-loop design philosophy was that the knowledge of the dynamics and stability characteristics of the aircraft then in use, particularly unsteady aerodynamic effects and structural flexibility, was not very well known. In any case, none of the servomechanisms then in use was sufficiently fast* to be capable of implementing active load alleviation. One advantage however, of open-loop control is that the stability of the aircraft is not affected by its presence, while improper choice of feedback gains for closed-loop control systems could seriously affect the stability of the aircraft with often disastrous effects. Because fast servomechanisms were unavailable, it was necessary to sense gusts well in advance in order to allow time for corrective controlling action to be taken. As servoactuator performance increased, it became feasible to provide countering action due to gusts almost instantaneously and all the necessary sensing could then be achieved by the use of strap-down+ accelerometers and gyros.

The earliest open-loop designs used aeromechanical control in order to alleviate gust loads. Waterman (1930), built an aircraft with wings attached to the fuselage by means of skewed

---

* Speed of actuation is necessary in the case of active load alleviation especially when travelling through atmospheric turbulence since the time delay between sensing and required countering action becomes very small.

\+ Strap-down devices are normally easily attached inside the surface (for example, on the wing of the aircraft). In addition, such devices are compacted in size and cheap to produce.

hinges. The wing was balanced in steady flight by means of pneumatic struts. In unsteady conditions, the wing deflected, thus changing the angle of attack. The system however caused lateral control of the aircraft to be affected since the deployment of ailerons also resulted in deflections of the wing.

In 1938, a French proposal for a flap-type load alleviation system was made by Hirsch (1957). Initially, only model tests were carried out and the system used a horizontal stabilizer as an angle of attack sensor. After World War II, the approach was further developed and in 1954, flight tests were made using a Douglas DC-3.

In 1957, work carried out on the implementation of Weiner's optimum filter theory for the minimisation of an aircraft's open-loop response to atmospheric turbulence was reported upon by Tobak, (1957). Tobak's proposal depended upon the accurate measurements of variations in the angle of attack of the aircraft. His analysis validated earlier work carried out by Phillips and Kraft (1951) using classical analysis techniques. The Weiner optimum filter theory applied to G.L.A. systems was not investigated until 1970, when, Coupry (1971) proposed such a system for a Mirage IIIB fighter. Both simulation and also flight tests were carried out using the system. The simulation tests indicated that by using vanes, gyroscopes and accelerometers, enough information could be obtained to effect substantial reductions in accelerations sustained by the aircraft. These results, however, were not confirmed from flight tests.

In 1949, a Bristol Brabazon was fitted with a G.L.A.S. specifically designed to reduce bending moments on the wing of the aircraft. As a result, the wing structure was made 20% weaker than the figure that would normally be required to meet gust levels in the absence of any G.L.A.S.The system was intended to employ symmetric deflection of ailerons to counteract the effect of gusts and sensing of the gust was to be done by means of a gust vane fitted at the nose of the aircraft. In 1953, the whole project was abandoned and the system remained untested. (Harpur, 1973).

In the U.S.A., in 1950, Douglas Aircraft Corp. carried out tests on a Dakota C-47 aircraft which employed auxiliary flaps to provide GLA (Hawk, Conner and Levy (1952)), and in 1952, tests were carried out by NACA on a C-47 aircraft (Kraft,(1956), Hunter and Kraft (1961)). In the U.K., a number of tests were at the time carried out by R.A.E. using an Avro Lancaster Bomber (Zbrozek, Smith and White (1957), Zbrozek (1961)). All these tests employed the use of gust vanes to detect either changes in pressure or sudden changes in the relative wind, and, with the exception of the Bristol Brabazon, only alleviation of gust loads on the rigid body motion was attempted. In tests with the Avro Lancaster, considerable loss of stability was experienced due to large pitching moments caused by aileron deployment. This led to a decrease in effectiveness of the gust vane systems at large gust gradient distances

The gust vane systems employed at the time were unsuccessful because it was not sufficiently appreciated that the gust has components normal to the plane of symmetry of the aircraft and because account was not taken of other secondary effects such as changes in flight conditions, the effect of downwash acting on the tailplane,and the time delay between the wing encountering the gust and then the tail. The gust vane systems, which were really feedforward systems, could not at the time be designed to provide the necessary speed of response required, or be made insensitive enough to the secondary effects. These problems were noted and avoided by Attwood, Cannon, Johnson, and Andrew, who, in 1955, put forward a patent application for a GLA system which, "would sense linear and angular accelerations and would use auxillary control surfaces to produce forces and moments required to minimise the accelerations." The patent application was granted in 1961 and specifically took into account airframe and wing flexibility by using blended outputs from a pair of accelerometers and a pair of rate gyros so that unwanted signals due to bending motion would be cancelled. This proposed system was however mainly considered from the point of view of ride quality of passengers, and the specific aim of using a control system to alleviate structural loading, although implicit, was not until the present time considered. In 1962, the prototype UK fighter bomber, the TSR-2 depended upon augmented static directional stability to reduce its sensitivity to a gusty environment when operating in a high-speed, low-level role. (Ostgaard, (1976)). In the USA, a system designed to re-

duce structural loads due to gusts was first tried in a USAF program involving the prototype bomber, the XB-70. The program involved a significant amount of development work and this has been reported upon in Davis and Swaim (1966), Wykes and Mori (1966), Smith and Lum (1966) and Smith, Lum and Yamamoto (1968).

In 1964, a B-52H bomber of the Strategic Air Command of the USAF on a low level mission over Western USA encountered severe turbulence of estimated peak velocities of about 35 m/s. About 6 seconds after penetration into the gust, the yaw damper of the aircraft saturated. The response of the now unaugmented rigid body dynamics was so pronounced that 80% of the tail fin broke off. This unfortunate incident however accelerated interest in the study of GLA. One such study became the start, in 1965, of an extensive program of flight control system development known as the Load Alleviations and Mode Suppression (LAMS) program. The program produced very encouraging results and were reported in some detail by Burris and Bender (1969). The ride control systems developed under the LAMS program were later extended to accomodate GLA (Stockdale and Poyneer (1973)). Another such program centered around the C-5A aircraft known as the Load Improvement Control System (LICS) and was conducted by Van Dierendonck, Stone and Ward (1973). The B-1 Bomber developed for use with the USAF has been fitted with a Low Altitude Ride Control (LARC) system with the aim of alleviating the effect of gusts encountered at low altitudes using specially developed active surfaces

in the form of foreplanes located just aft of the nose of the aircraft (Interavia (1976), Hinsdale, (1976)). A Quantas B-747 aircraft has been fitted with a sideslip gust vane which is used to suppress gust-induced lateral acceleration. A load alleviation system has for some time been available as an optional extra for the Lockheed L-1011 aircraft, Hoblit (1973), although, only one has so far been fitted*.

Gust load alleviation schemes have also been applied to a number of light aircraft, for instance, the Cessna Cardinal has been fitted with a GLA system acting through spoilers (Brainerd & Kohlman, (1972)). An aeromechanical system employing auxillary wings to sense changes in angle of attack and to drive the flaps to compensate the resulting lift has been applied to the Cessna 172 aircraft. Reductions in normal acceleration of up to 50% were achieved by this system, (Roech and Harlan (1974), Stewart (1975)). A NASA Jetsteam aircraft now incorporates a GLA system amongst other Active Control Technology (ACT) functions which has proved to be very successful. (Lange et.al. 1975)).

A number of more recent studies conducted by McLean, (1976, 1978), have established the feasibility of using modern optimal control methods to design very effective active control systems to alleviate structural loads on aircraft. In this research, studies were made of the practical implementation of such systems which must necessarily employ either reduced or-

---

* On a British Airways aircraft in 1980.

der control or the use of state-estimators to implement full state feedback control. Practical aspects of synthesizing such controllers with some attendant degree of flight integrity are also considered.

1.3. Scope of the Research Investigation.

This research investigation was concerned with a study of the application of optimal control theory, in conjunction with advanced electronic technology, to provide, in current and future operational aircraft, a means of alleviating structural loads on such aircraft when subjected either to deterministic manoeuvre demands or to flying through atmospheric turbulence, by the use of continuously active control surfaces.

The subject aircraft for the study was a large jet transport, the Lockheed C-5A. Because of the limited amount of data available, only longitudinal motion was studied, and then only for a single flight condition. Several mathematical models representing the aircraft were used. The model representing the most complete set of dynamics contained equations describing rigid body motion, structural flexibility effects, actuator dynamics and unsteady aerodynamics. In the structural flexibility equations up to fifteen bending modes associated with the wing of the aircraft were represented. The bending and torsional moments at five different wing stations including the wing root were described by a set of output equations.

Optimal control theory was used to derive a number of linear full-state feedback laws using mathematical models of different order. Control laws corresponding to 24, 17, 14, and 5 state variable feedback were derived. The effect which different orders of feedback had upon the bending and torsional moments associated with the 5 chosen stations on the wing of

the aircraft was extensively tested by means of digital simulation. The work completed up to this stage has been reported elsewhere (McLean and Prasad (1980A), Prasad, Saoullis and Tsitsilonis (1980), McLean and Prasad (1980B)).

Because reduced order feedback appeared to be an attractive proposition from the point of view of practically synthesising the control law in an economical manner, a number of observer or state-estimator algorithms were considered to see if it would be possible to recoup some of the advantages of full-state feedback control based upon the measurements of only a few motion variables. It is believed that development of an algorithm of the type considered for synthesising the full-order observer has not been attempted previously. The theory used in the consideration of reduced-order observers had to be modified slightly to allow quadratic weightings used in the performance index of the control problem to be placed upon the output vector instead of the state vector.

Finally, a microcomputer system (MCS) available to the author was used for demonstrating the feasibility of employing software reliability techniques for monitoring the behaviour of a typical flight controller. Simulation of failure of the flight controller to produce the correct controlling signals to the servo-actuators was achieved by means of a self-repairing controller test unit (SRCTU) designed by the author. The MCS was then used to show how distortion of the output signals may be detected and how a reconstructed signal may be produced by

using surrogate gain values stored in ROMS in the computer. This part of the work has also been reported elsewhere (McLean and Prasad, (1980C)).

In Chapter 2, an extensive analysis is made of the way in which the most complete mathematical model was derived. The other models used, (of lower order), are described in less detail because all were simplifications of the most complete model.

In Chapter 3, the theory relating to the derivation of the optimal control laws is considered. Obtaining of time responses by the use of transition matrix methods of solution of the aircraft's state equation also forms a section of this chapter. In a final section of the chapter, a scheme to evaluate the r.m.s. levels of bending and torsional moments acting on the wing of the aircraft as it 'flies' through simulated atmospheric turbulence is also considered.

In Chapter 4, extensive tests by digital simulation of the effectiveness of control laws derived are reported. Both full and reduced-order control are considered together with servoactuator requirements and the performance of the controlled aircraft in simulated atmospheric turbulence.

In Chapter 5, an algorithm for synthesising a full-order observer is developed. Optimal control theory is used for the solution of the observer parameters and several time response tests are made to assess the performance of the

observer and to compare with results obtained previously, which assumed that the full system state would always be available for feedback.

In Chapter 6, Miller's theory for the design of optimal minimal-order observers is used to derive a reduced order observer. A small addition was made to the theory to allow quadratic weightings on the output vector rather than the state vector to be made. The change however did not affect the final specifications of the observer design as proposed by Miller. Time responses were again obtained by digital simulation and comparisons were made with results obtained previously.

In Chapter 7, work done on establishing the feasibility of using a microcomputer system (MCS) to provide software reliability is reported upon. A Bell and Howell MCS available to the author was used to detect simulated failure of ~~an~~ the aircraft's flight controller and the 'servoactuator signals' were then reconstructed with the MCS by sampling the 'sensor signals' and by using surrogate gain values stored in ROM. Simulation of Flight Controller failure was accomplished by the use of a simple logic circuit designed by the author.

Chapter 8 contains a concluding summary of the work reported in this thesis. Several recommendations for further study are included in the closing section of the chapter.

CHAPTER 2: MATHEMATICAL REPRESENTATION OF THE AIRCRAFT

2.1 Introduction

The equations used to represent the motion of the flexible aircraft which was chosen for the research investigation took into account the geometric, aerodynamic and structural properties of that aircraft. The way in which such equations are presented, however, depends upon the coordinates chosen to describe the motion, (Milne (1964)), i.e. whether these coordinates are relative either to an inertial axis set fixed in the Earth, or to some non-inertial set fixed in the aircraft. Although the results obtained from either set will be the same, the body-fixed axis system was used in this research principally because many of the criteria for aircraft handling and performance are expressed in this set, (Schwanz (1972)), and because pilot response appears to be mostly based upon body-fixed motion cues, (Gundry (1977)).

The derivation of equations in the body-fixed axis system are normally most easily carried out by first writing down the Lagrange equations, (Milne (1964), Schwanz (1972)):

$$\frac{d}{dt}\left(\frac{\partial L_i}{\partial \dot{\underline{q}}}\right) - \frac{\partial L_i}{\partial \underline{q}} = \underline{F}_i \qquad \ldots(2.1)$$

where $\underline{q}$ is the coordinate vector, F_i is a forcing vector and L_i is the associated Lagrangian. There are two possible sets of equations which can result from using (2.1), viz.,

(a) Equations containing constant coefficients which have been derived from steady state aerodynamics with unsteady aerodynamics being approximated by Küssner and Wagner lift growth functions.

(b) Equations containing non-constant coefficients which depend upon the use of more exact methods for representing unsteady aerodynamics.

In this study the former set was employed primarily because such equations are easy to formulate, and, provided that some additional approximations ~~could~~ can be made on the Küssner and Wagner representations, solutions of which can be quickly determined. One disadvantage, however, of using linearised equations is that it is not easy to incorporate the effect of changes in flight conditions: some of the coefficients of the equations may vary over a wide range, even changing sign at different points of the aircraft's flight envelope. For example, the stability derivative, M_w, which represents the change in pitching moment due to a change in vertical velocity, w, is one of the most difficult derivatives to determine and consequently the derivative represents a significant uncertainty where the design of an AFCS is concerned. Also Küssner and Wagner lift growth functions used to represent unsteady aerodynamics, are more accurately represented graphically. The expressions which represent the Küssner and Wagner functions are extremely difficult to incorporate into model equations, and, approximations provided in the literature, (in particular, see Bisplinghoff et al (1955)), have been employed.

The form of the aircraft equations resulting from the Lagrangean approach is typically as shown in (2.2), viz.,

$$F_2\ddot{\underline{q}} + F_1\dot{\underline{q}} + F_o\underline{q} + G_2\ddot{\underline{q}}*W + G_1\dot{\underline{q}}*W = C_1\underline{\dot{F}}*K \qquad \ldots(2.2)$$

where,

F_2 = Matrix of generalised inertia of the aircraft structure

F_1 = Matrix of generalised structural damping

F_o = Matrix of generalised structual stiffness

G_2 = Matrix of generalised aerodynamic damping

G_1 = Matrix of generalised aerodynamic stiffness

C_1 = Matrix of coefficients of the generalised forcing function.

$\underline{F}$ is the forcing function: W is the Wagner lift function and K is the Küssner function. The * is used to denote convolution and $\underline{q}$ is the vector of generalised coordinates. The generalised coordinates are calculated assuming that the elastic behaviour of the structure is linear and that structural displacements are small.

When aircraft equations are derived on the basis of small perturbations and account is taken of unsteady aerodynamic effects, the resulting set is known as an EXACT formulation. Equations so derived are difficult to solve numerically, primarily because of their complexity: often, approximations are used. The equation set so derived may be referred to as:

(a) Quasi-Static

(b) Modal Substitution

(c) Residual Stiffness

(d) Residual Flexibility

(e) Modal Truncation

When the motions of the structure are assumed to be in phase with the rigid body motions, i.e., accelerations of the structure are instantaneous, the resulting formulation is known as the QUASI-STATIC set. In order that the AFCSs designed on the basis of using such a set be capable of providing sufficient damping of all modes, it has to be ensured that the frequency separation between the rigid body and the elastic motions are large.

When the motions of the structure are related to the orthogonal, in vacuo, eigenvectors, the resulting equations are known as the MODAL SUBSTITUTION set. The associated eigenvectors will normally be composed of real numbers only.

By RESIDUAL STIFFNESS is meant that only a number of modes from the modal substitution set are retained, although, a quasi-static aeroelastic correction factor is also employed relating to the deleted modes. The chief disadvantage of the residual stiffness formulation is that all mode shapes must be calculated including those associated with the deleted modes. These extra calculations may be avoided by re-developing the equations associated with the exact formulation using the 'free-free' flexibility matrix, (Schwendler and MacNeal (1962)). The resulting formulation is then known as the RESIDUAL FLEXIBILITY set.

The MODAL TRUNCATION set is obtained when the deleted modes of the residual flexibility set are not represented by any correction factor. It is the most common dynamic aeroelastic formulation reported in the literature.

2.2 The Subject Aircraft

The specific type of aircraft chosen for the study was the C-5A, a large jet transport manufactured by Lockheed, because much of the data needed for the mathematical models required for the research study were available in Stone (1972) and Harvey and Pope, (1977). However, only information about the longitudinal motion, and then only for a single flight condition, was provided. The chief parameters associated with the flight condition studied are given in Table 2.1.

Total weight (N)	3.107×10^6
Mach No.	0.448
Altitude (m)	2.3×10^3
Dynamic Pressure (N/m^2)	9.15×10^3
Airspeed (m/s)	1.43×10^2
C of G (%mac)	31
Trim angle of attack (deg)	5.15×10^{-2}
Load Factor	1

Table 2.1: Flight Condition Parameters

At the same flight condition six separate mathematical models, all of different dimensions, were used. For ease of identification, these models were named:

ARNE

BACH

CLEMENTI

FAURÉ

GERSHWIN

HANDEL

The model ARNE was the largest, its state vector being of dimension, 79, while the model HANDEL was the smallest, its state vector being of dimension, 5. Since all the models were derived from ARNE, only this model is described in some detail in this chapter. The other models however, are briefly described in the final section of the chapter. Also, the composition of the state, control and output vectors of each model are summarised in Appendix I. In Appendix VI is shown the data associated with the model CLEMENTI.

2.3 State Equation Representation

For work connected with AFCS design, it is convenient to arrange that the aircraft equations be expressed in state variable form; that is to say, as a set of first-order differential equations in which only the first derivatives of the state variables appear on the left hand side of the equation, and on the right hand side, appear terms containing the state variables, $\underline{x}^*$. When the control and disturbances are considered as separate vectors, say $\underline{u}$ and $\underline{z}_g$, then an appropriate form of the state variable equation is:

$$\dot{\underline{x}}^* = \tilde{A}\underline{x}^* + \tilde{B}\underline{u} + \tilde{D}\underline{z}_g \qquad \ldots(2.3)$$

where $\underline{x}^* \epsilon R^n$, $\underline{u} \epsilon R^m$ and $\underline{z}_g \epsilon R^r$. The disturbance vector $\underline{z}_g$ is usually solved through a second equation, viz.,

$$\dot{\underline{z}}_g = D\underline{z}_g + \tilde{G}\eta \qquad \ldots(2.4)$$

where η represents a scalar white noise input to the filter. For the models used in this research, it was found more convenient to combine (2.3) and (2.4) resulting in (2.5). viz.,

$$\begin{bmatrix} \dot{\underline{x}}^* \\ \dot{\underline{z}}_g \end{bmatrix} = \begin{bmatrix} \tilde{A} & \tilde{D} \\ o & D \end{bmatrix} \begin{bmatrix} \underline{x}^* \\ \underline{z}_g \end{bmatrix} + \begin{bmatrix} \tilde{B} \\ o \end{bmatrix} \underline{u} + \begin{bmatrix} o \\ \tilde{G} \end{bmatrix} \eta \qquad \ldots(2.5$$

or

$$\dot{\underline{x}} = A\underline{x} + B\underline{u} + G\eta \qquad \ldots(2.6)$$

where,

$$\underline{x} \triangleq \begin{bmatrix} \underline{x}^* \\ \underline{z}_g \end{bmatrix} \qquad \ldots(2.7)$$

$$A \triangleq \begin{bmatrix} \tilde{A} & \tilde{D} \\ o & D \end{bmatrix} \qquad \ldots(2.8)$$

$$B \triangleq \begin{bmatrix} \tilde{B} \\ o \end{bmatrix} \qquad \ldots(2.9)$$

$$G \triangleq \begin{bmatrix} o \\ \tilde{G} \end{bmatrix} \qquad \ldots(2.10)$$

The significance of sometimes separating (2.6) into its components (2.3) and (2.4) will be described in greater detail in Section 2.4.5. Since the main aim of the research was to achieve some reduction of bending and torsional loads on the wing of the aircraft, it was necessary to define an output vector, $\underline{y}$, which was related to the state vector, $\underline{x}$, and control vector, $\underline{u}$, in such a way that these loads may be determined at any time. Thus the appropriate output equation was:

$$\underline{y} = C\underline{x} + E\underline{u} \qquad \ldots(2.11)$$

where, $\underline{y} \in R^p$.

2.4 The Mathematical Model, ARNE

The state vector, $\underline{x}$, of ARNE had dimension n of 79. Its control vector had dimension m of 2. Its output vector had dimension p of 56. In table 2.2 is shown how the state vector of the model, ARNE was composed.

$x_1 - x_2$	rigid body dynamics
$x_3 - x_{17}$	bending mode velocities
$x_{18} - x_{32}$	bending mode displacements
$x_{33} - x_{35}$	control surface displacements
$x_{36} - x_{40}$	Küssner dynamics
$x_{41} - x_{42}$	Gust Dynamics
$x_{43} - x_{79}$	Wagner Dynamics

Table 2.2 Composition of the State Vector of the Model ARNE

2.4.1 Rigid Body Motion $(x_1 - x_2)$

The rigid body motion of the aircraft was represented by the linearised, small perturbation equations associated with the short period mode, viz.,

$$\dot{w} = Z_w w + U_o q/n_2 + \sum_{j=1}^{m} Z_{\delta_j} \delta_j \qquad \ldots(2.12)$$

$$\dot{q}/n_2 = M_w w + M_{\dot{w}} \dot{w} + M_q q/n_2 + \sum_{j=1}^{m} M_{\delta_j} \delta_j \qquad \ldots(2.13)$$

where,

w = vertical velocity (.0254 m/s)

q/n_2 = 'translational pitch rate* (.0254 m/s)

Z_i = dimensional stability derivatives associated with vertical motion

M_i = dimensional stability derivatives associated with pitching motion.

U_o = Forward speed (m/s.)

δ_j = deflection of the j^{th} control surface.

It is easy to arrange that all the first derivatives appear on the left hand side by substituting for $\dot{w}$ in (2.13) using (2.12), viz.,

$$\dot{w} = Z_w w + U_o q + \sum_{j=1}^{m} Z_{\delta_j} \delta_j \qquad \ldots(2.14)$$

$$\dot{q}/n_2 = (M_w + M_{\dot{w}} Z_w) w + (M_q + M_{\dot{w}} U_o) q/n_2 + \sum_{j=1}^{m} (M_{\delta_j} + M_{\dot{w}} Z_{\delta_j}) \delta_j \qquad \ldots(2.15)$$

w and q/n_2 were designated state variables x_1 and x_2 respectively. The control surface deflections employed were

δ_{ε_i} - Inboard section of elevator

δ_{ε_o} - Outboard section of elevator

δ_A - symetrically deflected ailerons

2.4.2 Structural Flexibility Equations ($x_3 - x_{32}$)

The usual structural dynamics equations given as (2.2) are in an unsuitable form for use in flight control work for two principal reasons:

---

* n_2 is a conversion factor of 0.6066×10^{-3} rad/m, valid over small angles <0.2 rad.

(a) the equations are expressed as 2nd order vector differential equations rather than 1st order scalar as required for state variable representation.

(b) the vector $\underline{q}$ contains control inputs, δ_j, (which are terms which should only appear on the right hand side of the state equation).

An alternative method of expressing the structural dynamic equations, is to represent each mode by an equation of the form:

$$A_i\ddot{q}_i + B_i\dot{q}_i + C_i q_i = Q_i \qquad \ldots(2.16)$$

where, q_i, $\dot{q}_i$ and $\ddot{q}_i$ correspond to generalised stiffness, damping and mass terms respectively. A_i, B_i and C_i are coefficients of the i^{th} generalised coordinate and Q_i is a generalised force, containing aerodynamic variables. not correct at all

Let,

$$\lambda_{1_i} \triangleq q_i \qquad \ldots(2.17)$$

$$\lambda_{2_i} \triangleq \dot{\lambda}_{1_i} = \dot{q}_i \qquad \ldots(2.18)$$

Substituting definitions (2.17) and (2.18) into (2.16) yields :

$$\dot{\lambda}_{2i} = \frac{-B_i}{A_i}\lambda_{2i} - \frac{C_i}{A_i}\lambda_{1i} + \frac{Q_i}{A_i} \qquad \ldots(2.19)$$

$$\therefore \quad \begin{bmatrix}\dot{\lambda}_{1i}\\ \dot{\lambda}_{2i}\end{bmatrix} = \begin{bmatrix}0 & 1\\ -\frac{C_i}{A_i} & -\frac{B_i}{A_i}\end{bmatrix}\begin{bmatrix}\lambda_{1i}\\ \lambda_{2i}\end{bmatrix} + \begin{bmatrix}0\\ \frac{1}{A_i}\end{bmatrix}\cdot Q_i \qquad \ldots(2.20)$$

* See The A matrix appendix VI. Structural modes are not defined as suggested by 2.2 .

Hence each bending mode can be represented by two first order differential equations of the form given by (2.20), where λ_{2_i} is the rate and, λ_{1_i}, the displacement associated with the i^{th} mode. For ARNE, the first fifteen bending mode rates were represented by the state variables x_3-x_{17} and the corresponding bending mode displacements by the state variables x_{18} - x_{32}. The damping ratios of each mode were small. all being <0.1. The units of λ_i were 0.0254m and those of $\dot{\lambda}_i$ were 0.0254m/s.

not correct at all

2.4.3 Control Surface Actuation (x_{33} - x_{35})

The deflections of the control surfaces were considered to arise as a result of control signals being applied to their servo-actuators. The dynamic responses of these actuators were considered to be linear and were assumed to be represented by simple time lags.

The three control surfaces used were:

Ailerons (symmetrically deflected)

Inboard section of elevator

Outboard section of elevator

However, only the signals to the actuators associated with the ailerons and the inboard section of the elevator were used as control inputs: the outboard section of the elevator was left free for receiving other commands such as would be required for carrying out normal inflight manoeuvres. Its dynamics were however represented in the state vector of ARNE.

The actuator dynamics associated with those control surfaces used were represented by:

Aileron:

$$\delta_A(s) = \frac{6.0}{s+6.0} \delta_{A_c}(s) \quad \ldots(2.21)$$

Inboard elevator:

$$\delta_{E_i}(s) = \frac{7.5}{s+7.5} \delta_{E_{i_c}}(s) \quad \ldots(2.22)$$

From (2.21),

$$\dot{\delta}_A = -6.0\delta_A + 6.0\,\delta_{A_c} \quad \ldots(2.23)$$

and from (2.22),

$$\dot{\delta}_{E_i} = -7.5\delta_{E_i} + 7.5\delta_{E_{i_c}} \quad \ldots(2.24)$$

The actuator dynamics associated with the outboard elevator was simply represented by the equation:

$$\dot{\delta}_{E_o} = -7.5\delta_{E_o} \quad \ldots(2.25)$$

For ARNE,

$$\delta_A = x_{33} \quad \ldots(2.26)$$

$$\delta_{E_i} = x_{34} \quad \ldots(2.27)$$

$$\delta_{E_o} = x_{35} \quad \ldots(2.28)$$

and,

$$\delta_{A_c} = u_1 \quad \ldots(2.29)$$

$$\delta_{E_{i_c}} = u_2 \quad \ldots(2.30)$$

2.4.4 The Küssner Dynamics (x_{36}- x_{40})

The Küssner function, K(c) , (Küssner (1936), is related to the change in lift on an aerofoil due to the incidence of a sharp-edged gust striking the aerofoil. The dimentionless lift development, L(c), based upon the aerofoil mean semichord, $\bar{c}$, is given as, (Bisplinghoff et al (1955):

$$L(c) = 2\pi\rho U_o b w_g K(c) \qquad \ldots(2.31)$$

where b is the aerofoil semispan and, w_g, is the vertical gust velocity. U_o is the forward speed of the aircraft and ρ is the air density. The form of $K(c)$ makes it difficult to express in simple algebraic terms, and approximations are often employed, (Fung (1955), Dowell (1978) . One approximation is the Sear's function (1940) which, for aerofoils with aspect ratio >6* is given by,

$$K(c) = 1 - 0.5e^{-0.13c} - 0.5e^{-c} \qquad \ldots(2.32)$$

where $c \triangleq \frac{U_o t}{\gamma \bar{c}/2}$. $\qquad \ldots(2.33)$

and γ is a Mach number correction factor. (2.32) is the expression for the output obtained when a step input (such as the edge of a gust) strikes the aerofoil. The appropriate transfer function for the wing of the chosen subject aircraft is

$$J_W(s) = \frac{0.5}{s+2.857} + \frac{0.5}{s+21.98} \qquad \ldots(2.34)$$

and for the tail, is:

$$J_T(s) = \frac{0.5}{s+5.781} + \frac{0.5}{s+61.37} \qquad \ldots(2.35)$$

The corresponding numerical values of U_o, γ and $\bar{c}$ have been substituted in (2.34) and (2.35). For the C-5A, these numerical values are:

$$U_o = 143 \text{ m/s}$$
$$\gamma = 1.38$$
$$\bar{c}_W = 9.429 \text{ m}$$
$$\bar{c}_T = 4.66 \text{ m}$$

---

* For the C-5A, the aspect ratio of the wing is 7.75.

In Harvey and Pope (1977), in the determination of (2.33), the value of the chord was used instead of that of the semi-chord and this error was noted in McLean and Prasad (1980B). However, the Harvey and Pope representation was followed in this work to permit valid comparison of results. Also some approximation was made to the transfer functions (2.34) and (2.35), which, in Harvey and Pope, was given as:

$$\tilde{J}_W(s) = \frac{10.983}{s + 10.983} \qquad \ldots (2.36)$$

$$\tilde{J}_T(s) = \frac{22.185}{s + 22.185} \qquad \ldots (2.37)$$

The corresponding equations describing the Küssner dynamics for the wing was:

$$\dot{x}_{40} = -10.983x_{40} + 10.983x_{42} \qquad \ldots (2.38)$$

and for the tail was:

$$\left.\begin{aligned} \dot{x}_{36} &= -22.185x_{36} + 22.185w_g \\ &= -22.185x_{36} + 22.185x_{42} \end{aligned}\right\} \qquad \ldots (2.39)$$

Because the edge of the gust will strike the wing first and then the tail some finite time after the aircraft penetrates the gust field, pure delays were used to represent this time delay. For the tail, a distance of 56.1m behind the nose, the time delay was:

$$\tau_T = \frac{56.1}{U_o} = 0.393s. \qquad \ldots (2.40)$$

This delay was represented by a 2nd order Padé approximation, (Richards (1979)), which was given as:

$$\dot{x}_{38} = x_{39} - \frac{2}{\tau_T} x_{36} \qquad \ldots (2.41)$$

$$\dot{x}_{39} = -\frac{6}{\tau_T^2} x_{38} - \frac{4}{\tau_T} x_{39} + \frac{14}{\tau_T^2} x_{36} \qquad \ldots(2.42)$$

$$\therefore \quad \dot{x}_{38} = x_{39} - 5.096\, x_{36} \qquad \ldots(2.43)$$

$$\dot{x}_{39} = -38.953\, x_{38} - 10.192\, x_{39} + 90.891\, x_{36} \qquad \ldots(2.44)$$

(2.39), (2.43) and 2.44) are easily expressed in terms of Laplace transformations, viz.,

$$sX_{36}(s) = -22.185\, X_{36}(s) + 22.185\, X_{42}(s) \ldots(2.45)$$

$$sX_{38}(s) = X_{39}(s) - 5.096\, X_{36}(s) \ldots(2.46)$$

$$sX_{39}(s) = -38.953\, X_{38}(s) - 10.199\, X_{39}(s) + 90.891 X_{36}(s) \ldots(2.47)$$

From (2.45)

$$\left.\begin{aligned} \frac{X_{36}(s)}{X_{42}(s)} &= \frac{22.185}{s + 22.185} \\ &= \frac{1}{1 + 0.045s} \end{aligned}\right\} \qquad \ldots(2.48)$$

Multiplying (2.47) throughout by s and substituting for $X_{38}(s)$ using (2.46) yields:

$$s^2X_{39}(s) = -38.953[X_{39}(s) - 5.096X_{36}(s)] - 10.199sX_{39}(s) + 90.891sX_{36}(s) \ldots(2.49)$$

$$\therefore \quad \frac{X_{39}(s)}{X_{36}(s)} = \frac{198.5\,(1 + 0.458s)}{s^2 + 10.199s + 38.953} \qquad \ldots(2.50)$$

In block diagram form, the Küssner dynamics associated with the tail is shown in Figure 2.1

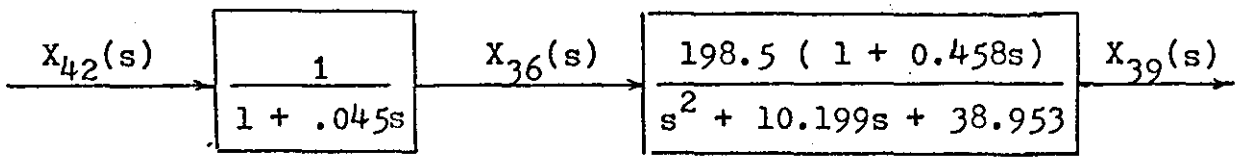


Figure 2.1 : Küssner Dynamics applied to Tail

The appearance of the gust at the wing, a distance of 16.772m from the nose of the aircraft, was delayed by:

$$\tau_W = \frac{16.772}{U_o} = 0.117s. \qquad ...(2.51)$$

This delay was represented by a simple time lag, viz.,

$$\dot{x}_{37} = -\frac{1}{\tau_W}x_{37} + \frac{1}{\tau_W}x_{40} \qquad ...(2.52)$$

or,

$$\dot{x}_{37} = -8.549x_{37} + 8.549x_{40} \qquad ...(2.53)$$

(2.38) together with (2.53) express the form of the Küssner dynamics applied to the wing of the subject aircraft. The equations, expressed in terms of Laplace transformations are:

$$sX_{40}(s) = -10.983X_{40}(s) + 10.983X_{42}(s) \qquad ...(2.54)$$

$$sX_{37}(s) = -\ 8.549X_{37}(s) + \ 8.549X_{40}(s) \qquad ...(2.55)$$

$$\therefore \quad \frac{X_{40}(s)}{X_{42}(s)} = \frac{10.983}{s + 10.983} = \frac{1}{1 + 0.091s} \qquad ...(2.56)$$

and,

$$\frac{X_{37}(s)}{X_{40}(s)} = \frac{8.549}{s + 8.549} = \frac{1}{1 + 0.117s} \qquad ...(2.57)$$

In Figure 2.2 is shown the appropriate block diagram representation of (2.56) and (2.57).

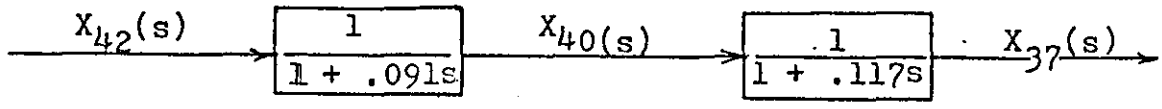


Figure 2.2 Küssner Dynamics applied to Wing

2.4.5 Model of Atmospheric Turbulence $(x_{41}-x_{42})$

A number of suitable representations of continuous atmospheric turbulence are available (Taylor (1937), Von Karman (1937)). Possibly the most faithful is that proposed by Von Karman since, of all such representations available, the Von Karman model is in closest correspondence with the observed behaviour of turbulence. The power spectral density (p.s.d) associated with the Von Karman model, for vertical gust velocity, w_g (which was the only component of the gust required for this research), is given as:

$$\Phi_{w_g}(\omega) = \frac{\sigma_{w_g}^2 \cdot L_w}{U_o} \frac{\left[1+8/3(1.339 L_w/U_o \cdot \omega)^2\right]}{\left[1+(1.339 L_w/U_o \cdot \omega)^2\right]^{11/6}} \quad \ldots(2.58)$$

The Von Karman model cannot easily be programmed for simulation in real time because of the non-integer exponent in (2.58). A suitable alternative, the Dryden model (Chalk et al (1969))provides a p.s.d which closely matches that of the Von Karman model. Some small differences occur at the higher frequencies but this is generally of small consequence in AFCS design. The Dryden p.s.d is:

$$\phi_w(\omega) = \sigma_{w_g}^2 \frac{L_w}{U_o} \frac{\left[1 + 3\left(\frac{L_w}{U_o}\cdot\omega\right)^2\right]}{\left[1 + \left(\frac{L_w}{U_o}\cdot\omega\right)^2\right]^2} \qquad \ldots(2.59)$$

It is easily shown, (Truxal (1955)), that:

$$\phi_{w_g}(\omega) = \left|G_{w_g}(j\omega)\right|^2 \qquad \ldots(2.60)$$

Thus, the transfer function of the Dryden filter may be obtained, viz.,

$$G_{w_g}(s) = \sigma_{w_g}\sqrt{\frac{L_w}{U_o}} \frac{\left(1 + \sqrt{3}\frac{L_w}{U_o}s\right)}{\left(1 + \frac{L_w}{U_o}s\right)^2} \qquad \ldots(2.61)$$

In figure 2.3 is shown the appropriate block diagram representation for the Dryden filter. The filter is excited by zero mean, white noise, η, and its output is the vertical gust velocity.

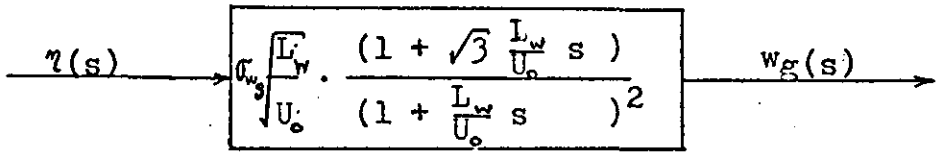


Figure 2.3 Block Diagram Representation of Dryden Filter

The transfer function (2.61) may be easily expressed in state variable form. Let:

$$x_{42} \triangleq w_g \qquad \ldots(2.62)$$

$$x_{41} \triangleq \dot{w}_g - \sigma_{w_g}\sqrt{\frac{3U_o}{L_w}} \cdot \eta(t) \qquad \ldots(2.63)^*$$

---

* This definition of x_{41} was employed in order to avoid terms in $\dot{\eta}(t)$ from the final expressions.

It can be shown, (see Appendix II), that:

$$\begin{bmatrix} \dot{x}_{41} \\ \dot{x}_{42} \end{bmatrix} = \begin{bmatrix} -2\frac{U_o}{L_w} & -\frac{U_o^2}{L_w^2} \\ 1 & 0 \end{bmatrix} \begin{bmatrix} x_{41} \\ x_{42} \end{bmatrix} + \begin{bmatrix} \sigma_{w_g}\sqrt{\frac{U_o^3}{L_w^3}}.(1-2\sqrt{3}) \\ \sigma_{w_g}\sqrt{\frac{3U_o}{L_w}} \end{bmatrix} \eta(t) \quad ..(2.64)$$

For the C-5A, the following parameters applied:

$$L_w = 576m$$
$$U_o = 143m/s \quad ...(2.65)$$

The standard deviation of the vertical gust velocity, σ_{w_g}, was chosen to be 0.3048m/s. See page 67 {There are not the Same.

Using (2.65), (2.64) becomes:

$$\begin{bmatrix} \dot{x}_{41} \\ \dot{x}_{42} \end{bmatrix} = \begin{bmatrix} -0.497 & -0.062 \\ 1 & 0 \end{bmatrix} \begin{bmatrix} x_{41} \\ x_{42} \end{bmatrix} + \begin{bmatrix} -0.093 \\ 0.263 \end{bmatrix} \eta \quad ...(2.66)$$

It should be noted that (2.64) is of the form of (2.4), where:

$$\underline{z}_g = \begin{bmatrix} x_{41} \\ x_{42} \end{bmatrix} \quad ...(2.67)$$

$$D = \begin{bmatrix} -2\frac{U_o}{L_w} & -\frac{U_o^2}{L_w^2} \\ 1 & 0 \end{bmatrix} \quad ...(2.68)$$

$$\tilde{G} = \begin{bmatrix} \sigma_{w_g}\sqrt{\frac{U_o^3}{L_w^3}}\ (1-2\sqrt{3}) \\ \sigma_{w_g}\sqrt{\frac{3U_o}{L_w}} \end{bmatrix} \quad ...(2.69)$$

2.4.6 The Wagner Dynamics (x_{43} - x_{79})

The Wagner function, W(c), (Wagner (1925)), represents the growth in lift on any of the lifting surfaces such as the wing, the tail or any of the control surfaces due to a step change in their angle of attack. The circulatory lift due to this motion is given as (Bisplinghoff (1955)):

$$L(c) = 2\pi\rho U_o^2 b\, \alpha_o . W(c) \qquad ..(2.70)$$

where α_o is the trim angle of attack and W(c) is the Wagner function. As with the Küssner function, the form of W(c) is such that it cannot be expressed in simple algebraic terms and often, approximations have to be made. One such approximation suggested by Fung (1955), for an aerofoil section of high aspect ratio (AR>6), is:

$$W(c) = 1-0.165e^{-0.455c}-0.335e^{-0.3c} \qquad ..(2.71)$$

where c is defined in (2.33). The associated transfer function of (2.71), in the case of the wing, is:

$$W_W(s) = \frac{0.165}{(s+1.0)} + \frac{0.335}{(s + 6.594)} \qquad ..(2.72)$$

and, in the case of the tail, is:

$$W_T(s) = \frac{0.165}{(s+2.024)} + \frac{0.335}{(s + 13.32)} \qquad ..(2.73)$$

The error made by Harvey and Pope concerning the evaluation of (2.38), (where the chord was used instead of the semichord), was again carried through in the determination of the Wagner function. Although this error was noted, the Harvey and Pope

representation was followed to permit comparison with previous results obtained. In Harvey and Pope the transfer functions (2.72) and (2.73) were taken as:

Wing:
$$\tilde{W}_W(s) = \frac{s + 10.49}{s + 10.99} \qquad ..(2.74)$$

Tail:
$$\tilde{W}_T(s) = \frac{s + 21.737}{s + 22.237} \qquad ..(2.75)$$

The Wagner dynamics are not incorporated into the aircraft dynamics in a straight-forward manner. Not only are contributions to the growth of lift on the flying surfaces made from the rigid body motion, but also from each of the fifteen bending modes represented. In table 2.3, are shown those state variables in the model, ARNE, representing the Wagner dynamics.

$\dot{w}_{wing}$	x_{43}
$\dot{q}/n_{2\ wing}$	x_{44}
$\dot{\lambda}_{1wing} - \dot{\lambda}_{15\ wing}$	$x_{45} - x_{59}$
$\dot{w}_{tail}$	x_{60}
$\dot{q}/n_{2tail}$	x_{61}
$\dot{\lambda}_{1tail} - \dot{\lambda}_{15\ tail}$	$x_{62}-x_{76}$
$\dot{\delta}_{A\ wing}$	x_{77}
$\dot{\delta}_{E\ tail}$	x_{78}
$\dot{\delta}_{E\ tail}$	x_{79}

Table 2.3: State Variables of ARNE associated with Wagner Dynamics.

The subscript, (wing), is used to indicate the Wagner dynamics associated with that variable having an effect on the wing and the subscript,(tail), indicates the corresponding effect on the tail.

Inspection of (2.74) and (2.75) indicates that the transfer functions associated with the representation of the Wagner dynamics are approximately unity. From the Bode diagram representations of (2.74) and (2.75), presented in Figure 2.4, it is clear that their contribution to the dynamic behaviour of the aircraft is unlikely to be of any significance. Consequently, it was decided to use a lower order model not incorporating the Wagner dynamics and this is further discussed in Section 2.5.

2.4.7 Output Variables.

Since levels of bending and torsional moments experienced in the wing of the aircraft were of particular significance for the research study, it was necessary to derive suitable expressions from which these moments could be evaluated. Five wing stations were chosen for the subject aircraft: wing station 1 (w.s.1) was at the wing root, w.s.3 was at the mid-span and w.s.5 was at the wing tip; w.s.2 was equidistant between w.s.1 and w.s.3, and, w.s.4 was equidistant between w.s.3 and w.s.5.

The bending moment (y_k) at wing station (k) is given as:

$$y_k = -EI \left. \frac{d^2 \xi_k}{dy^2} \right|_{y=o} \qquad ..(2.76)$$

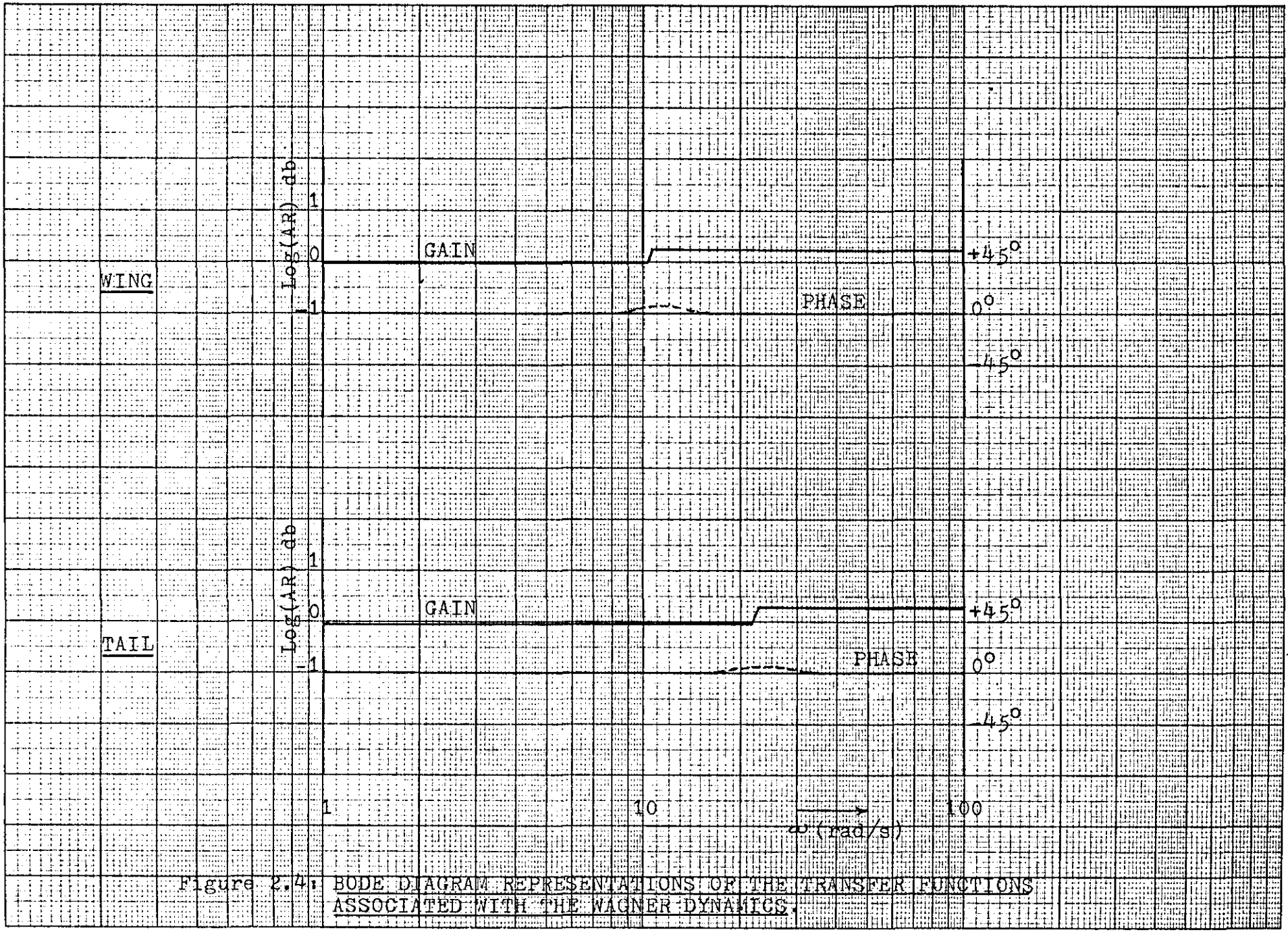


Figure 2.4: BODE DIAGRAM REPRESENTATIONS OF THE TRANSFER FUNCTIONS ASSOCIATED WITH THE WAGNER DYNAMICS.

where, (EI), is the flexural rigidity term and, ξ_k, is the generalised displacement at w.s(k). ξ_k, according to normal mode theory. is given as:

$$-\xi_k = \phi_{k1}h + \phi_{k2}\theta + \sum_{i=3}^{n}\phi_{ki}\lambda_{i-2} + \sum_{j=n+1}^{m}\phi_{kj}\delta_j \qquad ..(2.77)$$

where, λ_{i-2} represents the displacements associated with the bending modes, ($i = 3,..18$ in the case of ARNE). Also,

$$\dot{h} = U_o\theta - w \qquad ..(2.78)$$

$$\therefore -\frac{d^2\xi_k}{dy^2} = \frac{d^2\phi_{k1}}{dy^2}h + \frac{d^2\phi_{k2}}{dy^2}\theta + \sum_{i=3}^{n}\frac{d^2\phi_{ki}}{dy^2}.\lambda_{i-2} + \sum_{j=n+1}^{m}\frac{d^2\phi_{kj}}{dy^2}.\delta_j \qquad ..(2.79)$$

By substituting,(2.79), into (2.70), the general expression for the bending moment at any wing station, (k), is obtained, viz.,

$$y_k = EI\left\{\frac{d^2\phi_{k1}}{dy^2}.h + \frac{d^2\phi_{k2}}{dy^2}\theta + \sum_{i=3}^{n}\frac{d^2\phi_{ki}}{dy^2}\lambda_{i-2} + \sum_{j=n+1}^{m}\frac{d^2\phi_{kj}}{dy^2}.\delta_j\right\} \qquad ..(2.80)$$

By differentiating y_k,(2.80) with respect to time, it is possible to determine the expression for the bending rate associated with wing station, k. Also included in the output description were expressions for the torsional moments together with their associated rates of change at the five wing stations. In the case of the mathematical model, ARNE, the displacement

and rates of change of displacement associated with the first fifteen bending modes were also included in the output vector as well as the motion variables of the rigid body and both the deflections and rates of change of deflection of the control surfaces commanded. Thus the output vector, $\underline{y}$, (Equation (2.11)), of ARNE, had dimension, 56.

2.5. Reduced Order Models.

The other models used, viz., BACH, CLEMENTI, FAURÉ, GERSHWIN and HANDEL were all derived from the model, ARNE. In Table 2.4. is shown a comparison of the dimensions of the models considered.

MODEL	VECTOR DIMENSIONS		
	state n	control m	output p
ARNE	79	2	56
BACH	42	2	56
CLEMENTI	24	2	38
FAURÉ	17	2	38
GERSHWIN	14	2	38
HANDEL	5	2	38

Table 2.4 : Dimensions of Mathematical Models Used.

The model, ARNE, proved to be too difficult for computation, although it represented the most complete model by containing equations relating to both structural flexibility effects and unsteady aerodynamics.

The model, BACH, was represented by the same equations as the model, ARNE, but omitting the equations representing the Wagner dynamics. Its output vector was identical to that defined for ARNE. The reason for neglecting the Wagner dynamics was that the lift growth dynamics were being represented by the approximate transfer functions given as (2.74) and (2.75) and these were nearly unity.

The model, CLEMENTI, included in its description only the

first six structural bending modes but was otherwise identical to BACH. Quite early in the research program, it was found from the associated digital simulation studies that the responses obtained from BACH, did not differ significantly from those obtained when the nine upper bending modes were omitted Consequently, most of the research effort was directed to CLEMENTI.

The model FAURÉ included equations representing the same dynamics as the model CLEMENTI, but it excluded both the vertical gust and the Küssner dynamics. The model GERSHWIN, however reintroduced both the gust and the Küssner dynamics, but included in its description only the first bending mode and its rate, the higher bending modes being neglected. This model was used principally to test the hypothesis that much of the bending energy (60% or more)is contained in the first bending mode (Schwanz (1972)).

The model, HANDEL, only contained in its description, the rigid body motion variables and the variables associated with the actuator dynamics.

CHAPTER 3: THEORY FOR THE DESIGN OF A SLACS

3.1 Introduction

In this chapter, the major theoretical aspects relating to the design of a feedback controller to provide, for the subject aircraft, a certain amount of structural load alleviation are presented.

The analysis of the mathematical models described in Chapter 2 indicated that it was desired to use two of the control surfaces of the subject aircraft to affect up to 56 output variables. Such a control problem may not easily be solved by conventional methods, which are in the main more suitable to single-input, single-output systems, or even multi-input single-output systems. Such methods depend upon interpretation of time responses in order to determine settling time, time-to-peak overshoot, frequency of oscillation, time-of-half amplitude, and so on; inevitably the design procedure is slow and needless to say expensive since for the size of mathematical models studied, digital computation has to be employed*.

---

* Analogue computation would require an extremely large amount of integrators to be employed; for CLEMENTI at least 24 integrators would be required in addition to a substantial amount of summing amplifiers and potentiometers. The analogue computer available to the author, a TR-48, did not have the capacity for handling models of such complexity. However, the model HANDEL was patched on the TR 48 in relation to work to be reported in Chapter 7.

Optimal control methods are particularly suitable for designing automatic flight control systems to provide ACT* functions like Structural Load Alleviation. By such methods, it is possible to specify a desired performance which may be met exactly. When a particular performance criterion is employed subject to the constraints imposed by the chosen state equation formulation, the resulting design is unique. The control problem is most adequately represented as a regulator problem. A regulator is designed to keep a system within an acceptable deviation from a reference condition using acceptable amounts of control (Bryson and Ho (1969)). For dynamic systems, adequately represented by linear models, it is relatively easy to determine very satisfactory feedback controllers. However, a particular disadvantage of synthesising any feedback laws obtained as solutions of the optimal regulator problem is that full state feedback is required. In the research discussed here, tests were often made on the aircraft employing reduced state feedback. It was found that there was a limit to the number of variables which could be eliminated in the feedback loop and this limit is dictated by controllability and stabilisability criteria. These criteria are discussed in a subsequent section with particular reference to the models used.

---

* There are other active control technology (ACT) functions such as Fatigue Reduction, Flutter Mode Control, Ride Control and Augmented Stability.

3.2 OPTIMAL CONTROL

The basic principles presented in this section are due in great measure to Pontryagin (1962).

3.2.1. General Problem Formulation

It is usual practice to employ as a measure of the quality of performance of an optimal system, an integral of the form

$$J = \int_{t_o}^{T} L(\underline{x},\underline{u},t)dt \qquad \ldots(3.1)^*$$

subject to the constraint,

$$\dot{\underline{x}} = g(\underline{x},\underline{u},t) \qquad \ldots(3.2)$$

where $\underline{x} \in R^n$, $\underline{u} \in R^m$ and t is the independent variable, time. The scalar, J, is referred to as the performance index (p.i.) of the system; the functional $L(\underline{x},\underline{u},t)$ can be considered to be the cost of being at some specific point in the state space of the problem, with a particular value of control, at some particular time (Fuller (1959)). The problem is to find a control, $\underline{u}^o$, which minimises[+] the p.i over the interval t_o to T. A form of the p.i which is convenient to use in flight control work is:

$$J = \tfrac{1}{2}\int_{o}^{\infty}(\underline{x}'Q\underline{x} + \underline{u}'G\underline{u})dt \qquad \ldots(3.3)$$

By taking the limits of the integral over the semi-infinite

---

*Here the problem is assumed to be purely deterministic See 3.3.1.2

+In some cases the maximum of the p.i. is found in which case the sign of the integrand is simply the opposite to that used in (3.1).

interval, it turns out that the parameters of the resulting control law are constant. The $\frac{1}{2}$ is used simply for analytical convenience. The properties of the weighting matrices Q and G will be discussed in Section 3.2.1.1. When the system is described by a linear vector differential equation of the form:

$$\dot{\underline{x}} = A\underline{x} + B\underline{u} \qquad \ldots \quad (3.4)$$

and the associated performance index to be minimised is of the form of (3.3), the problem is referred to as the Linear Quadratic Problem (LQP). It has been shown (Kalman (1960), that the optimal control which minimises (3.3) is

$$\underline{u}^{o} = -G^{-1}B'K\underline{x} \qquad \ldots \quad (3.5)$$

where K is the positive definite solution of the algebraic matrix Riccati equation given as (3.6), viz.,

$$KA + A'K - KBG^{-1}B'K + Q = 0 \quad .. \quad (3.6)$$

3.2.1.1. Solution of the LQP

For a system described by the linear vector differential equation (3.4) with performance index given as (3.3), the procedure for determining the optimal control is quite straightforward, and, for small problems, computing requirements are not excessive.

The associated Hamiltonian (H) of the system (Athans and Falb (1966)) is expressed as:

$$H = \tfrac{1}{2}(\underline{x}'Q\underline{x} + \underline{u}'G\underline{u}) + \underline{\psi}'(A\underline{x} + B\underline{u}) \quad \ldots (3.7)$$

where $\underline{\psi}$ is the co-state vector of dimension, n, and,

$$\dot{\underline{\psi}} \triangleq -\frac{\partial H}{\partial \underline{x}} \quad \ldots(3.8)$$

Therefore,

$$-\frac{\partial H}{\partial \underline{x}} = \dot{\underline{\psi}} = -Q\underline{x} - A'\underline{\psi} \; ; \; \underline{\psi}(\infty) = 0 \quad \ldots(3.9)$$

and

$$\frac{\partial H}{\partial \underline{u}} = G\underline{u} + B'\underline{\psi} \quad \ldots.(3.10)$$

For H to be minimised with respect to $\underline{u}$, (hence J), then:

$$\frac{\partial H}{\partial \underline{u}} = 0 \quad \ldots..(3.11)$$

$$\therefore \quad \underline{u}^{o} = -G^{-1}B'\underline{\psi} \quad \ldots.(3.12)$$

For G^{-1} to exist, the weighting matrix G must be positive definite (p.d).

For (3.10) and hence (3.12) to be true, (i.e; for the system to be at least locally optimal), the associated Jacobian matrix must be p.d., viz.,

$$\begin{bmatrix} \dfrac{\partial^2 H}{\partial \underline{x}^2} & \dfrac{\partial^2 H}{\partial \underline{x}.\partial \underline{u}} \\ \dfrac{\partial^2 H}{\partial \underline{u}.\partial \underline{x}} & \dfrac{\partial^2 H}{\partial \underline{u}^2} \end{bmatrix} > 0 \quad \ldots(3.13)$$

(3.9) and (3.10) are differentiated appropriately to form the elements of the Jacobian matrix of (3.13) i.e.,

$$\begin{bmatrix} Q & 0 \\ 0 & G \end{bmatrix} > 0 \quad \ldots.(3.14)$$

To ensure that the Jacobian matrix is p.d., it is essential that Q be made at least non-negative definite (n.n.d), (since G is positive definite).

Substituting for $\underline{u}$ in (3.4) using (3.12) yields

$$\dot{\underline{x}} = A\underline{x} - BG^{-1}B'\underline{\psi} \qquad \ldots (3.15)$$

Combining (3.15) and (3.9), gives:

$$\begin{bmatrix} \dot{\underline{x}} \\ \dot{\underline{\psi}} \end{bmatrix} = \begin{bmatrix} A & -BG^{-1}B' \\ -Q & -A' \end{bmatrix} \begin{bmatrix} \underline{x} \\ \underline{\psi} \end{bmatrix} \qquad \ldots (3.16)$$

Since the problem must satisfy the transversality conditions i.e. $\underline{x}(t_\infty) = 0$; $\underline{\psi}(\infty) = 0$, $\underline{\psi}$ is related to $\underline{x}$ by (3.17), viz.,

$$\underline{\psi} = K\underline{x} \qquad \ldots (3.17)$$

where K is the p.d. solution of the algebraic Riccati equation (3.6). Substituting (3.17) into (3.12) yields (3.5). Also, it can be shown that the minimum value of J is given as

$$J = \tfrac{1}{2}\underline{x}'(0)K\underline{x}(0) \qquad \ldots (3.18)$$

where $\underline{x}(0)$ is the initial state vector.

3.2.1.2. The Linear Quadratic Gaussian (LQG) Problem

Explicit account may be taken of the effects of atmospheric turbulence and measurement noise by determining the feedback controller as a solution of the Linear Quadratic Gaussian (LQG) problem.

For the completely controllable and observable*, linear, time-invariant system described by:

$$\dot{\underline{x}} = A\underline{x} + B\underline{u} + G\eta \qquad \ldots (3.19)$$

$$\underline{y}^* = C^*\underline{x} + \epsilon \qquad \ldots (3.20)$$

---

* Complete controllability and observability are properties of the system normally required for obtaining a linear feedback law. These properties are normally required regardless of whether the problem is LQP or LQG. (see Section 3.2.4)

where both η and ϵ are Gaussian, white, zero mean, mutually independent, stationary noise signals, i.e.,

$$\text{cov}\left[\eta(t);\eta(\tau)\right] = \Xi\delta(t-\tau);\ \Xi=\Xi'\geqslant 0 \quad \ldots (3.21)$$

$$\text{cov}\left[\varepsilon(t);\varepsilon(\tau)\right] = \text{Ⓗ}\delta(t-\tau);\ \text{Ⓗ}=\text{Ⓗ}'\geqslant 0 \quad \ldots (3.22)$$

and $\underline{y}^*$ is an output vector comprising elements which have a linear relationship with the elements of the state vector; the LQG problem is to find $\underline{u}(t)$, for all t, such that the cost functional,

$$J_o = \lim_{T\to\infty} \frac{1}{2T}\cdot\int_{-T}^{T} (\underline{x}'Q_o\underline{x} + \underline{u}'G_o\underline{u})dt \quad \ldots (3.23)$$

is minimised, where the weighting matrices Q_o and G_o are such that*,

$$Q_o = Q_o' \geqslant 0 \quad \ldots (3.24)$$

$$G_o = G_o' > 0 \quad \ldots (3.25)$$

It can be shown, (Athans (1971)), that the optimal control is given by:

$$\underline{u}^o = -G_o^{-1}B'K_o\underline{x} = F\underline{x} \quad \ldots (3.26)$$

where K_o is the solution of an algebraic Riccati equation, viz.,

$$K_oA + A'K_o - K_oBG_o^{-1}B'K_o + Q_o = 0 \quad \ldots (3.27)$$

It is seen that the control law (3.26) will be the same as that obtained for the LQP (see Equation 3.5), provided that the associated weighting matrices are chosen to be the same. However, in this case it is assumed that the state vector $\underline{x}$, which from (3.19) can be seen to be affected by η, is not [available for feed-

---

* The matrices Q_o and G_o are usually assumed to be diagonal. Since weighting values are chosen empirically, such an assumption facilitates the assessment of each particular choice of weighting values.

back; rather, a Kalman-Bucy filter‡ driven by the output, $\underline{y}^*$, and the control, $\underline{u}$, are used to form an estimate, $\hat{\underline{x}}$, on-line and this estimate is then used to implement the feedback control. The expression for the Kalman-Bucy filter is

$$\dot{\hat{\underline{x}}} = A\hat{\underline{x}} + B\underline{u} + H[\underline{y}-C\hat{\underline{x}}] \qquad \ldots(3.28)$$

where,

$$H = \bar{K}C' \Theta^{-1} \qquad \ldots(3.29)$$

and where, $\bar{K}$ satisfies an algebraic Riccati equation associated with the filter, viz.,

$$\bar{K}A + A'\bar{K} - \bar{K}C'H^{-1}C\bar{K} + \Xi = 0 \qquad \ldots(3.30)$$

If a filter can be designed so that the estimate, $\hat{\underline{x}}$, is always very close to the actual state, $\underline{x}$, then (3.26) is the same as (3.31), viz,

$$\underline{u}^o = F\hat{\underline{x}} \qquad \ldots(3.31)$$

Substituting (3.27) into (3.28), yields

$$\dot{\hat{\underline{x}}} = [A + BF - HC]\hat{\underline{x}} + H\underline{y}^* \qquad \ldots(3.32)$$

In block diagram form, the controlled aircraft with Kalman-Bucy filter incorporated is as shown in figure 3.1+.

A Kalman filter is in practice difficult to synthesise because of its dimensionality. However, if no account is to be taken of noise, a Luenberger observer of reduced dimension (which may also be regarded as a form of filter), may be used in place of the Kalman filter. The principal advantage of these filters is that they may be designed to be driven only by those signals which can be easily measured

‡ The equations associated with such a filter have been derived by Kalman and Bucy (1961).

+ The control, $\underline{u}$, has been taken into account implicitly in (3.32) by means of (3.31).

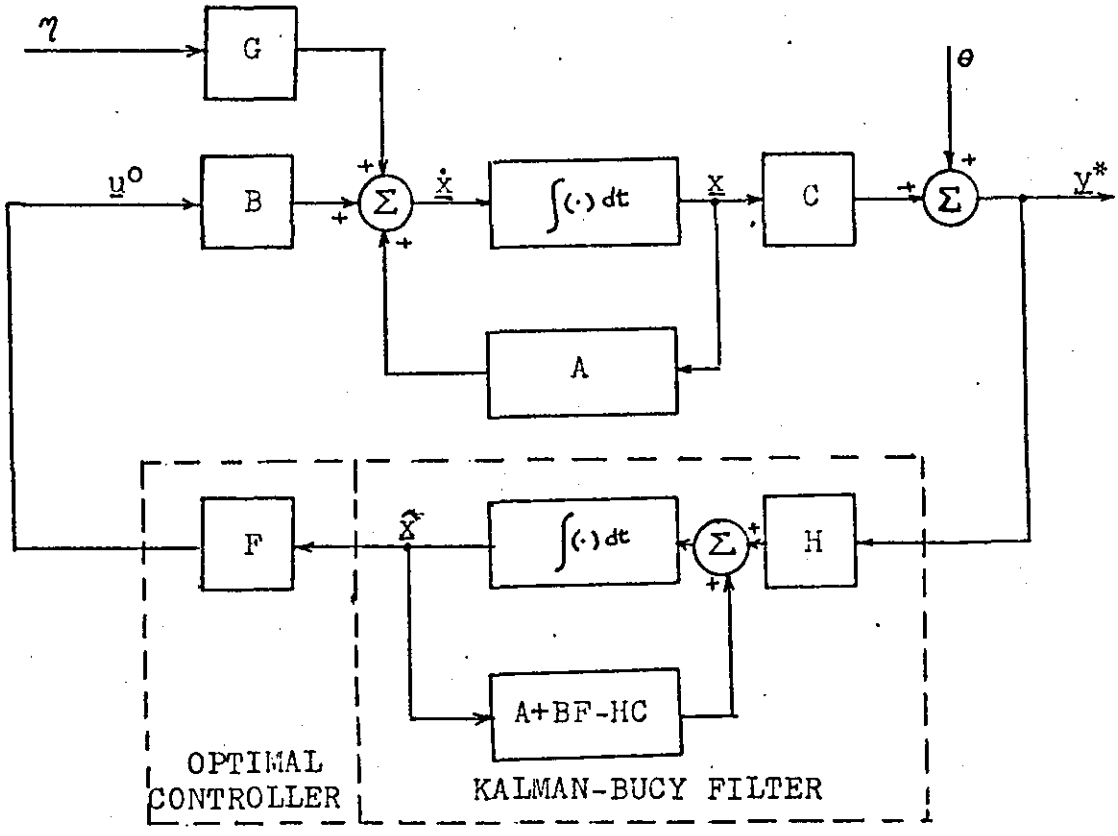


Figure 3.1 Controlled Aircraft with Kalman Filter Incorporated.

and will have as their output an estimate of the full state of the system. It is considered that since the optimal feedback control obtained will be the same whatever the approach, if full state feedback were to be employed and a Kalman filter was not implemented, the worst that would be likely to occur is that some decrease in the performance cost will result. With strong feedback control, the performance degradation is not likely to be great. However, because it was realised from the onset in this research investigation that it would not be possible practically to implement

full state variable feedback (FSVF), two approaches to the problem have been considered:

(a) use of reduced-order control

and (b) use of observers; in particular, reduced-order observers, to see whether it is possible to recoup some of the advantages of full state feedback control.

The assessment of (a) and (b) are reported upon in detail in subsequent chapters.

3.2.2 Specific Problem Statement - Optimal Output Regulator

Since the primary aim of the research was to determine some means of alleviating the structural loads on the wing of the subject aircraft by the use of active control, it was decided to include those variables associated with bending and torsional moments into the performance index (p.i.) Thus the problem was cast as an optimal output regulator and and the chosen performance index, J, was

$$J = \tfrac{1}{2}\int_0^\infty (\underline{y}'Q\underline{y} + \underline{u}'G\underline{u})\,dt \qquad \ldots(3.33)$$

The Hamiltonian, H, is expressed as:

$$H = \tfrac{1}{2}(\underline{y}'Q\underline{y} + \underline{u}'G\underline{u}) + \underline{\psi}'(A\underline{x} + B\underline{u})$$

$$= \tfrac{1}{2}[(C\underline{x} + E\underline{u})'(C\underline{x}+E\underline{u})+\underline{u}'G\underline{u}] + \underline{\psi}'(A\underline{x} + B\underline{u}) \ldots(3.34)$$

For H to be minimised w.r.t $\underline{u}$, (hence J), then:

$$\frac{\partial H}{\partial \underline{u}} = E'QC\underline{x} + (G + E'QE)\underline{u}^o + B'\underline{\psi} = 0 \qquad \ldots(3.35)$$

$$\therefore \quad \underline{u}^o = -(G + E'.QE)^{-1}[E'QC\,\underline{x} + B'\underline{\psi}] \qquad \ldots(3.36)$$

Also,

$$\frac{\partial H}{\partial \underline{x}} \triangleq -\dot{\underline{\psi}} = C'QC\underline{x} + C'QE\underline{u} + A'\underline{\psi} \qquad \ldots(3.37)$$

Substituting for $\underline{u}$ in (3.4) and 3.37) using (3.36), yields the canonical equation of the optimal system, viz.,

$$\begin{bmatrix}\dot{\underline{x}}\\ \dot{\underline{\psi}}\end{bmatrix} = \left[\begin{array}{c|c} A-B(G+E'QE)^{-1}E'QC & -B(G+E'QE)^{-1}B' \\ \hline -C'[Q-QE(G+E'QE)^{-1}E'Q]C & -[A-B(G+E'QE)^{-1}E'QC]' \end{array}\right]\begin{bmatrix}\underline{x}\\ \underline{\psi}\end{bmatrix} \qquad \ldots.(3.38)$$

or,

$$\dot{\underline{z}} = M\underline{z} \qquad \ldots(3.39)$$

where

$$\underline{z} \triangleq \begin{bmatrix}\underline{x}\\ \underline{\psi}\end{bmatrix} \qquad \ldots(3.40)$$

and M is the system matrix of (3.38) of order 2n x 2n. The optimal solution is obtained from the solution of (3.38) with the known boundary conditions $\underline{x}(t_0) = 0$ and $\underline{\psi}(\infty) = 0$. An explicit solution of (3.38) may be obtained in the form of two single-point boundary-value problems using eigen-analysis. As in (3.17), $\underline{\psi}$ is found to be related to $\underline{x}$ by the equation:

$$\underline{\psi} = \hat{K}\underline{x} \qquad \ldots(3.41)$$

where $\hat{K}$ is the p.d. solution of an algebraic Riccati equation, viz.,

$$\hat{K}\hat{A} + \hat{A}'\hat{K} - \hat{K}B\hat{G}^{-1}B'\hat{K} + \hat{Q} = 0 \qquad \ldots(3.42)$$

and where,

$$\hat{A} = A - B\hat{G}^{-1}E'QC \qquad \ldots(3.43)$$

$$\hat{G} = G + E'QE \qquad \ldots(3.44)$$

$$\hat{Q} = C'[Q - QE\hat{G}^{-1}E'Q]C \qquad \ldots(3.45)$$

3.2.3 Numerical Solution of the Optimal Control Laws

The time response associated with (3.38) may be defined in terms of the eigenvalues and the eigenvector components of the matrix M, viz., (Marshall and Nicholson (1970)): If U is the modal matrix made up of columns of eigenvectors and if Λ is a diagonal matrix made up of the elements,* $\lambda_1, \lambda_2, \lambda_3, \ldots\ldots\lambda_{2n}$,

---

*Assuming that the eigenvalues, λ_i, of the system are distinct.

then,

$$\underline{z}(t) = Ue^{\Lambda\tau}U^{-1}\underline{z}(t_o) \qquad \ldots (3.46)$$

where,

$$\tau = t_f - t_o \qquad \ldots (3.47)$$

Also,

$$MU = U\Lambda \qquad \ldots (3.48)$$

M consists of convergent and divergent mode pairs with eigenvalues, equal in magnitude but opposite in sign. Partitioning Λ into two sets of eigenvalues, with $\Lambda_1=[\lambda_i]$, $i = 1,2,\ldots\ldots n$ consisting of negative real parts and $\Lambda_2 = [\lambda_j]$, $j = 1,2,\ldots\ldots n$ consisting of positive real parts. Similarly partitioning (3.46) yields:

$$\begin{bmatrix}\underline{x}(t)\\ \underline{\psi}(t)\end{bmatrix} = \begin{bmatrix}U_{11} & U_{12}\\ U_{21} & U_{22}\end{bmatrix}\begin{bmatrix}e^{\Lambda_1\tau} & 0\\ 0 & e^{\Lambda_2\tau}\end{bmatrix}\begin{bmatrix}V_{11} & V_{12}\\ V_{21} & V_{22}\end{bmatrix}\begin{bmatrix}\underline{x}(t_o)\\ \underline{\psi}(t_o)\end{bmatrix} \qquad \ldots (3.49)$$

where,

$$VU = I \qquad \ldots (3.50)$$

From (3.49)

$$\underline{x}(t) = U_{11}e^{\Lambda_1\tau}[V_{11}\underline{x}(t_o)+V_{12}\underline{\psi}(t_o)]+ U_{12}e^{\Lambda_2\tau}[V_{21}\underline{x}(t_o)+V_{22}\underline{\psi}(t_o)] \qquad \ldots (3.51)$$

The divergent modes corresponding to the unstable roots must be eliminated in order to satisfy conditions of [asymptotic stability, viz.,

$$\underline{\psi}(t_o) = -V_{22}^{-1}\ V_{21}\ \underline{x}\ (t_o) \qquad \ldots (3.52)$$

or, using (3.50),

$$\underline{\psi}(t_o) = U_{21}\ U_{11}^{-1}\ \underline{x}(t_o) \qquad \ldots (3.53)$$

$$\therefore\ \underline{x}(t) = U_{11}e^{\Lambda_1\tau}(V_{11}-V_{12}V_{22}^{-1}V_{21})\underline{x}(t_o)$$
$$= U_{11}e^{\Lambda_1\tau}U_{11}^{-1}\underline{x}(t_o) \qquad \ldots (3.54)$$

Similarly from (3.49),

$$\underline{\varphi}(t) = U_{21} e^{\Lambda_1 \tau} U_{11}^{-1} \underline{x}(t_o)$$

$$= U_{21} U_{11}^{-1} \underline{x}(t) \qquad \ldots(3.55)$$

By substituting for $\underline{\varphi}$ in (3.36), using (3.55), the required control law applying for all time, t, was obtained. The method outlined is by far the fastest* and was used in the program, OUTREG (Appendix IV). For inversion of the U_{11} sub-matrix of the modal matrix, U, the method of Lanczos (1957) was used, Although simple to program, the method of Lanczos required that the real and imaginary n x n matrices associated with U_{11} to be used to form a 2n x 2n matrix for inversion. The approach did pose some computational difficulty when the program OUTREG was run for the model, BACH. Consequently it was decided to break the program into a two-pass one and these programs were then run on a CDC 7600 computer at the Regional Computing Centre of the University of Manchester All the computations of the feedback law associated with the low order models were completed on an ICL 1904S computer and subsequently a PRIME 400 at Loughborough University of Technology.

As regards the choice of suitable weights for the matrices Q and G, (which were chosen to be diagonal) in the performance index (3.33), no specific technique other than a method of trial and error was employed. A number of methods to assist in the

---

* Golub et al (1979) have published an algorithm which is reputed to be faster (30%-70% is claimed by the authors); however, the approach still requires eigenvector methods (involving the Schur vector), and transformation techniques.

choice of Q and G have been proposed (Bryson and Ho (1969) Harvey and Stein (1979)). The method proposed by Bryson and Ho suggests that the matrices Q and G be diagonal. Each diagonal element of Q and G is determined from the expressions:

$$q_i = \frac{1}{n\tau}\left[\frac{1}{x_i^2}\right]_{max} \quad \ldots (3.56)$$

$$g_j = \frac{1}{m\tau}\left[\frac{1}{u_j^2}\right]_{max} \quad \ldots (3.57)$$

where,

n is the dimension of the state vector

m is the dimension of the control vector

τ is the interval over which the time response is to be obtained

$x_{i_{max}}$ is the maximum possible value attained by the ith state variable

$u_{j_{max}}$ is the maximum possible value attained by the jth control vector.

The method allows initial values of q_i and g_j to be easily determined and is helpful in situations where particular difficulty is experienced in selecting a set of weighting values. However, in the research study, it was found that weighting values selected in this way did not have any special relationship with the performance of any feedback law derived. In addition, the method proposed by Harvey and Stein was not considered since it appears that a restriction must be placed on the dimension of the output vector to that of the control vector. It was found that in all cases studied, empirical selection of the weighting values for the Q and G matrices proved to be adequate.

3.2.4 Controllability and Stabilisability Requirements.

Often in this research, the closed-loop behaviour of the aircraft was assessed using reduced order feedback control. The concepts of complete state controllability and stabilisability of the aircraft were found to be important considerations whenever a new feedback law was to be evaluated and tested.

It was shown by Larson and Dressler, (1968), that complete state controllability is only a sufficient but not a necessary condition for closed-loop system stability. If the original state description of the aircraft was itself stable, then this alone was a necessary and sufficient condition for obtaining a feedback law which would guarantee the stability of the closed-loop system. In a number of cases in this study, it was found that some of the mathematical models of the aircraft which were used, were not completely state controllable. This fact then required that additional tests be made to determine whether the aircraft was at least stabilisable. The dynamic stability of the uncontrolled aircraft is most easily checked by observing the signs of the eigenvalues of the coefficient matrix of the state equation, i.e. matrix A of,

$$\dot{\underline{x}} = A\underline{x} + B\underline{u} \qquad ..(3.4)$$

The concept of complete controllability is due mainly to Kalman (1960). By complete controllability is meant, that property of a system which will allow the system to be transferred from any given state to another state in a

finite time. (3.4) is completely controllable if the controllability matrix, X, given as:

$$X = (B,\ AB,\ A^2B\ \ldots.A^{n-1}B) \qquad ..(3.58)$$

spans the n-dimensional space, i.e.

$$\text{rank}\ (X) = n \qquad ..(3.59)$$

A simple check for controllability may be achieved by means of a state transformation (De Russo et al (1966)), of (3.4) into a canonical form. The most convenient transformation is the matrix of eigenvectors ~~columns~~ of A. Thus using the transformation:

$$T\underline{x}' = \underline{x} \qquad ..(3.60)$$

(3.4) is then written in the form:

$$\dot{\underline{x}}' = T^{-1}AT\,\underline{x}' + T^{-1}B\underline{u} \qquad ..(3.61)$$

Provided that the eigenvalues of A are distinct, $(T^{-1}AT)$ is a diagonal matrix. Thus (3.61) represents a decoupled form of (3.4). It can be easily shown that for (3.4) to be completely controllable, the rows of $(T^{-1}B)$ of (3.61) must all contain non-zero elements. This check was used in the computer program CONOBS (see Appendix IV).

3.3 A SCHEME TO EVALUATE THE MODEL'S PERFORMANCE IN SIMULATED ATMOSPHERIC TURBULENCE

In this section, a method for assessing a particular SLACS scheme when the aircraft is subjected to atmospheric turbulence, is outlined. In particular, a method for evaluating the r.m.s. values of bending and torsional moments experienced at each wing station of the aircraft, for light turbulence* is described. The method is due to Swaim et al (1977), and is presented below.

The state equation given as (3.19) is repeated here for convenience, i.e.,

$$\dot{\underline{x}} = A\underline{x} + B\underline{u} + G\eta \qquad \ldots (3.19)$$

A linear control law may be derived by the method outlined in section 3.2.3 and given as (3.26), i.e.,

$$\underline{u}^{o} = F\underline{x} \qquad \ldots (3.26)$$

Substituting for $\underline{u}$ in (3.19) using (3.26), the equation representing the controlled aircraft results, viz.,

$$\dot{\underline{x}} = (A+BF)\underline{x} + G\eta \qquad \ldots (3.62)$$

or,

$$\dot{\underline{x}} = \hat{A}\underline{x} + G\eta \qquad \ldots (3.63)$$

where,

$$\hat{A} \triangleq (A+BF) \qquad \ldots (3.64)$$

---

* To allow comparison with dynamic response tests, described in Section 4.1, a vertical gust having an r.m.s. intensity of about 1.0m/s. was assumed throughout the research. This was considered adequate for the purposes of tests since only percentage reductions in bending and torsional loads were of interest.

The output equation given as (2.9), is:

$$\underline{y} = C\underline{x} + E\underline{u} \qquad \ldots (3.65)$$

Again substituting for $\underline{u}$ in (3.65) using (3.26), yields:

$$\underline{y} = (C+EF)\underline{x} \qquad \ldots (3.66)$$

or,

$$\underline{y} = \hat{C}\underline{x} \qquad \ldots (3.67)$$

where,

$$\hat{C} \triangleq (C+EF) \qquad \ldots (3.68)$$

The mean squared value of $\underline{y}$, which is the expected value of $\underline{y}^2$, is:

$$\xi[\underline{y}^2] = \xi[(\hat{C}\underline{x})(\hat{C}\underline{x})'] \qquad \ldots (3.69)$$

or,

$$\xi[\underline{y}^2] = \hat{C}\xi[\underline{x}.\underline{x}']\hat{C}' \qquad \ldots (3.70)$$

where, $\xi(\cdot)$ is the expectation operator. $\xi[\underline{x}.\underline{x}']$ is the covariance matrix and can be obtained in the following way:

Post-multiplying (3.63) by $\underline{x}'$ and taking the expected value, yields:

$$\xi[\dot{\underline{x}}.\underline{x}'] = \hat{A}\xi[\underline{x}.\underline{x}'] + G\xi[\eta.\underline{x}'] \qquad \ldots (3.71)$$

Transposing (3.63) throughout, pre-multiplying by, $\underline{x}$, and then taking the expected value, yields:

$$\xi[\underline{x}.\dot{\underline{x}}'] = \xi[\underline{x}.\underline{x}']\hat{A}' + \xi[\underline{x}.\eta]G' \qquad \ldots (3.72)$$

For a linear system of state vector, $\underline{x}$, driven by zero mean, unit Gaussian white noise, the correlation between $\underline{x}$ and η is (Swaim et al (1977), Bryson and Ho (1969)):

$$\xi[x.\eta] = \frac{G}{2} \qquad \ldots (3.73)$$

Substituting (3.73) into (3.71) and (3.72) and adding the resulting equation yields:

$$\xi[\dot{x}.x'] + \xi[x.\dot{x}'] = \hat{A}\,\xi[x.x'] + \xi[x.x']\,\hat{A} + GG' \qquad \ldots (3.74)$$

For the covariance matrix $\xi[x.x']$ to be time-varying requires that the statistical properties of the state vector, x, vary with time. But since the noise source is, η, (white noise) and of zero mean, then:

$$\frac{d}{dt}\{\xi[x.x']\} = 0 = \xi[\dot{x}.x'] + \xi[x.\dot{x}'] \qquad \ldots (3.75)$$

Thus, (3.74) becomes:

$$\hat{A}\,\xi[x.x'] + \xi[x.x']\,\hat{A}' + GG' = 0 \qquad \ldots (3.76)$$

By solving for the covariance matrix in (3.76), and then substituting the result into (3.70), the r.m.s. values of the variables which constitute the output vector, y, was obtained.

(3.76) is of the form,

$$\hat{A}\tilde{X} + \tilde{X}\hat{A}' = -\hat{Q} \qquad \ldots (3.77)$$

where,

$$\tilde{X} \triangleq \xi[x.x'] \qquad \ldots (3.78)$$

$$\hat{Q} \triangleq GG' \qquad \ldots (3.79)$$

Let,

$$\tilde{A} = \hat{A}' \qquad \ldots (3.80)$$

Substituting for $\hat{A}$ in (3.77) using (3.80), yields:

$$\tilde{A}'\tilde{X} + \tilde{X}\tilde{A} = -\hat{Q} \qquad \ldots (3.81)$$

(3.81) is in the form of a Lyapunov equation and is a degenerate case of an algebraic matrix Riccati equation. The equation may be solved using the method of Golub et al (1979), or of Marshall and Nicholson (1970). The latter method is simple to program and was used in the computer program COVRNC (Appendix IV). The results of the tests carried out are presented in section 4.5.

CHAPTER 4: ASSESSMENT OF VARIOUS SLACS SCHEMES.

4.1. Introduction.

The computer programs OUTREG and RESPON (Appendix IV) were used extensively in order to carry out tests on the mathematical models discussed in Chapter 2. The control laws obtained using OUTREG were tested using both simulated deterministic and simulated turbulent situations. In this research study, a number of artificial test situations were used for assessing and comparing various SLACS schemes. Table 4.1 shows the test situations employed for the deterministic cases studied, while in Table 4.2 are shown those test situations employed for simulation in atmospheric turbulence. For the simulation of vertical gust, which was the only component of the gust required in the tests, a Dryden filter was used with zero mean white noise as its input. The simulated gust signal which was the output of the Dryden filter also had the property of zero mean and was of an intensity which depended upon the amplitude of the noise input.* Test cases D and E allowed a qualitative assessment to be made of a number of SLACS schemes. A quantitative assessment was also made using the computer program COVRNC, (Appendix IV) to evaluate the r.m.s bending and torsional levels achieved in the wing of the subject aircraft. These results are discussed in Section 4.6.

---

* The amplitude of the noise input was adjusted until the evaluated r.m.s intensity of the gust field was approximately 1.0m/s.

CASE	SITUATION		
	Initial State	Commanded Control Surface Deflection (rad.)	
		Aileron δ_{A_c}	Inboard Elevator $\delta_{E_{i_c}}$
A	w=~~7.15 m/s~~ 281.5 All other states set to zero.	0.0	0.0
B	All states set to zero.	0.025	0.0
C	All states set to zero.	0.01	0.01

Table 4.1 : Test situations employed for deterministic case.

CASE	SITUATION		
	Initial state	Forcing Terms*	Standard Deviation of vertical Gust Velocity (w_g) (m/s)
D	All states set to zero	None	1.0+
E	w = ~~7.15 m/s~~ 281.5 All other states set to zero.	None	1.0

See page 36

Table 4.2 : Test Situations employed for atmospheric turbulence.

???

* No commanded control surface deflections were used.

\+ These values correspond to light turbulence.

4.2 Derivation of Optimal Control Laws.

The model, ARNE, proved too large to be handled by any computer available to the author, even when the computer program, OUTREG, (Appendix 1V) was broken into a two-pass one. The main difficulty always arose when it was necessary to invert the n/xn matrix partition of eigenvector columns (which often had complex elements) of the modal matrix associated with the optimal canonical matrix (see Eqn 3.49). Complex inversion by the method of Lanczos (1957), was used which involved the formation and inversion of a 2n x 2n matrix. This matrix in the case of ARNE was of dimension 158 x 158.

Feedback laws associated with the model BACH were found by using the 'two-pass' version of the OUTREG program on a CDC 7600 computer at the University of Manchester Regional Computer Centre (UMRCC). For the lower order models, no further difficulty was experienced and it was possible to make all the required runs on an ICL 1904S computer at Loughborough University of Technology Computer Centre (LUTCC). It is possible that the recent report by Laub (1979) using the Shur method for solving the A.RE may remove most of the numerical difficulties previously experienced.

4.2.1 Selection of Weighting Matrices.

A number of trial runs of the program, OUTREG, were made for the model CLEMENTI in order to establish a suitable weighting scheme for the output vector weighting matrix, Q, and the

control vector weighting matrix, G. Although a number of methods are available to assist in the choice of Q and G (Bryson and Ho (1969), Harvey and Stein (1979)), none of these methods could be relied upon to give adequate results. A typical set of weighting values found to be suitable for the model BACH, is given as (4.1) and (4.2), viz.,

$$Q = \text{diag.}\begin{Bmatrix} 10^{-4} & 10^{-4} & 10^{-4} & 10^{-4} & 10^{-4} & 10^{-4} & 10^{-4} & 10^{-4} & 10^{-4} & 10^{-4} \\ 10^{-5} & 10^{-5} & 10^{-5} & 10^{-5} & 10^{-5} & 10^{-5} & 10^{-5} & 10^{-5} & 10^{-5} & 10^{-5} \\ .1 & .1 & .1 & .1 & .1 & .1 & .1 & .1 & .1 & .1 \\ .1 & .1 & .1 & .1 & .1 & .1 & .1 & .1 & .1 & .1 \\ .1 & .1 & .1 & .1 & .1 & .1 & .1 & .1 & .1 & .1 \\ 1 & 1 & 10 & 10 & 10 & .5 & & & & \end{Bmatrix} \quad (4.1)$$

$$G = \text{diag.}\ (\ .01 \quad .01\ ) \qquad \ldots \quad (4.2)$$

The resulting optimal control gain matrix, F, (Equation (3.26)), was determined to be:

$$F = \begin{bmatrix} -3.07E\text{-}2 & -6.582E\text{-}2 & 5.178E\text{-}2 & 5.035E\text{-}3 & 1.472E\text{-}1 & -9.786E\text{-}2 \\ -6.111E\text{-}2 & 1.867E\text{-}1 & 2.007E\text{-}2 & -1.948E\text{-}3 & 3.370E\text{-}2 & 1.463E\text{-}3 \\ 8.248E\text{-}3 & -3.506E\text{-}2 & 2.855E\text{-}3 & 4.161E\text{-}3 & -1.172E+0 & -1.898E\text{-}1 \\ 9.101E\text{-}2 & 9.646E\text{-}1 & -1.317E+0 & -3.263E\text{-}2 & 7.996E\text{-}1 & 8.725E\text{-}1 \\ -6.218E\text{-}1 & -2.142E\text{-}1 & -1.252E\text{-}3 & 1.960E\text{-}1 & -2.316E\text{-}1 & -5.585E\text{-}1 \\ -1.974E+0 & -4.484E+0 & -2.987E+1 & -1.370E+1 & -1.827E+0 & 2.672E\text{-}2 \\ -1.874E\text{-}1 & 7.729E\text{-}2 & 1.579E\text{-}2 & -1.604E\text{-}1 & -2.857E\text{-}3 & -1.949E\text{-}1 \\ \\ -7.001E\text{-}2 & 4.250E\text{-}2 & 7.523E\text{-}2 & 2.213E\text{-}2 & 5.773E\text{-}2 & 3.019E\text{-}1 \\ -1.823E\text{-}1 & 2.239E\text{-}1 & 3.239E\text{-}2 & 6.729E\text{-}1 & 2.790E\text{-}1 & 1.022E\text{-}1 \\ 1.460E\text{-}1 & 8.010E\text{-}2 & -4.846E\text{-}1 & -8.017E\text{-}1 & -5.637E+0 & 9.564E\text{-}1 \\ -8.617E\text{-}1 & 3.152E\text{-}1 & -4.300E+0 & 3.470E+0 & -6.046E+0 & -1.270E+1 \\ -2.459E+1 & -2.604E+1 & 1.055E+1 & 1.053E+1 & 1.543E+1 & -2.849E+1 \\ -4.637E+1 & -3.957E+1 & -1.084E+2 & -3.907E+2 & -2.909E+1 & 1.799E\text{-}1 \\ -9.764E\text{-}1 & -1.244E+0 & -5.769E\text{-}3 & -1.895E\text{-}1 & 2.971E\text{-}1 & 6.700E\text{-}1 \end{bmatrix}$$

... (4.3)

Since the model CLEMENTI had an output vector similar to that of BACH except only that the upper nine bending mode variables were omitted, the weighting scheme adopted for CLEMENTI was similar to that given as (4.1) and (4.2). Thus for CLEMENTI:

$$Q = \text{diag}\ \{10^{-4},\ 10^{-4},\ 10^{-4},\ 10^{-4},\ 10^{-4},\ 10^{-4},\ 10^{-4},10^{-4},10^{-4},10^{-}$$
$$10^{-5},\ 10^{-5},\ 1-^{-5},\ 10^{-5},\ 10^{-5},\ 10^{-5},\ 10^{-5},10^{-5},10^{-5},10^{-}$$
$$.1 \quad .1 \quad .1 \quad .1 \quad .1 \quad .1 \quad .1 \quad .1 \quad .1 \quad .1 \quad .1$$
$$1, \quad 1, \quad 10, \quad 10, \quad 10, \quad .5\}$$

..(4.4)

$$G = \text{diag}\ \{.01,\ .01\} \qquad \ldots (4.5)$$

The resulting optimal control was determined to be:

$$u^{o} = \begin{bmatrix} -.015 & -.0066 & .026 & .021 & .141 & -.196 & -.019 & .12 & .019 & -.078 \\ .005 & .714 & -1.079 & 3.724 & -19.434 & -12.846 & -2.904 & .022 & -.1 & \\ -.063 & .003 & -.032 & .0072 & -.032 & & & & & \\ -.037 & .158 & -.434 & .109 & 1.289 & -.877 & -.512 & 1.312 & -.473 & \\ .202 & .306 & -3.864 & .425 & .602 & -97.373 & -378.7 & -67.869 & .347 & \\ .058 & -1.789 & -.0011 & .114 & .239 & .162 & & & & \end{bmatrix}$$

.. (4.6)

The effectiveness of control laws such as (4.6) were carried out initially by inspection of the eigenvalues of the closed loop system and then by making appropriate response checks under the test conditions specified in Tables 4.1 and 4.2. If it was found that a particular control law derived did not produce a desired effect on the controlled aircraft then the appropriate elements of the weighting matrices Q and G were made heavier (or 'lighter', as the case may be) and the program, OUTREG re-run to produce a new law.

4.3. Eigenvalue Analysis.

Eigenvalue analysis was carried out primarily to determine the extent to which damping of the structural bending modes had been augmented by the use of a particular SLACS scheme. The assessment was made by comparing with the eigenvalues of the controlled aircraft.

From Table 4.3., it may be seen that, for the uncontrolled aircraft, all bending modes were only very lightly damped where in every case, $\zeta \leq 0.1$. Also, it should be noted that the frequency of the short period mode was only separated from the frequency of the first bending mode by a factor of four. For the controlled aircraft however, this frequency separation has been increased by a factor of eight. Such frequency separation has the desirable effect of reducing the possibility of frequency coupling between the rigid body motion and any of the flexural modes. With close coupling at these frequencies, it may not be possible to generate sufficient controlling action to reduce the amplitude of the attending motion.

It can also be seen that the short period frequency of the rigid body motion has been slightly reduced in the case of the controlled aircraft although the damping ratio has remained unchanged. Thus, there has been little change to the handling qualities of the basic uncontrolled aircraft.

For the controlled aircraft, the damping ratios of bending modes 1,3,5 and 6 were increased as were the frequencies of

	UNCONTROLLED AIRCRAFT	CONTROLLED AIRCRAFT
Short Period Mode	-.877 + j 1.27	-.73 + j 1.07
Bending Mode 1	-.51 + j 5.46	-3.93 + j 8.49
" " 2	-.23 + j 11.12	-.23 + j 11.15
" " 3	-.58 + j 13.79	-2.1 + j 15.1
" " 4	-.6 + j 15.59	-.36 + j 17.62
" " 5	-.43 + j 17.48	-2.25 + j 18.94
" " 6	-.62 + j 18.78	-35.43 + j 23.99
Inboard Elevator Servo	-7.5	-2869.0
Outboard Elevator Servo	-7.5	-7.5
Aileron Servo	-6.0	-6.68
Küssner Dynamics	-0.2	-0.2
" "	-0.3	-0.3
" "	-8.55	-8.55
" "	-10.98	-10.98
" "	-22.19	-22.19
" "	-5.1 + j 3.6	-5.1 + j 3.6

Table 4.3: EIGENVALUES OF MODEL CLEMENTI WITHOUT AND WITH FEEDBACK CONTROL.

modes 1.3.4.5 and 6. The damping ratio of mode 4 was halved from 0.04 to 0.02. However the frequencies associated with all bending modes are relatively well spaced. It should also be noticed that the dynamic characteristics associated with mode 2 ~~has~~ have remained unchanged by the use of feedback control. It was pointed out by Harvey and Pope (1977), that mode 2 was uncontrollable and this gave cause for some concern in the research study. Also, it may be seen from Table 4.3. that the Küssner dynamics also have remained unaffected under the action of feedback control. A check for state controllability using the program CONOBS (Appendix IV), showed that mode 2 was controllable although those states associated with the Küssner dynamics and the servo-actuator dynamics connected with the outboard sections of the elevator were not controllable. These phenomena are discussed further in Section 4.4.3a under the heading of controllability and stabilisability.

4.4. Responses.

4.4.1 Response of the Uncontrolled Aircraft to Deterministic Commands

A number of evaluations were first carried out on the mathematical models of the uncontrolled aircraft. In Figure 4.1a. is shown the response of one of the rigid body motion variables (vertical velocity, w) when the models BACH and CLEMENTI were subjected to a case A test situation. It is seen that there is little significant difference between the responses of these two models. There also appears to be little noticeable difference in the plots of wing-root bending moment (WRBM) as can be seen from Figure 4.1b.

Figures 4.2 and 4.3 show the corresponding responses for the case B and case C test situations respectively. All the responses indicate that there is little significant difference between the models BACH and CLEMENTI. However, in the case C test situation, although the transient responses are identical, it is seen that there is a small but finite steady-state error in the responses produced by the two models. Since this research was aimed at obtaining substantial reductions in bending and torsional loads in the wing of the aircraft, it was considered that these small steady-state differences would not greatly influence the accuracy of the end result . In the later stages of the research, a method was devised whereby the value of the steady-state bending and torsional moments could be easily evaluated provided that the magnitude of the command vector and the aircraft dynamics were known. The method used

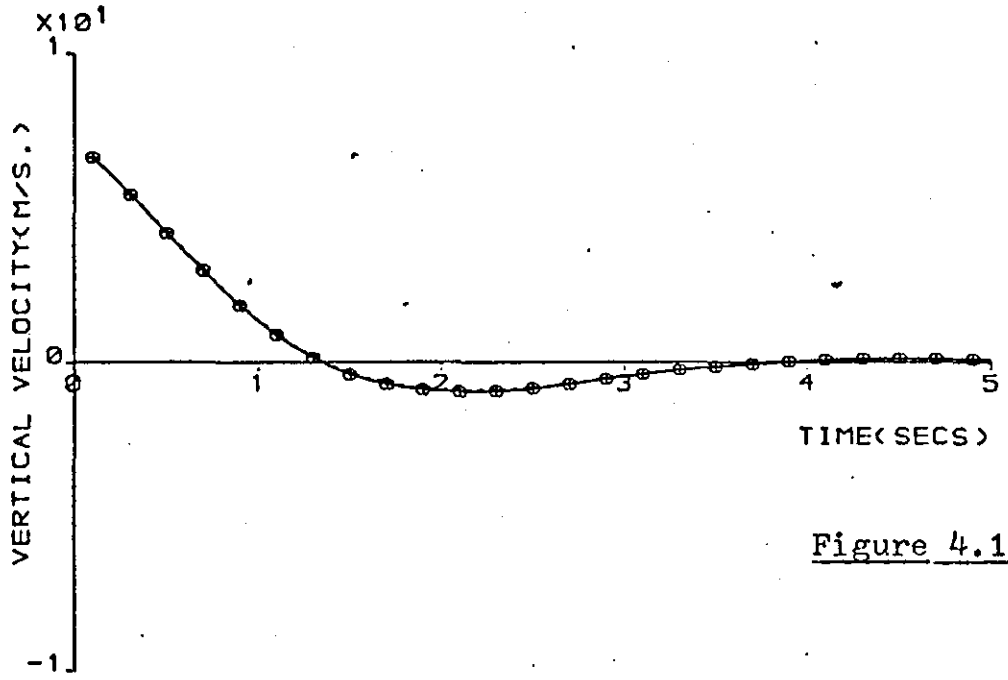


Figure 4.1a

+ UNC. RESPONSE :MODEL CLEMENTI : :CASE A
o UNC. RESPONSE :MODEL BACH : :CASE A

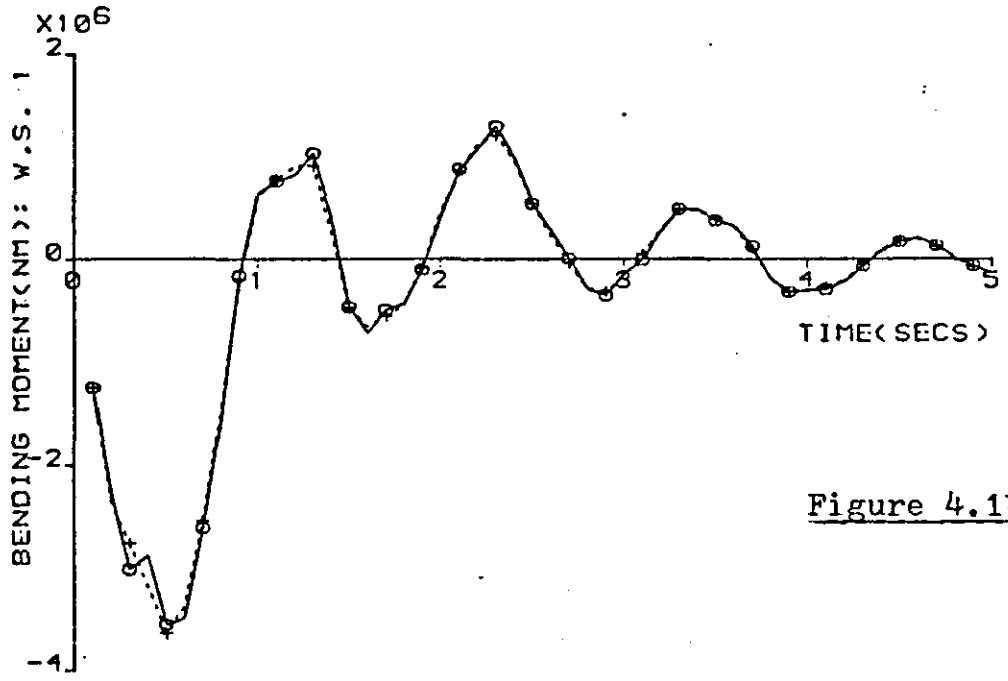


Figure 4.1b

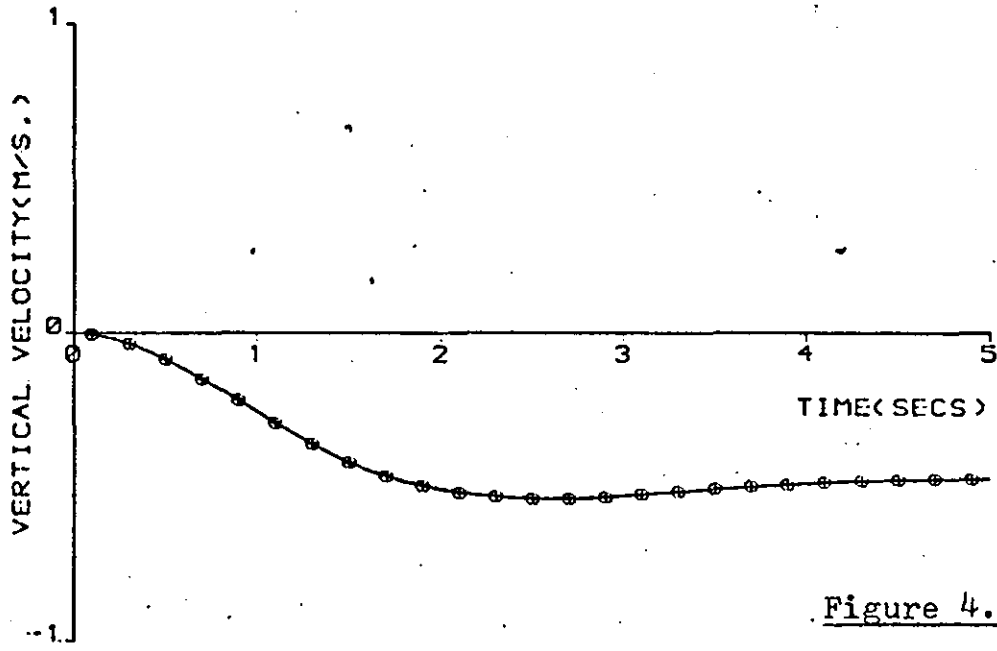


Figure 4.2a

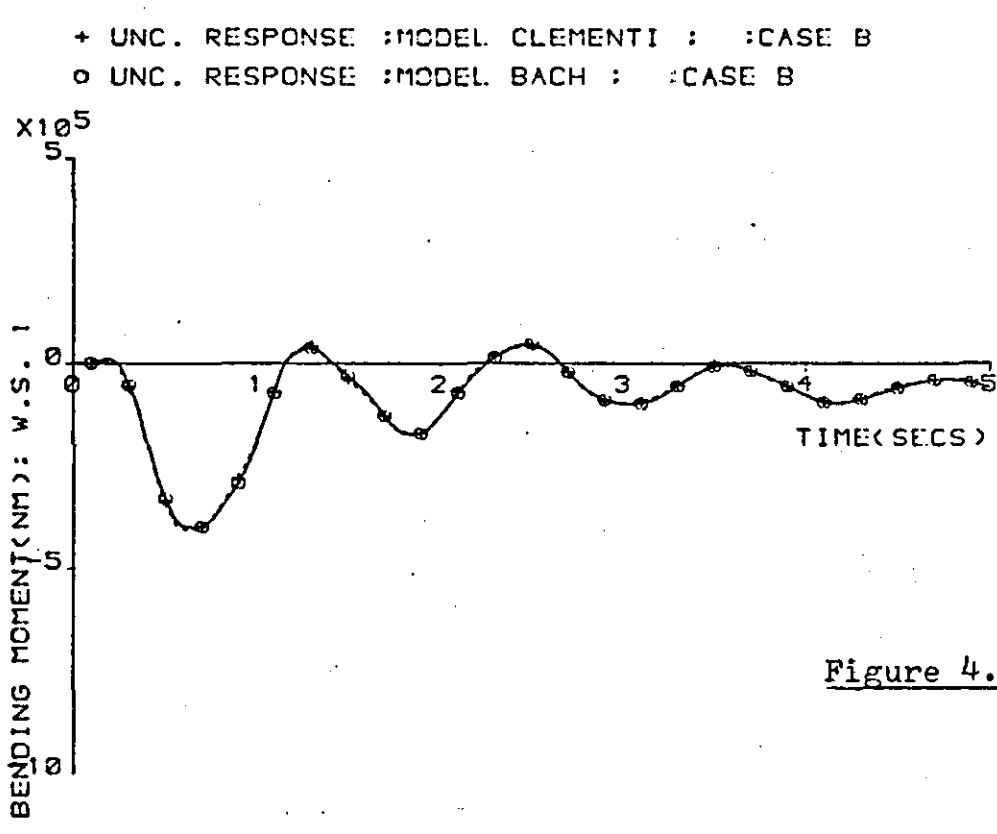


Figure 4.2b

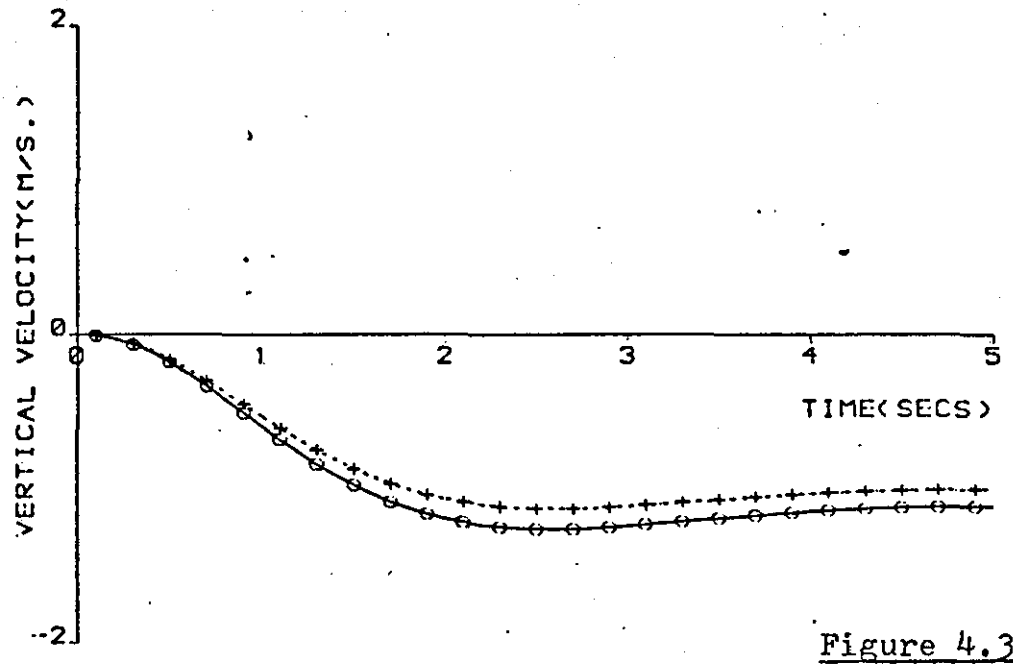


Figure 4.3a

+ UNC. RESPONSE :MODEL CLEMENTI : :CASE C
o UNC. RESPONSE :MODEL BACH : :CASE C

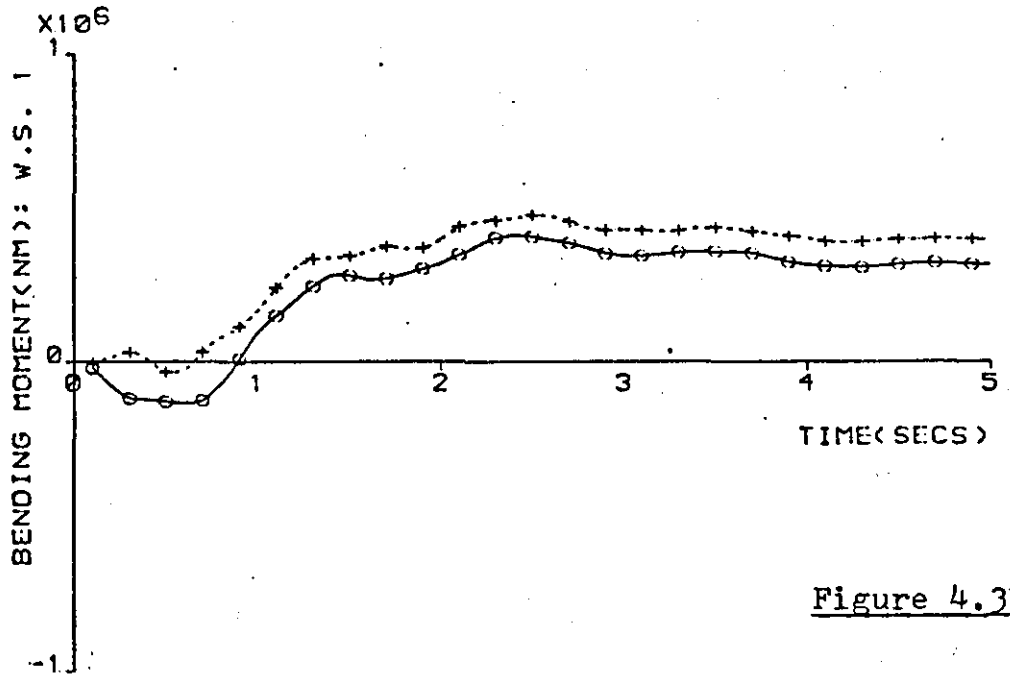


Figure 4.3b

is described in Section 4.4.3c. The results discussed above indicated that the model CLEMENTI was suitable for all work connected with the design of a structural load alleviation control system for the subject aircraft and these results also suggested that most of the aeroelastic energy of concern is contained in the first six bending modes.

4.4.1a. Forcing the Controlled Aircraft.

The artificial test situations B and C given in Table 4.1 were only used for forcing the uncontrolled aircraft. The chief reason for this is that when the same control surface demands were made on the controlled aircraft, the latter did not experience the same rigid body motion as the uncontrolled aircraft: in particular the steady-state levels of vertical velocity, w, and pitch rate, q, experienced in the uncontrolled and controlled situations were different.

In order to validly compare the performance of the controlled with the uncontrolled aircraft, and to assess any SLACS scheme, a method of forcing the controlled aircraft to the same state-state levels of rigid body motion, as experienced by the uncontrolled aircraft, was devised.

The equation representing the uncontrolled aircraft is:

$$\dot{\underline{x}} = A\underline{x} + B\underline{u} \quad + \qquad .. (4.7)$$

The optimal control law is:

$$\underline{u}^{o} = F\underline{x} \qquad ..(4.8)$$

+ In the absence of turbulence.

By substituting (4.8) into (4.7), the equation representing the co trolled aircraft is obtained, viz.,

$$\dot{\underline{x}}_c = (A+BF)\,\underline{x}_c \qquad ..(4.9)$$

(4.9) was forced by adding to the right hand side, an additional vector, $\underline{r}$, acting through a driving matrix, H, i.e.

$$\dot{\underline{x}}_c = (A + BF)\,\underline{x}_c + H\underline{r} \qquad ..(4.10)$$

where,

$$\underline{r} \triangleq \begin{bmatrix} w_{ss} \\ q/n_2 \text{ s.s.} \end{bmatrix} \qquad ..(4.11)$$

$$H \triangleq \begin{bmatrix} 1 & 0 \\ 0 & 1 \\ 0 & 0 \\ \cdot & \cdot \\ \cdot & \cdot \\ \cdot & \cdot \\ 0 & 0 \end{bmatrix} \qquad ..(4.12)$$

Figure 4.4. shows a block diagram representation of the uncontrolled aircraft while in Figure 4.5 is shown the block diagram of the controlled aircraft with forcing vector, $\underline{r}$, included. Figure 4.6 shows plots of rigid body heave motion (i.e. vertical velocity, w) for test situations A,B and C. Similar graphs were obtained for pitch rate,q and the steady-state values attained for the uncontrolled aircraft were used to form table 4.3. These values then formed the elements of vector,$\underline{r}$, (4.11) and were used to force the controlled aircraft. From Figure 4.6 it is seen that the method was very

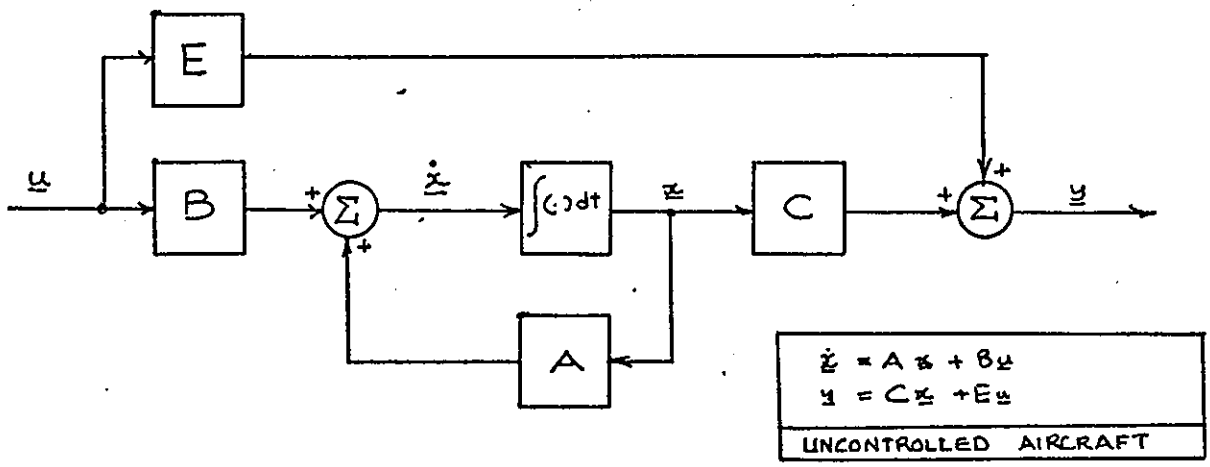


Figure 4.4: SIMULATION BLOCK STRUCTURE: UNCONTROLLED AIRCRAFT

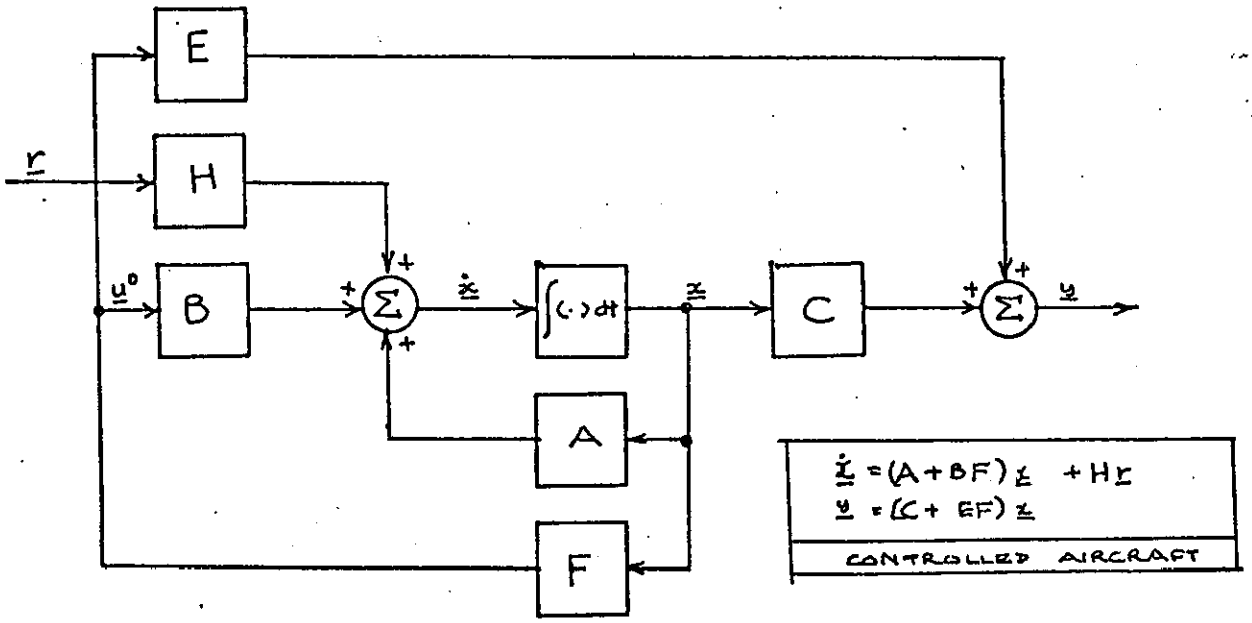


Figure 4.5: SIMULATION BLOCK STRUCTURE: CONTROLLED AIRCRAFT

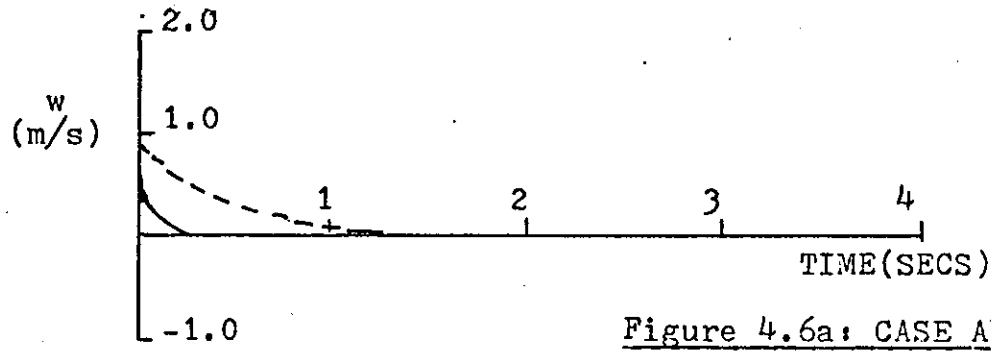


Figure 4.6a: CASE A

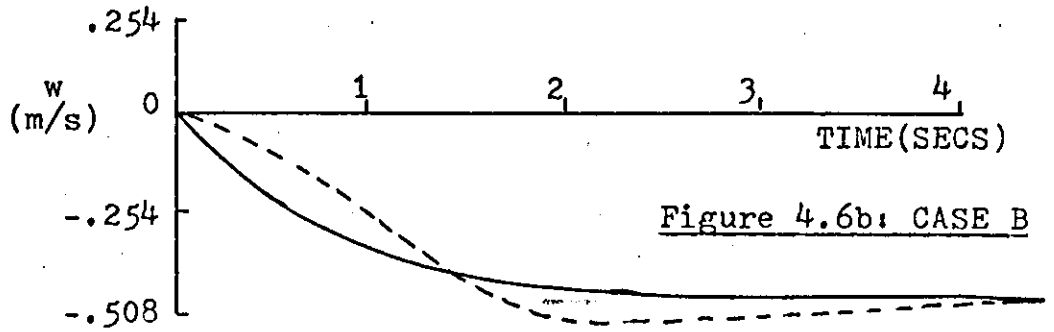


Figure 4.6b: CASE B

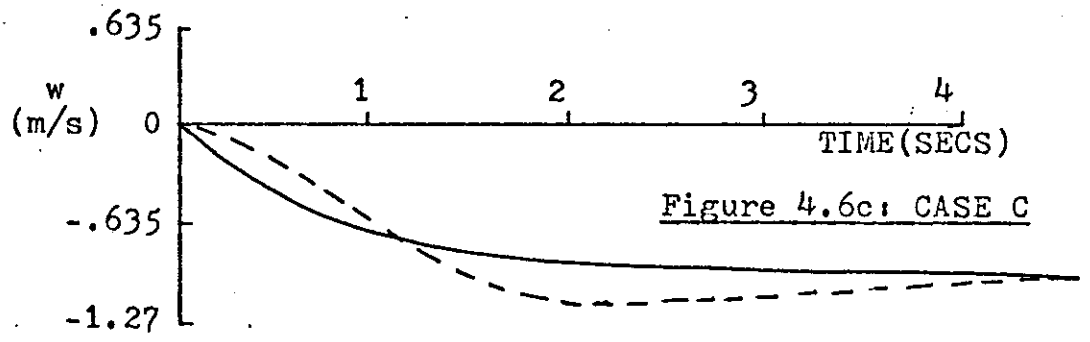


Figure 4.6c: CASE C

——— CONTROLLED

- - - - - - - UNCONTROLLED

RIGID BODY HEAVE MOTION.

effective in producing the same steady level of vertical

CASE	w_{ss} in/s (m/s)	$q/n_{z_{ss}}$ in/s (rad/s)
A	0.0	0.0
B	-18.75 (0.48)	-25 (1.52×10^{-3})
C	-39.5 (1.00)	-6.9 (4.19×10^{-3})

Table 4.4 : Steady State Values: Rigid Body Motion.

velocity within about 5 seconds. Table 4.4 was used extensively in all tests relating to an assessment of each SLACS scheme.

4.4.2 Responses of the Controlled Aircraft Employing Full state Feedback.

The feedback law (4.6) derived on the basis of the model CLEMENTI was tested using the program RESPON (Appendix IV). Figures 4.7 and 4.8 show the bending responses at the wing root and at wing station 3 (w.s.3) for the case B and case C* test situations respectively. It can be seen how effective the presence of feedback was in causing reductions of 50% or more at these wing stations. All the plots associated with the other wing stations studied indicated a similar pattern. An additional welcome feature of the feedback control was the reduction in oscillatory motion in the bending response at each wing station. Such reductions were achieved by augment-

---

* The responses associated with the case A test are not indicated in this case because they were all small deviations about the abscissa which tended to obscure portions of the other responses.

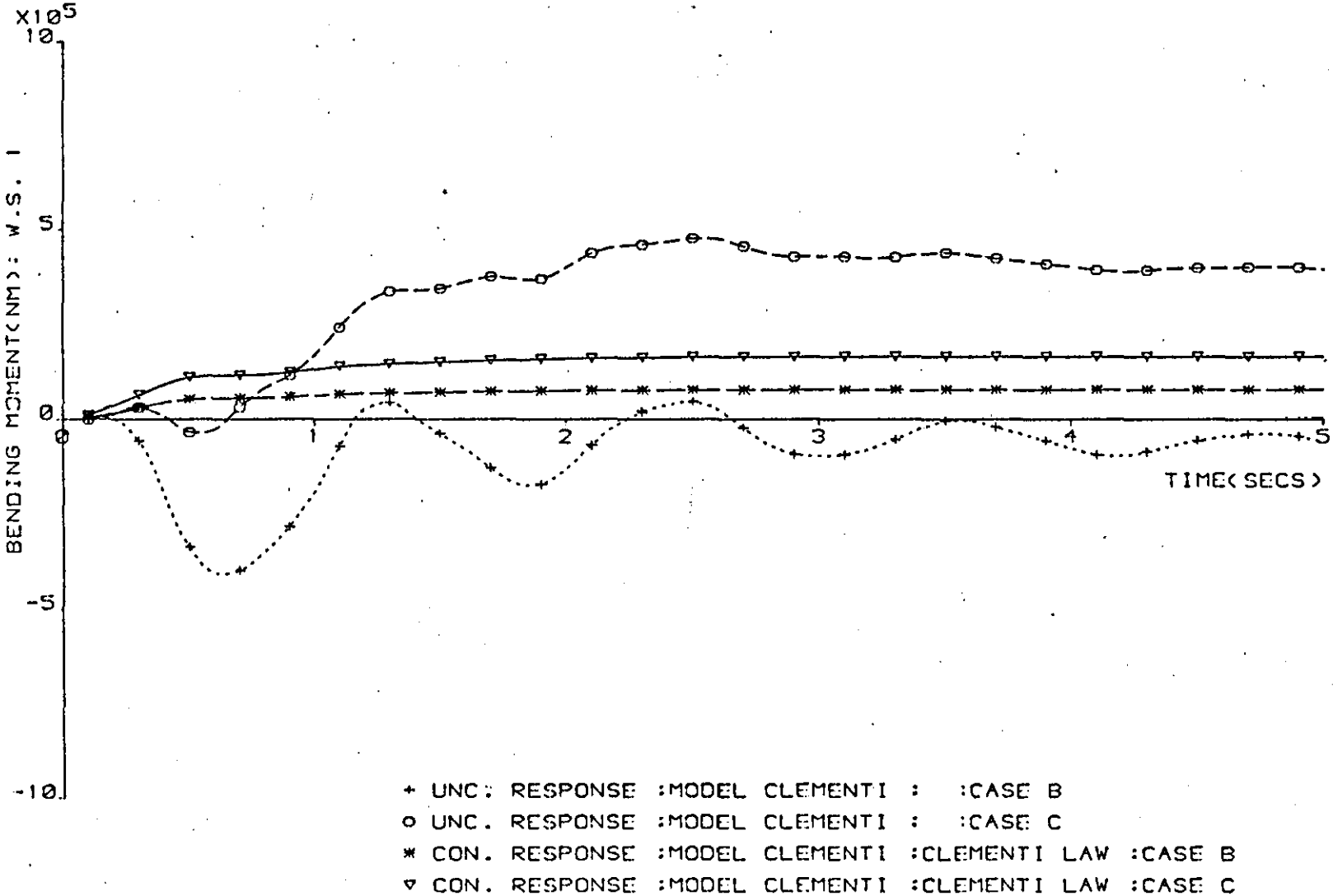


Figure 4.7: BENDING MOMENTS AT THE WING ROOT: LAW 4.6

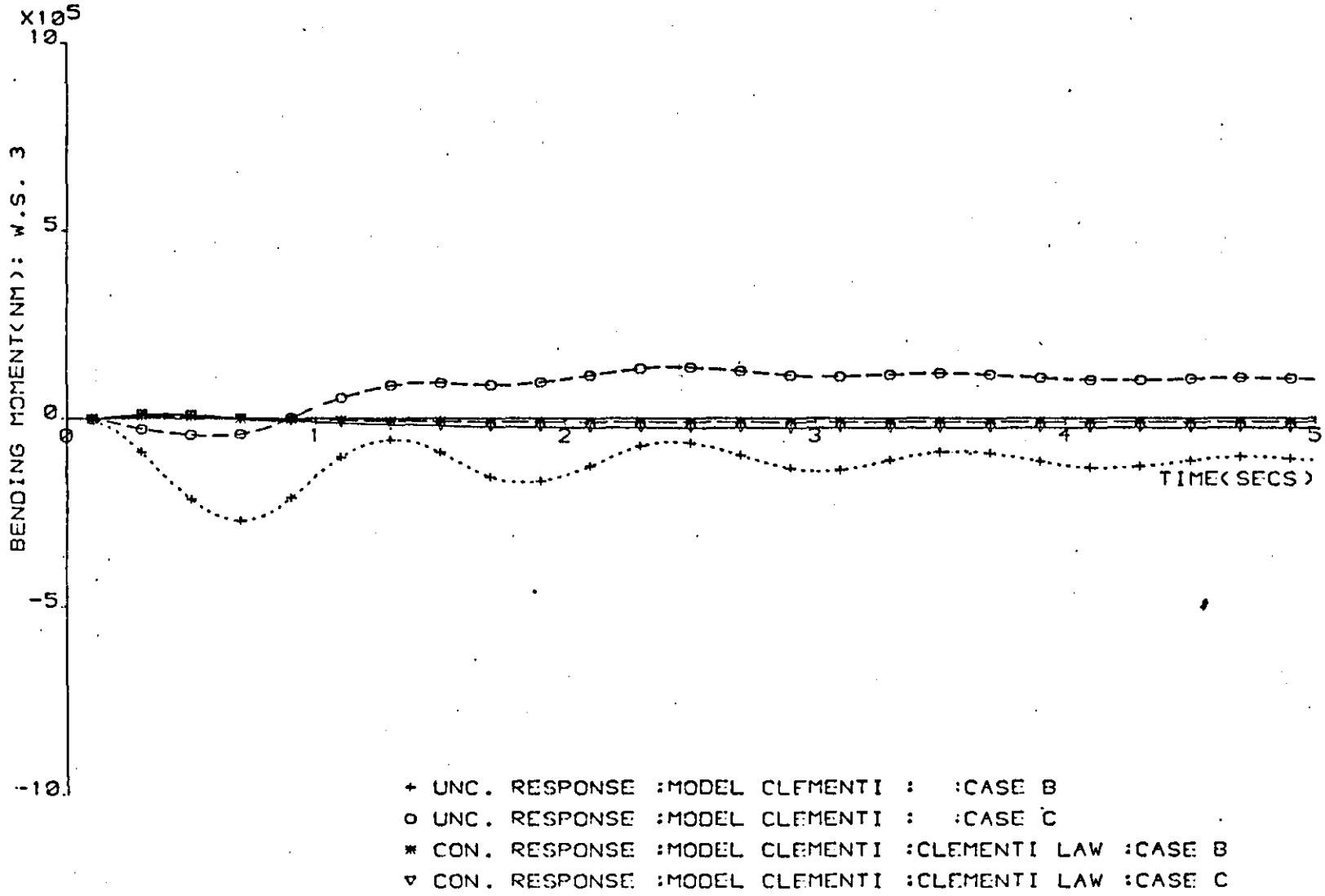


Figure 4.8: BENDING MOMENTS AT W.S.3: LAW 4.6.

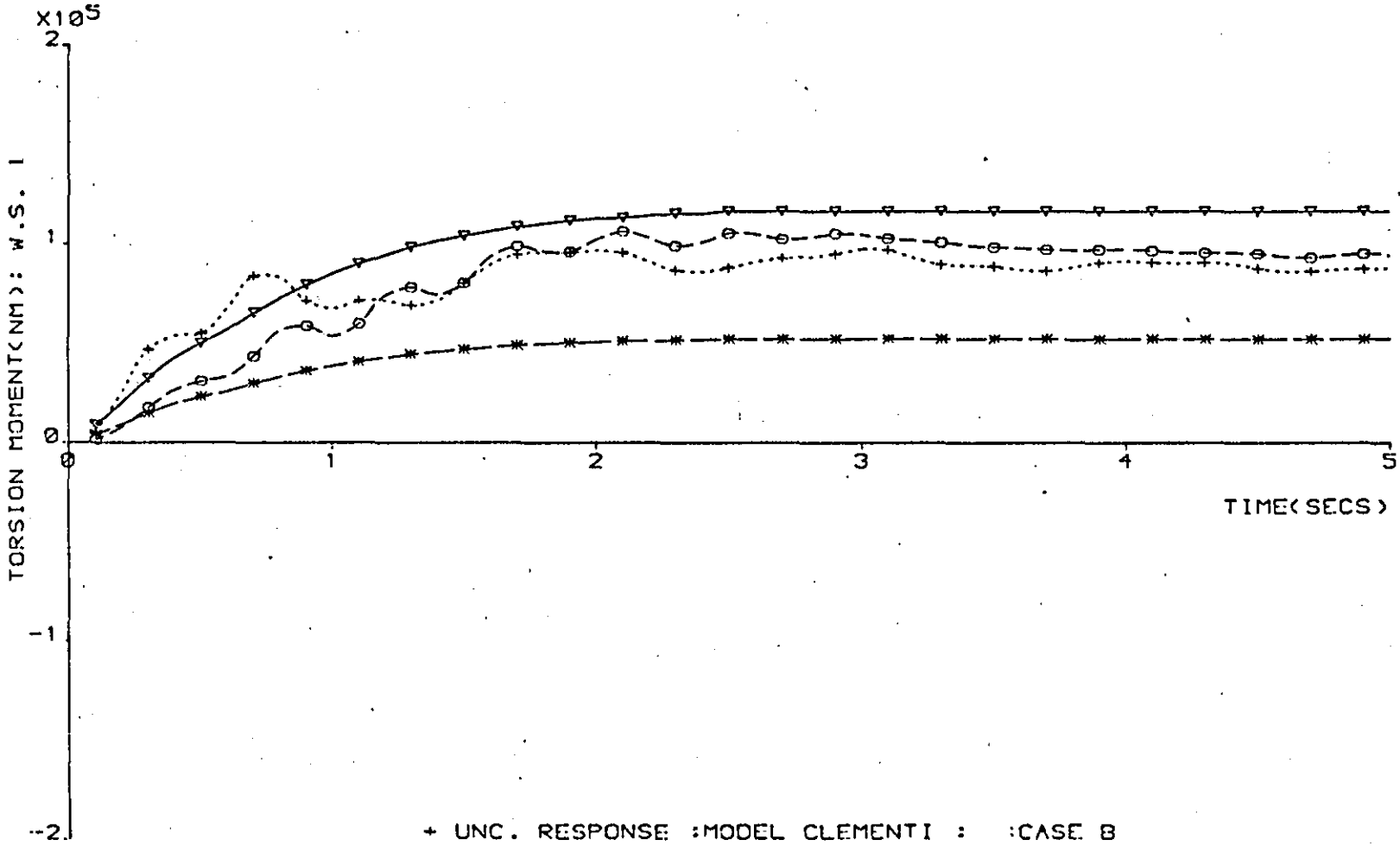
ing the damping of the elastic modes and will contribute to a reduction in the accumulation of the fatigue of the wing structure, i.e. if it is accepted that fatigue accumulates according to Minor's Hypothesis (Burris and Bender (1969)).

Although substantial reductions in bending moments were obtained, it was not possible, with the same control law, for all the test situations studied to simultaneously achieve a reduction in torsional moments. If Figure 4.9 is shown a comparison plot, of torsional moments at the wing root, between the uncontrolled and controlled aircraft. It is seen that for the Case B situation, a reduction of about 50% in torsional moment was possible. However, for the case C situation, there was a 15% increase in torsional moment. As a result, a number of tests were made which involved only different choices of Q and G weighting matrices from which it was shown that it would be feasible to produce a feedback law which would effect a reduction of both bending and torsional moments. A typical set of weighting matrices used are:

$$Q = \text{diag} \begin{Bmatrix} 10^{-7} & 5\times10^{-7} & 10^{-9} & 5\times10^{-8} & 10^{-7} & 5\times10^{-7} & 10^{-9} & 5\times10^{-8} \\ 10^{-9} & 5\times10^{-8} & 10^{-8} & 10^{-9} & 10^{-8} & 10^{-9} & 10^{-9} & 10^{-8} & 10^{-9} \\ 10^{-9} & 10^{-8} & 10^{-9} & 10^{-2} & 10^{-2} & 10^{-2} & 10^{-2} & 10^{-2} & 10^{-2} \\ 10^{-2} & 10^{-2} & 10^{-2} & 10^{-2} & 10^{-2} & 10^{-2} & 1 & 1 & 10 & 10 & 10 & 0.5 \end{Bmatrix} \quad ..(4.13)$$

and,

$$G = \text{diag} (.01 \quad .01) \quad ...(4.14)$$



?? Table 4.7 Says WRT M is lower than in the uncontrolled case ??? Boy oh boy!!

Figure 4.9: TORSIONAL MOMENTS AT THE WING ROOT: LAW 4.6.

The corresponding control law was calculated to be:

$$\underline{u}^{\circ} = \begin{bmatrix} -.0605 & -.0022 & .15 & .0098 & .364 & -.356 & -.151 & .739 & .0212 \\ .151 & 2.38 & -3.44 & -4.26 & 12.7 & -35.4 & -37.8 & -10.4 & .0567 \\ -.443 & -.164 & .0009 & -.189 & .090 & -.0505 & & & \\ & & & & & & & & \\ -.1670 & .0102 & -.0778 & .11 & 1.970 & -1.510 & -.951 & 3.08 & \\ -.0822 & .289 & 5.22 & -9.06 & -11.1 & 33.9 & -151.0 & -438.0 & \\ -87.4 & -464 & -1.08 & -2.03 & .0022 & -.307 & .515 & .237 & \end{bmatrix} \underline{x}$$

.. (4.15)

The responses associated with control law (4.15) are shown in Figures 4.10 - 4.12. From the plots, it is evident that the magnitude of reductions achieved was not the same as was possible with control law (4.6). However, in the case where control law (4.15) was employed, it was possible to contain the torsional moments experienced by the wing of the aircraft to within an acceptable level, i.e. even in an acute manoeuvre situation such as case C, it was still possible to effect a small reduction in torsional moments. In none of the control laws applied so far ~~were~~ the basic handling qualities of the aircraft found to be impaired. The reduction in bending moment at the wing root were in the case of control law (4.15), in the region of 40% while, with control law (4.6), a reduction of 55% was obtained. Thus, if it is necessary to maintain torsional moments at their original level, or even to effect some small reductions, it would still be possible to achieve substantial reductions in wing root bending moments. Similar reductions were recorded at all other wing stations although only the results for wing station 3 have been pre-

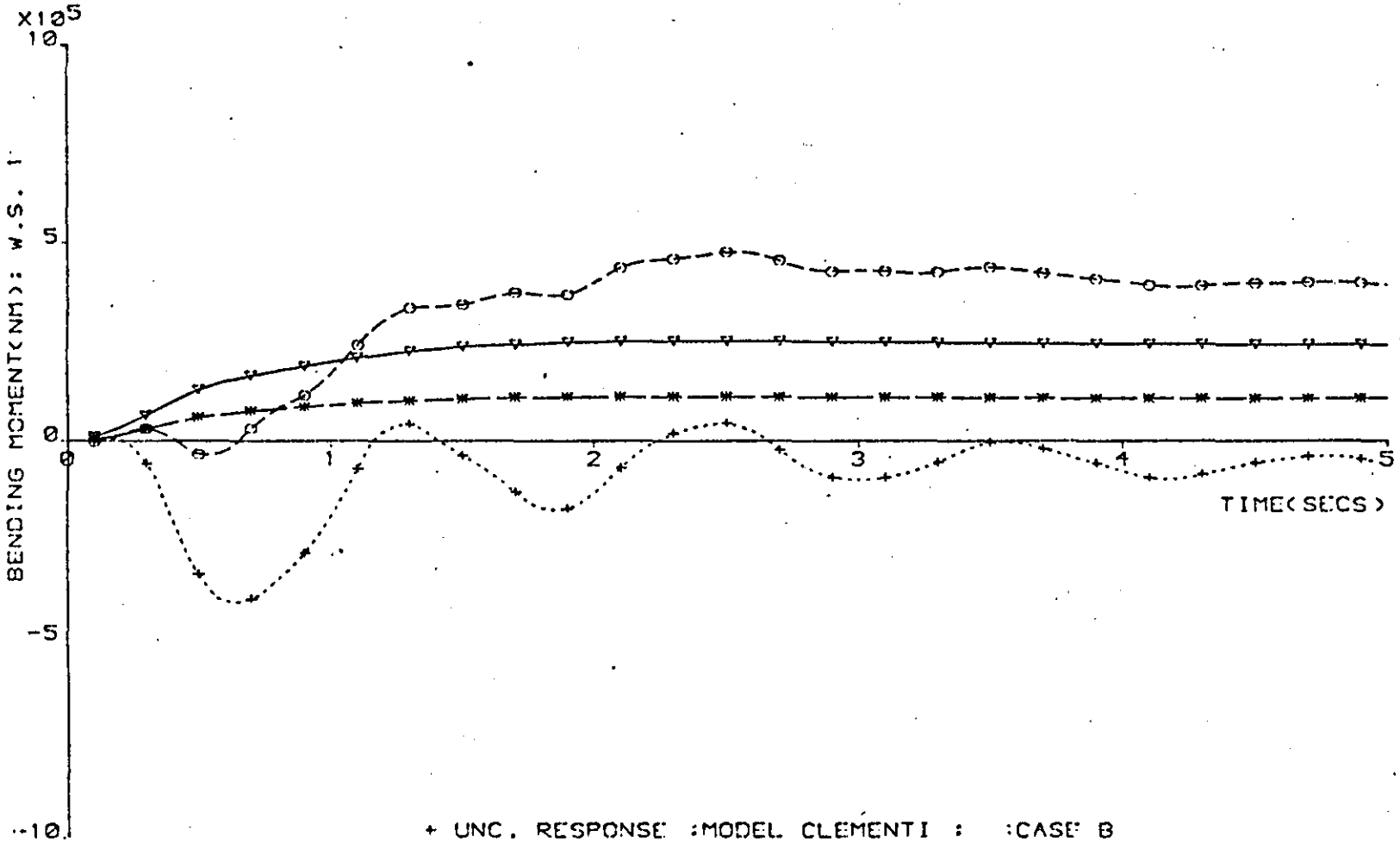


Figure 4.10: BENDING MOMENTS AT THE WING ROOT: LAW 4.15.

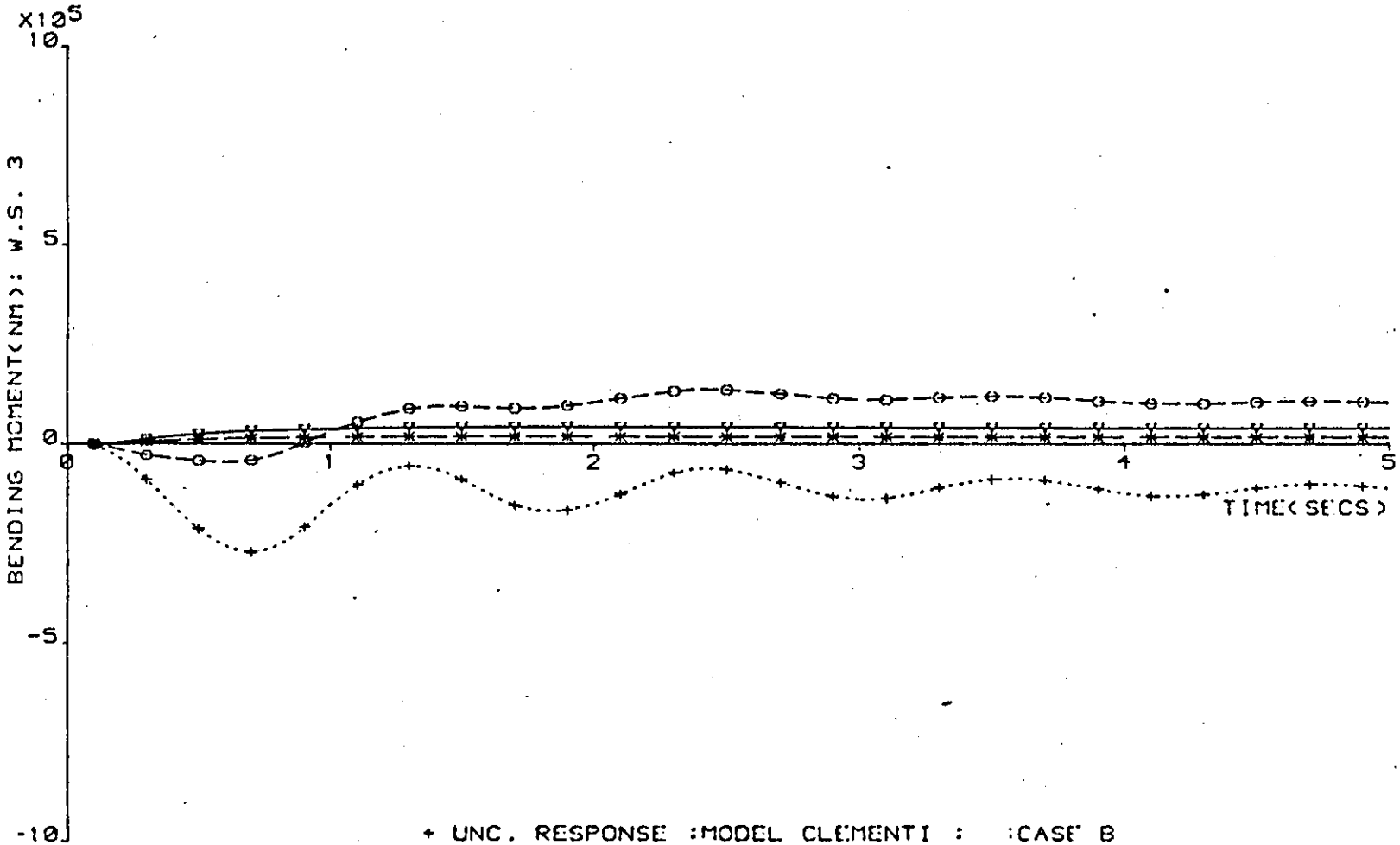


Figure 4.11: BENDING MOMENTS AT W.S.3: LAW 4.15.

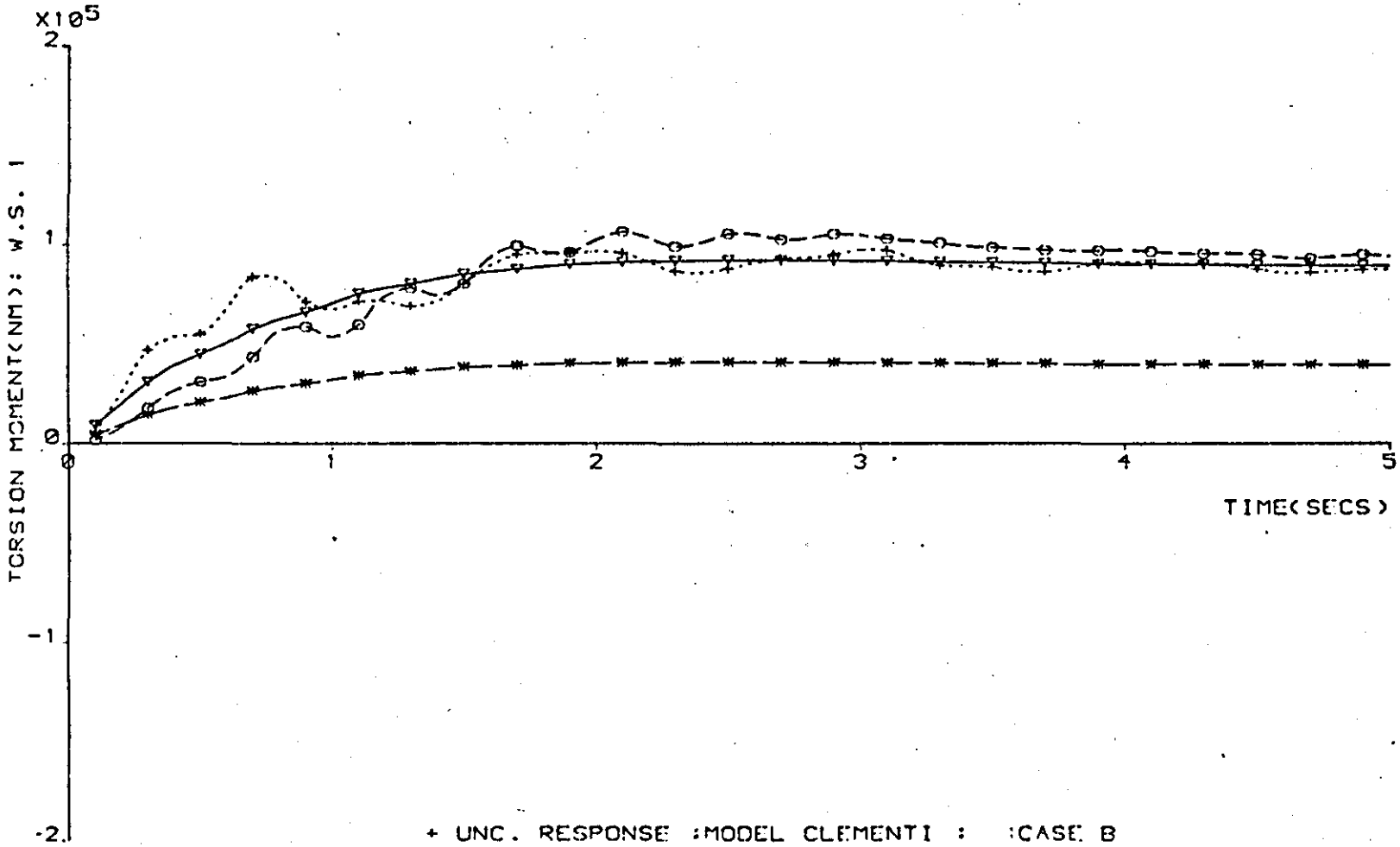


Figure 4.12: TORSIONAL MOMENTS AT THE WING ROOT: LAW 4.15.

sented in Figure 4.11.

4.4.3. Controlled Aircraft Employing Reduced State Feedback.

The feedback laws derived so far, based upon the model CLEMENTI, employed full state variable feedback (FSVF), which, in practice, would be extremely difficult to synthesise. Not only are those state variables involving the displacements and the rates of each of the six bending modes required, but also the six variables associated with the Küssner dynamics* in addition to the gust velocity, which, is an extremely difficult quantity to measure. A number of further tests were therefore carried out to determine the robustness properties of the feedback laws used previously (see section 4.4.2.). A robust flight controller is considered to be one which, without replication of equipment, or switch-over to stand-by equipment does not lead to a loss of control or to system instability when some motion sensor or controller failure occurs (Steinhauser,(1978)). These tests involved the derivation of new feedback laws using less complete models such as FAURÉ, GERSHWIN and HANDEL, but applying these laws to the model CLEMENTI. By this means, it was possible to determine the effect which the absence of one or even an entire group of feedback variables had upon the overall stability of the aircraft. Since robustness must take into account the controllability and stabilisability properties

---

* These variables have no explicit physical existence.

of the system, these properties were investigated and reported upon in the following section.

4.4.3a Controllability and Stabilisability.

Inspection of the eigenvalues of the uncontrolled aircraft, considered to be adequately represented by the mathematical model CLEMENTI, showed that the aircraft was stable. However, further checks using the program CONOBS (Appendix IV) indicated that CLEMENTI was not completely state controllable. In Section 3.2.4., /it was indicated that only stabilisability was necessary and sufficient for evaluating a feedback law which would guarantee the stability of the controlled aircraft. The closed loop stability of the aircraft can be judged from an inspection of the eigenvalues given in Table 4.3.

A more detailed comparison of the eigenvalues given in Table 4.3 will show that those eigenvalues associated with the Küssner states and the outboard-elevator servo have remained unchanged. It is these which account for the result that CLEMENTI was not completely state controllable. Similar results were obtained when the models FAURÉ, GERSHWIN and HANDEL were tested. In all cases either the presence of the Küssner dynamics or the outboard elevator dynamics, or both, resulted in the models being not completely state controllable. However, because the Küssner dynamics and the outboard-elevator dynamics are themselves stable, the closed-loop model was always found to have stable roots. In Table 4.5 is shown the

feedback gains obtained when the output regulator problem was solved for each model. Each set of feedback gains was then applied to the model CLEMENTI: and the eigenvalues of the new 'closed-loop' system found (Table 4.6).

In Table 4.6, 17-SVF/ for instance, is used to indicate that feedback law evaluated on the basis of using the model FAURÉ but applied to the model CLEMENTI. Where some of the gain values are missing, these were replaced by zero, and assumed unavailable for feedback. The eigenvalues for the uncontrolled aircraft and for CLEMENTI with FSVF listed in Table 4.3 have been reincluded in Table 4.6 for convenience. It can be seen from Table 4.6 that, even with what appears to be a severe loss of feedback, as is the case with 5-SVF, there appears to be no significant effect on the stability of the aircraft. The results obtained with 5-SVF$_4$ were of particular significance since as it turns out all five state variables are relatively easy to measure. It was however necessary to investigate the effects of any further loss of feedback. A systematic scheme of testing was made on the model CLEMENTI with various combinations of the gains associated with 5-SVF in the feedback loop. By means of eigenanalysis, it was possible to establish the condition that both pitch rate, q, (i.e. $^{q}/_{n_2}$) and aileron deflection, δ_A, must always be available as feedback signals to guarantee the stability of the closed-loop SLACS. However, in all subsequent tests in this research, it was assumed that all five variables would be available for feedback and consequently 5-SVF is referred to as the 'safety law'.

	w	q/n_2	$\dot{\lambda}_1$	$\dot{\lambda}_2$	$\dot{\lambda}_3$	$\dot{\lambda}_4$	$\dot{\lambda}_5$	$\dot{\lambda}_6$	λ_1	λ_2	λ_3	λ_4	λ_5	λ_6
CLEMENTI	-.0605 .1670	-.0022 .0102	.150 -.0778	.0098 .1100	.364 1.970	-.356 -1.510	-.151 -.951	.739 3.080	.0212 -.0822	.151 .289	2.38 5.22	-3.44 -9.06	-4.26 -11.10	12.7 33.9
FAURÉ	-.019 -.044	-.0052 -.0033	.031 -.433	.010 .118	.126 1.296	-.161 -.943	-.030 -.480	.154 1.188	.012 -.121	.039 -.089	.298 -1.734	-.250 -.975	-.897 .600	3.124 1.220
GERSHWIN	.0138 .0111	.0225 .0536	.0524 -.388						.847 1.64					
HANDEL	.0003 -.0027	.054 .187												

	δ_A	δ_{E_i}	δ_{E_o}	p_1	p_2	p_3	p_4	p_5	p_6	w_g
CLEMENTI	-35.4 -151.0	-37.8 -438.0	-10.4 -87.4	.0567 .4640	-.443 -1.080	-.164 2.030	.0009 .0022	-.189 -.307	.090 .515	-.0505 .237
FAURÉ	-17.44 -101.3	-13.80 -377.7	-3.068 -67.6							
GERSHWIN	-28.2 -134.0	-38.7 -440.0	-6.77 77.5	.0432 .463	.0246 .0105	.181 -2.070	.0002 .0006	.0486 .255	.0798 .482	.169 .798
HANDEL	-31.3 -144.0	-40.4 -446.0	-5.85 -76.0							

Table 4.5: COMPARISON OF FEEDBACK GAINS OBTAINED USING DIFFERENT MODELS

	UNCONTROLLED AIRCRAFT,	CONTROLLED AIRCRAFT			
		FSVF - CLEMENTI	17-SVF	14-SVF	5-SVF
Short Period Mode	-.877±j1.27	-1.14 ± j0.849	-.985 ± j0.785	-1.0 ± j0.973	-1.13 ± j1.12
Bending Mode 1	-.51 ± j5.46	-3.35 ± j7.96	-3.37 ± j8.60	-11.9± j10.4	-0.53 ± j5.47
" " 2	-.23 ± j11.12	-.23 ± j11.12	-0.22 ± j11.12	-0.24± j11.12	-0.24 ± j11.12
" " 3	-.58 ± j13.79	-1.92 ± j15.6	-2.12 ± j14.7	-0.74± j13.5	-0.64 ± j13.8
" " 4	-.6 ± j15.59	-0.37 ± j17.6	-0.37 ± j17.6	-0.79± j15.1	-0.58 ± j15.6
" " 5	-.43 ± j17.48	-1.68 ± j27.6	-2.31 ± j18.8	-0.43 ± j17.5	-0.43 ± j17.5
" " 6	-.62 ± j18.78	-58.0 ± j51.4	-35.2 ± j23.7	-0.62 ± j18.7	-0.61 ± j18.8
Inboard Elev. Servo.	-7.5	-3380.0	-2860.0	-3380.0	-3430.0
Outboard Elev. Servo.	-7.5	-7.5	-7.5	-7.5	-7.5
Aileron Servo.	-6.0	-5.71	-5.98	-79.9	-113.0
Küssner Dynam.	-0.2	-0.2	-0.2	-0.2	-0.2
" "	-0.3	-0.3	-0.3	-0.3	-0.3
" "	-8.55	-8.55	-8.55	-8.55	-8.55
" "	-10.98	-10.98	-10.98	-10.98	-10.98
" "	-22.19	-22.19	-22.19	-22.19	-22.19
" "	.51 ± j3.6	-5.1 ± j3.6	-5.1 ± j3.6	-5.1 ± j3.6	-5.1 ± j3.6

Table 4.6 Comparison of Eigenvalues of the Controlled Model CLEMENTI Using Reduced Order Feedback

4.4.3b. Responses.

The feedback laws evaluated using the models FAURÉ, GERSHWIN and HANDEL were tested using the model CLEMENTI. A typical set of dynamic responses are shown for the wing root and w.s.3 in Figures 4.13-4.15. It can be seen from these plots how effective reduced-order feedback was in still securing substantial levels of bending moment reductions both at the wing root and at w.s. 3. Although no significant reduction in torsional moments was possible, in no circumstance did these moments turn out to be greater than those experienced by the uncontrolled aircraft. Although not included in this set, the responses obtained for wing stations 2,4 and 5 followed a similar pattern. Also because the responses obtained from using the feedback law based on the model FAURÉ did not differ significantly from the responses of CLEMENTI with FSVF, these responses were not included in the plots. The result is however not unexpected since FAURÉ only differs from CLEMENTI in the absence of the Küssner and gust dynamics. Since the tests made so far are all deterministic, the gust dynamics were not excited.

The response obtained using the law derived from the model GERSHWIN presents an interesting result since it confirms the general belief in Aeronautical Engineering that much of the aeroelastic energy is contained in the first bending mode. The results of Figure 4.13 indicate that it is possible to achieve the same level of reductions in WRBM even when only those state variables associated with the first bending mode are fed back.

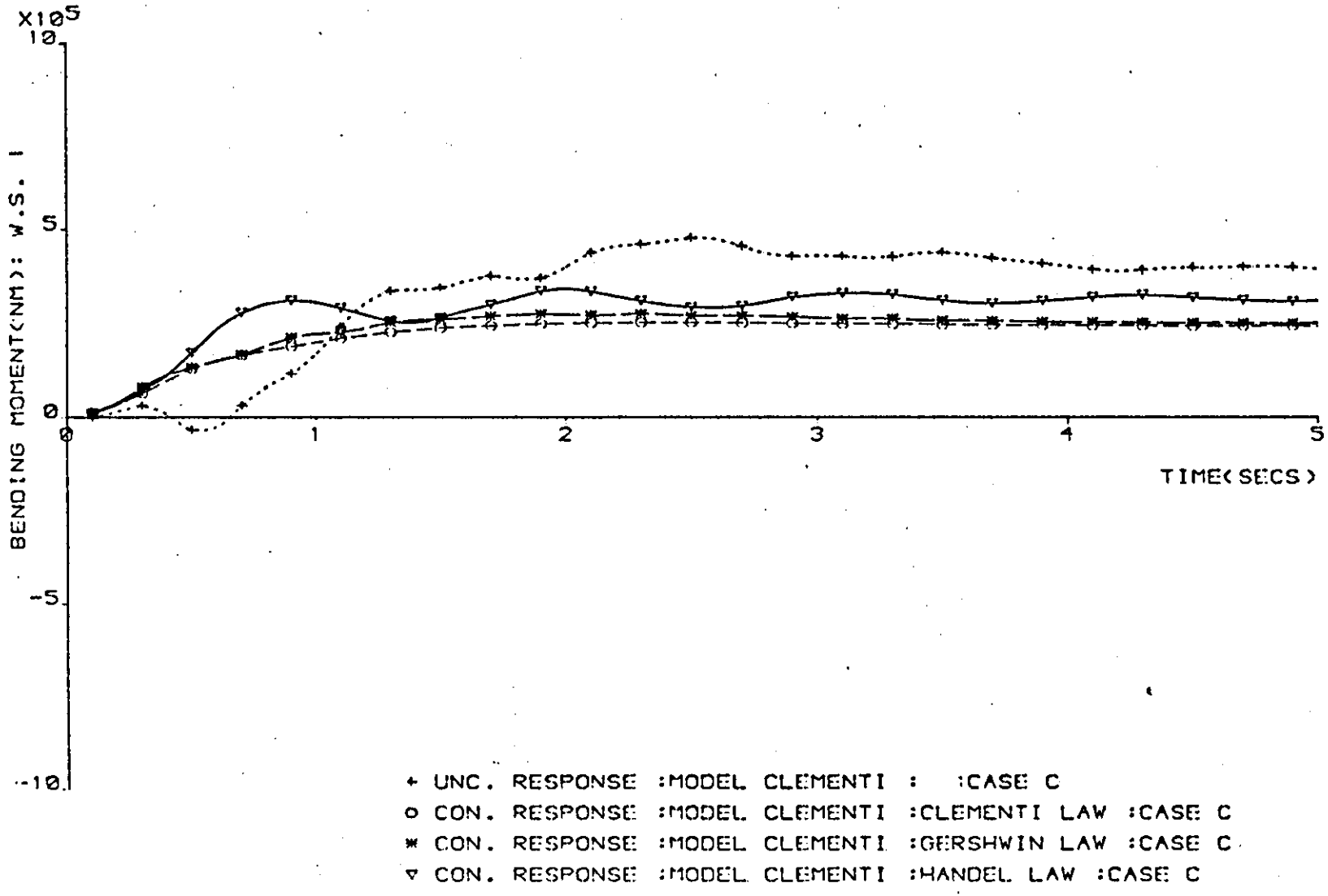


Figure 4.13: EFFECT OF REDUCED-ORDER FEEDBACK ON WRBM.

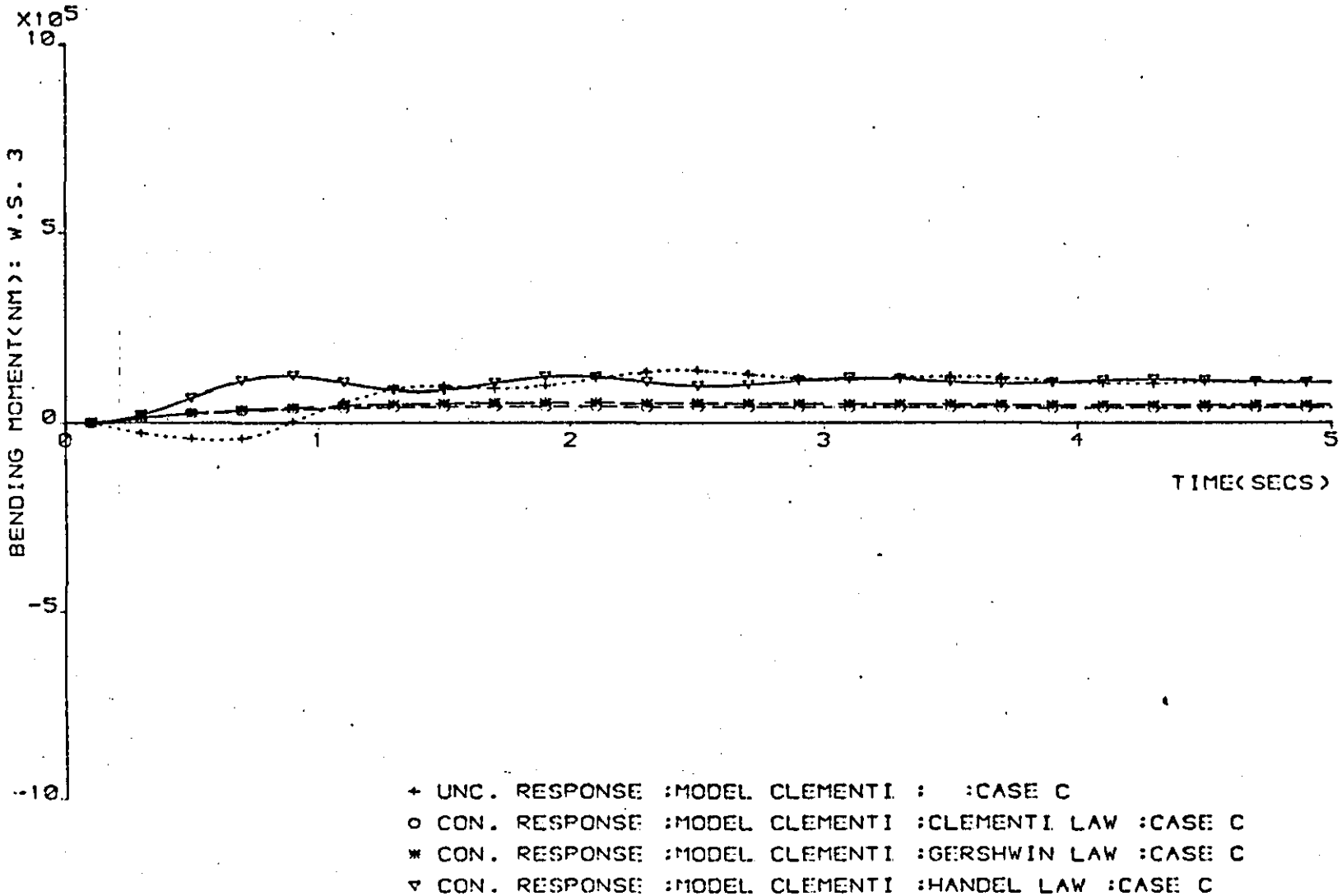


Figure 4.14: EFFECT OF REDUCED-ORDER FEEDBACK ON BENDING MOMENT AT W.S.3.

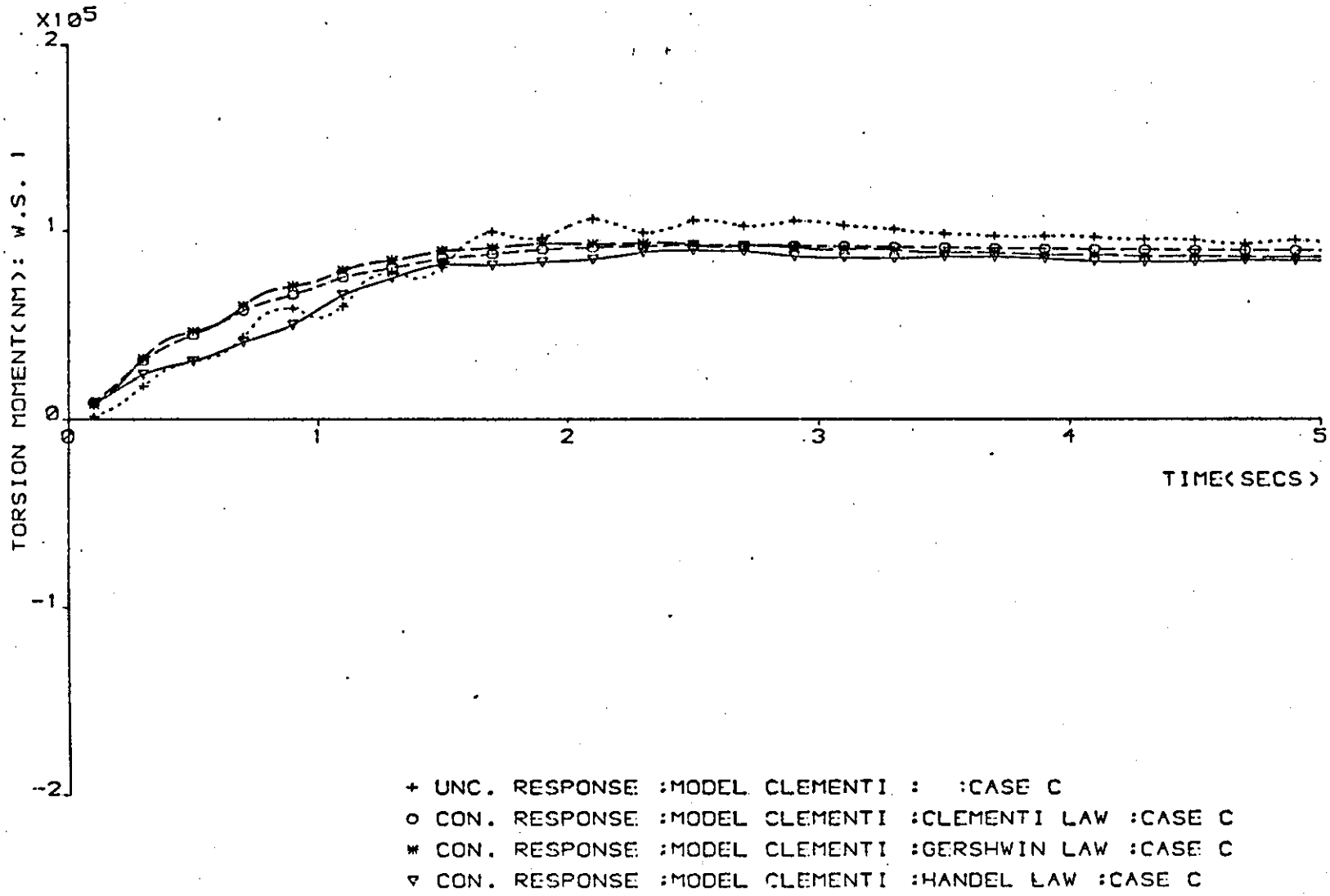


Figure 4.15: EFFECT OF REDUCED-ORDER FEEDBACK ON WRTM.

With 5-SVF it was not possible to achieve the same level of bending moment reductions as was possible with either 14-SVF, 17-SVF or full state-variable feedback. At the wing root bending moment reductions were in the region of 20% when 5-SVF was used, compared with 40% for the FSVF case. Also, with 5-SVF, it was not possible to augment the damping of the bending modes to the extent achievable with higher orders of feedback. As a result there is some oscillation associated with the bending responses when the 'safety law' was employed. From these results, it may be inferred that the use of 5-SVF, although an attractive proposition from the point of view of being easy to synthesise, has associated with it a number of limitations. Reduced state feedback, which may result, because enough sensors cannot be provided, or, when present, cannot provide accurate measurements, or may have failed in their operation, may be expressed in terms of the increased level of bending moments which will result together with the presence of some oscillation in the bending responses.

4.4.3c Steady-State Checks.

Since this research was primarily concerned with the reduction of structural loads on the wing of the subject aircraft and since, in all tests carried out so far, each SLACS was judged principally by the steady-state level of load reduction it provided, a method was developed for quickly evaluating the steady-state loads from a knowledge of the aircraft dynamics and the command vector being applied.

EASTER VACATION BORROWING

Books may be borrowed for the Easter vacation from Monday March 16th. However all books are still subject to recall and must be returned if required by another reader.

Consider the aircraft equations given as:

$$\dot{\underline{x}} = A\underline{x} + B\underline{u} \qquad ..(4.7)$$

$$\underline{y} = C\underline{x} + E\underline{u} \qquad ..(4.16)$$

In the steady-state,

$$\dot{\underline{x}} \triangleq 0 \qquad ..(4.17)$$

Therefore from (4.7),

$$\underline{x}_{ss} = - A^{-1}B\underline{u} \qquad ..(4.18)$$

and from (4.16)

$$\underline{y}_{ss} = (-CA^{-1}B + E)\underline{u} \qquad ..(4.19)$$

(4.19) was used to determine the steady-state level of any of the variables constituting the vector, $\underline{y}$, (chiefly the bending and torsional moments), which was achieved by the uncontrolled aircraft when subjected to a case B or a case C test situation. In order to compare these load levels with those achieved when feedback was present, it was first necessary to take into account, in (4.7), the change in the basic aircraft dynamics, i.e., for an optimal control law given as:

$$\underline{u}^{o} = F\underline{x} \qquad ..(4.8)$$

the equations representing the controlled aircraft are:

$$\dot{\underline{x}}_c = (A + BF)\underline{x}_c \qquad ..(4.20)$$

and,

$$\underline{y}_c = (C + EF)\underline{x}_c \qquad ..(4.21)$$

where $\underline{x}_c$ is a vector identical to $\underline{x}$, but only used to distinguish between the controlled and the uncontrolled situations. In order to force the controlled aircraft, an extra vector, $\underline{r}$, was introduced into (4.20) acting through a driving matrix, H, (see section 4.4.2) i.e.

$$\dot{\underline{x}}_c = (A + BF)\underline{x}_c + H\underline{r} \qquad ..(4.22)$$

Again, in the steady state,

$$\dot{\underline{x}}_c \triangleq 0 \qquad ..(4.23)$$

$$\therefore \underline{x}_{c_{ss}} = -(A + BF)^{-1} H\underline{r} \qquad ..(4.24)$$

From (4.21)

$$\underline{y}_{c_{ss}} = -(C+EF)(A+BF)^{-1} H\underline{r} \qquad ..(4.25)$$

(4.25) was used for determining the steady state levels of bending and torsional loads induced in the wing of the controlled aircraft and these were then compared for the equivalent test situation with those levels induced in the wing of the uncontrolled aircraft. Both full and reduced state feedback was studied i.e. F took a range of values (from Table 4.5) dependent upon the order of feedback studied. The vector, $\underline{r}$, took the values appropriate to a case B or a case C test situation (see Table 4.3). For a solution of (4.25) to exist, (A+BF) must be non-singular. The feedback matrix, F, is the solution of a linear quadratic problem (LQP) and that solution guaranteed that (A+BF) must be at least positive semi definite (p.s.d); that is to say, that the eigenvalues of (A+BF) have negative real parts

and (A+BF) is therefore a stability matrix and is invertible.

Some results obtained for the wing root and wing station 3 are presented in table 4.7. The table allows steady-state bending levels of the uncontrolled aircraft to be compared with those achieved by the controlled aircraft for the Case B and Case C test situations. Results for the controlled aircraft with reduced feedback down to 5-state variables are shown. It is seen that in almost every case where feedback was implemented, it was possible to achieve some reduction in bending and torsional loads. All the results were confirmed independently through response tests. Since, from previous response tests, it was evident that the transient response of the aircraft with SLACS incorporated, did not alter significantly, even with a severe loss of feedback down to five motion variables, the method provides a fast and accurate way of predicting the effect that different types of reduced order control would have on the aircraft. Also the results of table 4.7 lends support to the suggestion made earlier in Section 4.43b that the cost of providing more sensors, or alternatively, the cost of a failure, to provide measurements, can be expressed in terms of the resultant increase in the load levels experienced in the wing of the aircraft. Even when only 5-SVF is employed, (a much simpler and hence cheaper engineering task), the reduction in bending moment that was possible at the wing root was in the region of 18%. However, in practice it will be necessary that the wing of the aircraft be designed to withstand loads incurred with the minimum of SLACS action.

Aircraft Control Condition	WRBM		WRTM		W.S.3 BM	
	B	C	B	C	B	C
Uncontrolled	-.535	3.54	.784	.843	-1.01	.932
FSVF	.976	2.17	.362	.801	.155	.352
17-SVF	.871	2.17	.490	.801	-.019	.352
14 SVF	1.01	2.25	.348	.773	.184	.418
5-SVF	1.00	2.30	.351	.751	.179	.464

All Moments quoted in 10^6 Nm.

Table 4.7: COMPARISON OF STEADY-STATE BENDING AND TORSIONAL MOMENTS

See graph (figure 4.9)

WRTM for case C is 1.16 . (Rodle)????

From the response tests carried out on the uncontrolled aircraft represented by the mathematical models BACH and CLEMENTI, it was evident that the transient and steady-state behaviour of these models were identical (see Figures 4.1 - 4.3). (4.25) was used to confirm these results. Furthermore, when the feedback law evaluated on the basis of the model CLEMENTI was used with BACH, the steady-state loads predicted were identical to those predicted for CLEMENTI with FSVF. Thus CLEMENTI was regarded as being of the highest dimension required for any work connected with the design of a suitable SLACS for the subject aircraft. The results also clearly indicate that the upper nine bending modes, represented only in BACH, ~~was~~ were not contributing significantly to the total aeroelastic energy involved.

4.4.3d Servo-Actuator Requirements.

In all cases involving full and reduced-order control, it was noticed from the eigenvalues obtained (see for instance table 4.6), that the root associated with the inboard section of the elevator shifted over a very wide range: from -7.5 to about -3000.0. This suggested that the response time of the inboard elevator was required to be reduced by some 400 times in order to achieve the required structural load alleviation. Such a requirement implied almost instantaneous action from the servo-actuator associated with the inboard elevator, a requirement which cannot be met in practice. In an attempt to more fully appreciate the need for

such a fast response, a number of tests were carried out which enabled the dynamic response of each actuator used in the study to be plotted. The tests were made using the model CLEMENTI and employing both full and reduced-order control. In Figures 4.16 and 4.17 are shown the results of the tests made for the case C situation in which the control surfaces were found to be the most active. In none of the plots ~~are~~ the requirements for control surface deflection, or its rate, so high as to be beyond the capability of currently available servo-actuators. However, it is evident from Figure 4.17, that the use of 17-SVF and 14-SVF may require sudden demands for control surface rate and this is certainly likely to cause practical difficulties with the duty-cycle ratings of currently available servo-actuators.

All responses for Case C

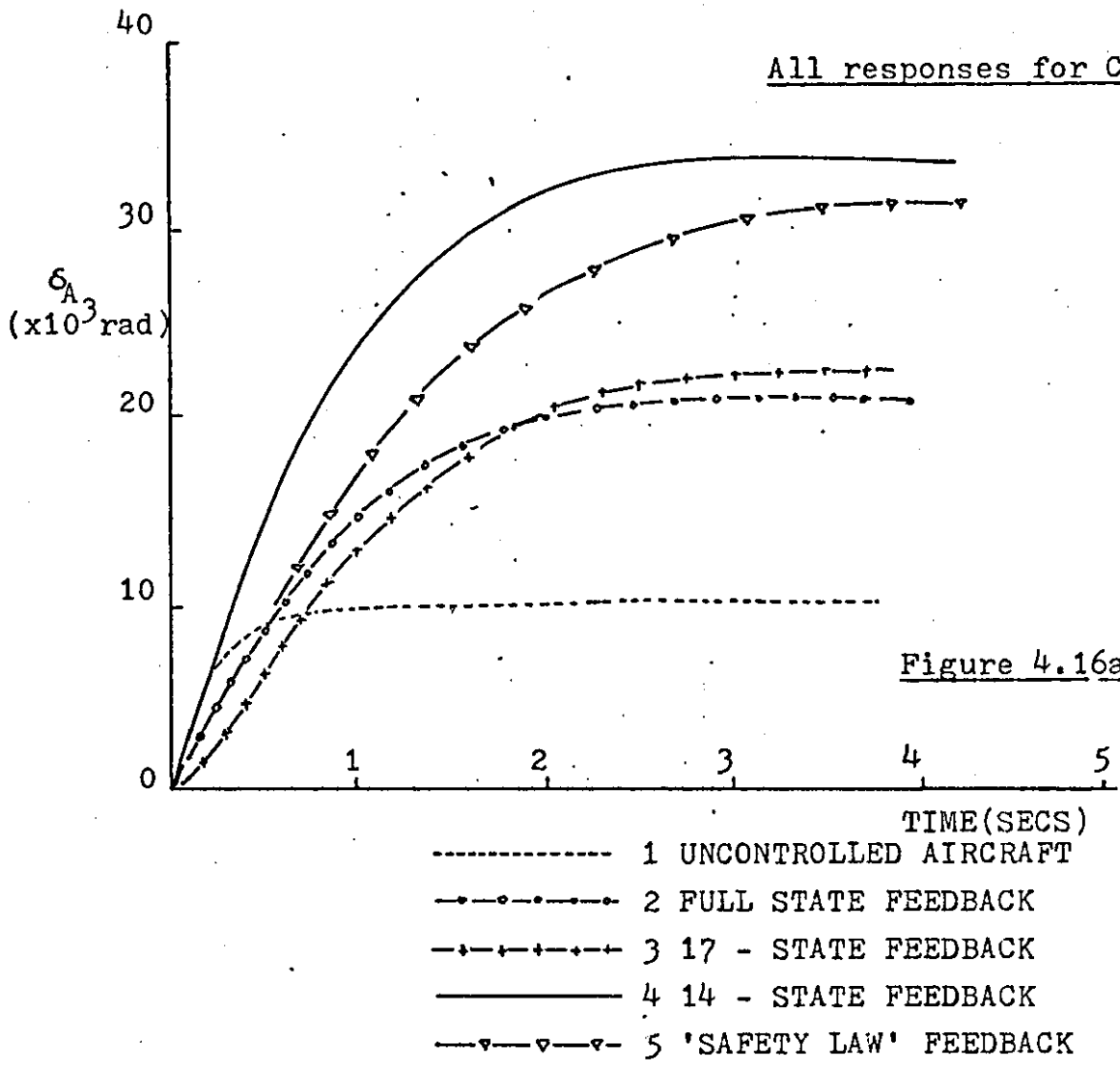


Figure 4.16a

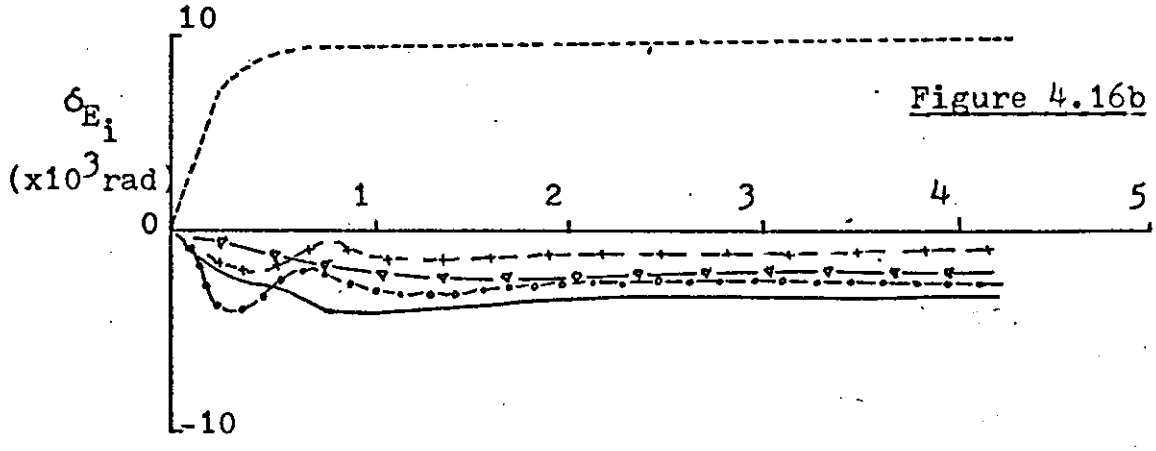


Figure 4.16b

CONTROL SURFACE DEFLECTIONS NEEDED FOR LOAD ALLEVIATION

All responses for Case C

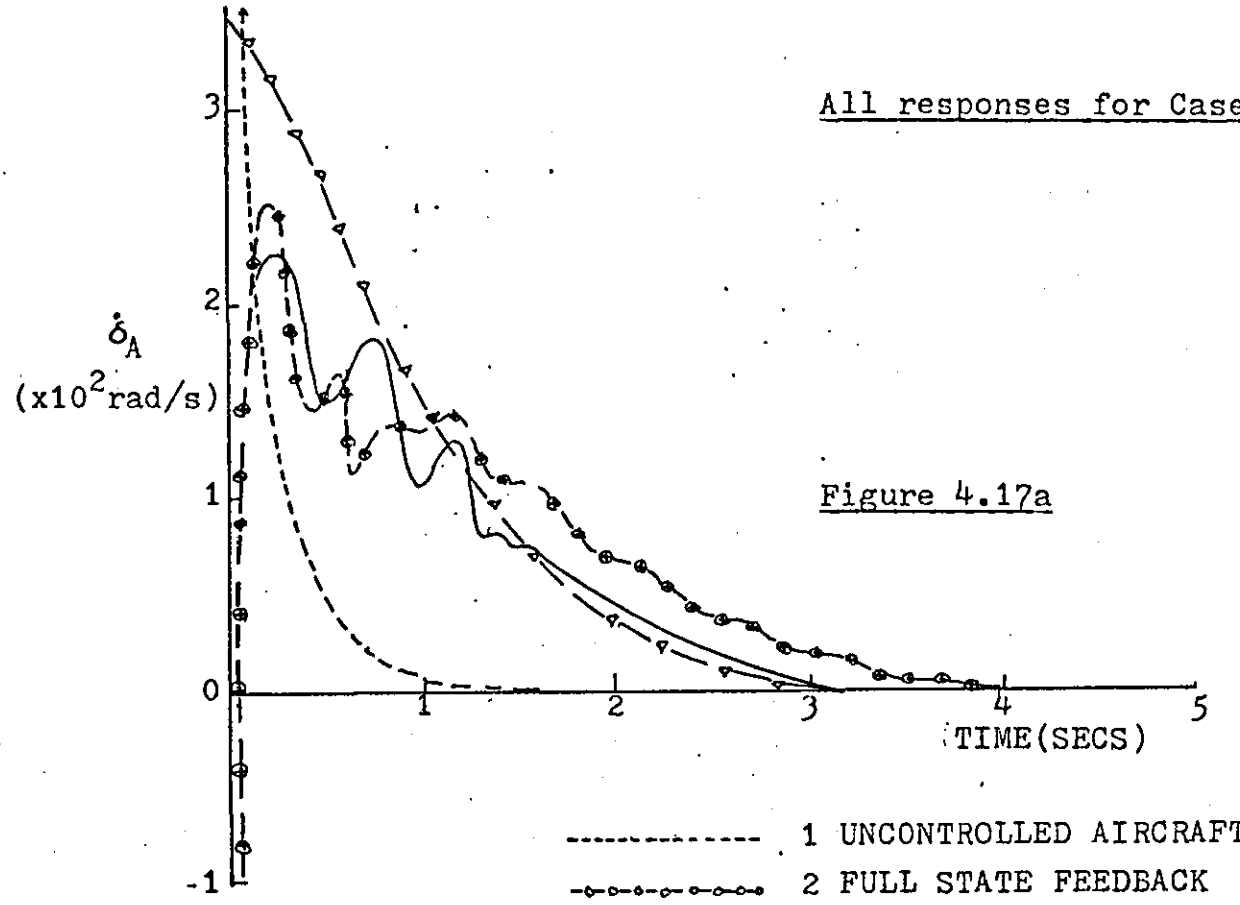


Figure 4.17a

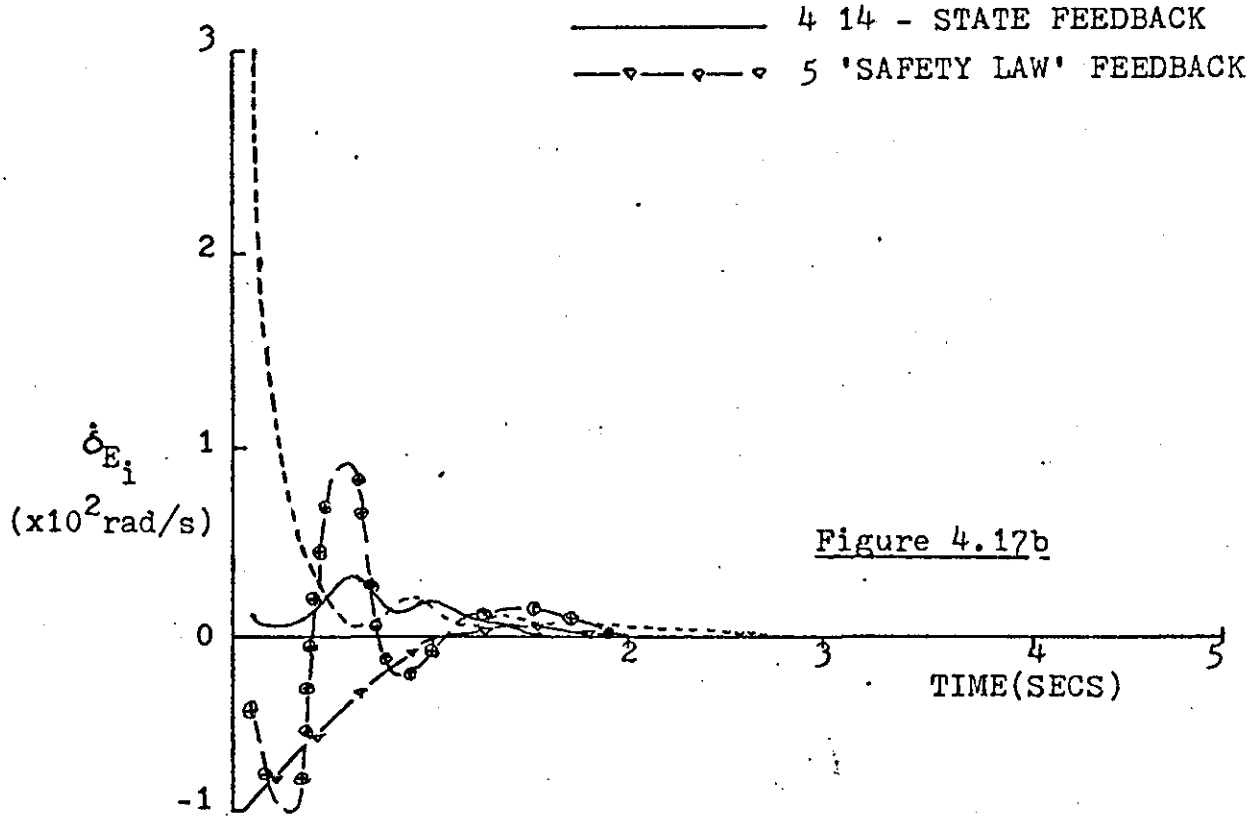


Figure 4.17b

CONTROL SURFACE RATES NEEDED FOR LOAD ALLEVIATION.

4.5 Aircraft Response in Atmospheric Turbulence.

Only a limited number of tests were carried with the aircraft model (again considered to be adequately represented by CLEMENTI) in simulated atmospheric turbulence since each response required a large amount of computing time for its generation. For the input noise to the Dryden Filter, random number generation was used and these were provided by standard NAG* library routines . The sequence of numbers approximated to the white noise input required for the Dryden filter and had the property of zero mean and of standard deviation which was adjusted to give an r.m.s. value of vertical gust velocity, (the Dryden filter output). of about 1.0 m/s. In Figure 4.18a is shown the input to the Dryden filter while its output has been plotted in Figure 4.18b. Some of the responses of the uncontrolled and controlled aircraft for test situations D and E are shown in Figures 4.19 and 4.20 respectively. In the case D test situation, no initial conditions on the state variables were used and no commanded control surface deflections were employed. Thus the case D situation approximated to the aircraft travelling in steady level flight and suddenly encountering atmospheric turbulence. From the graphs it is seen that this type of turbulence resulted in the highest peak levels of bending moment at the wing root, greater than any of those experienced in the deterministic command situations. In the case E situation, the aircraft was assumed to have an initial vertical velocity of 7.15 m/s.

---

* NAG = Numerical Algorithms Group, University of Oxford.

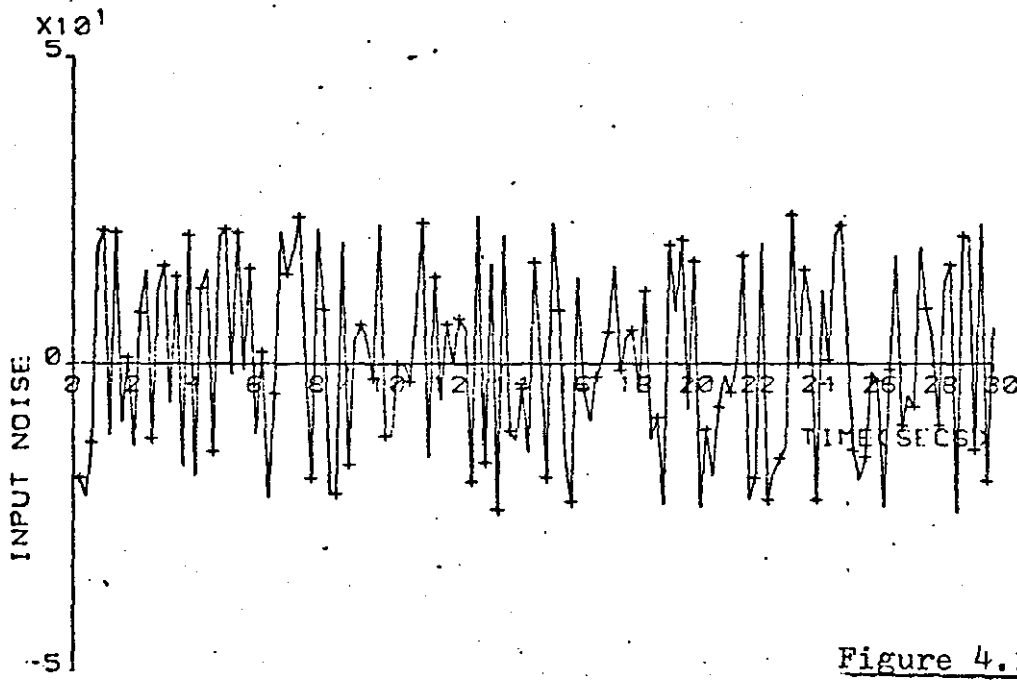


Figure 4.18a

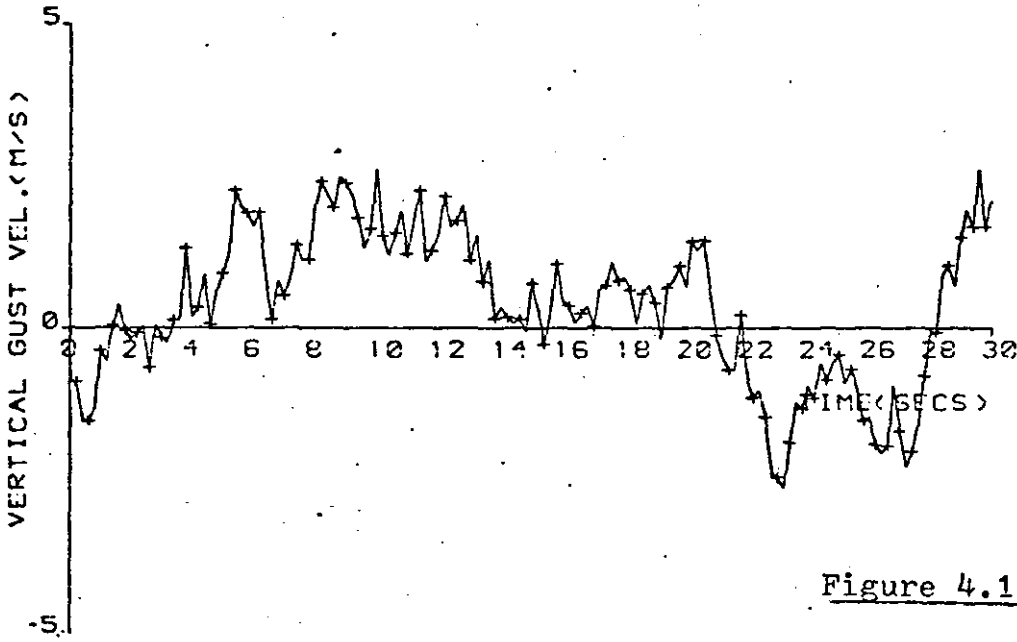


Figure 4.18b

SIMULATION OF ATMOSPHERIC TURBULENCE

Overall, little difference was noticed between the case D and the case E situations. However, the initial state values of bending moment induced at the wing root in the case E situation was quite high, approaching -3×10^6 Nm.

For the tests on the controlled aircraft, the full-state feedback law, which secured in the deterministic situations wing-root bending moment reductions of up to 40% without causing an increase in the corresponding torsional moments, was used, i.e. control law (4.15). In none of the tests with simulated atmospheric turbulence was reduced-order control used. The reason for this was primarily because the tests were expensive to carry out in terms of CPU time and the heavy computational burden did not permit further tests to be made. However, for those tests reported upon, the responses were obtained for 30 seconds, (only 5 seconds were used in the deterministic tests) chiefly to ensure that any tendency of the SLACS to cause either sudden changes of stress or excessive levels of peak loads would be detected.

Figures 4.19 and 4.20 show that even in turbulence, the SLACS was very effective in securing for the aircraft, substantial reductions in bending moment at the wing root. Although not shown here, similar levels of reductions were obtained at the other wing stations. It is also seen from the responses of the controlled aircraft that vertical velocity is also reduced by the action of the SLACS and this implies lower rigid body accelerations which will contribute towards improving the ride

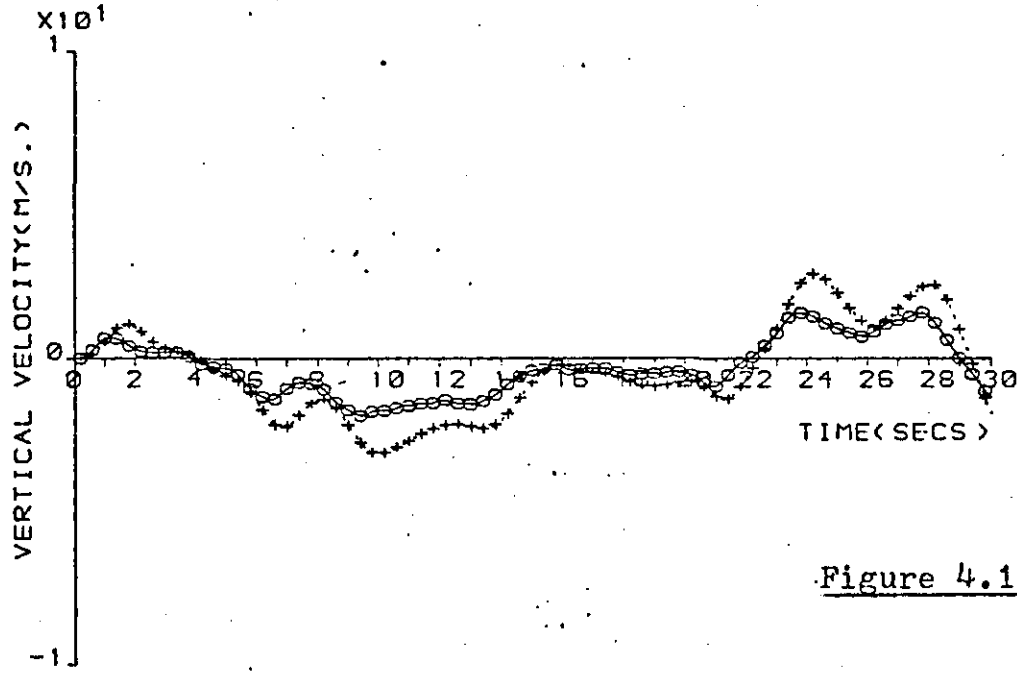


Figure 4.19a

+ UNC. RESPONSE :MODEL CLEMENTI : :CASE D
o CON. RESPONSE :MODEL CLEMENTI :CLEMENTI LAW :CASE D

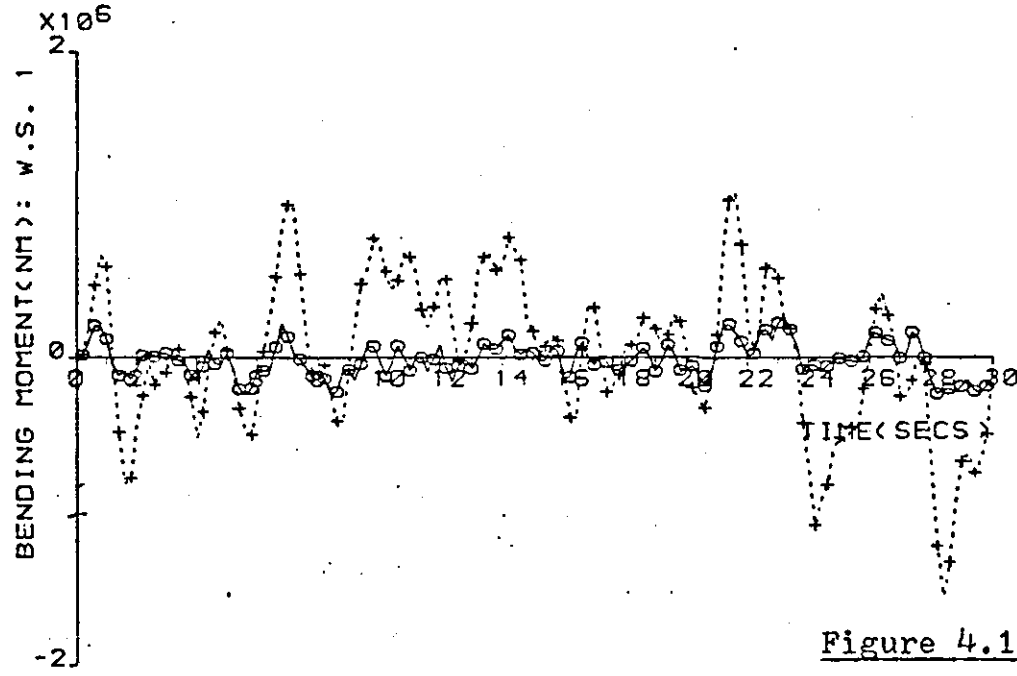


Figure 4.19b

RESPONSE TO TURBULENCE

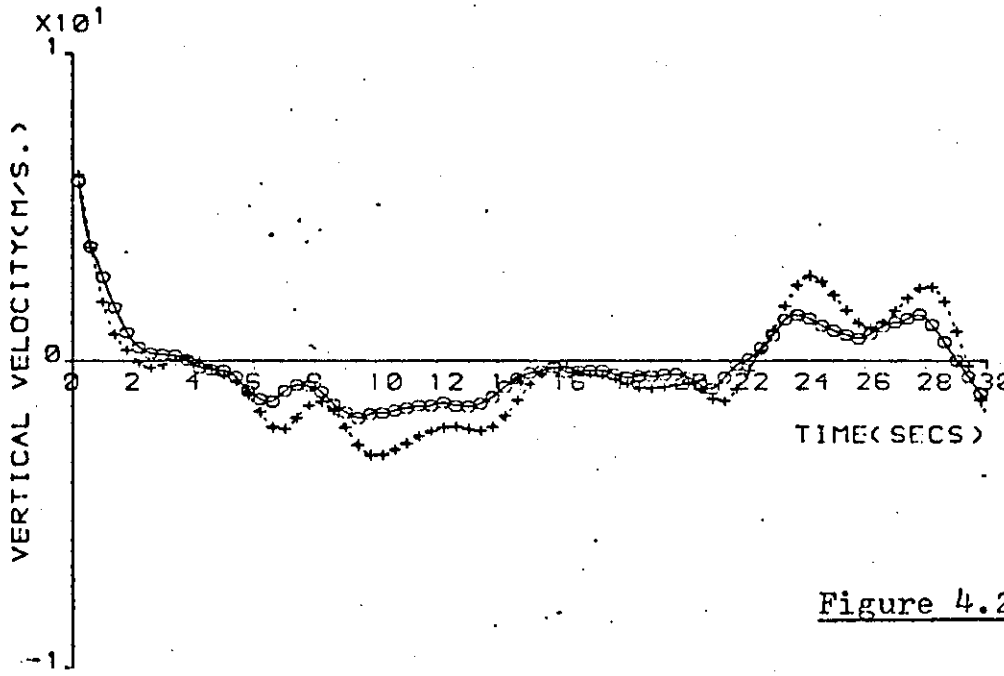


Figure 4.20a

+ UNC. RESPONSE :MODEL CLEMENTI : :CASE E
o CON. RESPONSE :MODEL CLEMENTI :CLEMENTI LAW :CASE E

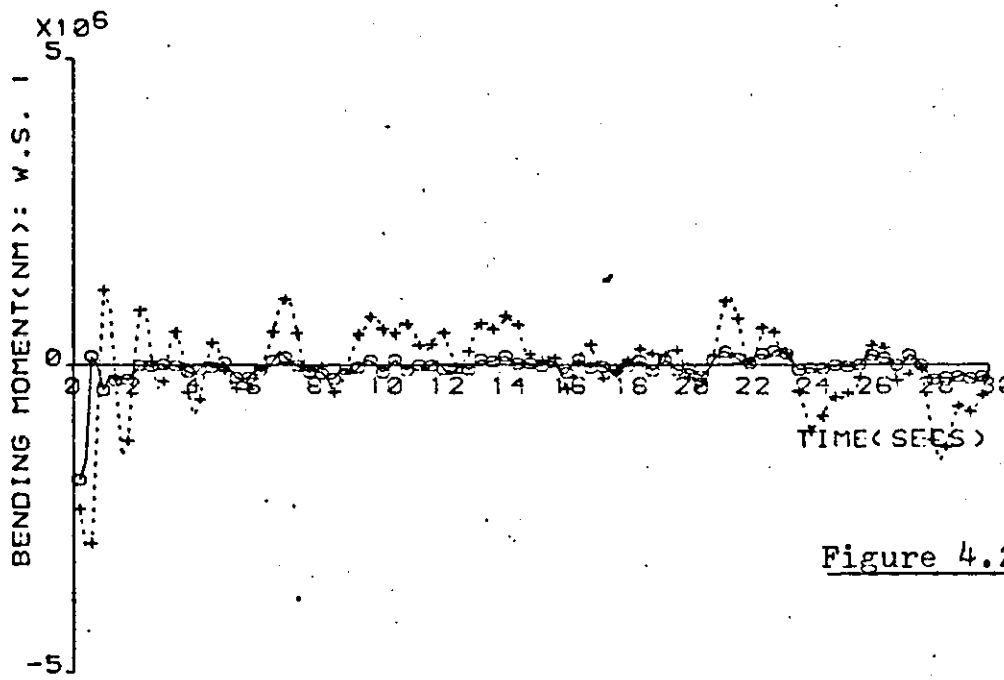


Figure 4.20b

RESPONSE TO TURBULENCE

quality of the aircraft.

4.5.1 Predicting r.m.s. reductions in Wing loads.

The method of predicting the levels of bending and torsional moment reductions achieved for an aircraft fitted with a SLACS, which was outlined in Section 3.3, was employed here for the full state feedback case. In table 4.8 is shown the percentage reductions predicted to be possible with full state feedback control. Results for each wing station are presented in the table.

	Percentage Reductions.				
	Wing Root	WS2	WS 3	WS 4	WS 5
Bending Moments	95.5	98.3	99.1	95.3	83.9
Rates of Change of Bending Moments	99.5	99.0	97.1	93.0	85.3

Table 4.8 Percentage reductions of r.m.s values of Bending and Torsional moments in the Presence of Turbulence using full state feedback control.

It is seen that the greatest reductions are possible at the mid-span although the reductions overall are quite substantial. At the wing tip, the reductions possible was somewhat less than those achievable at the other wing stations, being only 84%, at the wing root, up to 95% was possible.

CHAPTER 5 : OBSERVERS FOR THE SLACS: FULL ORDER

5.1. Introduction.

A serious impediment to any practical implementation of the SLACS considered is the requirement that the number of state variables fed back is large. Most of these variables either cannot be measured or are not physically realisable, having arisen only as a result of mathematical manipulation. Previous work reported upon in Chapter 4 showed that substantial reductions in bending moment, ($\approx$40% at the wing root) can be achieved, for the aircraft under consideration, by implementing full state-variable feedback (FSVF). However, because of the practical difficulties of implementing FSVF, a number of digital simulation studies were carried out using reduced-order feedback control. It was demonstrated, (see Section 4.4.3.), that even with 5-SVF, some reductions in bending moment, ($\approx$ 25% at the wing root), were still achievable, although further loss of state variable feedback could lead to the aircraft becoming unstable. Thus, the control law associated with 5-SVF was referred to as the 'safety law'. While the 'safety law' has the advantage of being relatively easy to synthesise, when compared with the problem of providing FSVF, the principal disadvantage associated with its use is that the same level of bending moment reductions could not be achieved as with FSVF. Another disadvantage, observed from time responses of the aircraft in deterministic situations, was that the transients associated with bending moments were

much more prolonged when compared with the transients of those responses obtained as a result of applying higher orders of feedback. A typical example of the effect different orders of feedback had upon the wing-root bending response of the aircraft was plotted in Fig. 4.13. It was considered that the oscillatory nature of the bending response, caused as a result of the safety law being operational, may affect the fatigue life of the structure, if it is accepted that fatigue accumulates according to Minor's hypothesis (Burris & Bender (1969)).

In an attempt to recover some of the advantages associated with implementing FSVF, further investigations were made at this stage in the research study to determine whether FSVF may be effectively implemented by obtaining a reconstruction of the missing state variables. There are several methods available for determining, on-line, an estimate of the state vector. One such method is due to Kalman and Bucy, (1961) where, the state vector is formed on-line by means of a Kalman-Bucy filter using available measurements of the output vector, $\underline{y}$, and of control inputs, $\underline{u}$. The filter design takes explicit account of the presence of noise due to both atmospheric turbulence effects and sensor signal measurements and is derived as a solution of a Linear Quadratic Gaussian (LQG) problem. It is well-known, (Athans (1971)), that the control law obtained from the solution of the LQG problem is identical to that obtained from the solution of the LQP (considered in this study) provided that the

same weightings on the appropriate Q and G matrices are used (see Sec. 3.2.1.). Thus, in the case where the two solutions matched, the worst that is likely to occur if the Kalman-Bucy filter was ignored, is that an increase in the performance cost, (given as Equation 3.18), would result. In practice, if strong feedback control were to be used, the resulting performance degradation is not likely to be great.

An alternative, and somewhat simpler, design approach is to use a sub-system (in a strictly deterministic setting) often referred to as a Luenberger observer (Luenberger (1966, 1971)). Like the Kalman filter, the observer has, as its inputs, the inputs and available outputs of the system whose state is to be approximated; however, the characteristics of the observer system are, to some extent free to be determined by the designer. This chapter is concerned with the theory, and test, by digital simulation, of an observer designed to reconstruct the full state vector based upon one or more of the measurements of the five state variables of the "safety law". The error between the actual state and the observed state was used to form part of a performance index (p.i.) to be minimised. Minimisation of this performance index resulted in the solution of the "gain matrix" of the observer and ensured that the error in the estimate of the state vector decayed exponentially to zero. To the knowledge of the author, neither the approach used nor the algorithm developed for the full-order observer studies has been reported in the literature, although some suggestions as to how a suitable p.i. may be set up has been sketched in Kuo (1975).

5.2. Theory.

For convenience, some of the equations used for the derivation of the full-state feedback law are repeated in this section. The flexible aircraft, subject only to commanded manoeuvres, can be described by the differential equation:

$$\dot{\underline{x}} = A\underline{x} + B\underline{u} \qquad .(5.1)$$

where $\underline{x} \in R^n$, $\underline{u} \in R^m$ and A and B are of appropriate order.

Assuming that only a few output variables (defined as the constituents of a new vector, $\underline{y}^*$), are available for measurement, a suitable output equation is:

$$\underline{y}^* = C^* \underline{x} \qquad ..(5.2)$$

where $\underline{y}^* \in R^p$. The matrix C^* depends upon which variables of the state vector were available for measurement. If, for example, only the first two variables x_1 and x_2 were available then C^* takes the form.

$$C^* = \begin{bmatrix} 1 & 0 & 0 & \ldots\ldots\ldots 0 \\ 0 & 1 & 0 & \ldots\ldots\ldots 0 \end{bmatrix} \qquad ..(5.3.)$$

In section 3.2. it was shown that the optimal feedback control was of the form†:

$$\underline{u}^o = D\underline{x} \qquad ..(5.4.)$$

Since normally only the estimated state vector, $\underline{x}_e$, and not the actual state, $\underline{x}$, will be available for feedback, and since the system will be designed so that, $\underline{x}_e$, approaches

† In this Chapter, the matrix, D, is used to denote the feedback gain matrix instead of the matrix, F, which was used in previous chapters.

$\underline{x}$; with time, $t \to \infty$, (5.4.), is written as, (5.5.), where:

$$\underline{u}^{o} = D\underline{x}_{e} \qquad t \to \infty \qquad ..(5.5.)$$

Miller (1973) has shown that a separation-type theorem holds for the design of observers where the matrix, D, is solved assuming that the full state is available for feedback; the observer design may then be considered quite separately regardless of the parameters chosen for the solution of the full state feedback problem.

Let the equation of the full-order observer for (5.1.) and (5.2.) be given by:

$$\dot{\underline{x}}_{e} = F\underline{x}_{e} + G\underline{y}^{*} + H\underline{u} \qquad ..(5.6)$$

Subtracting (5.1.) from (5.6.) and substituting for $\underline{y}^{*}$ from (5.2.) results in :

$$(\dot{\underline{x}} - \dot{\underline{x}}_{e}) = (A - GC^{*})\underline{x} - F\underline{x}_{e} + (B-H)\underline{u} \qquad ..(5.7)$$

If,

$$H = B \qquad ..(5.8)$$

and, if a stable observer can be designed, then, in the steady-state, for any control input, $\underline{u}$,

$$\underline{x} = \underline{x}_{e} \qquad ..(5.9)$$

$$F = A - GC^{*} \qquad ..(5.10)$$

Let an error vector $\underline{e}$ be defined by:

$$\underline{e} = \underline{x} - \underline{x}_{e} \qquad ..(5.11)$$

$$\therefore \quad \dot{\underline{e}} = \dot{\underline{x}} - \dot{\underline{x}}_{e} \qquad ..(5.12)$$

Using (5.8), (5.10), (5.11) and (5.12), (5.7) may be written as,

$$\dot{\underline{e}} = (A - GC^*)\underline{e} \qquad .. (5.13)$$

Thus, a stable observer will result if (A-GC*) is a stability matrix and the problem reduces to the determination of an observer 'gain matrix', G, which will ensure that the error vector, $\underline{e}$, decays to zero with time.

Consider the deterministic optimal control problem given by:

$$\dot{\underline{e}} = A'\underline{e} + C^{*\prime}\,\underline{v} \qquad ..(5.14)$$

$$J = \tfrac{1}{2}\int_0^\infty (\underline{e}'\,\hat{Q}\,\underline{e} + \underline{v}'\,\hat{R}\,\underline{v})\,dt \qquad ..(5.15)^\dagger$$

(5.14) and (5.15) defines the well-known state regulator problem. and sufficient conditions for the existence of an optimal control law for (5.14) and (5.15), are, that the pair, $[A', C^{*\prime}]$, be completely controllable and that, $\hat{R}$, be positive definite and, $\hat{Q}$, be at least non-negative definite (Kalman (1960), Athans and Falb (1966)). The optimal control law is then given by:

$$\underline{v}^o = -\hat{R}^{-1}C^*\,P\underline{e} \qquad ..(5.16)$$

where P is the positive definite solution of an algebraic matrix Riccati equation given by:

$$PA' + AP - PC^{*\prime}\hat{R}^{-1}C^*P + \hat{Q} = 0 \qquad ..(5.17)$$

Let,

$$G' \triangleq \hat{R}^{-1}C^*P \qquad ..(5.18)$$

---

† To avoid confusion with the use of G as the observer 'gain matrix', $\hat{R}$ is used in this chapter and in Chapter 6, as the weighting matrix on the control vector, $\underline{u}$.

then, substituting (5.18) into (5.16) gives:

$$\underline{v}^{o} = -G'\underline{e} \qquad ..(5.19)$$

Thus the optimally controlled system is found by substituting $\underline{v}^{o}$ of (5.19) for $\underline{v}$ in (5.14) giving:

$$\dot{\underline{e}} = (A' - C^{*'}G')\,\underline{e} \qquad ..(5.20)$$

Let,

$$S' \triangleq (A' - C^{*'}G') \qquad ..(5.21)$$

Since the eigenvalues of any square matrix, S', are the same as those of S, the stability of the closed-loop system implies that the eigenvalues of,

$$S = (A - GC^{*}) \qquad ..(5.22)$$

have negative real parts.

Equations (5.14) - (5.19) provided a design algorithm for ensuring that (5.13) was a stability matrix and that the decay of the error in the estimated state vector is, in a sense optimal depending upon the choice of weightings used for the matrices $\hat{Q}$ and $\hat{R}$ of (5.15). The design is seen to be an exact dual of that employed for the linear, time invariant, optimal state regulator problem. The controllability requirement was met by ensuring beforehand that the pair, $[A',C^{*}]$, was completely controllable or alternatively that $[A,C^{*}]$ was completely observable (Kuo, (1975)). It was also easy to select a matrix, $\hat{R}$, that was positive definite, and a matrix, $\hat{Q}$, that was at least non-negative definite in forming the performance index given by (5.15). Several solution methods of the algebraic matrix Riccati equation of the

form given by (5.17) were available although the eigenvector solution with asymtotic stability proposed by Marshall and Nicholson (1970), proved the easiest to program.

5.3. Modelling the Observed System.

Let the estimated output vector, $\underline{y}_e^*$, be given by:

$$\underline{y}_e^* = C^* \underline{x}_e \qquad ..(5.23)$$

C^* was defined in (5.2).

Substituting for F and H in (5.6) using (5.10) and (5.8) respectively, gives,

$$\dot{\underline{x}}_e = (A - GC^*)\underline{x}_e + G\underline{y}^* + B\underline{u} \qquad ..(5.24)$$

Using (5.2) and (5.23), (5.24) may be written as,

$$\dot{\underline{x}}_e = A\underline{x}_e + B\underline{u} + G(\underline{y}^* - \underline{y}_e^*) \qquad ..(5.25)$$

(5.25) shows that the observer model is very similar in structure to the original model of the aircraft, (Equation 5.1), except only that the error between the available outputs and the estimated outputs forms an additional forcing term in the observer equation.

Substituting for $\underline{y}^*$ in (5.24), using (5.2), yields (5.26) viz.,

$$\dot{\underline{x}}_e = (A - GC^*)\underline{x}_e + GC^*\underline{x} + B\underline{u} \qquad ..(5.26)$$

For the purposes of assessing the performance of the controlled aircraft incorporated with an observer, an output vector, $\underline{y}_e$, similar to that used in (2.25) is defined, i.e.

$$\underline{y}_e = C\underline{x}_e + E\underline{u} \qquad ..(5.27)$$

For the optimally controlled aircraft, the control $\underline{u}$, of (5.26) is substituted by $\underline{u}^0$, and, using (5.5), (5.26) becomes,

$$\dot{\underline{x}}_e = (A - GC^* + BD)\underline{x}_e + GC^*\underline{x} \qquad ..(5.28)$$

In the controlled situation, it should be still possible to manoeuvre the aircraft to some desired flight state; for example in response to a demand for a certain value of vertical velocity. Such demands were considered by using an additional forcing vector, $\underline{r}$, acting through a matrix H^* as had been used in earlier studies. (See Section 4.4)

(5.1) was therefore augmented after substituting for $\underline{u}$ using (5.4). Thus,

$$\dot{\underline{x}} = (A + BD)\underline{x} + H^*\underline{r} \qquad ..(5.29)$$

The output equations were also written in the form,

$$\underline{y} = (C + ED)\underline{x} \qquad ..(5.30)$$

$$\underline{y}_e = (C + ED)\underline{x}_e \qquad ..(5.31)$$

(5.28) and (5.29) and also (5.30) and (5.31) were combined to allow comparison, by digital simulation, of the controlled aircraft without and with the observer incorporated, viz.,

$$\begin{bmatrix} \dot{\underline{x}} \\ \dot{\underline{x}}_e \end{bmatrix} = \begin{bmatrix} A + BD & 0 \\ GC^* & A + BD - GC^* \end{bmatrix} \begin{bmatrix} \underline{x} \\ \underline{x}_e \end{bmatrix} + \begin{bmatrix} H^* \\ 0 \end{bmatrix} \underline{r} \qquad ..(5.32)$$

$$\begin{bmatrix} \underline{y} \\ \underline{y}_e \end{bmatrix} = \begin{bmatrix} C + ED & 0 \\ 0 & C + ED \end{bmatrix} \begin{bmatrix} \underline{x} \\ \underline{x}_e \end{bmatrix} \qquad ..(5.33)$$

A block diagram of the observed system is shown in Fig 5.1.

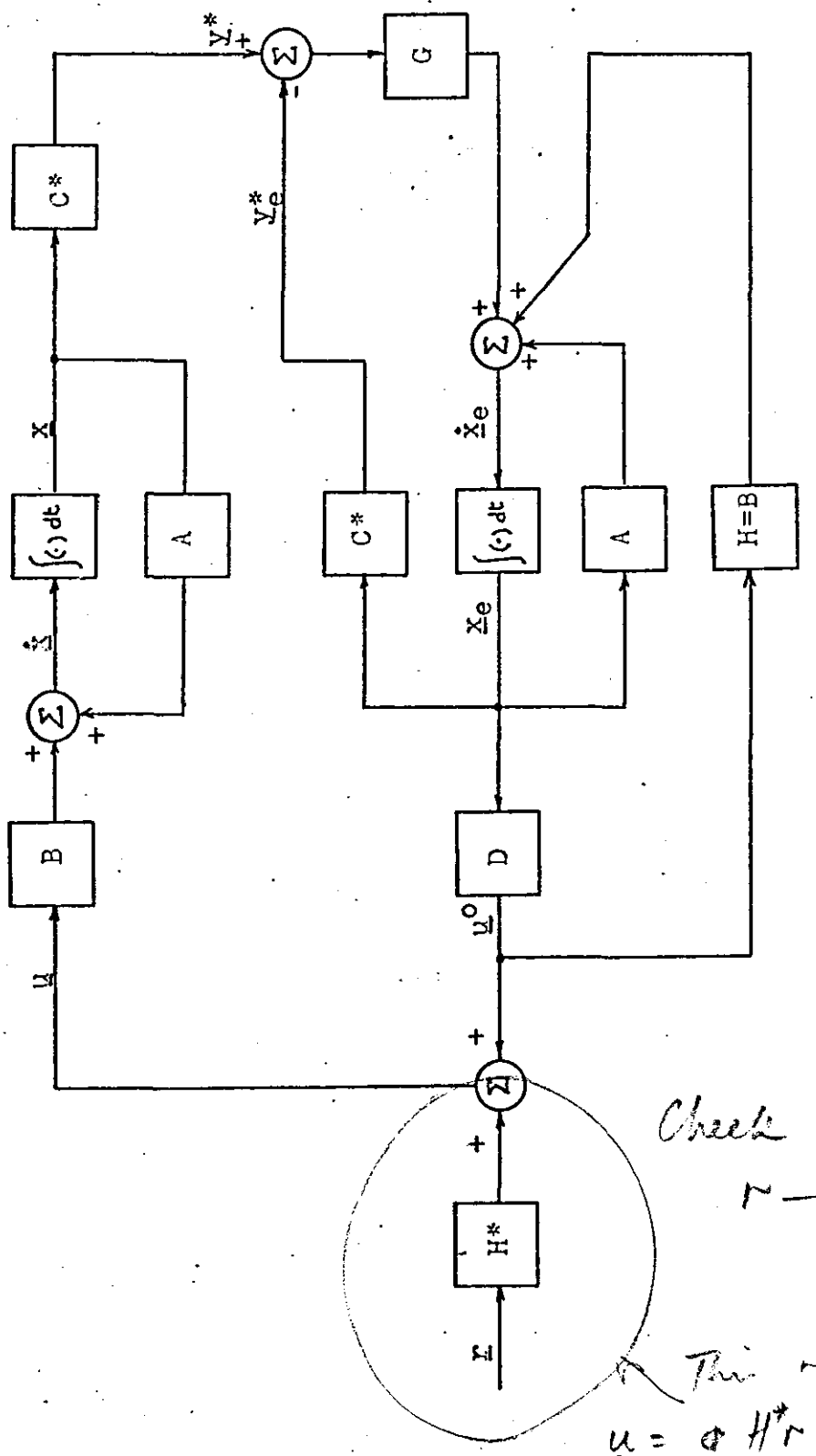


Figure 5.1: BLOCK DIAGRAM OF THE OBSERVED SYSTEM

Check where r — [H] — $\dot{x}$ goes

This results in $u = \phi H^* r + D x_e$

where as Section 9.4

$\dot{x} = Ax + Bu$
$u = Dx$

$\dot{x} = (A+BD)x + Hr$

5.4. Selection of Observer Weighting Matrices.

Equations (5.32) and (5.33) were used to assess the performance of the observer design. Only deterministic test situations were considered. Once all the observer parameters had been solved, it was decided that the relevant matrices of (5.32) and (5.33) be formed directly to allow simultaneous comparison of full state-variable feedback (FSVF) with full reconstructed state-variable feedback (FRSVF). Simultaneous comparison implied that the order of a particular model studied was effectively doubled. For CLEMENTI, this would have meant computations on a system with a state vector of dimension, 48, and an output vector of dimension, 76. Since the model, FAURÉ differed from CLEMENTI only in the absence of Küssner dynamics and since in all deterministic tests made, the bending responses associated with FAURÉ did not differ significantly from those obtained with CLEMENTI (see Figs. 4.13 - 4.16) it was considered that FAURÉ was adequate enough for the purposes of testing the observer design. In the case where the controlled aircraft with FRSVF is to be further tested, in response to simulated atmospheric turbulence, the Küssner dynamics would have to be reincluded. i.e. the model CLEMENTI will have to be used.

Thus the chosen system, based upon FAURÉ, had a state vector of dimention, 34, and an output vector of dimension, 76. Previous tests (see Sec. 4.4.3) had shown that the model, FAURÉ was not completely controllable. This was found to be

due to the presence of the state associated with the outboard elevator servo in the state description of FAURÉ. The lack of complete state controllability did not however prevent a feedback law from being determined. Also the resulting closed-loop system was stable as will be evident from the eigenvalue tables to be presented later in this section.

The weighting matrices associated with the determination of the optimal control law for the model FAURÉ were chosen to be:

$$\hat{Q} = \text{diag} \left\{ \begin{array}{ccccc} 0.1E\text{-}6 & 0.5E\text{-}6 & 0.1E\text{-}8 & 0.5E\text{-}7 & 0.1E\text{-}6 \\ 0.5E\text{-}6 & 0.1E\text{-}8 & 0.5E\text{-}7 & 0.1E\text{-}8 & 0.5E\text{-}7 \\ 1.0E\text{-}8 & 1.0E\text{-}9 & 1.0E\text{-}8 & 1.0E\text{-}9 & 1.0E\text{-}8 \\ 1.0E\text{-}9 & 1.0E\text{-}8 & 1.0E\text{-}9 & 1.0E\text{-}8 & 1.0E\text{-}9 \\ .01.01 & .01 & .01 & .01 & .01 \quad .01 \quad .01 \quad .01.01 \quad .01 \\ 1 & 1 & 10 & 10 & 10 \quad 0.5 \end{array} \right\}$$

..(5.34)

$$\hat{R} = \text{diag} \{.01 \quad .01\}$$

The corresponding control law was found to be:

$$\underline{u}^o = \left[\begin{array}{cccccccc} -.019 & -.0052 & .031 & .010 & .126 & -.161 & -.030 & .154 \\ .012 & .039 & .298 & -.250 & -.897 & 3.142 & -17.44 & -13.80 \quad -3.068 \\ -.044 & -.003 & -.433 & .118 & 1.296 & -0.943 & -.480 & 1.188 \\ -.121 & -.089 & -1.734 & -.975 & .600 & 1.220 & -101.30 & -377.7 \quad -67.6 \end{array} \right] \underline{x}$$

..(5.36)

The computer program, RAPEST, (Appendix IV), was used to evaluate the observer matrices together with the relevant matrices of (5.32) and (5.33) in order to allow assessment by digital simulation to be made. RAPEST was used to evaluate the matrix, P, of (5.17) by the eigenvector solution method

proposed by Marshall and Nicholson (1966). Once the matrix, P, had been obtained, the 'observer gain matrix', G, was easily evaluated using (5.18) The solution of, P, required that suitable weighting values be assigned to the matrices $\hat{Q}$ and $\hat{R}$ of (5.15). The dimensions of, $\hat{Q}$, which was square, were the same as the dimension of the state vector while the dimension of, $\hat{R}$, depended upon the number of state variables assumed available for measurement. As an example, a typical weighting scheme chosen for solution of the observer matrices for the model FAURÉ, assuming only the measurement of the vertical velocity, w , was to be used, is:

$$\hat{Q} = \text{diag} \begin{Bmatrix} 5.0 & 5.0 & & & & \\ .01 & .01 & .01 & .01 & .01 & .01 \\ .01 & .01 & .01 & .01 & .01 & .01 \\ 10 & 10 & 10 & & & \end{Bmatrix} \qquad ..(5.37)$$

$$\hat{R} = \{2.0\} \qquad ...(5.38)$$

The corresponding observer gain matrix was evaluated as:

$$G = \begin{bmatrix} 32.2 & 229.0 & -291.0 & 24.0 & 170.0 & 171.0 \\ 44.5 & -41.8 & -2.24 & 0.486 & 2.64 & 8.32 \\ 1.99 & -3.44 & -0.88 & -2.26 & -0.318 & \end{bmatrix} \qquad ..(5.39)$$

In Table 5.1. is shown the eigenvalues of the observer matrix, S, of (5.22) when compared with the eigenvalues of the controlled aircraft with FSVF. It is seen that the real parts of the eigenvalues of the observer should at least have been greater than those of the eigenvalues of the controlled aircraft (considered in this case to be adequately represented by the model FAURÉ). This observer design was nevertheless tested

with the controlled aircraft by means of digital simulation and using the same deterministic test situations employed previously (Table 4.1).

	FAURÉ	OBSERVER
Short Period Mode	$-.985 \pm j0.785$	$-.517 \pm j5.45$
Bending Mode 1	$-3.37 \pm j8.60$	$-.225 \pm j11.10$
" " 2	$-0.22 \pm j11.12$	$-.442 \pm j13.30$
" " 3	$-2.12 \pm j14.7$	$-.908 \pm j15.50$
" " 4	$-0.37 \pm j17.6$	$-.395 \pm j17.50$
" " 5	$-2.31 \pm j18.8$	$-.529 \pm j18.70$
" " 6	$-35.2 \pm j23.7$	$-12.50 \pm j32.4$
Inboard Elevator Servo	-2860.0	-23.3
Outboard Elevator Servo	-7.5	-7.5
Aileron Servo	-5.98	-6.06

Table 5.1: Comparison of Eigenvalues: FAURÉ (FVSF) with OBSERVER

5.5 Time Response Tests.

The same test situations that were used earlier, (see Table 4.4) were used again here to evaluate the performance of the 'observed' system. All comparisons were made using the model FAURÉ. The particular type of feedback used was distinguished by FSVF, (assuming all the variables of the state vector could be measured directly), and by FRSVF, assuming that the variables of the state vector were reconstructed by an observer of the type reported upon in this chapter. In Figs. 5.1 - 5.4 are shown comparative responses* using FSVF and FRSVF for test situations A - C. In order to produce a reconstruction of the state vector, only a measurement of vertical velocity, w was required by this particular observer design; also all initial conditions were set to zero. It is remarkable how effective was the observer in predicting the state and as a consequence, the output of the original system.

In a number of reports, (Newmann(1970), Arimoto and Hino (1974)), it has been suggested that the performance of an observer will deteriorate substantially if the initial conditions on its states are not matched with those of the system being observed. In an attempt to confirm the validity of this proposition, a number of tests were made for the situation

---

* Only the wing root bending moment together with either pitch rate (q) or vertical velocity (w) are plotted although the other responses were found to be just as closely matched.

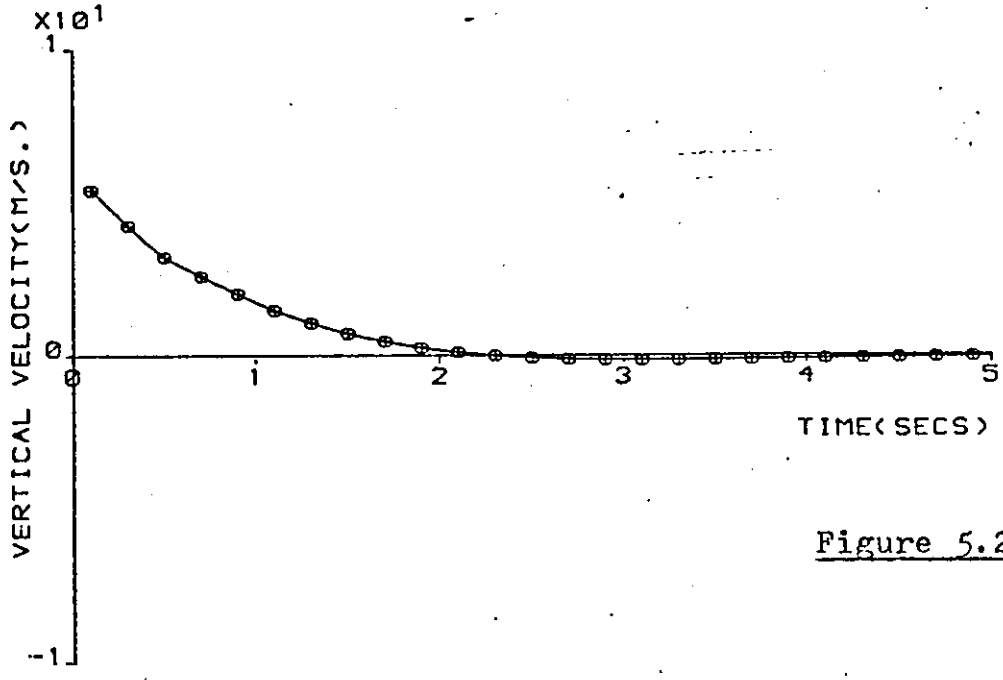


Figure 5.2a

+ FSVF
o RSVF

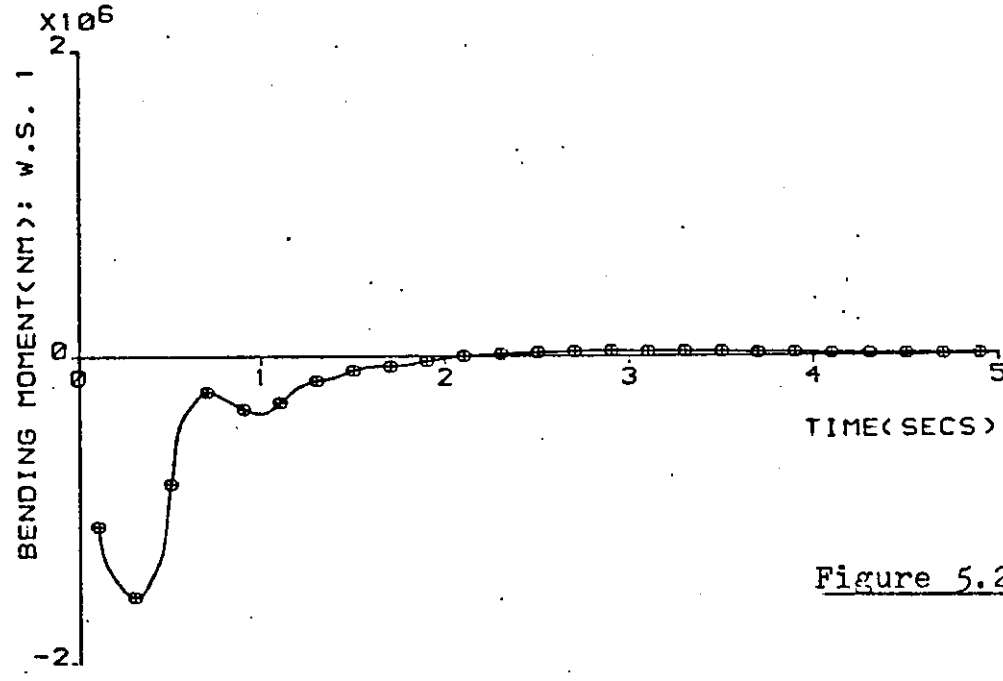


Figure 5.2b

COMPARISON RESPONSE: FSVF WITH FULL-ORDER OBSERVED SYSTEM: CASE

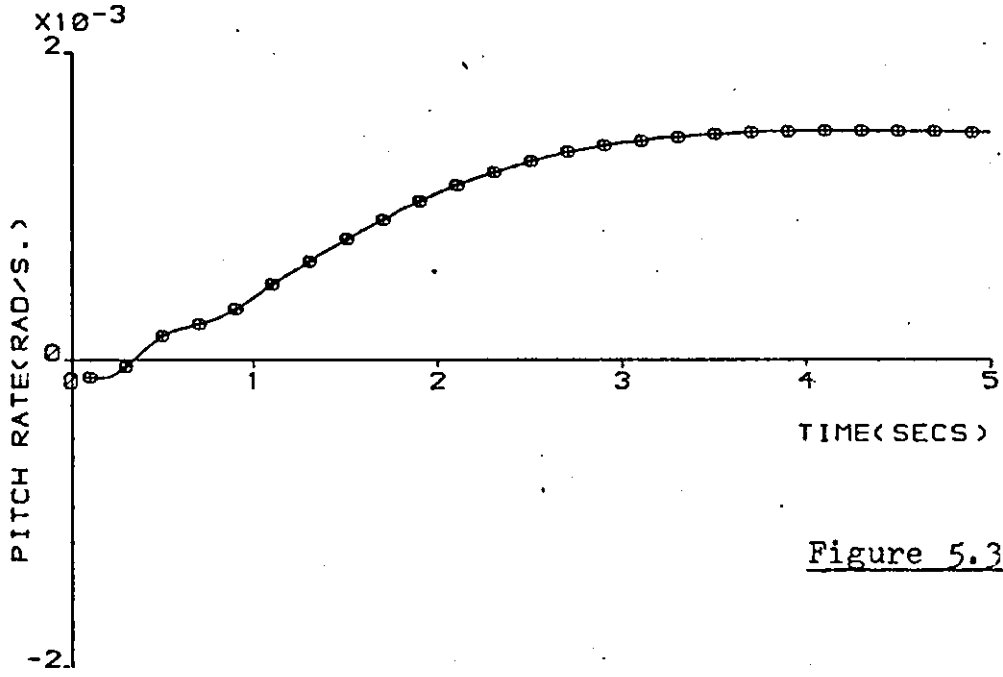


Figure 5.3a

+ FSVF
o RSVF

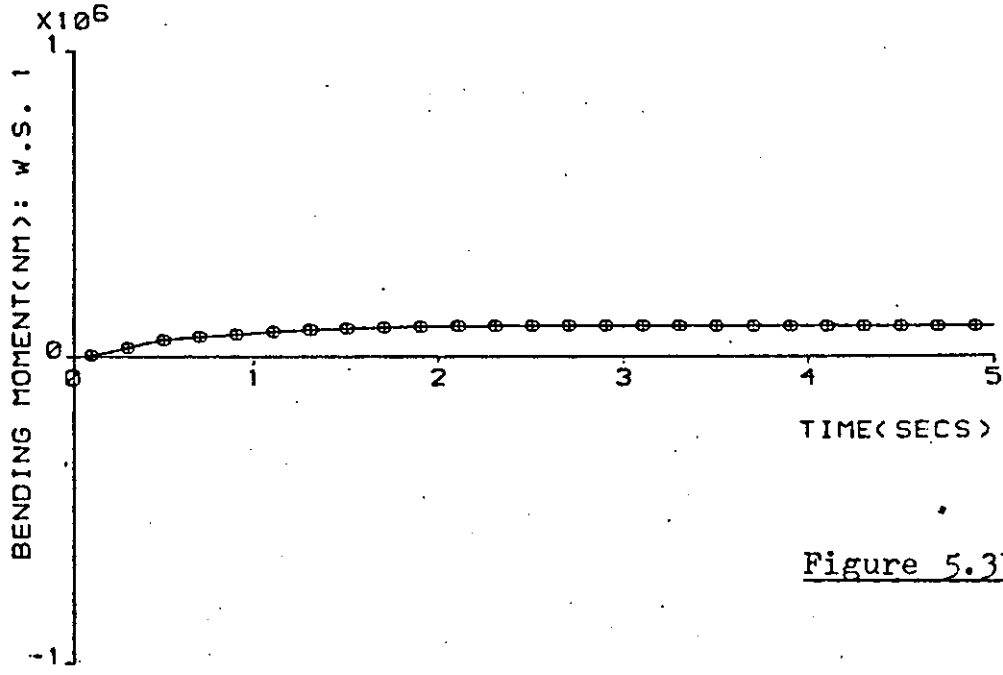


Figure 5.3b

COMPARISON RESPONSE: FSVF WITH FULL-ORDER OBSERVED SYSTEM: CASE B

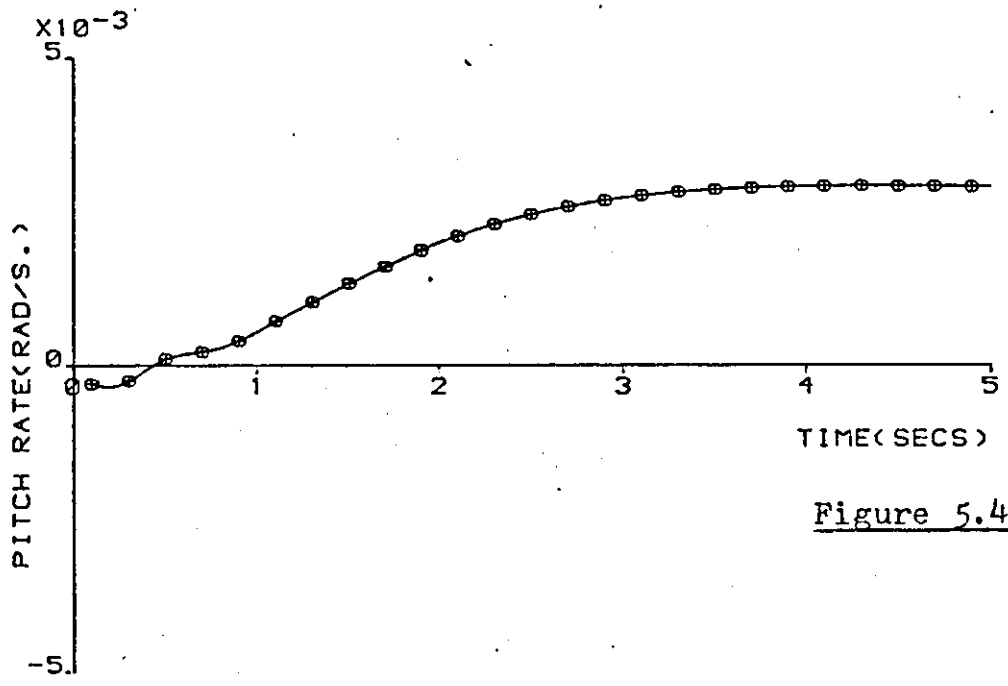


Figure 5.4a

+ FSVF
o RSVF

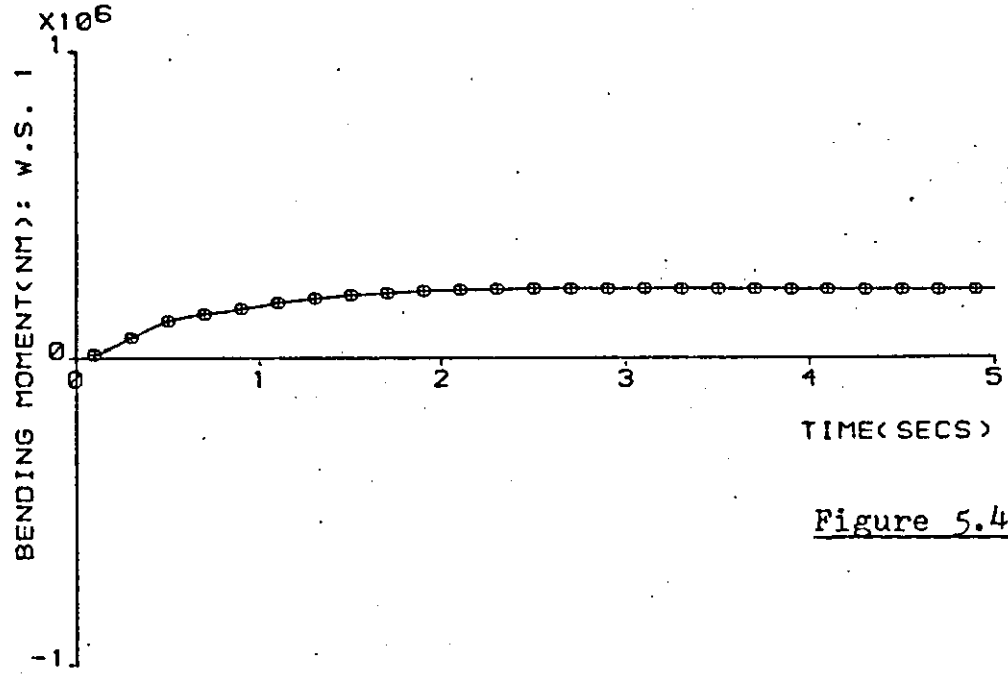


Figure 5.4b

COMPARISON RESPONSE: FSVF WITH FULL-ORDER OBSERVED SYSTEM: CASE C

where the initial conditions of the observer did not agree exactly with those of the model being observed. Figure 5.5 shows the case where all the initial states of the observer were set to zero and the aircraft was considered to have an initial pitch rate of about 0.06 rad.s^{-1}. The plots indicate that the observer dynamics are not fast enough to cope with the mismatch in initial conditions, a result which was evident when the eigenvalues were compared in Table 5.1. The observer design was however found to be less sensitive to a mismatch of initial conditions on inboard elevator deflection. Such a result is evident from Figure 5.6, where, the initial states of the observer were again set to zero and the inboard elevator was considered to have an initial deflection of about 0.1 rad. When there was a mismatch of initial conditions on vertical velocity, (w), substantial variations on wing root bending moment occurred (Figure 5.7) before the observer transients decayed. These large variations may in some manner be related to the original specification of the particular observer design being tested, i.e. reconstruction of the system state was achieved by using measurements of vertical velocity, (w) . A number of tests made using observer designs based upon the availability of other measurements viz., q, δ_A and δ_{E_i} are reported upon later in this section.

In an attempt to reduce the sensitivity of the observer to mismatching of initial conditions, further tests were made using only different choices of the weighting matrices assoc-

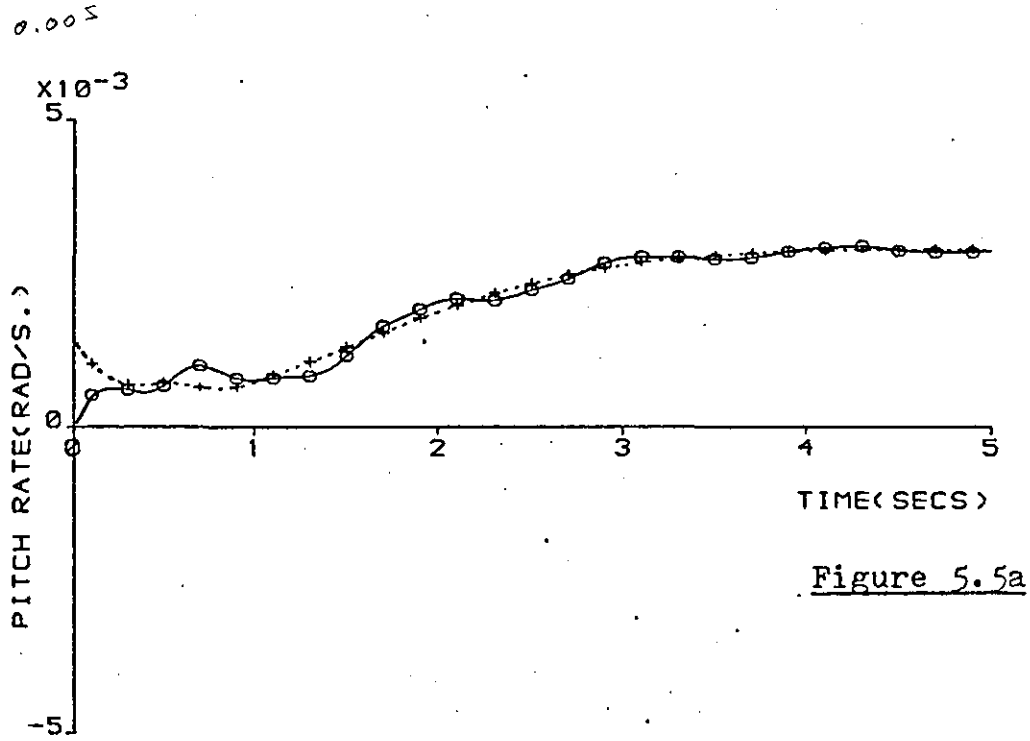


Figure 5.5a

+ FSVF
o RSVF

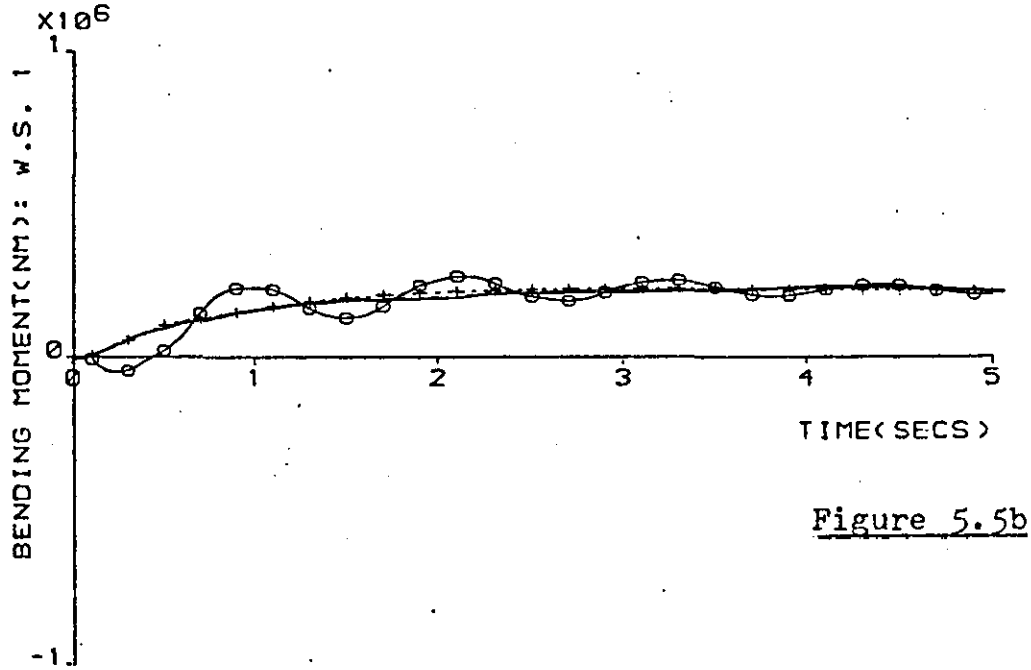


Figure 5.5b

EFFECT OF MISMATCH IN INITIAL CONDITIONS ON PITCH RATE

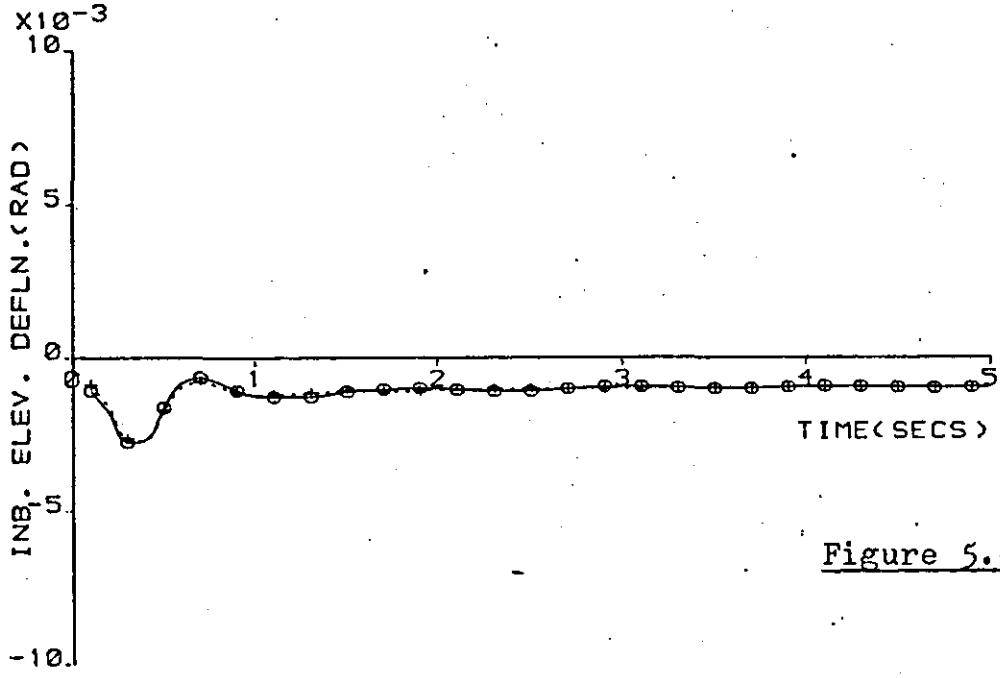


Figure 5.6a

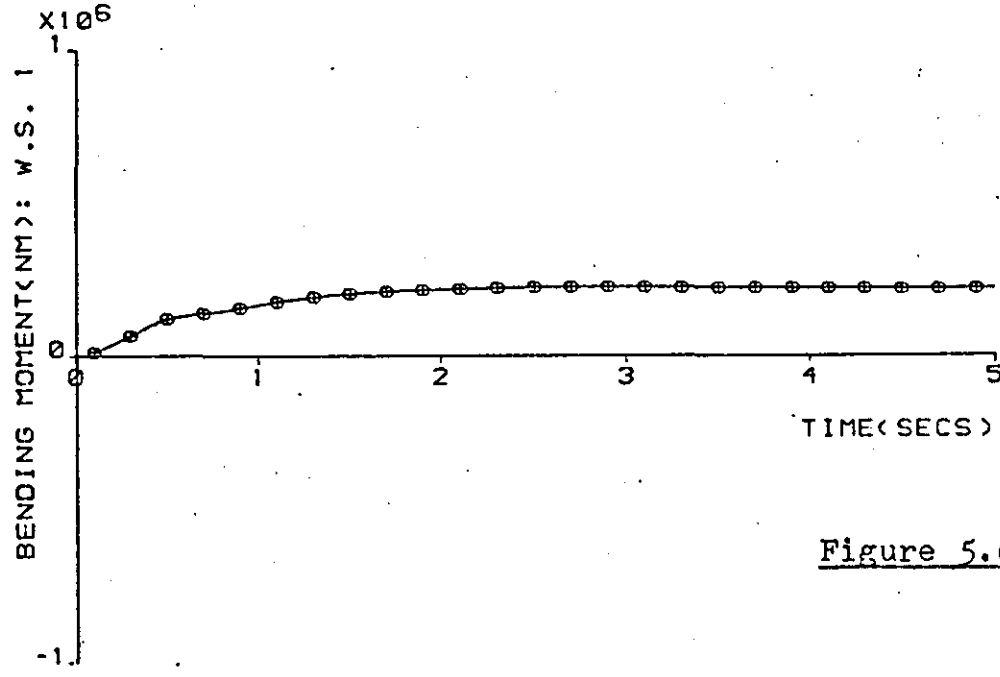


Figure 5.6b

EFFECT OF MISMATCH IN INITIAL CONDITIONS ON INBOARD ELEVATOR DEFLECTION.

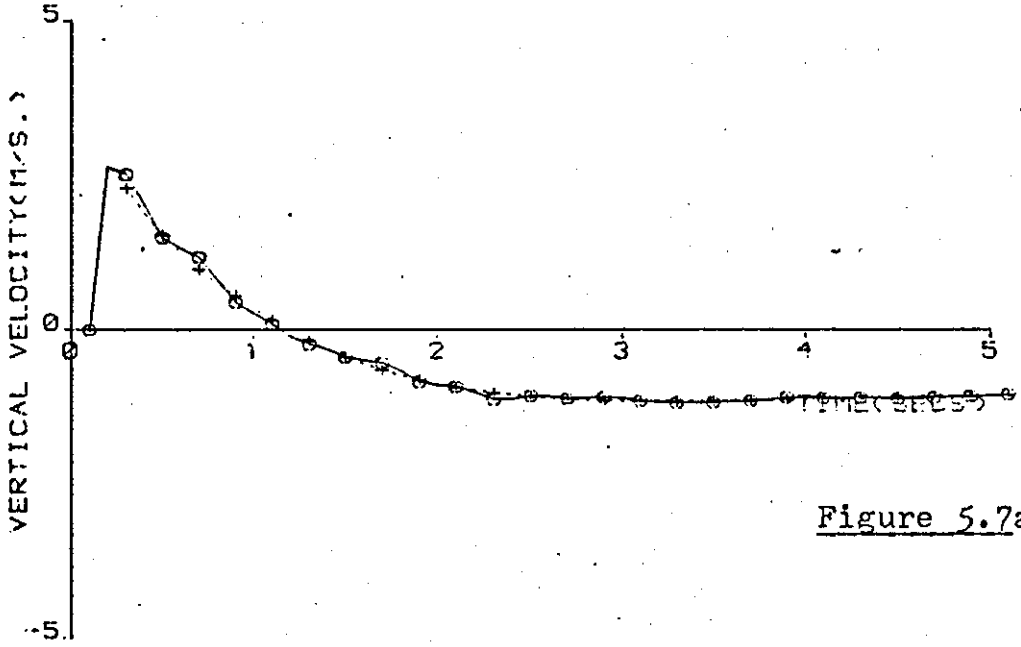


Figure 5.7a

+ FSVF
o RSVF

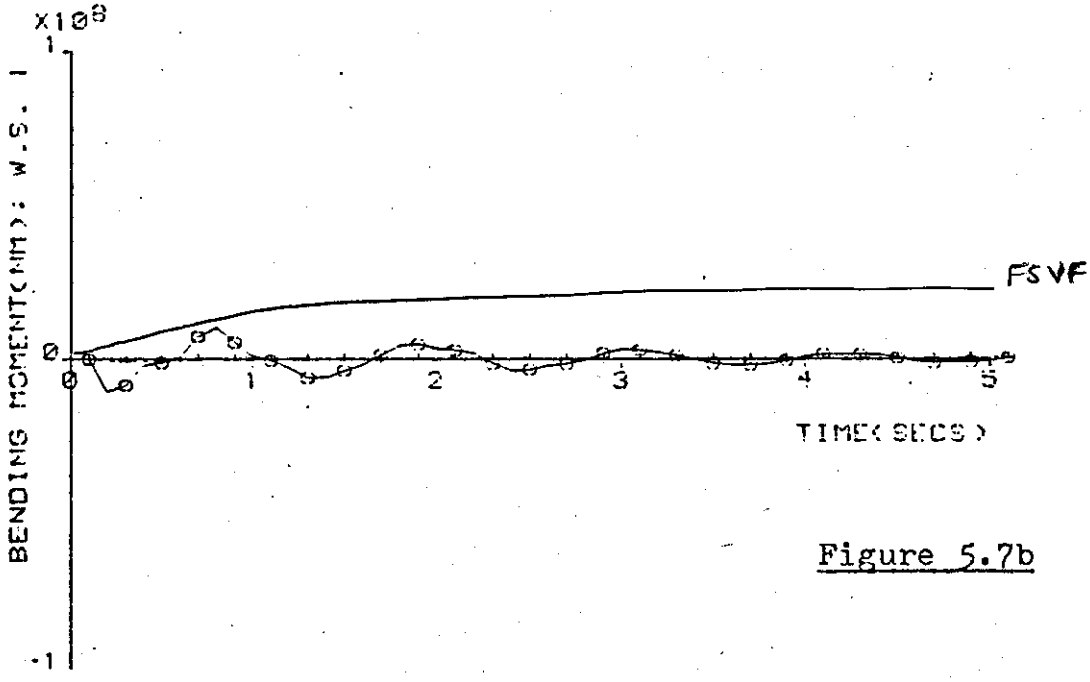


Figure 5.7b

EFFECT OF MISMATCH IN INITIAL CONDITIONS ON VERTICAL VELOCITY

iated with the design. It was found that in general, it was possible to obtain a desired set of dynamics associated with each observer design although it was not possible to establish any fixed pattern for a suitable choice of weighting matrices. A workable design can therefore result from carrying out a large number of test computer runs, during which, both the locations of the observer's eigenvalues and its response need to be checked.

A representative set of tests is shown in Figures 5.8 - 5.10, where, the same disparities in initial conditions, used earlier for tests shown in Figures 5.5 - 5.7, have been implemented. In general, it is seen that the settling time of the observer design has been reduced to within three seconds although the transient excursions experienced are much higher when compared with those obtained in the previous design. To achieve this reduced settling time, the error weightings on vertical velocity, w, and pitch rate, q, had to be increased. However, there was a limit as to how much these weightings could be increased as it was not then possible to obtain a solution to the Riccati equation (5.17).

Most of the tests used until now were repeated for the condition where only the pitch rate, q, was available for measurement. The tests however did not record any significant change in the observer performance when compared with that of the former design based upon the availability of vertical velocity, w, for measurement.

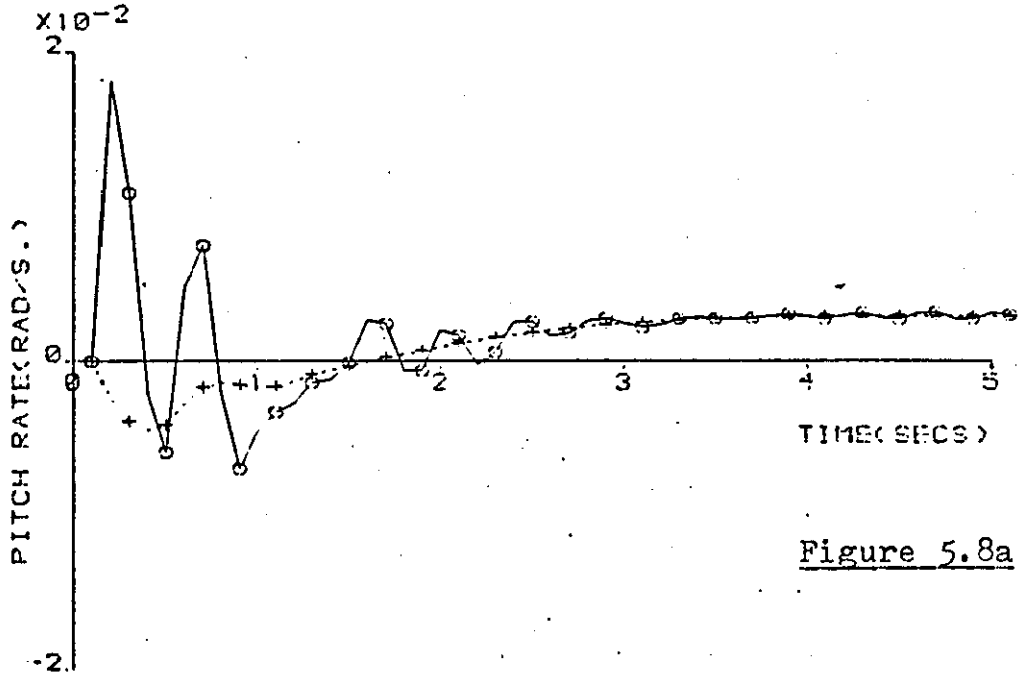


Figure 5.8a

+ FSVF
o RSVF

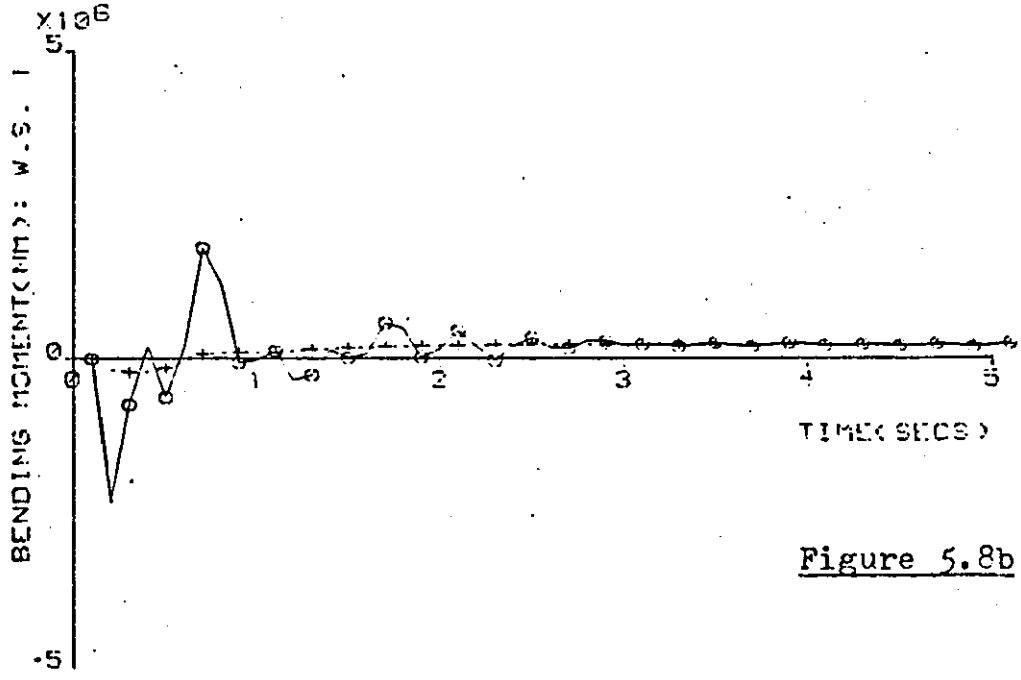


Figure 5.8b

EFFECT OF MISMATCH IN INITIAL CONDITIONS ON PITCH RATE

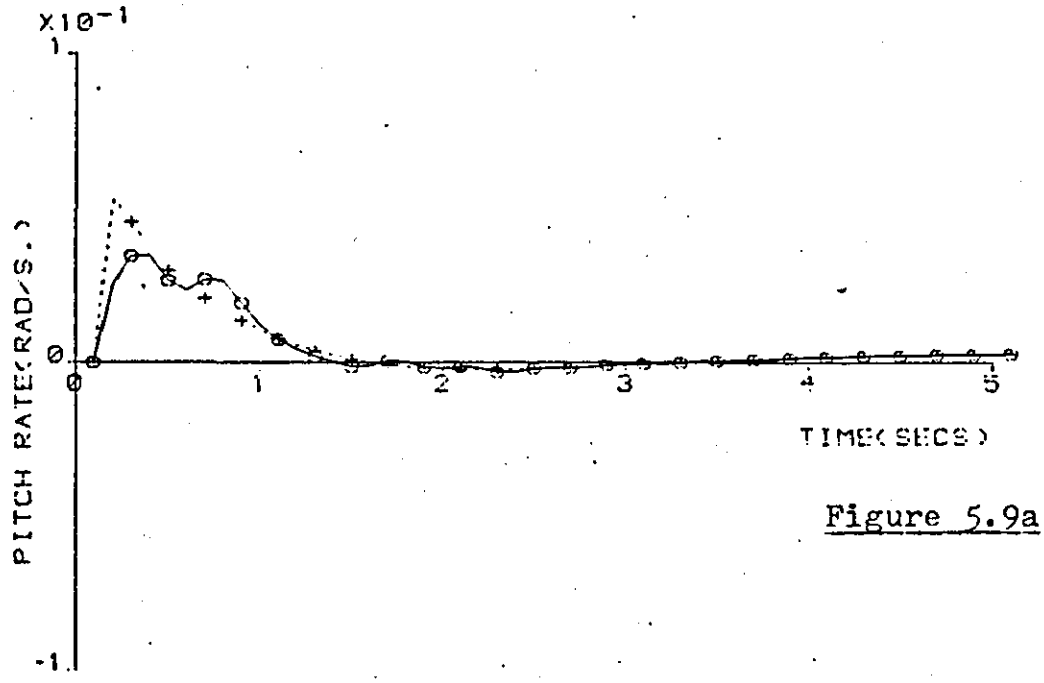


Figure 5.9a

+ FSVF
o RSVF

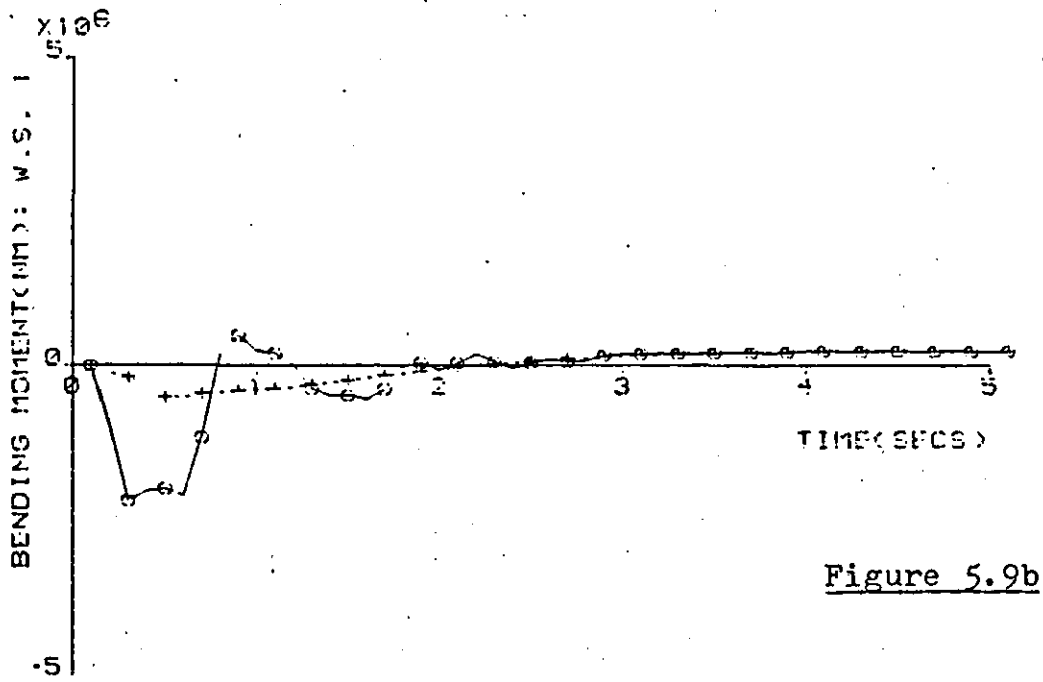


Figure 5.9b

EFFECT OF MISMATCH IN INITIAL CONDITIONS ON INBOARD ELEVATOR DEFLECTION.

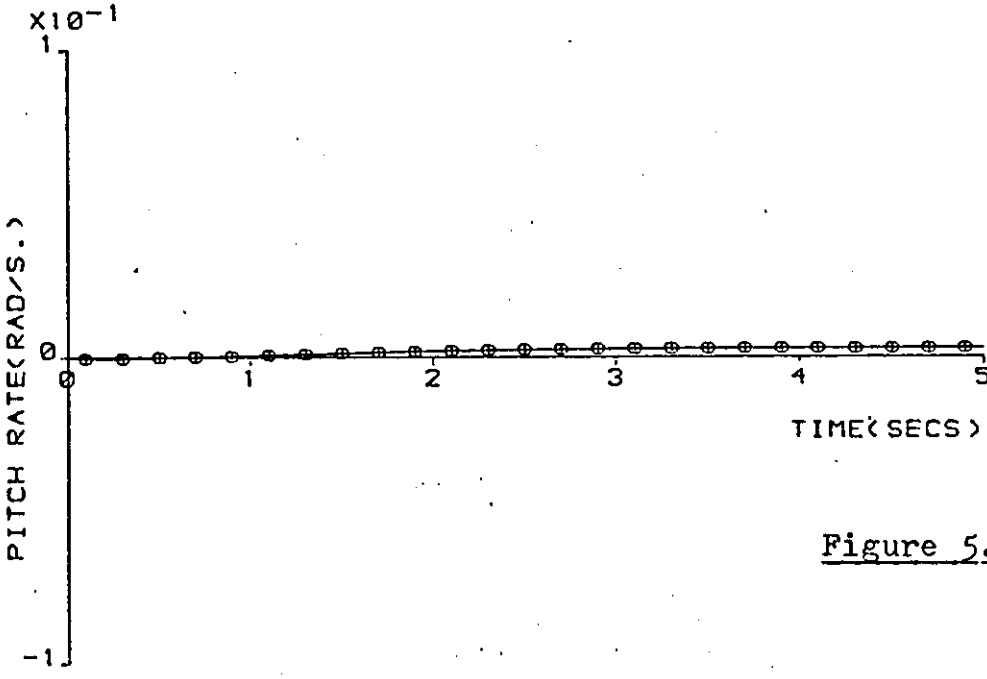


Figure 5.10a

+ FSVF
o RSVF

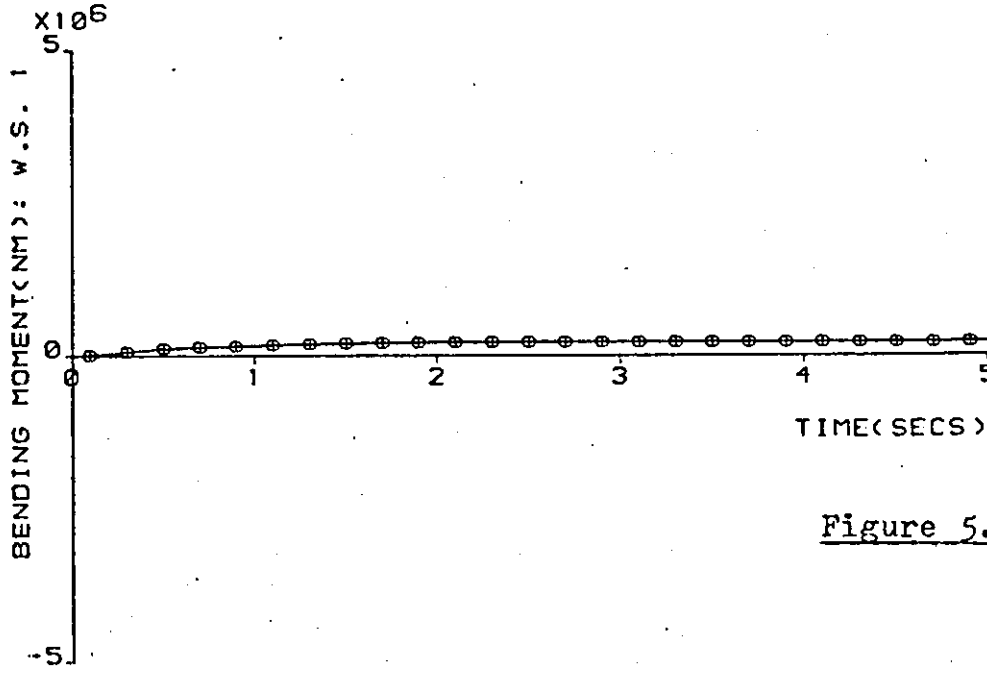


Figure 5.10b

EFFECT OF MISMATCH IN INITIAL CONDITIONS ON VERTICAL VELOCITY

A number of checks were made to determine the effect of making more sensor signals available for measurement. Two such checks are presented here, where it is assumed that:

(i) both w and q were available simultaneously for measurement, and,

(ii) the signals $w, q, \delta_A, \delta_{E_i}$, were all being measured.

A set of example results are presented below. For test (i), the weighting matrices were chosen to be:

$$\hat{Q} = \text{diag} \left\{ \begin{matrix} 1.0E{+}4 & 1.0E{+}7 & 1.0E{-}2 & 1.0E{-}2 & 1.0E{-}2 & 1.0E{-}2 \\ 1.0E{-}2 & 1.0E{-}2 & 1.0E{-}2 & 1.0E{-}2 & 1.0E{-}2 & 1.0E{-}2 \\ 1.0E{-}2 & 1.0E{-}2 & 25.0 & 10.0 & 10.0 & \end{matrix} \right\} \quad ..(5.40)$$

$$\hat{R} = \text{diag} \{2 \quad 10\} \quad ..(5.41)$$

The observer 'gain matrix' was found to be:

$$G = \begin{bmatrix} 77.6 & 17.4 & 59.1 & 17.4 & 155.0 & .280 & 1.01 & 24.4 & -82.7 \\ .958 & 3.64 & 9.15 & .657 & -.089 & -1.48 & -.587 & -.096 & \\ 3.51 & 999.0 & -7.76 & 2.40 & 7.71 & 6.30 & 2.79 & -2.59 & \\ -.282 & .173 & 0.40 & 0.76 & 0.135 & -.204 & -.0503 & & \\ -0.127 & -.022 & & & & & & & \end{bmatrix} \quad ..(5.4\ )$$

For test (ii), the weighting matrices were chosen to be:

$$\hat{Q} = \text{diag} \left\{ \begin{matrix} 1.0E{+}4 & 1.0E{+}6 & 1.0E{-}2 & 1.0E{-}2 & 1.0E{-}2 & 1.0E{-}2 \\ 1.0E{-}2 & 1.0E{-}2 & 1.0E{-}2 & 1.0E{-}2 & 1.0E{-}2 & 1.0E{-}2 \\ 1.0E{-}2 & 1.0E{-}2 & 5.0E{+}1 & 1.0E{+}2 & 1.0E{+}1 & \end{matrix} \right\} \quad ..(5.4\ )$$

$$\hat{R} = \text{diag}\{1.0E\text{-}1 \quad 1.0E\text{-}1 \quad 1.0E\text{-}3 \quad 1.0E\text{-}3\} \qquad ..(5.44)$$

The corresponding observer 'gain matrix' was calculated to be:

$$G = \begin{bmatrix} 1000.0 & 4.35 & -24.6 & 11.3 & 139.0 & 68.4 & -3.97 & 2.04 \\ -24.6 & -7.40 & 3.74 & 16.5 & .615 & -.761 & -4.07 & -4.42 \\ -2.23 & & & & & & & \\ 4.35 & 10000.0 & -53.3 & 10.4 & 74.3 & 69.3 & 26.6 & -42.3 \\ -6.08 & .724 & 2.32 & 1.91 & 0.667 & -.954 & -1.21 & -7.43 \\ -2.52 & & & & & & & \\ -40.8 & -12.1 & -3300.0 & -16.5 & -1280.0 & 808.0 & 23.3 & \\ -386.0 & -3.03 & 14.7 & 20.7 & 2.15 & -1.95 & 1.66 & 217.0 \\ -.503 & -.534 & & & & & & \\ -44.2 & -74.3 & 1380.0 & -69.6 & -2450.0 & -2370.0 & -228.0 & \\ 1110.0 & -1.25 & 2.80 & 6.73 & 12.4 & -16.3 & -9.42 & -.501 \\ 308.0 & -0.884 & & & & & & \end{bmatrix} \qquad (5.4$$

The comparative time responses corresponding to tests (i) and (ii) are shown in Figures 5.11 and 5.12 respectively. It appears that, as would be expected, the availability of more measurements had a beneficial effect upon the aircraft response. With only w and q available as measurements, (Figure 5.11), the bending moments experienced in the wing of the aircraft are initially quite severe although the transients oscillations decay rather faster than those associated with measurements of all four signals, (Figure 5.12). However it will be noticed that some of the elements of the observer gain matrix for test (ii), (5.45), are very large, ($\gg 10^3$), when compared with those of test (i), (Equation 5.42). It would in practice be inappropriate to use gains $>10^2$ because not only the pure signal will be amplified but so is any noise present

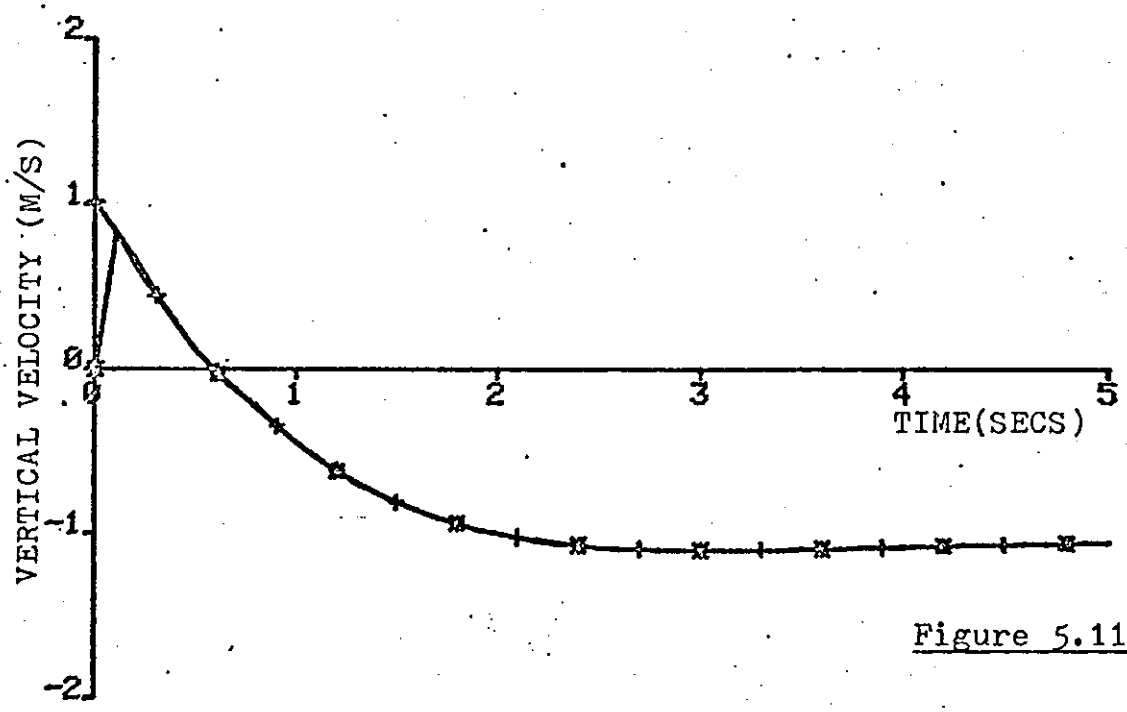


Figure 5.11a

+ FSVF
* RSVF

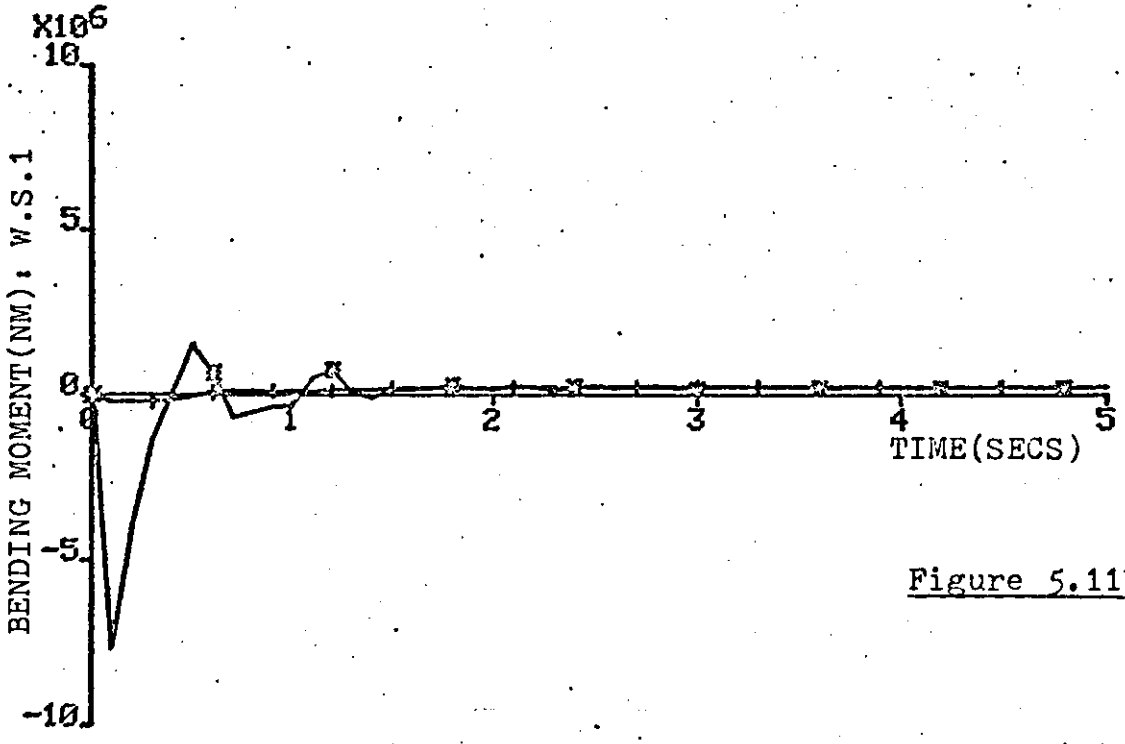


Figure 5.11b

RESPONSES OBTAINED WITH A RECONSTRUCTION ON w AND q.

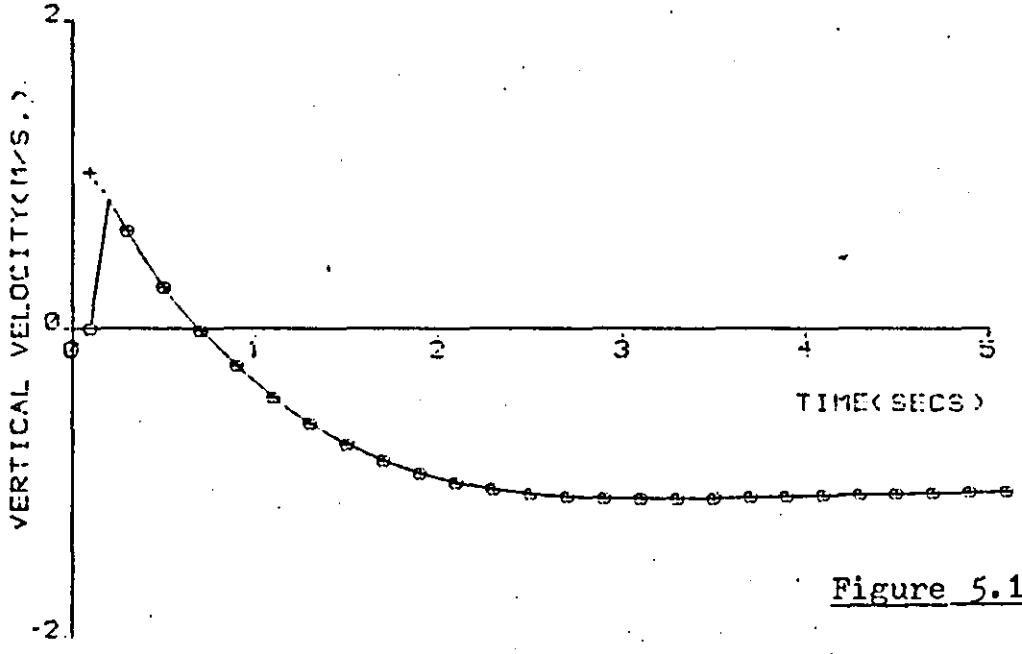


Figure 5.12a

+ FSVF
o RSVF

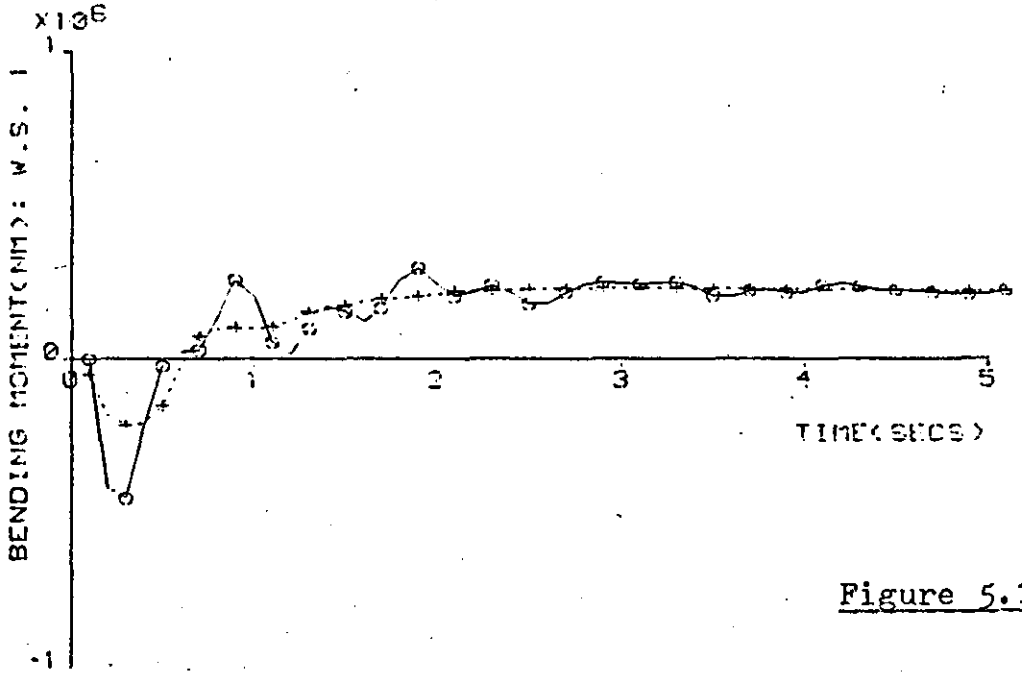


Figure 5.12b

RESPONSES OBTAINED WITH A RECONSTRUCTION ON w,q, δ_A and δ_{E_i}.

in the feedback path. Thus the results of Figure 5.12, although the best so far, even in situations where there are great disparities between initial conditions, cannot be guaranteed with the observer design considered for test (ii). However, it is possible that further experimentation with different weightings on the $\hat{Q}$ and $\hat{R}$ matrices may produce a workable design with the type of performance demonstrated in Figure 5.12.

CHAPTER 6: OBSERVERS FOR THE SLACS: REDUCED ORDER.

6.1 Introduction.

The full-order observer designs considered in the previous chapter were all extremely sensitive to mismatching of initial conditions between the state vector of the aircraft and those of the observer model. Unless the initial conditions were perfectly matched, the observer could not be relied upon to accurately estimate the system state with the result that the peak structural loads experienced in the wing of the aircraft tended to be high. Although it was possible to design by numerical experimentation an observer with a fast or slow settling time, it was not always possible to, in addition, reduce the peak levels of bending and torsional oscillations induced at every wing station.

In this chapter, studies made on an optimal reduced - order observer design are reported. It was considered that if an observer were to be used to provide some measure of reliability, (in software), to the SLACS in reconstructing any missing feedback signals, then it would be wasteful of computer storage and time to reconstruct signals which were in any case already being measured. Such was the case of the full-order observer designs considered earlier, (see Chapter 5), where those signals associated with the 'safety law' were being reconstructed within the observer system. For the implementation of a SLACS it is expected that the presence of those motion variables connected with the

'safety law' will always be guaranteed by using a suitable hardware redundancy scheme. Thus it will not be necessary to re-construct these signals using an observer; furthermore, a reduced-order observer will pose a much simplified synthesis problem. Since it was important that the aircraft with observer system should perform comparably with the FSVF designs considered earlier, (see Chapter 4), only reduced-order observer designs using optimal control techniques were investigated.

The problem of the decrease in performance of the optimal regulator when an observer is incorporated to estimate some or all of the state variables of a linear system occupied the interest of many authors* for over a decade. However, it was the paper of Sarma and Deekshatulu (1968) which encouraged further interest in performance deterioration due to the use of observers. A number of errors in this paper led to an incorrect expression for the decrease in performance of the observed system. Porter and Woodhead (1968) have published as part of their paper, a corrected version of the problem considered by Sarma and Deekshatulu, but it was Newmann(1969) who further suggested that the result of Sarma and Deekshatulu was incorrect due to a misunderstanding of the way in which errors arise when using an observer.

In a second paper, Newmann (1970) considered two separate optimal control approaches to the design of observers for

---

* See Eisenberg and Sage (1966), Sims and Melsa (1968), Burns and Kumar (1967), Bongiorno and Youla (1968).

linear systems using quadratic performance measures. One approach constrained the feedback gain to be the gain matrix, which solves the quadratic optimal control problem assuming that complete state measurements were available. The second approach left the feedback matrix as a design variable in the specific optimal control problem. Miller (1973) showed that due to an error in Newmann's paper, (Newmann (1970)), the two approaches considered led to different results and further showed that the optimal feedback gain matrix was the same whatever the approach. Arimoto and Hino (1974) have shown that the amount of performance deterioration, ΔJ, can only be made arbitrarily small if $n-p = 1$, where n is the order of the system whose state is to be observed and p is the order of the observer. For the case where $n-p \geq 2$, the performance deterioration, ΔJ, is finite and may be large.

An assumption made for analytical convenience in the design of a full-order observer, (reported in Chapter 5), was that the initial state, $\underline{x}(o)$, was always known. Newmann (1969), showed that setting the initial state, $\underline{x}_e(o)$, of the observer equal to the initial state of the system satisfied the optimal performance criterion used for the observer design. In practice, it is unlikely that the initial state of the system would be known and Newmann(1970), and more importantly Miller (1973), have proposed a theory for design of optimal minimal order observers where only the mean values and the covariance of the initial state of the system needed

to be known. Maeda and Hino (1974) have also proposed a design algorithm for optimal minimal-order observers but preferrad to use as a basis for their derivations, a frequency domain approach of the Luenberger observer (Luenberger, (1966)).

In Section 6.2 of this chapter, the theory for optimal minimal-order observer design, proposed by Miller (1973), is briefly outlined. Since the work reported has been conducted entirely in the time domain it was decided that the design method proposed by Miller was the most appropriate for investigating the feasibility of using minimal-order observers. A small addition was however made in the specification of the optimal performance criterion proposed by Miller: the performance index was chosen to take the same form as that used for obtaining previous results, (see Chapter 3) i.e. the output vector was weighted instead of the state vector as proposed by Miller. This addition was necessary in order that weightings may be placed directly upon those variables appropriate to the bending and torsional moments at each wing station considered. The change, however, did not affect the final design specification of the reduced-order observer.

In Section 6.3., the method used for modelling the observed system is described and in Section 6.4., is included some of the results obtained which illustrate the effectiveness of the performance of the observer design.

6.2. THEORY.

The theory outlined in this section is, with the exception of a small addition in Section 6.2.2., principally due to Miller (1973). To avoid duplication, detailed proofs have been omitted and only the main results presented.

6.2.1. Specifications of the Minimal-Order Observer Design.

For convenience, some of the equations derived previously are re-included in this section. The system under consideration is described by,

$$\dot{\underline{x}} = A\underline{x} + B\underline{u} \qquad ..(6.1)$$

$$\underline{y} = C\underline{x} + E\underline{u} \qquad ..(6.2)$$

where $\underline{x} \in R^n$, $\underline{u} \in R^m$, $\underline{y} \in R^p$ and matrices A,B,C and E are of appropriate dimensions. (6.1) is the state equation which was given as (3.4); (6.2) is the output equation given earlier as (2.11). It is required to design a reduced-order Luenberger observer represented by the equations:

$$\dot{\underline{z}} = F\underline{z} + G\underline{y}^* + H\underline{u} \qquad ..(6.3)$$

$$\hat{\underline{x}} = L\underline{y}^* + M\underline{z} \qquad ..(6.4)$$

$$\left.\begin{array}{l} \text{as } t \to \infty .\ \hat{\underline{x}} \to \underline{x} \\ \quad \therefore D\hat{\underline{x}} \to D\underline{x} \ \text{ie.}\ \underline{u}^o \end{array}\right\} \qquad ..(6.5)$$

where $\underline{z} \in R^r$, $\underline{y}^* \in R^{n-r}$, and where F is $(r \times r)$, G is $(r \times (n - r))$, H is $(r \times m)$; L is $(n \times (n - r))$, M is $(n \times r)$ and D is $(m \times n)$. (6.5) is the control law defined earlier as (5.4). Since the vector, $\underline{x}_e$, was used previously to indicate a vector composed entirely of reconstructed states, here, $\hat{\underline{x}}$ is used to indicate that vector which is composed of some measured state var-

iables with its remainder consisting of reconstructed state variables. The measured state variables are represented as in (5.2) by the equation:

$$\underline{y}^* = C^*\underline{x} \qquad ..(6.6.)$$

C^* is the p x n, (in this case $(n-r) \times n$), matrix defined in (5.2).

For (6.3) to be an observer, the following must hold,

$$\dot{\underline{e}} = F\underline{e} \qquad ..(6.7)$$

$$\underline{e} = \underline{z} - T\underline{x} \qquad ..(6.8)$$

where $\underline{e}$ is defined as an error vector, ($\underline{e} \in R^r$) and T is defined as an $(r \times n)$ transformation matrix and where,

$$TA - FT = GC^* \qquad ..(6.9)$$

$$H = TB \qquad ..(6.10)$$

$$LC^* + MT = I \qquad ..(6.11)$$

If matrices T, M and L can be found which satisfy (6.11), by making use of the relation,

$$(L \quad M)\begin{pmatrix} C^* \\ T \end{pmatrix} = I \qquad ..(6.12)$$

the substitutions:

$$F = TAM \qquad ..(6.13)$$

$$G = TAL \qquad ..(6.14)$$

are necessary and sufficient for the satisfaction of (6.9). By postmultiplying (6.12) by $\begin{pmatrix} C^* \\ T \end{pmatrix}^{-1}$ and premultiplying the resulting equation by $\begin{pmatrix} C^* \\ T \end{pmatrix}$ it is easy to show that:

$$TM = I_n \qquad ..(6.15)$$

$$C^*L = I_{n-r} \qquad ..(6.16)$$

and,

$$TL = 0 \qquad ..(6.17)$$

$$C^*M = 0 \qquad ..(6.18)$$

Substituting for $\underline{z}$ in (6.4), using (6.8) and making use of (6.11), gives:

$$\hat{\underline{x}} = \underline{x} + M\underline{e} \qquad ..(6.19)$$

The optimal control, $\underline{u}^o$, of (6.5) may then be given by:

$$\underline{u}^* = (D\underline{x} + DM\underline{e}) \to \underline{u}^o; \quad t \to \infty \qquad ..(6.20)$$

It is seen that when the observer transients have decayed, the error vector, $\underline{e}$, is zero and (6.20) reduces to the optimal control law determined earlier as (3.26).

Substituting (6.20) into (6.1) and (6.13) into (6.7) and combining the resulting equations yields:

$$\begin{bmatrix} \dot{\underline{x}} \\ \dot{\underline{e}} \end{bmatrix} = \begin{bmatrix} A + BD & BDM \\ 0 & TAM \end{bmatrix} \begin{bmatrix} \underline{x} \\ \underline{e} \end{bmatrix} \qquad ..(6.21)$$

(6.21) can be used to model the closed-loop response of the observed system†, where, from (6.8),

$$\underline{e}(o) = \underline{z}(o) - T\underline{x}(o) \qquad ..(6.22)$$

Thus the observer matrices may be solved by determining T, M, L, D AND $\underline{z}(o)$ and the problem constraints are equations (6.4), (6.21) and (6.22).

---

† It was proposed to carry out these tests in a slightly different way from those reported upon in Chapter 5. In Chapter 5, the responses of the FSVF system and the observed system were obtained by combining the equations associated with each system i.e. (5.32) and (5.33) were used. Although this required only a single computer run, it repeated some results already obtained in the FSVF tests (reported upon in Chapter 4). Thus for the tests reported upon in this Chapter, it was only necessary to make response checks on the observed system (by using (6.21)).

6.2.2 The Optimal Control Problem.

The performance index (p.i.) was chosen to take the same form† as that used for obtaining previous results (see Section 3.3.2): the output vector was weighted instead of the state vector as used by Miller, (1973). Thus:

$$\xi(J) = \int_0^\infty \xi(\underline{y}'.\hat{Q}.\underline{y} + \underline{u}'.\hat{R}.\underline{u})\, dt \qquad ..(6.23)$$

where $\xi(.)$ denotes the expectation operator.

It is easily shown that by substituting for $\underline{y}$ and $\underline{u}$ using (6.2) and 6.20), (6.23) may be rewritten as:

$$\xi(J) = \int_0^\infty \xi\left[(\underline{x}'\underline{e}')\begin{pmatrix} Q + (YD)' + YD + D'RD & YDM + D'RDM \\ M'(YD)' + M'D'RD & M'D'RDM \end{pmatrix}\begin{pmatrix}\underline{x}\\ \underline{e}\end{pmatrix}\right]dt \qquad ..(6.24)$$

where,

$$Q = C'\hat{Q}C \qquad ..(6.25)$$

$$R = E'\hat{Q}E + \hat{R} \qquad ..(6.26)$$

$$Y = C'\hat{Q}E \qquad ..(6.27)$$

Assume that P is an $(n + r) \times (n + r)$ constant positive definite matrix, which in partitioned form, satisfies:

$$\begin{pmatrix} P_{11} & P_{12} \\ P_{21} & P_{22} \end{pmatrix}\begin{pmatrix} A+BD & BDM \\ 0 & TAM \end{pmatrix} + \begin{pmatrix} (A+BD)' & 0 \\ (BDM)' & (TAM)' \end{pmatrix}\begin{pmatrix} P_{11} & P_{12} \\ P_{21} & P_{22} \end{pmatrix} + \begin{pmatrix} Q + (YD)' + YD + D'RD & YDM + D'RDM \\ M'(YD)' + M'D'RD & M'D'RDM \end{pmatrix} = 0 \qquad ..(6.28)$$

† To retain consistency with Miller's derivations, the $\frac{1}{2}$, previously used for analytical convenience is omitted from the p.i (Equation 6.23).

Then as long as $\underline{x}(t)$ and $\underline{e}(t)$ approach zero with time,

$$\xi(J) = \xi\left[\underline{x}'(0)\underline{e}'(o)\begin{pmatrix} P_{11} & P_{12} \\ P_{21} & P_{22}\end{pmatrix}\begin{pmatrix}\underline{x}(o) \\ \underline{e}(o)\end{pmatrix}\right] \quad ..(6.29)$$

Since for any vector $\underline{p}$ and matrix P, the following equality holds (Brockett,1970):

$$\underline{p}'P\,\underline{p} = \text{tr}\,(P\underline{p}\underline{p}') \quad ..(6.30)^{\dagger}$$

(6.29) may be written as:

$$\xi(J) = \text{tr}\left[\begin{pmatrix} P_{11} & P_{12} \\ P_{21} & P_{22}\end{pmatrix}\begin{pmatrix}\xi(\underline{x}(o).\underline{x}'(o)) & \xi(\underline{x}(o)\ \underline{e}'(o)) \\ \xi(\underline{e}(o).\underline{x}'(o)) & \xi(\underline{e}(o)\ \underline{e}'(o))\end{pmatrix}\right] .(6.31)$$

It is assumed that the initial conditions $\underline{x}(o)$ are unknown, but that the mean and covariance of the initial state are known and given by:

$$\xi(\underline{x}(o)) = \underline{m} \quad ..(6.32)$$

$$\xi\left[(\underline{x}(o) - \underline{m}).(\underline{x}(o) - \underline{m})'\right] = \Sigma_o \quad ..(6.33)$$

By using (6.32) and (6.33), (6.31) may be shown to be given by:

$$\xi(J) = \text{tr}\left[\begin{pmatrix} P_{11} & P_{12} \\ P_{21} & P_{22}\end{pmatrix} x \right.$$

$$\left.\begin{pmatrix} \Sigma_o + \underline{m}\underline{m}' & -\Sigma_o T' + \underline{m}(\underline{z}(o)-T\underline{m})' \\ -T\Sigma_o + (\underline{z}(o)-T\underline{m})\underline{m}' & T\Sigma_o T' + (\underline{z}(o)-T\underline{m})(\underline{z}(o)-T\underline{m})'\end{pmatrix}\right] \quad ..(6.34)$$

---

† 'tr' is in this case used to denote the trace of a matrix.

Thus the optimal control problem is to determine the matrices $M, T, L, P_{11}, P_{12}, P_{21}, P_{22}$ and the vector $\underline{z}(o)$ subject to the constraints (6.11) and (6.28).

The constrained optimization problem is converted to an unconstrained problem by adjoining the constraints (6.11) and (6.28) to the performance measure (6.34) via Lagrange multipliers. The resulting Lagrangian, $\mathcal{L}$, is:

$$\mathcal{L} = \operatorname{tr}\left\{ \begin{pmatrix} P_{11} & P_{12} \\ P_{21} & P_{22} \end{pmatrix} \left[\begin{array}{c|c} \Sigma_o + \underline{m}\underline{m}' & -\Sigma_o T' + \underline{m}(\underline{z}(o) - T\underline{m})' \\ \hline -T\Sigma_o + (\underline{z}(o)-T\underline{m})\underline{m}' & T\Sigma_o T' + (\underline{z}(o)-T\underline{m})(\underline{z}(o)-T\underline{m})' \end{array}\right] \right.$$
$$+ \begin{pmatrix} P_{11} & P_{12} \\ P_{21} & P_{22} \end{pmatrix} \begin{pmatrix} A+BD & BDM \\ 0 & TAM \end{pmatrix} \begin{pmatrix} (A+BD)' & 0 \\ (BDM)' & (TAM)' \end{pmatrix} \begin{pmatrix} P_{11} & P_{12} \\ P_{21} & P_{22} \end{pmatrix}$$
$$+ \begin{pmatrix} Q + (YD)' + (YD) + D'RD & YDM + D'RDM \\ M'(YD)' + M'D'RD & M'D'RDM \end{pmatrix} \begin{pmatrix} \Gamma_{11}' & \Gamma_{21}' \\ \Gamma_{12}' & \Gamma_{22}' \end{pmatrix}$$
$$\left. + 2\,(LC^* + MT - I)\Omega' \right\} \qquad ..(6.35)$$

Γ and Ω are matrices of Lagrange Multipliers and the number 2, in the expression is used for analytical convenience. Necessary conditions for optimality are, (Athans and Schweppe, (1965)),

$$\frac{\partial \mathcal{L}}{\partial P} = 0 \quad \frac{\partial \mathcal{L}}{\partial M} = 0 \quad \frac{\partial \mathcal{L}}{\partial T} = 0 \quad \frac{\partial \mathcal{L}}{\partial L} = 0 \quad \frac{\partial \mathcal{L}}{\partial D} = 0 \text{ and } \quad \frac{\partial \mathcal{L}}{\partial \underline{z}(o)} = 0$$

The gradient matrix notation is described in some detail in the Matrix Minimum Principle of Athans, (1968). Differentiating (6.35) with respect to P, M, T, L, D and $\underline{z}(o)$ in turn gives:

$$\frac{\partial \Phi}{\partial P} = \begin{pmatrix} \Sigma_o + \underline{m}\underline{m}' & -\Sigma_o T' + \underline{m}.(\underline{z}(o) - T\underline{m})' \\ -T\Sigma_o + (\underline{z}(o)-T\underline{m})\underline{m}' & T\Sigma_o T' + (\underline{z}(o) - T\underline{m})(\underline{z}(o)-T\underline{m})' \end{pmatrix}$$

$$+ \begin{pmatrix} \Gamma_{11} & \Gamma_{12} \\ \Gamma_{21} & \Gamma_{22} \end{pmatrix} \begin{pmatrix} (A+BD)' & 0 \\ (BDM)' & (TAM)' \end{pmatrix} + \begin{pmatrix} A+BD & BDM \\ 0 & TAM \end{pmatrix} \begin{pmatrix} \Gamma_{11} & \Gamma_{12} \\ \Gamma_{21} & \Gamma_{22} \end{pmatrix} = 0$$

..(6.36)

$$\frac{\partial \Phi}{\partial M} = \Omega T' + \left[D'.(B'P_{11} + RD + Y') + A'T'P_{21}\right]\Gamma_{12}$$

$$+ \left[D'(B'P_{12} + RDM) + A'T'P_{22}\right]\Gamma_{22} = 0$$

..(6.37)

$$\frac{\partial \Phi}{\partial T} = M'\Omega + P_{21}\left[\Gamma_{12}M'A' - \Sigma_o - \underline{m}\underline{m}'\right]$$

$$+ P_{22}\left[\Gamma_{22}M'A' + T\Sigma_o - (\underline{z}(o) - T\underline{m})\underline{m}'\right] = 0$$

..(6.38)

$$\frac{\partial \Phi}{\partial L} = \Omega C^{*'} = 0 \qquad ..(6.39)$$

$$\frac{\partial \Phi}{\partial D} = (B'P_{11} + RD + Y').(\Gamma_{11} + \Gamma_{12}M')$$

$$+ (B'P_{12} + RDM).(\Gamma_{21} + \Gamma_{22}M') = 0 \qquad ..(6.40)$$

$$\frac{\partial \Phi}{\partial \underline{z}(o)} = P_{21}\underline{m} + P_{22}(\underline{z}(o) - T\underline{m}) = 0 \qquad ..(6.41)$$

(6.36) → (6.41) will be considered in the following section.

6.2.3. The Optimal Observer.

The Lemmas used by Miller to develop the design procedure for the optimal observer are stated in this section. In particular, it was shown that the design parameters for the optimal observer can be found by essentially solving two algebraic Riccati equations.

Let the feedback matrix, D, of (6.5) be defined as:

$$D \triangleq (\hat{R} + E'\hat{Q}\,E)^{-1}\left[\,E'\hat{Q}\,C + B'K\right] \qquad ..(6.42)$$

It is seen that provided the weighting matrices are the same, (6.42) is exactly the same as (3.36) which was derived earlier.

Statement of Lemma 1.

Let T, L and M be matrices of appropriate dimension such that (6.11) is satisfied. Assume that (TAM) is a stability matrix and let:

$$D_o = (\hat{R} + E'\hat{Q}\,E)^{-1}.\left[\,E'\hat{Q}\,C + B'P_{11}\right] \qquad ...(6.43)$$

where, P_{11} is the solution of:

$$P_{11}(A - BR^{-1}E'QC) + (A - BR^{-1}E'QC)'P_{11} - P_{11}BR^{-1}B'P_{11} + C'(Q - QER^{-1}E'Q)C = 0 \qquad ..(6.44)$$

Then (6.28) has a unique solution with:

$$P_{12} = P_{21}' = 0 \qquad ..(6.45)$$

$$D_o = D \qquad ..(6.46)$$

Statement of Lemma 2.

Assuming that Lemma1 holds, (6.37) and (6.39) may be satisfied simultaneously, if:

$$\Omega = -(D'RDM + A'T'P_{22}) \cdot \Gamma_{22} M' \qquad ..(6.47)$$

Statement of Lemma 3.

Assume that Lemma 1 holds; assume that P_{22} is the positive definite solution of the equation obtained by taking the lower right ~~partition~~ submatrix of (6.28), i.e.,

$$P_{22}(TAM) + (TAM)'P_{22} + M'D'RDM = 0 \qquad ..(6.48)$$

and set,

$$\underline{z}(o) = T\underline{m} \qquad ..(6.49)$$

then the matrix of Lagrange multipliers Γ_{11} exists and the necessary conditions for optimality are satisfied if and only if:

$$T\Sigma_o + \Gamma_{22}M'A' + TAM\Gamma_{22} M' = 0 \qquad ..(6.50)$$

and,

$$\Gamma_{21} = -\Gamma_{22}M' \qquad ..(6.51)$$

Statement of Lemma 4.

Let S, V and M be any $(r \times n)$, $(n \times p)$ and $(n \times r)$ matrices which satisfy,

$$\begin{pmatrix} C^* \\ S \end{pmatrix}^{-1} = (V \quad M) \qquad ..(6.52)$$

then there exists matrices L, T and Γ_{22} of appropriate dimensions such that (6.11) and (6.50) are satisfied simultaneously if and only if:

$$L = (M\Gamma_{22}M'A' + \Sigma_o).C^{*'}(C^* \Sigma_o C^{*'})^{-1} \quad ..(6.53)$$

$$T = S - SLC^* \quad ..(6.54)$$

and Γ_{22} satisfies the algebraic Riccati equation

$$\Gamma_{22}\bar{A}' + \bar{A}\Gamma_{22} - \Gamma_{22}\bar{B}' \bar{R}^{-1} \bar{B}\Gamma_{22} + \bar{Q} = 0 \quad ..(6.55)$$

where:

$$\bar{A} \triangleq S\left[I - \Sigma_o C^{*'}(C^*.\Sigma_o.C^{*'})^{-1}C^*\right] AM \quad ..(6.56)$$

$$\bar{B} \triangleq C^*.AM \quad ..(6.57)$$

$$\bar{R} \triangleq C^*\Sigma_o C^{*'} \quad ..(6.58)$$

$$\bar{Q} \triangleq S\Sigma_o (I - C^{*'}(C^*.\Sigma_o.C^{*'})^{-1}.C^*.\Sigma_o)S' \quad ..(6.59)$$

The optimal observer is virtually solved by Lemmas 1-4. Furthermore, (6.44) has already been solved. (see Section 3.3.3.) It only remains to show that a solution can be obtained for (6.55) and that the resulting observer is stable.

Consider the deterministic optimal control problem given by:

$$\dot{\underline{w}} = \bar{A}'\underline{w} + \bar{B}'\underline{v} \quad ..(6.60)$$

$$J = \int_o^\infty (\underline{w}'\bar{Q}\ \underline{w} + \underline{v}'\bar{R}\underline{v})\ dt \quad ..(6.61)$$

(6.60) and (6.61) defines the well-known state regulator problem, and sufficient conditions for the existence of an op-

timal control law for (6.60) are that, $\bar{R}$, be positive definite, $\bar{Q}$, be at least non-negative definite and that the pair $[\bar{A}', \bar{B}']$ be completely controllable. (Kalman (1960), Athans and Falb, (1966)). The optimal control law is then given by:

$$\underline{v}^* = -\bar{R}^{-1}\bar{B}\Gamma_{22}\underline{w} \qquad ..(6.62)$$

where Γ_{22} is the positive definite solution of (6.55)

From definition (6.58), $\bar{R}$ is clearly positive definite if it is ensured that, Σ_0 , is positive definite.

To show that $\bar{Q}$ is positive definite, consider the change of variables,

$$\underline{v} = \underline{s} + \bar{R}^{-1}.C\Sigma S'.\underline{w} \qquad ..(6.63)$$

$$\underline{v}'\bar{R}\,\underline{v} = (\underline{s} + \bar{R}^{-1}C^*\Sigma_0 S'\underline{w})'\,\bar{R}(\underline{s} + \bar{R}^{-1}C^*\Sigma_0 S'\underline{w}) \qquad ..(6.64)$$

Substituting for $\bar{R}$ using (6.58) and expanding the r.h.s. of (6.64) yields.

$$\underline{v}'\bar{R}\,\underline{v} = \underline{s}'(C^*\Sigma_0 C^{*\prime})\underline{s} + \underline{s}'(C^*\Sigma_0 S')\underline{w} + \underline{w}'(S\Sigma_0 C^{*\prime})\underline{s} + \underline{w}'(S\Sigma_0 C^{*\prime})(C^*\Sigma_0 C^{*\prime})^{-1}(C^*\Sigma_0 S')\underline{w} \qquad ..(6.65)$$

$$\underline{w}'\bar{Q}\,\underline{w} = \underline{w}'(S\Sigma_0 S')\underline{w} - \underline{w}'(S\Sigma_0 C^{*\prime})(C^*\Sigma_0 C^{*\prime})^{-1}(C^*\Sigma_0 S')\underline{w} \qquad ..(6.66)$$

The integrand of (6.61) is therefore the sum of (6.65) and (6.66) which is:

$$\underline{w}'\bar{Q}\,\underline{w} + \underline{v}'\bar{R}\,\underline{v} = \underline{s}'(C^*\Sigma_o C^{*\prime})\underline{s} + \underline{w}'(S\Sigma_o C^{*\prime})\underline{s} + \underline{s}'(C^*\Sigma_o S')\underline{w} + \underline{w}'(S\Sigma_o C^{*\prime})\underline{w}$$

$$= (\underline{s}'\underline{w}') \begin{bmatrix} C^*\Sigma_o C^{*\prime} & C^*\Sigma_o S' \\ S\Sigma_o C^{*\prime} & S.\Sigma_o S' \end{bmatrix} \begin{pmatrix} \underline{s} \\ \underline{w} \end{pmatrix} \qquad ..(6.67)$$

$$= (\underline{s}'\underline{w}') \begin{pmatrix} C \\ S \end{pmatrix} \Sigma_o .(C'S') \begin{pmatrix} \underline{s} \\ \underline{w} \end{pmatrix}$$

By definition, (6.52), $\begin{pmatrix} C^* \\ S \end{pmatrix}$ is nonsingular; thus the integrand of (6.61) is zero, if and only if $\underline{s}$ and $\underline{w}$ are both zero and this implies that $\bar{Q}$ must be at least non-negative definite.

Controllability requirement.

It is shown indirectly below that the controllability of $[\bar{A}', \bar{B}']$ is guaranteed if the system defined by:

$$\dot{\underline{x}} = A\underline{x} \qquad ..(6.68)$$

$$\underline{y}^* = C^*\underline{x} \qquad ..(6.69)$$

is completely observable.

Substituting (6.63) into (6.60) and making the relevant substitution for $\bar{A}$, $\bar{B}$ and $\bar{R}$ using (6.65) - (6.58) respectively yields:

$$\dot{\underline{w}} = (SAM)'\underline{w} + (C^*AM)'\underline{s} \qquad ..(6.70)$$

If $\underline{w}$ can be controlled through $\underline{s}$ in (6.70), $\underline{w}$ can be controlled through $\underline{v}$ in (6.60) because of the linear relationship (6.63). For $[SAM', CAM']$ to be completely controllable,

$$\text{Rank}\,\Lambda = \text{Rank}\begin{bmatrix} (C^*AM) \\ (C^*AM)(SAM)_2 \\ (C^*AM)(SAM)^2 \\ \vdots \\ (C^*AM)(SAM)^{r-1} \end{bmatrix} = r \qquad ..(6.71)$$

Consider the similarity transformation,

$$\begin{pmatrix} \underline{x}_1 \\ \underline{x}_2 \end{pmatrix} = \begin{pmatrix} C^* \\ S \end{pmatrix} \underline{x} \qquad ..(6.72)$$

$$\therefore \quad \begin{pmatrix} \dot{\underline{x}}_1 \\ \dot{\underline{x}}_2 \end{pmatrix} = \begin{pmatrix} C^*A \\ S\ A \end{pmatrix} \underline{x} \qquad ..(6.73)$$

(6.52) may be rewritten as,

$$(V\ M)\begin{pmatrix} C^* \\ S \end{pmatrix} = I \qquad ..(6.74)$$

$$\therefore \quad (C^*AV\ C^*AM)\begin{pmatrix} C^* \\ S \end{pmatrix} \underline{x} = C^*A\underline{x} \qquad ..(6.75)$$

and,

$$(SAV\ SAM)\begin{pmatrix} C^* \\ S \end{pmatrix}\underline{x} = SA\underline{x} \qquad ..(6.76)$$

or,

$$\begin{pmatrix} \dot{\underline{x}}_1 \\ \dot{\underline{x}}_2 \end{pmatrix} = \begin{pmatrix} C^*AV & C^*AM \\ SAV & SAM \end{pmatrix}\begin{pmatrix} \underline{x}_1 \\ \underline{x}_2 \end{pmatrix} \qquad ..(6.77)$$

and,

$$\underline{y} = \underline{x}_1 \qquad (6.78)$$

Luenberger, (1971), has shown that complete observability of the system (6.77), (6.78) implies complete observability of the partitions $[(C^*AM), (SAM)]$. Thus matrix Λ will have rank r, since transposing a matrix does not change its rank. (Kuo, (1975))

It only remains to show that the resulting observer will be stable. The closed loop system of (6.60) with control law (6.62) will have a system matrix, K', defined by:

$$K' = \bar{A}' - \bar{B}'\bar{R}^{-1}\bar{B}\,\Gamma_{22} \qquad ..(6.79)$$

since, the eigenvalues of the square matrix, K', will be the same as those of its transpose, K, where,

$$K = \bar{A} - \Gamma_{22}\bar{B}'\bar{R}^{-1}\bar{B} \qquad ..(6.80)$$

Substituting for $\bar{A}$, $\bar{B}$ and $\bar{R}$ using (6.56) - (6.58) respectively and using (6.52), the r.h.s. of (6.80) becomes,

$$K = SAM - S(M\Gamma_{22}M'A' + \Sigma_0)C^* (C^*\Sigma_0 C^{*\prime})^{-1}C^*AM \qquad ..(6.81)$$

Substituting (6.58) and (6.54) into the above expression results in:

$$\begin{aligned} K &= (S - SHC^*)AM \\ &= TAM \end{aligned} \qquad ..(6.82)$$

The r.h.s. of (6.82) is seen to be identical to the observer partition of (6.21)

6.3. Modelling the Observed System.

To test the design of the reduced order observer using the model, CLEMENTI, it was assumed that the mean value of the initial state vector was zero, i.e.

$$\mathcal{E}(\underline{x}(0)) = \underline{m} = 0 \qquad .. (6.83)$$

The covariance matrix, Σ_0, was the solution of the degenerate algebraic Riccati equation given as (3.76); because the state equation was linear, this covariance matrix is constant:

$$\therefore \quad \mathcal{E}\left[\underline{x}(t) \cdot \underline{x}'(t)\right] = \mathcal{E}\left[\underline{x}(0).\underline{x}'(0)\right] \qquad .. (6.84)$$

Also, from (6.83),

$$\mathcal{E}\left[(\underline{x}(0) - \underline{m})(\underline{x}(0) - \underline{m})'\right] = \Sigma_0 = \mathcal{E}\left[\underline{x}(0).\underline{x}'(0)\right] \qquad .. (6.85)$$

There was no need to solve the Riccati equation, (6.44) since the feedback law thus obtained was identical to that derived previously (see Equation 3.36), provided only that the weighting matrices $\hat{Q}$ and $\hat{R}$ were chosen to be identical to the corresponding matrices defined in (4.13) and (4.14) respectively. The feedback law (4.15) was used in every test associated with the reduced order observer. To obtain the observer parameters, it is necessary to form the matrices defined in (6.56) - (6.59). Since it was found from previous tests, (reported in Chapter 5), that the presence of four measurements, viz., w, q, δ_A and δ_{E_i} gave the best results in terms of the transient behaviour of a proposed observer design, the permanent and assured avail-

ability of these measurements was again assumed in subsequent studies on the reduced observer. The matrix C* was arranged to be of the form:

$$C^* = \begin{bmatrix} 1 & 0 & 0 & 0 & 0 & \cdots\cdots & 0 \\ 0 & 1 & 0 & 0 & 0 & \cdots\cdots & 0 \\ 0 & 0 & 1 & 0 & 0 & \cdots\cdots & 0 \\ 0 & 0 & 0 & 1 & 0 & \cdots\cdots & 0 \end{bmatrix} \qquad ..(6.86)$$

In practice, this was achieved simply by redefining the state vector of the model CLEMENTI so that the states w, q, δ_A and δ_{E_i} formed the first four elements of the state vector, $\underline{x}$. Since the matrix, S, of (6.52) could be selected arbitrarily, a convenient definition of S was,

$$S = \begin{bmatrix} 0 & 0 & 0 & 0 & 1 & 0 & 0 & \cdots\cdots\cdots\cdots & 0 \\ 0 & 0 & 0 & 0 & 0 & 1 & 0 & \cdots\cdots\cdots\cdots & 0 \\ 0 & 0 & 0 & 0 & 0 & 0 & 1 & & 0 \\ \cdot & \cdot & \cdot & \cdot & \cdot & \cdot & \cdot & \ddots & \\ \cdot & \cdot & \cdot & \cdot & \cdot & \cdot & \cdot & & \\ \cdot & \cdot & \cdot & \cdot & \cdot & \cdot & \cdot & & \\ \cdot & \cdot & \cdot & \cdot & \cdot & \cdot & \cdot & & \\ 0 & 0 & 0 & 0 & 0 & 0 & 0 & \cdots\cdots\cdots\cdots & 1 \end{bmatrix} \qquad ..(6.87)$$

(6.87) thus ensured that the matrix $\begin{pmatrix} C^* \\ S \end{pmatrix}$ of (6.52) was an identity matrix and thus avoiding the need for inversion to solve for the matrices V and M.

The computer program MILEST was used both to determine V and M, and to solve the equations (6.56) - (6.59). The algebraic Riccati equation (6.55) was next solved which then permitted matrices, L of (6.53) and, T of (6.54) to be obtained. It only remained to obtain the matrix of (6.21) to test the closed-loop

response of the observed system. The observer matrices were fixed as a result of the choice of, $\underline{m}$, and, Σ_0 , and they were used in all subsequent tests. (6.22) was solved to determine the appropriate initial conditions to be used for the error vector, $\underline{e}$. Substituting (6.83) into (6.49) for $\underline{m}$ results in:

$$\underline{z}(0) = T\underline{m} = 0 \qquad ..(6.88)$$

From (6.22),

$$\begin{aligned} \underline{e}(0) &= \underline{z}(0) - T\underline{x}(0) \\ &= -T\underline{x}(0) \end{aligned} \qquad ..(6.89)$$

(6.21) was forced by including into the equation, a vector, $\underline{r}$, acting through a driving matrix*, H. Thus for the purposes of making response tests, (6.21) was of the form:

$$\begin{bmatrix} \dot{\underline{x}} \\ \dot{\underline{e}} \end{bmatrix} = \begin{bmatrix} A + BD & BDM \\ 0 & TAM \end{bmatrix} \begin{bmatrix} \underline{x} \\ \underline{e} \end{bmatrix} + \begin{bmatrix} H \\ 0 \end{bmatrix} \underline{r} \qquad ..(6.90)$$

For comparison with previous results, vector, $\underline{r}$, was set to the values specified in Table 4.4. , i.e. the aircraft with its observer system was forced to the same values of vertical velocity, $\underline{w}$, and pitch rate, q, as used in the test situations A,B and C. In the case of the test situation A, the initial state vector, x(0) was defined by:

$$\underline{x}'(0) \triangleq [7.15 \quad 0 \quad 0 \quad 0 \quad \ldots\ldots\ldots \quad 0] \qquad ..(6.91)$$

Hence for test situation A, the vector $\underline{e}(0)$ was finite. For cases B and C, $\underline{x}(o)$, hence $\underline{e}(o)$ were zero.

---

* See Section 4.4 of Chapter 4.

The time responses obtained by assuming that only measurements of w, q, δ_A, and δ_{E_i} were available, with the observer being used to reconstruct the remaining states are presented in Figures (6.1) - (6.3). Time responses which were obtained earlier by employing FSVF* have been included in the plots for comparison.

Figure (6.1) shows a representative set of time responses+ for test situation A. The plots indicate that in flight situations such as case A, the observer would be very effective in accurately estimating the unmeasured states of the aircraft. This close matching with FSVF designs considered earlier (Chapter 4) was however not possible in all test situations: a demand for a finite value of vertical velocity, (Figures 6.2 and 6.3), indicated that the observer dynamics could be pronounced enough to affect the wing bending and torsional moments. These fluctuations in bending and torsional moments were however not substantial and certainly not as great as those when full recon-

---

* In the description of the time responses the following abbreviations are used:
FSVF - Full State Variable Feedback.
RSVF - Reconstructed State Variable Feedback.

\+ Only the wing root bending moment together with either pitch rate (q) or vertical velocity (w) are included in time-responses presented in this Chapter. The other responses did not show any unusual features which were not already evident from those responses presented.

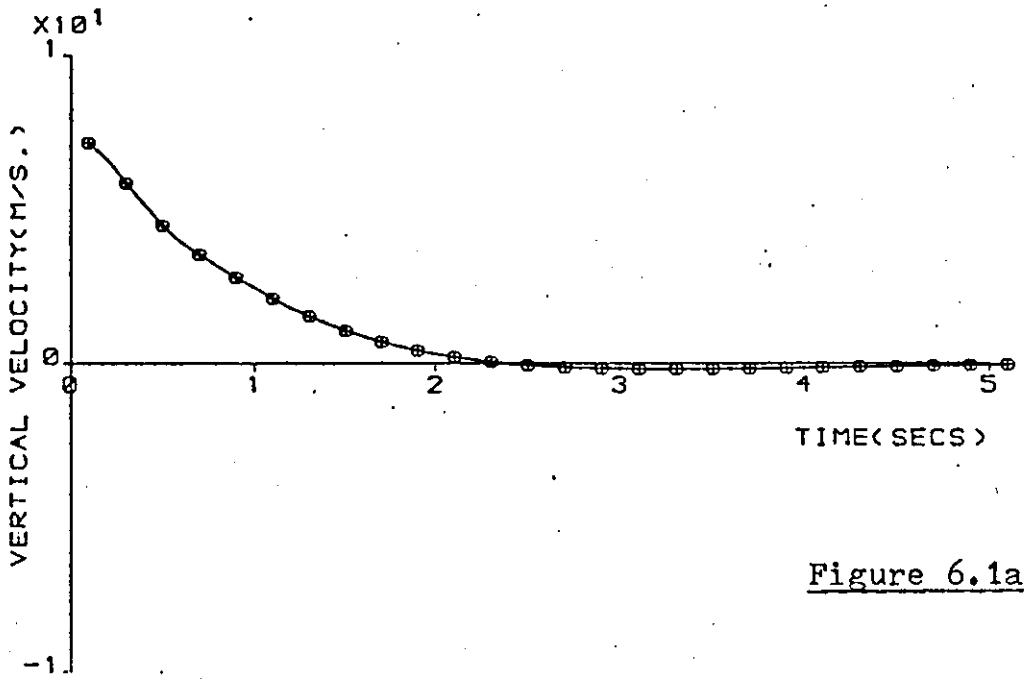


Figure 6.1a

+ FSVF
o RSVF

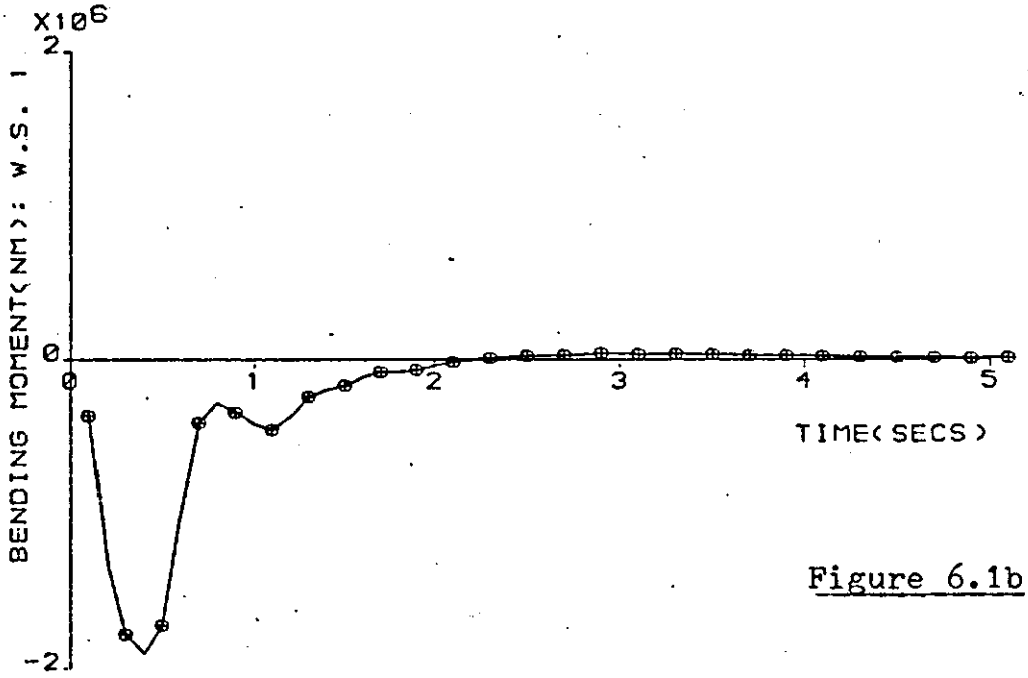


Figure 6.1b

COMPARISON RESPONSE: FSVF WITH REDUCED-ORDER OBSERVED SYSTEM: CASE A.

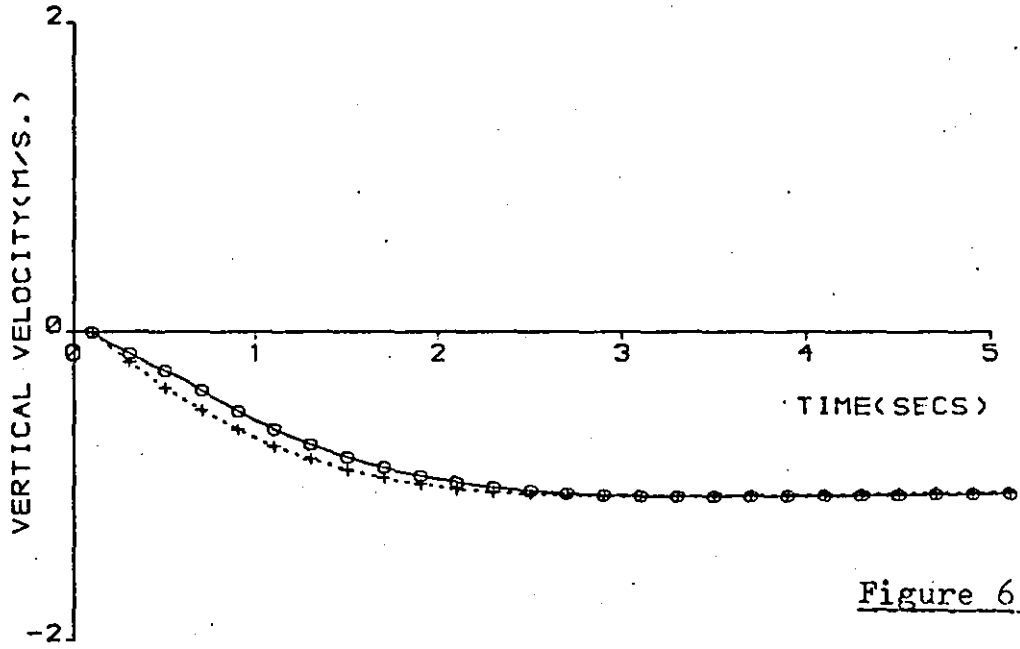


Figure 6.2a

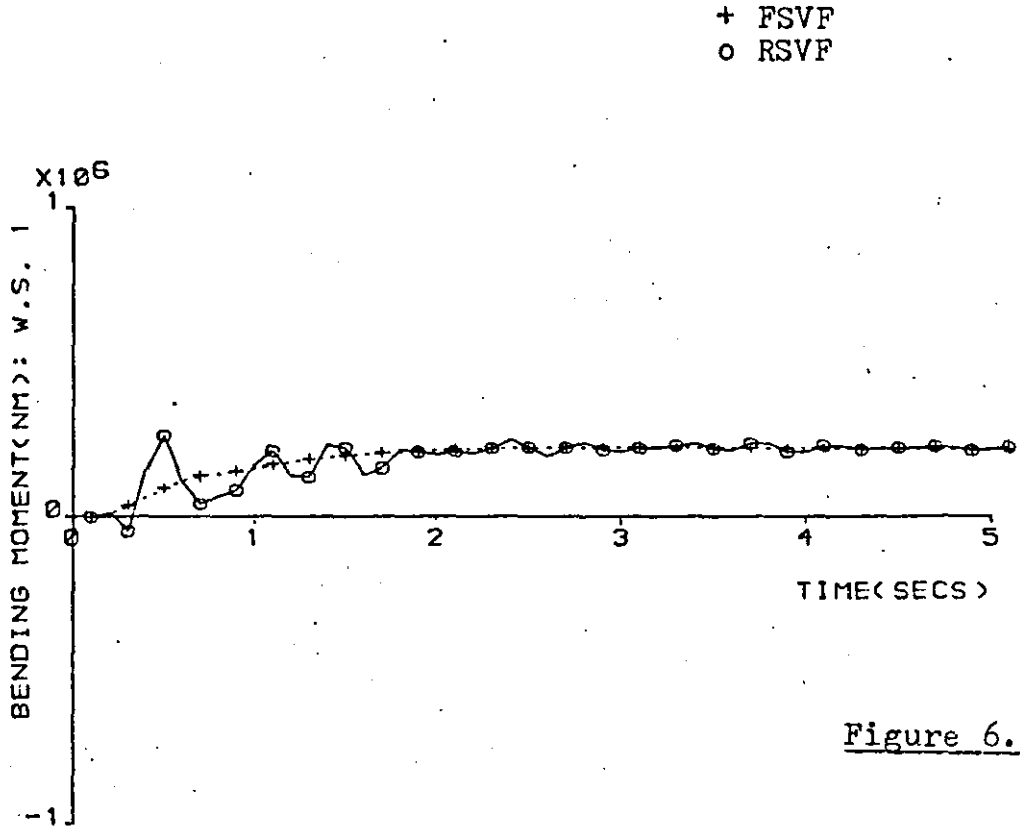


Figure 6.2b

COMPARISON RESPONSE: FSVF WITH REDUCED ORDER OBSERVED SYSTEM: CASE B.

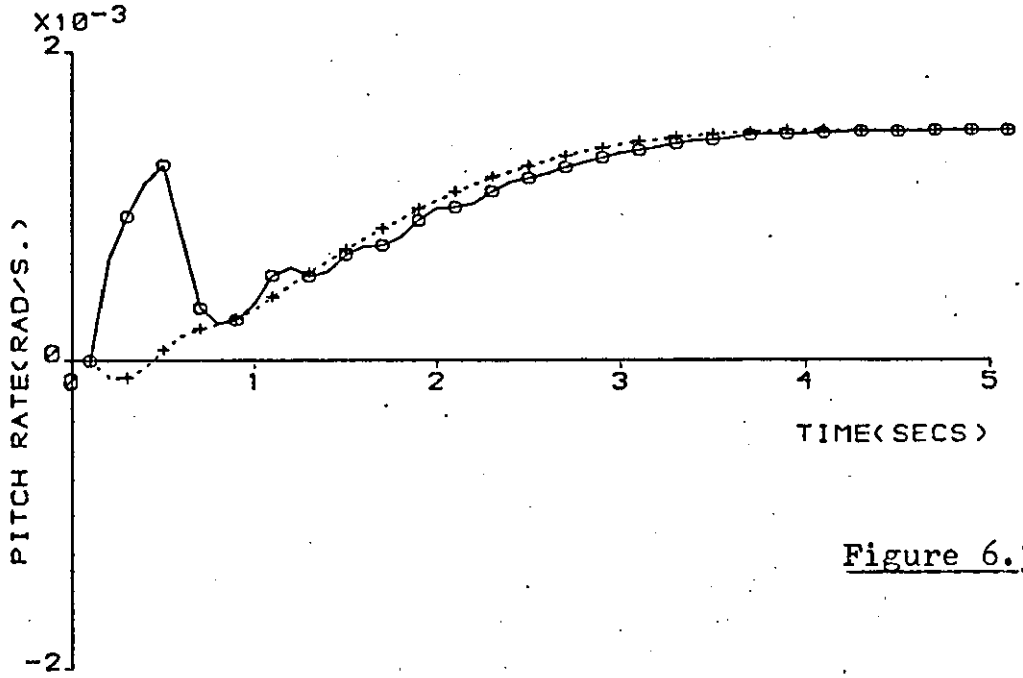


Figure 6.3a

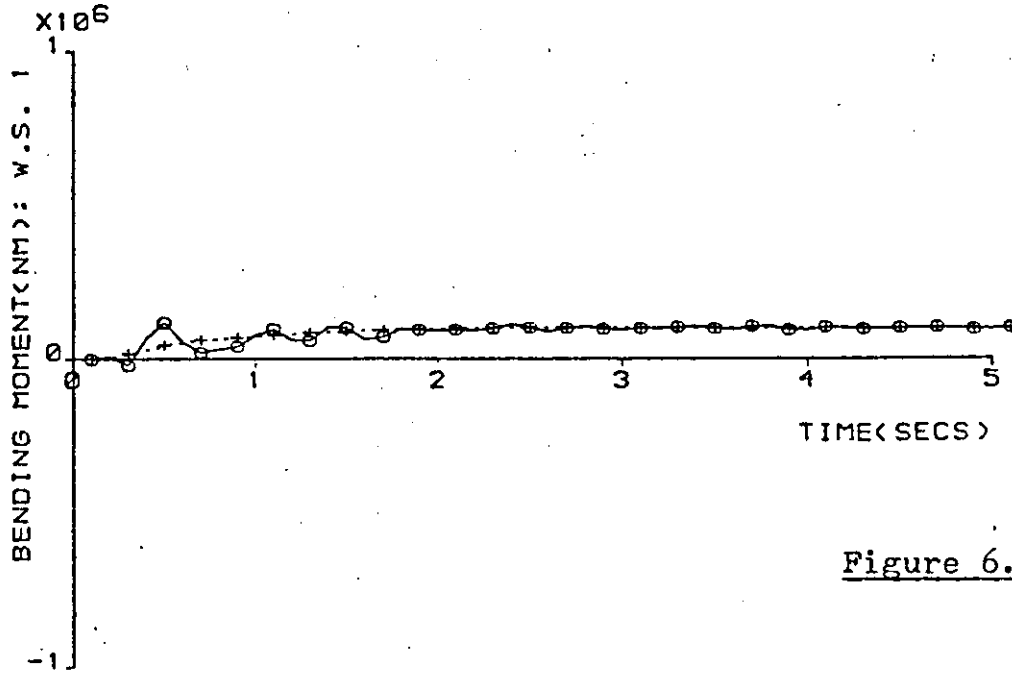


Figure 6.3b

COMPARISON RESPONSE: FSVF WITH REDUCED-ORDER OBSERVED SYSTEM: CASE C.

structed state feedback was used,(described in the previous chapter). In all cases, the observer transients settled within two seconds.

It appears that the reduced-order observer besides being simpler to synthesize than the full-order observer, has another advantage: it produces closer matching to the aircraft responses expected if full state variable feedback were to be used. Use of the mean and covariance of the initial state vector has served the purpose of making the resulting observer design less sensitive to imperfect matching of initial conditions.

CHAPTER 7: USE OF A MICROPROCESSOR AS A SELF-REPAIRING CONTROLLER (SRC).

7.1. Introduction.

A consequence of either reducing the strength of the wing of the aircraft or increasing its span*, as a result of employing an active load alleviation scheme, is that a considerable degree of reliability of the control system, higher than that of both the basic airframe and its propulsive system, will be required. For provision of a SLACS, such reliability cannot be accomplished solely by hardware redundancy techniques because of the large increase in cost that this would incur: not only triplex (and often quadruplex) systems have to be provided, but the attendant increase in weight would inevitably result in a reduction of payload capability. Some enhancement of the system reliability is possible by using software redundancy techniques, where, with the "safety law" operational, one of the observers of the type reported upon in Chapters 5 and 6 may be used to reconstruct any missing feedback signals. With an effective full-state feedback scheme implemented, the bending and torsional moments at various wing stations will be reduced and it may then be possible to reduce the weight of the wing by as much as 3% of the aircraft gross weight. (The net

---

* For commercial aircraft principally, it is, in view of the mounting costs of fuel, an economically attractive scheme to take advantage of the reductions in bending and torsional moments by increasing the span of the wing. The increased span reduces the induced drag and improves the fuel efficiency of the aircraft. Such a scheme has been implemented on the Lockheed L-1011 Tristar (Fink, 1980).

weight saving may be slightly lower when account is taken of the need to provide extra hydraulic systems and actuators and, perhaps, providing extra strengthening of the areas around the active surfaces). 2% of gross weight can, in some aircraft, represent 7-10% of the payload. A hardware redundancy scheme will still be required for the servo-actuators and those motion sensors required for measuring* the variables of the safety law, viz., w, q/n_z, δ_A, δ_{E_i}, and δ_{E_o}.

In recent years, with the advent of small dedicated microprocessor units (MPU's), it has become possible to synthesise complex control systems such as those which will be required for providing structural load alleviation. Such systems may for instance be used to enhance the safety and reliability of operation of the SLACS considered, by:

(a) Flight controller monitoring, i.e., ensuring that the 5-SVF feedback control law is available at all times during flight.

(b) State-estimation, i.e., employing a suitable observer algorithm to recreate any missing states from whatever feedback signals are available, in addition to those five states always available for the 'safety law'.

(c) Sensor signal monitoring, i.e., use of a suitable "voter" routine to provide "majority rule" output from monitoring three identical signals associated

---

* An accelerometer may be used to measure vertical acceleration and the signal integrated to obtain vertical velocity; for pitch rate, a rate gyro will be required, and for the control surface deflections, position transducers could be employed.

with each state variable of the 'safety law'. Such a system would replace the mechanical voter used with the triplex motion sensor.

(d) Self-checking, i.e., use of computer routines to check the logic outputs of one or more of the MPU's required for synthesising the SLACS.

The final exercise of this research investigation was concerned with a demonstration of how (a) may be achieved. The microcomputer system (MCS) available for use was a Bell and Howell PMS-500 Polynomialised Microcomputer, discussed in section 7.2. of this chapter. The MCS was used to detect a simulated failure of a linear feedback controller; once the failure in the feedback signal was detected by the MCS, a surrogate gain was employed which restored the feedback signal to its proper value. When used in this way, the MCS was referred to as a self-repairing controller (SRC) which is discussed in detail in Section 7.3. The available MCS did not have sufficient core space to allow any of (b), (c), or (d), to be adequately demonstrated, and, in the course of the development work on the SRC, it was established that the need to use floating-point software techniques was a serious performance limitation in respect of the sampling rate which could be achieved. A number of suggestions, based upon the experience gained in this work, about necessary performance features needed in any MCS employed for similar purposes in future are given in the Conclusions.

7.2. The Microcomputer System.

The Bell and Howell, PMS-500, is a dedicated microcomputer system (MCS) which can be ~~dedicated to~~ used for a particular application by means of PROM programming. All the arithmethic processing is carried out using word lengths of 20-bit* while 16-bit word working is used for system processing. The MCS has a set of 256 instructions: each instruction is an 8-bit binary word. Figure 7.1 shows the necessary hardware composing the MCS.

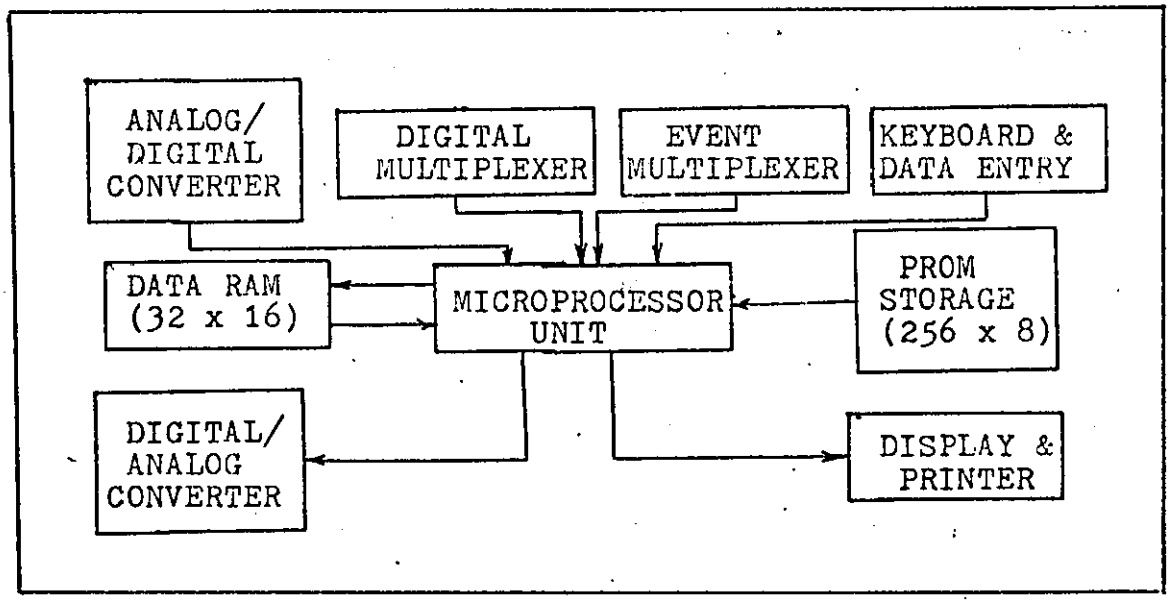


Figure 7.1: B & H Microcomputer System

The basic system was slow when compared with other available systems+ having a cycle time of 1.3μs. for 20-bit word-working. Timing also affected A-D conversion rates: the Analog - Digital converter provided with the basic

---

* To maintain a degree of accuracy to about 5 significant places, 20-bit arithmetic is used.

\+ For instance systems based upon the M6800 and 8086 with typical cycle times of 500ns. and 200ns. respectively.

system could not be used because the total time* required for a conversion was in excess of 5540μs. As a result, an external system (an Analogic MP6812) was used in place of the A-D converter in the PMS-500. With the MP-6812 in operation the total conversion time achieved was in the region of 60μs. The MP-6812 also contained a sample-and-hold amplifier which enabled any particular signal to be held at its current value until sampled again. In the case of Digital-to-Analog conversion, the D-A conversion unit on the PMS-500 was retained since it was possible to achieve a total conversion time of at least 40μs. In the PMS-500 MCS, all arithmetic was carried out using floating-point software. This inevitably affected the 'cycl time' of any program used.

---

* the expressions 'total time' or 'total conversion time' are used in this section to indicate the sum of the 'software' and 'hardware' times required to achieve a single conversion.

7.3. Self-Repairing Controller (SRC)

Figure 7.2. shows the way in which a self-repairing controller may be implemented in practice. MPU #1 represents the flight controller, while MPU #2 represents the self-repairing controller.

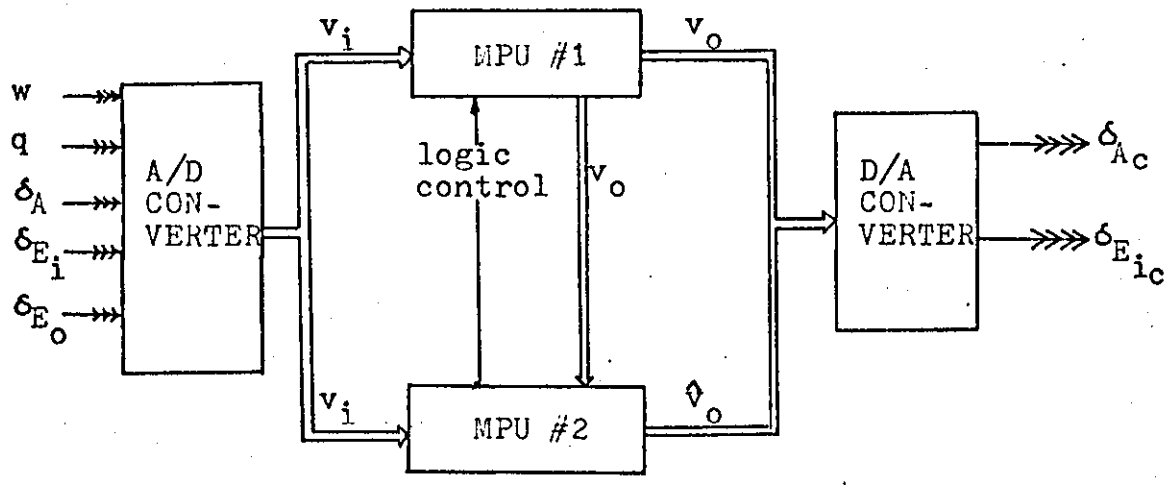


Figure 7.2. Self-Repairing Controller.

An input signal v_i is related to the corresponding output signal v_o by the equation:

$$v_o = k_i . v_i \qquad ..(7.1)$$

where k_i is the feedback gain. MPU #2 samples the inputs v_i and output v_o of the flight controller (MPU #1). MPU #2 would have its own voter program to select the correct sensor signal based upon a 'majority rule' output* and would also have surrogate gain values $\hat{k}_i$ stored in ROM. An estimate ($\hat{v}_o$) of the output signal is made by MPU #2 using the relationship:

$$\hat{v}_o = \hat{k}_i . v_i \qquad ..(7.2)$$

---

* See note (c), Section 7.1

The two output signals v_o and $\hat{v}_o$ are compared to within a prescribed tolerance (see Figure 7.3) by using some logic control (to be discussed later) between MPU #1 and MPU #2; it can be arranged that only the correct signal (i.e. v_c, Fig.7.3) is chosen. The appropriate signals are then summed to obtain the actuator signals δ_{A_c} and δ_{Ei_c}.

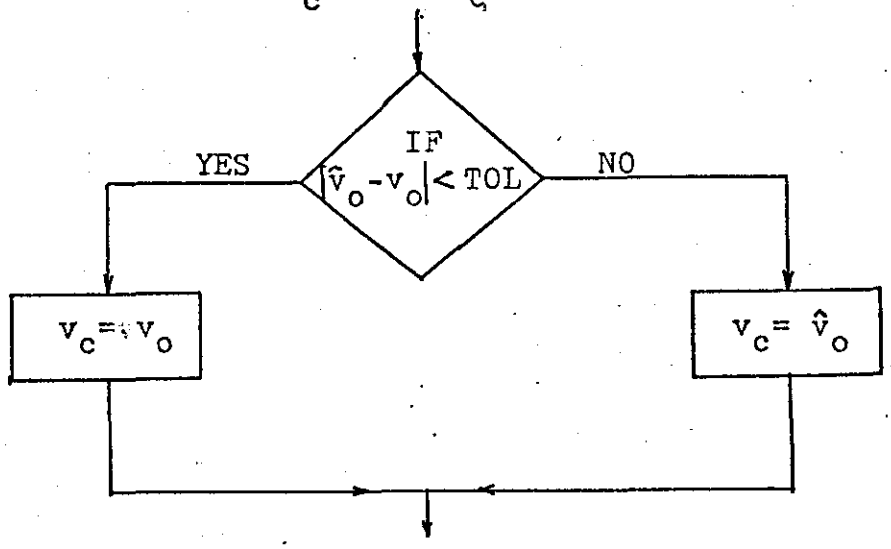


Figure 7.3: Selection of Correct Output.

The failure of signals in the flight controller, i.e. MPU #1, was simulated. MPU #2 together with A-D and D-A conversion hardware were represented by the PMS-500 microcomputer system. For simulation of failures, a test unit, referred to as a Self-Repairing Controller Test Unit (SRCTU) was designed. Figure 7.4. shows a functional diagram of the SRCTU, while in Figure 7.5. is shown a photograph of the SRCTU in its case. In Figure 7.6, is shown a photograph of the hardware* used for simulating the self-repairing controller.

* The TR-48 Analog Computer was not used in these tests but for subsequent tests on self-repairing control for the SLACS (reported in Section 7.4.)

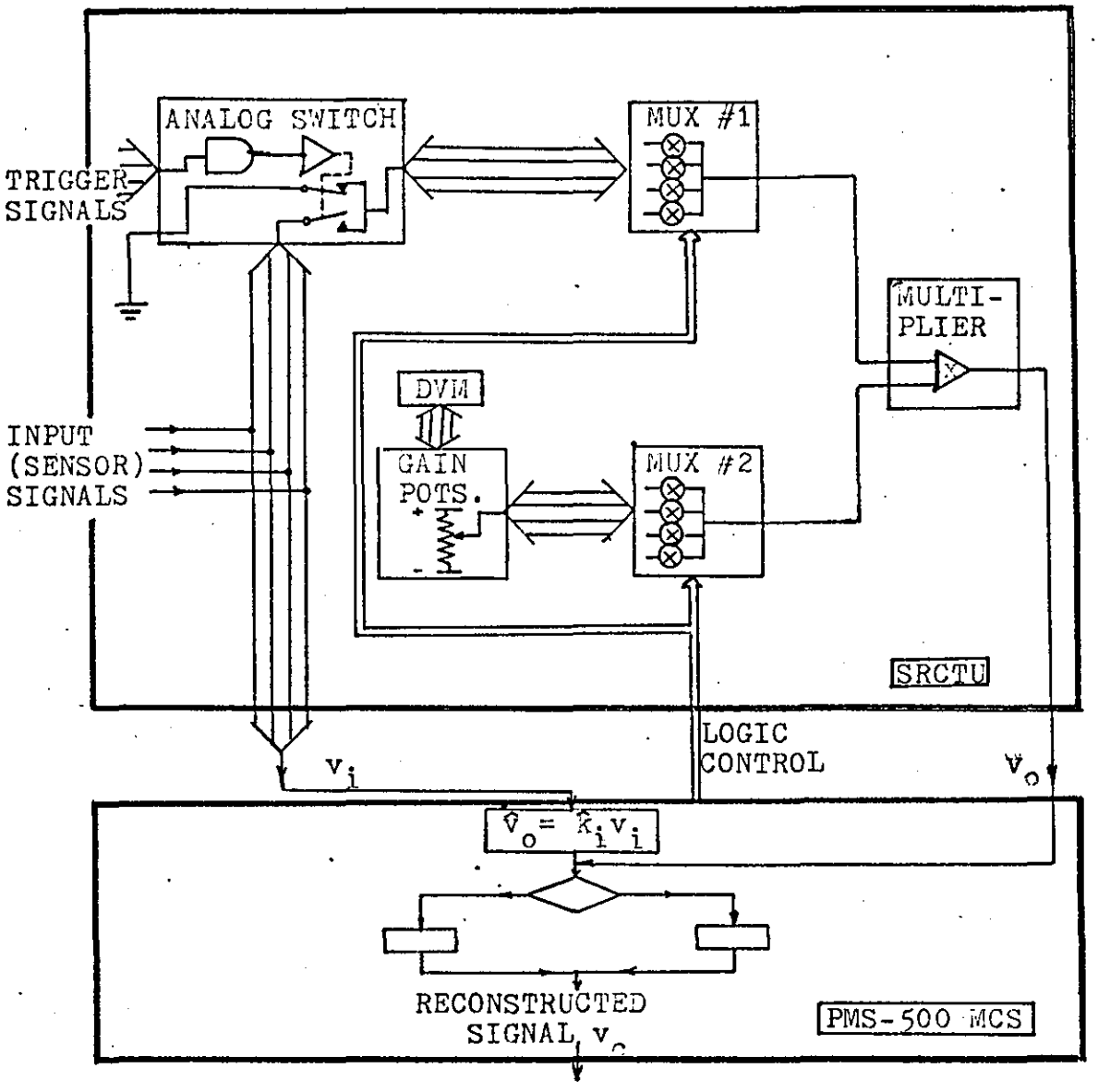


FIGURE 7.4. - FUNCTIONAL DIAGRAM OF SRCTU.

The triggering signals were used to activate the analog switches. SPDT switches were used with one terminal connected to the input (sensor) signal, and the other connected to signal ground. The triggering signals were pseudo-random TTL signals, which, when the frequencies were properly selected, resulted in a high degree of distortion

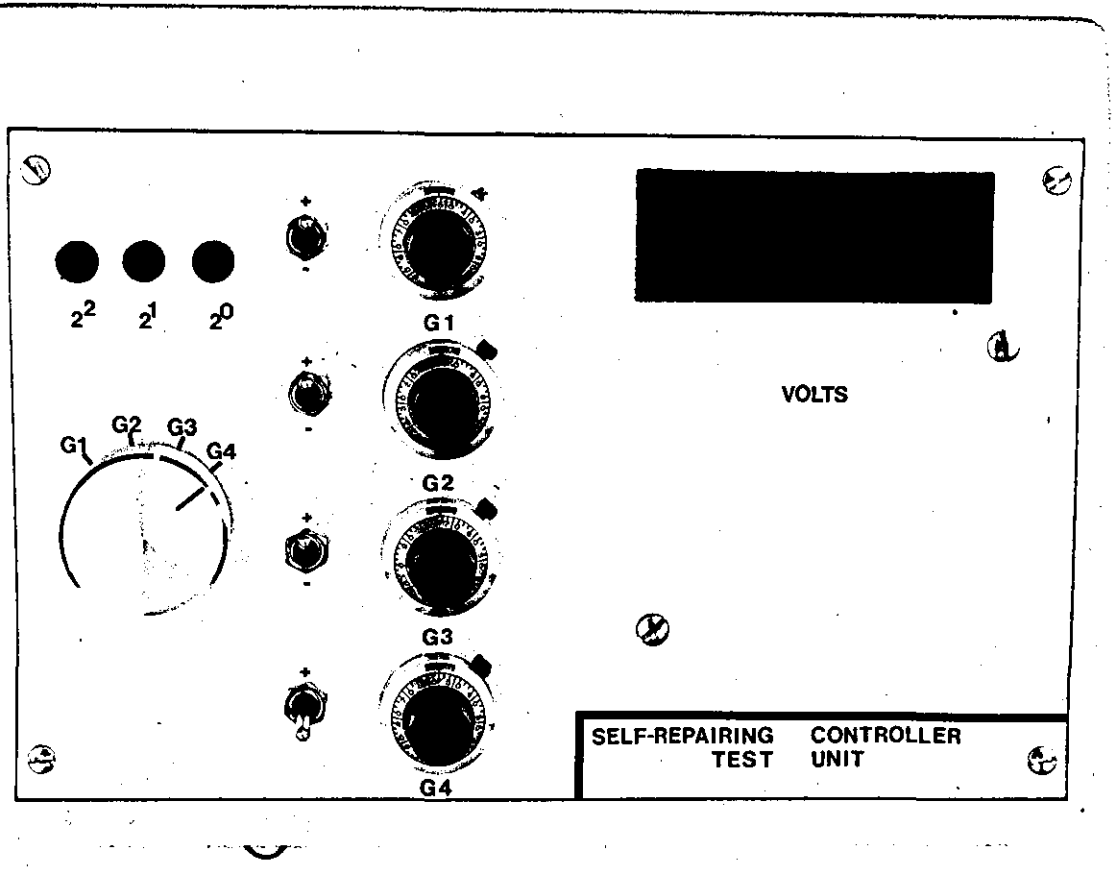


Figure 7.5: SELF-REPAIRING CONTROLLER TEST UNIT



Figure 7.6: PMS-500 MCS AND ASSOCIATED TEST HARDWARE

to the input signals. A typical set of input and output signals associated with one of the analog switches is shown in Figure 7.7. The gains, k_i, were set up on the SRCTU by the use of linear 10-turn potentiometers, the end terminals of which were connected to positive and negative supply rails. A selector switch was used to connect each potentiometer wiper to a digital volt meter (DVM) in order to set up the gain values accurately. The potentiometer wipers were also connected to the input terminals of multiplexer #2 (MUX2). The distorted signals from the analog switches were connected to MUX1. The signals were multiplexed to ensure that each signal was scaled by its corresponding gain value in the multiplier unit before being routed to the PMS-500 MCS for checking. The multiplexing was controlled by the PMS-500 to ensure an ordered and repetitive sequence of sampling. Thus $v_i(1)$ and $v_o(1)$ were sampled, followed by $v_i(2)$ and $v_o(2)$ and so on.

In the PMS-500 MCS, a program was written to sample the signals v_i and v_o, to determine the estimate $\hat{v}_o$ using (7.2), (where the gain $\hat{k}_i$ was stored in ROM) to compare the signals v_o and $\hat{v}_o$ using the logic arrangement shown in Figure 7.3 and to output the reconstructed signal, v_c. In Table 7.1, is shown a segment of the program used to compare and select the appropriate signal according to Figure 7.3.

In Figure 7.8 is shown a typical result where the reconstructed signal v_c, obtained by sampling the input signal v_i, and the distorted output signal v_o (Figure 7.7), has been plotted. The gain k_i has been assumed to be unity. To determine

PAPER SPEED: 25mm/s.
SENSITIVITY: 200mV/div.

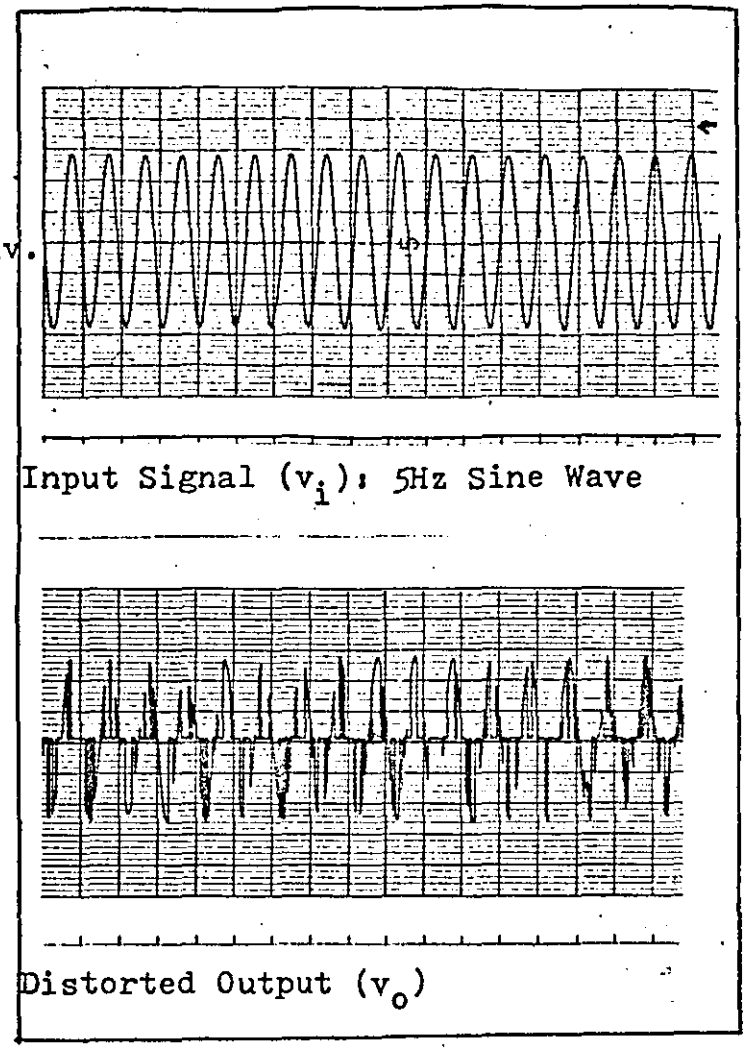


Figure 7.7: Plot of Input and Output Signals Associated with Analogue Switches.

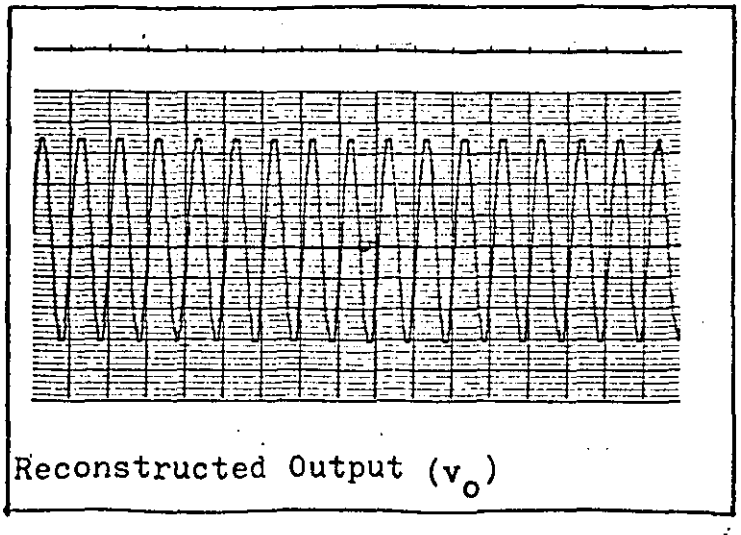


Figure 7.8: Plot of Reconstructed Output Signal from B&H PMS-500 MCS.

the maximum rate of processing each signal, a pure sine wave was used as an input signal. Figure 7.9 shows some results for a pure 20Hz. sine wave. By counting the number of sampling steps clearly evident from the plot of the reconstructed signal, it was found that with the PMS-500 MCS programmed to process 4 independent sensor signals in sequence, a sampling rate of 100 samples/s. could be achieved. As the frequency of the sine wave increased, the quality of reconstruction of the signal in the PMS-500 MCS deteriorated. In Figure 7.10, are shown some plots associated with a signal frequency of 50Hz. 50Hz. was regarded as the limiting frequency above which the

ADDRESS	8-BIT CODE	INSTRUCTION
0	10100000	Complement Multiplex Toggle
1	10010000	Input from Digital Source 0
2	10100000	Complement Multiplex Toggle
3	00101001	Write Reg 'A' to RAM Location 9
4*	10010000	Staticise Multiplexer Address 0
5	10100010	Complement Output Control Line
6	10100000	Complement Multiplex Toggle
7	10010000	Input from Digital Source 0
8	10100000	Complement Multiplex Toggle
9	00101000	Write Reg 'A' to RAM Location 8
10	01000010	Subtract A from B
11	10110001	Absolute Value of A
12	00001010	Read RAM Location 10
13	01001000	Compare
14	00001000	Read RAM Location 8
15	10101010	Skip if 1 in P Flag
0	00001001	Read Ram Location 9
1		etc.
2		

Table 7.1 : PROGRAM SEGMENT USED TO COMPARE v_o and $\hat{v}_o$

* although having the same 8-bit code as Instruction 0, this instruction is different because the Multiplex Toggle was complemented in Instruction 2.

SENSITIVITY:
0.2V/div.

TIME BASE:
1ms/div.

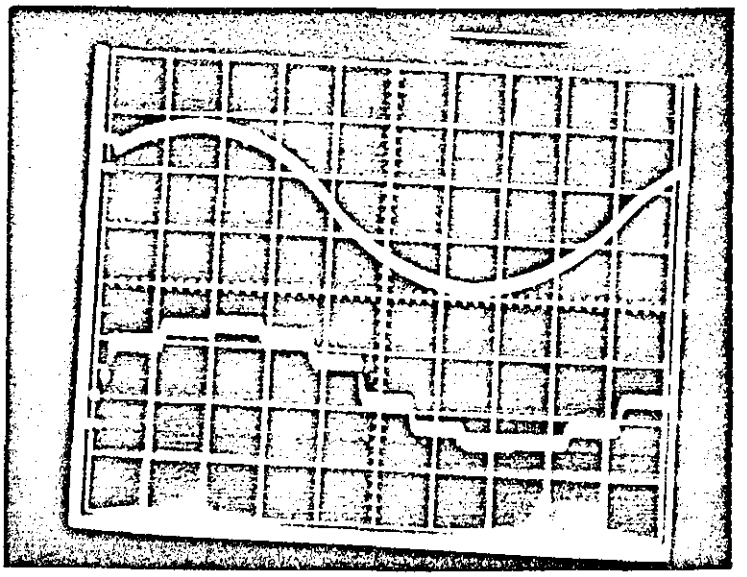


Figure 7.9: Input and Reconstructed Output Using 20Hz. Sine Wave. Gain (k_i)=1.

SENSITIVITY:
0.2V/div.

TIME BASE:
0.4ms/div.

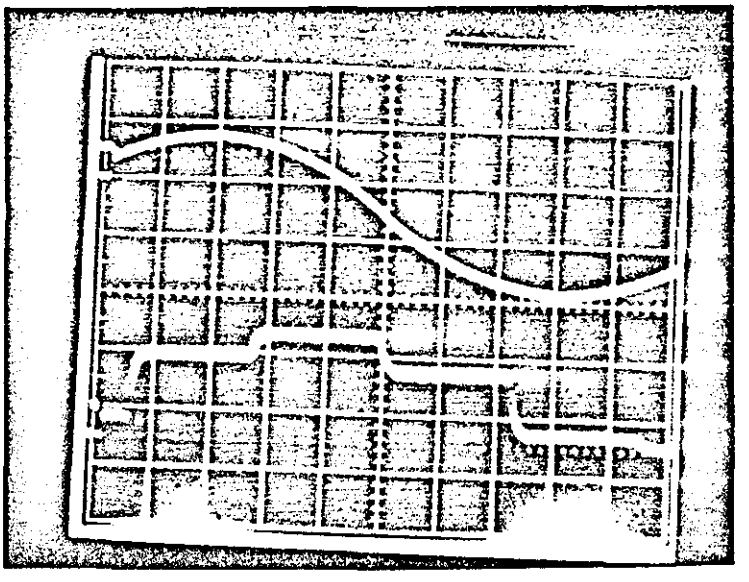


Figure 7.10: Input and Reconstructed Output Using 50Hz. Sine Wave. Gain (k_i)=1.

PMS-500 could not be relied upon to give an adequate reconstruction of the input signals for this application. However, from the results obtained in previous chapters, when the rigid body variables and the control surface deflections were plotted out, it was considered that a processing rate of 50 Hz. would be adequate if a micro-computer system such as the PMS-500 was used to act as a self-repairing controller.

7.4 SRC for the SLACS

As mentioned in Section 7.1, MPU's may be used to enhance the safety of operation of a SLACS in a variety of ways; these were described briefly in the same section. A possible scheme employing such MPU's to provide flight controller monitoring, state-estimation and sensor signal monitoring is shown in Figure 7.11. It is assumed that only those state variables connected with the 'safety law' are being measured and in addition, using a triple redundant scheme for the associated motion sensors. A 'voter' routine to provide 'majority rule' output may be incorporated into MPU(C1) and MPU(C2). MPU(C1) can be used to check each of three identical signals associated with each variable of the 'safety law'. MPU's B1 - B4 will contain reduced-order observer* algorithms, which can be used to reconstruct missing state variables required, for instance, for implementing a 17-SVF law. MPU(B1) will reconstruct those missing state variables based upon a measurement of vertical velocity, w. MPU(B2) will provide an independent reconstruction of the state vector based upon a measure of pitch rate, q. The reconstructions provided by MPU's B3 and B4 will be based upon the presence of w and q and of w,q, δ_A and δ_{E_i} respectively. The presence of 4 separate estimates of the state vector will again require a 'voter' and this function can be fulfilled by MPU(C2).

---

* Such observers will require less storage and CPU time than full-order observers for their implementation.

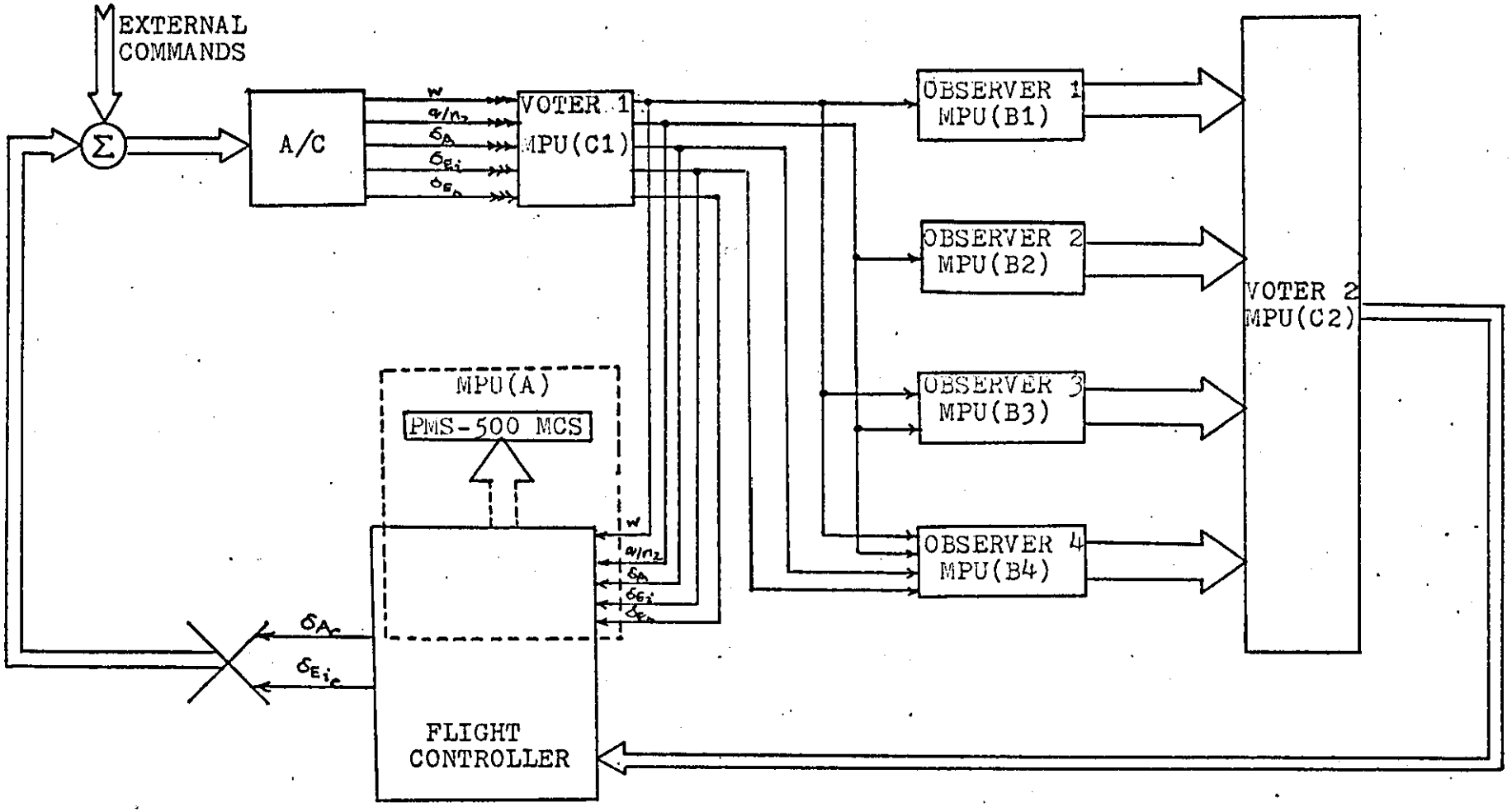


Figure 7.11: A PROPOSED 'SAFETY' SCHEME FOR THE SLACS.

The 'measured' state variables together with the 'estimated' state variables must then be scaled using the appropriate gain values connected with the optimal feedback law and summed to provide the actuator signals. Scaling and summing forms part of the function of the flight controller of the aircraft. Because the presence of those signals associated with the 'safety law' must be continually assured, it is proposed that an additional microprocessor unit (MPU(A)), be incorporated to monitor the signal path through the flight controller. It is this function which dictated the form of the study reported upon in this chapter.

In order to assess the performance of the SRC in a more realistic situation having typical aircraft sensor signals*, the mathematical model HANDEL, was patched on an EAI TR-48 Analogue computer. It was not possible to consider models of higher order for this test because of the limited amount of integrators available on the TR-48. In Figure 7.12 is shown a functional diagram of the way in which the test was carried out. The signals+ w, q, δ_A and δ_{E_i} were connected to the SRCTU where they were multiplexed with their appropriate feedback

---

* A vertical 'gust' signal was used to drive the model. The gust signal was produced as the output from a Butterworth filter which was one of the components of the gust generator shown in Figure 7.6. The gust generator was designed in an earlier study, (McLean,1976).

\+ Since the PMS-500 MCS was limited to 4 output channels on the D-A converter, and since for all tests, the outboard elevator deflection δ_{E_o} was zero, this signal was not used as part of the SRC tests.

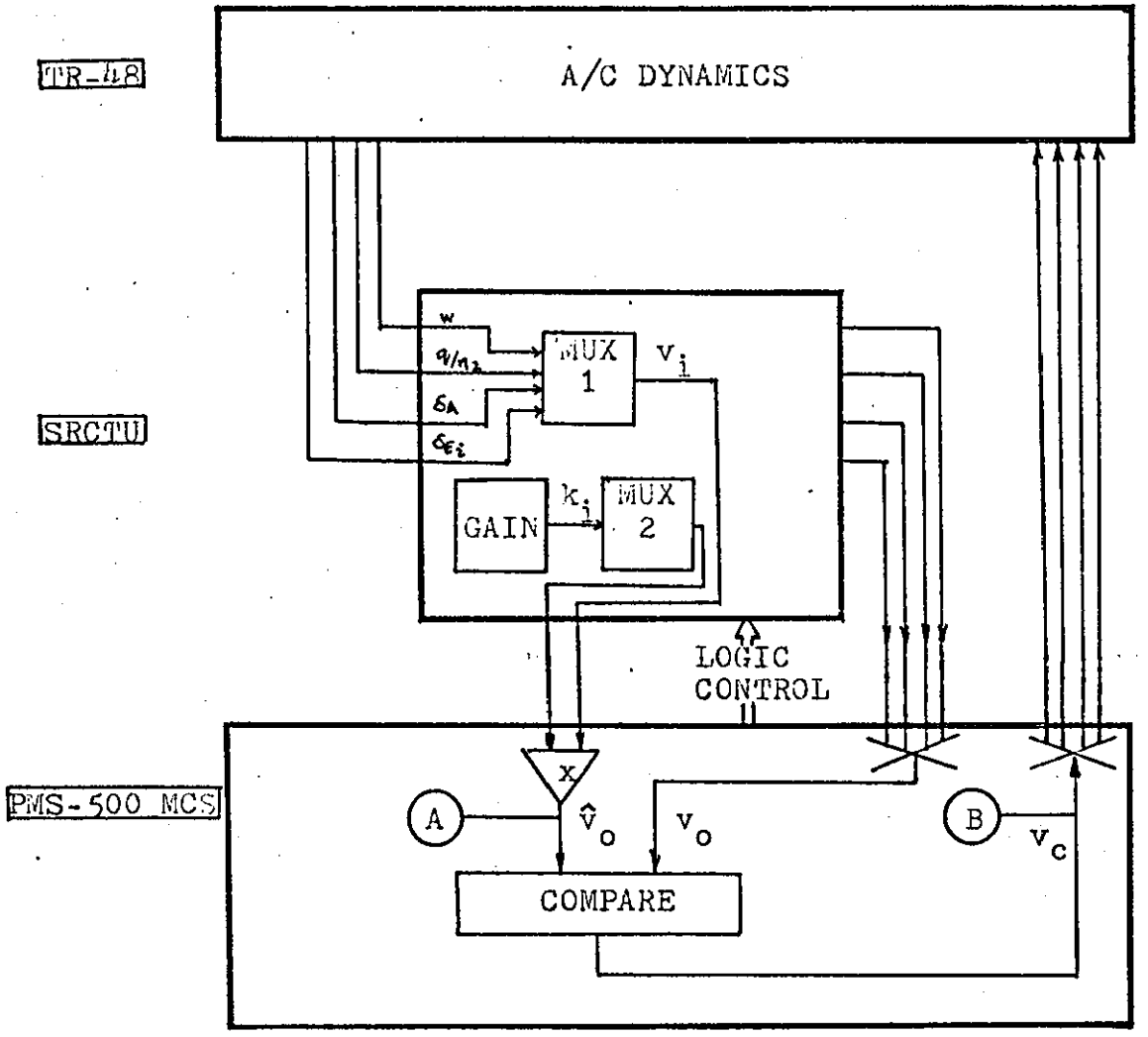


Figure 7.12: FUNCTIONAL DIAGRAM: SRC FOR THE SLACS

gains* using logic control from the PMS-500 MCS. Each signal, together with its appropriate gain, was then scaled and the resulting signal sampled by the PMS-500 MCS, (at point A, Figure 7.12). The SRCTU was also used to simulate a serious flight controller failure by providing as its output the appropriate scaled signals with a high degree of distortion associated with each of them.

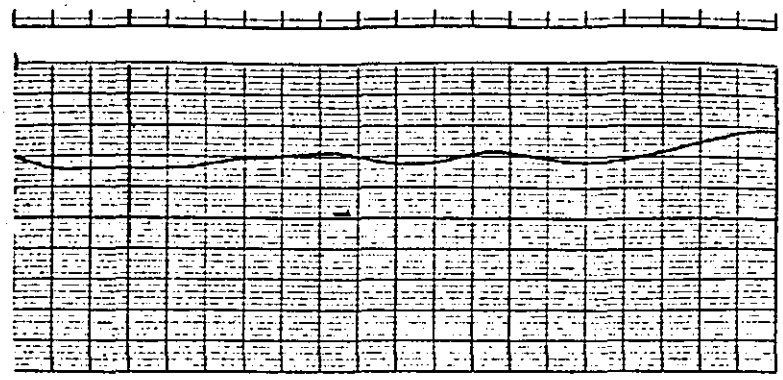
A program was then written (Appendix V), for the PMS-500 MCS which sampled the pure and distorted signals. These signals were compared according to Figure 7.3 and as described in Section 7.3. The correct signal 'sample' was then stored in an 8-level data stack. A second pair of signals was then compared and stored in the 8-level stack and so on. After all 4 sets of signals had been sampled, the first four locations of the 8-level stack were output to the D-A converter and the whole program cycle repeated.

In Figure 7.13 are shown the pure signals (point A, Figure 7.12) plotted together with the corresponding reconstructed output (point B,Figure 7.12). It is seen that as predicted from the results reported upon in Section 7.3, the sampling rate of the system used was quite adequate in providing a reasonable amount of self-repair to distorted feedback signals.

---

* These gains were in this instance not stored in the PMS-500 MCS but were set up independently as analogue voltages using the gain potentiometers on the SRCTU. This approach was used to minimise the need for data transfers through the A-D and D-A converters.

SENSITIVITY:
0.254m/s/div.

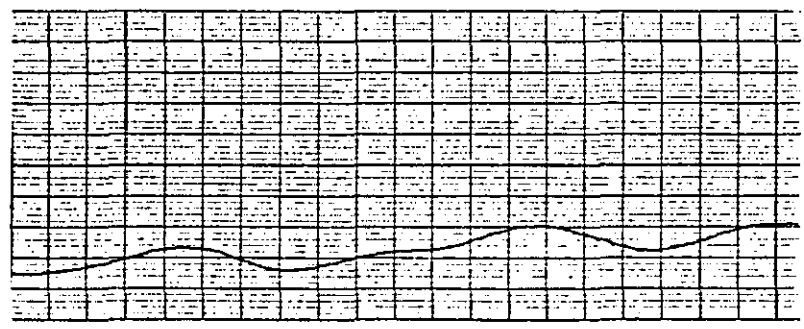




PAPER SPEED:
25mm/s.

Figure 7.13a: SIGNALS v_o AND v_c ASSOCIATED WITH VERTICAL VELOCITY(w).

SENSITIVITY:
0.012rad/s/div.



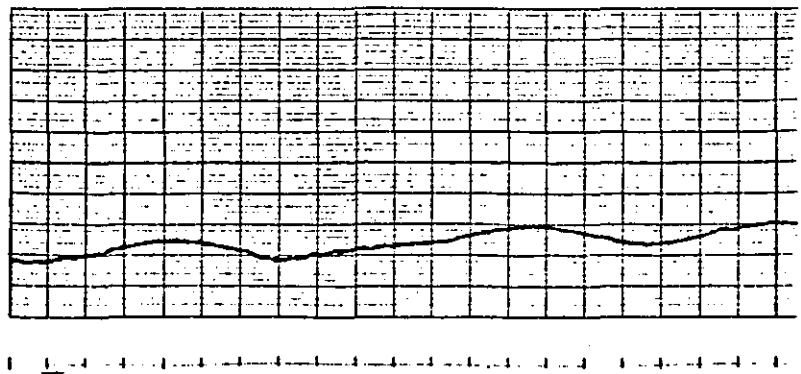


Figure 7.13b: SIGNALS v_o AND v_c ASSOCIATED WITH PITCH RATE (q/n_2).

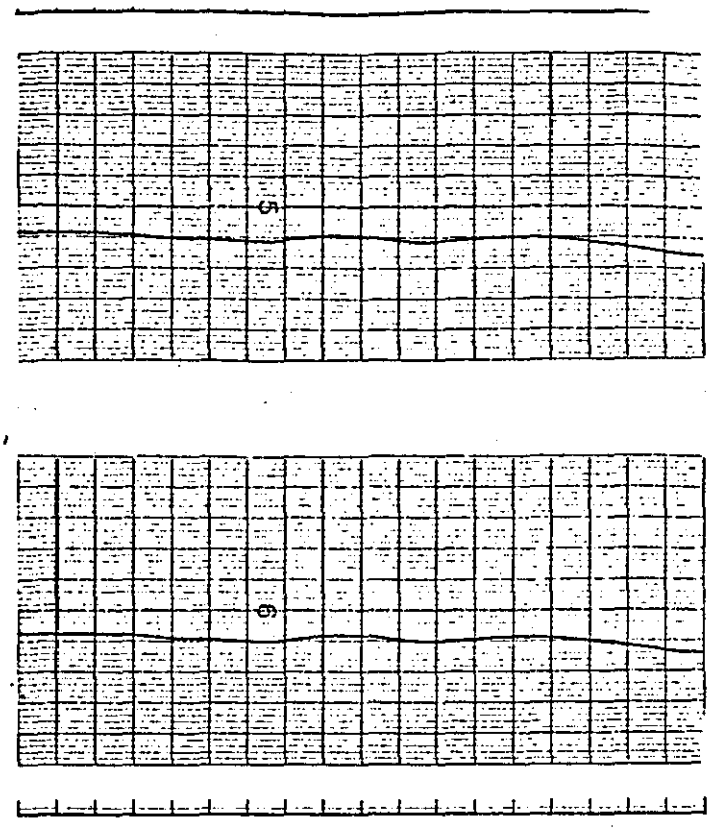


Figure 7.13c: SIGNALS v_o AND v_c ASSOCIATED WITH AILERON DEFLECTION (δ_A).

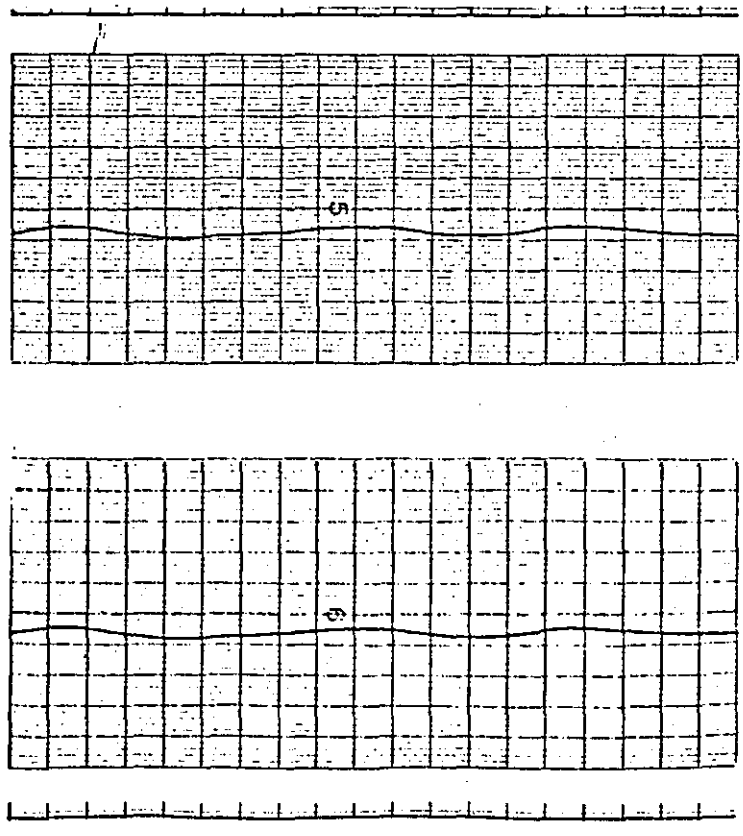


Figure 7.13d: SIGNALS v_o AND v_c ASSOCIATED WITH INBOARD ELEVATOR DEFLECTION (δ_E).

CHAPTER 8: CONCLUSIONS

8.1 Concluding Summary

This research investigation was concerned with a study of the application of optimal control theory, in conjunction with advanced electronic technology, to provide for current and future operational aircraft a means of alleviating structural loads (on such aircraft) when subjected either to deterministic manoeuvre demands or to flying through atmospheric turbulence, or both, by the use of continuously active control surfaces.

The aircraft type chosen for the study was the Lockheed C-5A and the specific aim was to design an active control system which would reduce the bending and torsional moments acting on the wing of the aircraft. This choice of aircraft was made because all the data required were available in Stone (1972) and Harvey and Pope (1977), although only information about the longitudinal motion, and then only for a single flight condition, was provided. A body-fixed axis system was employed principally because the criteria for aircraft handling and performance are normally expressed in this set (Schwanz (1972)), and because pilot response appears to be mostly based upon body-fixed motion cues (Gundry (1977)).

The most complete mathematical model employed for the subject aircraft was referred to as ARNE and was discussed in detail in Chapter 2 of this report. The model, ARNE, was of order, 79, and contained representations of rigid body motion, structural flexibility effects, actuator dynamics, gust dynamics and unsteady aerodynamics.

The rigid body motion of the aircraft was represented by the linearised, small perturbation equations associated with the short period mode: the long-period variation of the forward speed, known as the phugoid mode, was not believed to be significant. The chief reason for this is that it was considered that the variations in α and q (the variables associated with the short period motion), are unlikely to affect u and θ (the variables normally affecting the phugoid mode), in any significant way. Thus only vertical velocity, w, and pitch rate, q, were included in the state vector of ARNE.

For the representation of structural flexibility effects, up to fifteen bending modes associated with the wing of the aircraft were included, with frequencies ranging from 0.8Hz (for mode 1) to 8Hz (for mode 15). However, it was observed that the frequency associated with the short-period motion was only separated from the frequency of the first bending mode by a factor of 4 and this gave cause for some concern since it was known that if any frequency coupling occurred, it might not be possible with any AFCS design, to sufficiently augment the damping of coupled modes. It was found in all tests carried out that it was possible to obtain a feedback law which resulted in a separation of a factor of 8 or more between the two frequencies.

Three control surfaces were employed and these were: symmetrically deflected ailerons, and separately driven inboard and outboard sections of the elevator. However, only signals to the actuators associated with the ailerons and the inboard sections of the elevator were used as control inputs for the SLACS: the outboard section of the elevator was left free to respond to other commands such as may be required for carrying out normal in-flight manoeuvres.

A Dryden filter was employed for the simulation of atmospheric turbulence. Although a Von Karman model is in closest correspondence with the observed behaviour of turbulence, this model cannot easily be programmed because of a non-integer exponent in its p.s.d.,(See Eq.2.58). However, the Dryden model provides a p.s.d.,(See Eq.2.59), which closely matches that of the Von Karman model, although some small differences do occur between these models at the higher frequencies. It was considered that any AFCS designed to provide load alleviation will cause the damping of the bending modes to be so augmented that most of the energy will then be contained in the rigid body motion. As a result, the differences at high frequencies between these models will be of little consequence.

Unsteady aerodynamics were represented in the model, ARNE, by Küssner and Wagner lift growth functions. Although these functions are more accurately represented graphically, such representations are extremely difficult to incorporate into the model equations, and, therefore, well-established approximations (for instance,Bisplinghoff et al (1966)), were employed. In Harvey and Pope (1977), in the evaluation of the Küssner and Wagner functions an error was noted (McLean and Prasad (1980B)), where the value of the chord of any aerofoil sections considered, was used instead of the semi-chord. However, the Harvey and Pope representation was followed in this work to permit valid comparison of results.

Since the chief aim of the research was to achieve some reduction of bending and torsional loads on the wing of the aircraft, it was necessary to form an output equation, Eq.2.11, from which such loads could be determined at any time. Normal mode theory was used to derive such equations.

Quite early in the research study it became evident that in terms of computational requirements, ARNE would be too large to handle on the computing facilities available at LUT. As a result a number of lower order models were considered, viz., BACH, of order 42; CLEMENTI, of order 24; FAURÉ, of order 17; GERSHWIN, of order 14; and HANDEL, of order 5. However, because all the lower order models were derived from the model, ARNE, only this model was described in detail in Chapter 2.

In Chapter 3, those aspects of the theory relating to the design of a feedback controller to provide for the subject aircraft a certain amount of structural load alleviation were presented. Because of the nature of the problem, i.e., the requirement that two of the control surfaces of the subject aircraft be used to affect up to 56 output variables, application of optimal control methods were considered to be the most appropriate. Specifically, the problem was cast as the optimal output regulator. A particular disadvantage, however, of synthesising any feedback laws obtained as solutions of the optimal regulator problem is that full-state variable feedback (FSVF), is required and it was therefore proposed to make some tests employing reduced-order control. However, it was first decided that some consideration be given to establishing the controllability and stabilisability of each model employed.

In Chapter 3, it was stated that complete state controllability is a sufficient, but not a necessary, condition for closed-loop system stability (Larson and Dressler (1968)). If the original state description of the aircraft was itself stable, then this alone was a necessary and sufficient condition for

obtaining a feedback law which would guarantee the stability of the closed-loop system. The dynamic stability of the uncontrolled aircraft was most easily checked by observing the signs of the eigenvalues of the coefficient matrix of the state equation (i.e., matrix A of Eq.(3.4)).

All the questions raised so far, and reported upon in Chapter 3, were considered in the following Chapter. However, some aspects of the theory still remained to be considered, in respect of the type of problem formulation to be pursued, i.e., whether a solution of the Linear Quadratic Problem (LQP), as opposed to the Linear Quadratic Gaussian (LQG) Problem, was to be attempted. Solution of the LQP involves a purely deterministic approach, while solution of the LQG attempts to take account of the effects of atmospheric turbulence and of any measurement noise present. It is usual to employ a quadratic performance index (p.i) as a means of assessing the quality of performance achieved by the use of any feedback law derived. Such a performance index was characterised by the use of weighting matrices (typically Q and G matrices, see Eq.(3.3)), on the state and control vectors in its integrand. It is very difficult to determine the most appropriate values which must be used in the selection of Q and G matrices and, although a few methods have been proposed (Bryson and Ho (1969b), Harvey and Stein (1978)), none of these were found to be suitable and therefo empirical methods were employed.

In the solution of the LQP, or the LQG, provided that the weighting matrices are in each case chosen to be identical, the resulting control law will be the same. However, in the case

of the LQG, it is assumed that the state vector, $\underline{x}$, is not available for feedback: instead, an estimate of $\underline{x}$ has to be formed for which a Kalman-Bucy filter driven by the output, $\underline{y}$, and the control, $\underline{u}$, can be employed. However a Kalman-Bucy filter is in practice difficult to synthesise because of its dimensionality. It was considered that since the feedback law obtained will be the same, whatever the approach, if full state feedback were to be employed and a Kalman-Bucy filter not implemented, the worst that would be likely to occur is that some decrease in the performance cost will result. With strong feedback control, the attendant performance degradation is not likely to be great. Thus the solution of the LQP was adopted in all further tests. However, since it was realised from the onset in the research study that it will not be possible to implement FSVF, two separate approaches to the problem were proposed, viz.,

(a) use of reduced-order control,

and (b) use of Luenberger observers, in particular reduced-order observers, (which would be simpler to synthesise, although they do not take explicit account of the presence of noise), to see whether it will be possible to recoup some of the advantages of full state feedback control.

(a) formed the basis of Chapter 4, while work on observers, (b), was reported in Chapters 5 and 6.

From a closer study of the model, ARNE, it became evident that the transfer functions representing the Wagner dynamics

in this model were almost identically unity (see Figure 2.4). Since BACH only differed from ARNE by the omission of the Wagner dynamics, BACH was used in subsequent tests to represent the aircraft. However, further tests made by comparing the time responses to identical inputs obtained for the models BACH and CLEMENTI (in Chapter 4), indicated that a further reduction in model complexity was possible, for these time responses did not differ greatly even when what appeared to be severe manoeuvre demands were made on either model. (See Figures 4.1-4.3). CLEMENTI only differed from BACH in the omission of the upper nine bending modes, and, from considering the responses, it appeared that these higher bending modes were not contributing significantly to the total aeroelastic energy contained in the wing of the aircraft. Thus the model CLEMENTI was regarded as being of the highest order needed for any work associated with the design of a suitable SLACS for the subject aircraft.

The remaining models were used principally in those investigations employing reduced-order feedback control. By the use of these models, it was possible to determine the effect which the absence of one, or an entire group of, feedback variables had upon the performance of a SLACS. All reduced-order feedback laws were however tested in conjunction with the model, CLEMENTI. FAURÉ included equations representing the same dynamics as the model CLEMENTI, but excluded both the vertical gust and the Küssner dynamics. The model GERSHWIN, however, reintroduced both the gust and the Küssner dynamics, but included in its description only the first bending mode and its

rate, the higher modes being neglected. This model was used primarily to test the hypothesis that much of the bending energy (60% or more), is contained in the first bending mode (Schwanz,(1972)). The model, HANDEL, only contained in its description the rigid body motion variables and the variables associated with the actuator dynamics.

In the study, all the control laws derived, and the aircraft dynamics, were tested by means of digital simulation. A number of artificial test situations, (see Tables 4.1 and 4.2), involving both manoeuvre command inputs and disturbing the aircraft with simulated atmospheric turbulence were employed for assessing and comparing various SLACS schemes.

The effectiveness of any control law derived was carried out initially by inspection of the eigenvalues of the closed-loop system and then by making appropriate response checks using the artificial test situations.

Eigenvalue analysis was carried out primarily to determine the extent to which the damping of the structural bending modes had been augmented by the use of a particular SLACS scheme. From a comparison of eigenvalues of the uncontrolled aircraft with the controlled aircraft (Table 4.3), it was found that the frequency separation between the first bending mode and the short period mode had been increased from a factor of 4 to a factor of 8 although the basic handling qualities of the aircraft had remained essentially unaltered. The damping ratios of modes 1,3,5 and 6 were increased as were the frequencies of modes 1,3,4,5 and 6. The damping ratio of mode 4 was halved from 0.04

to 0.02. The dynamic characteristics of mode 2 remained unchanged. It was also noticed that the roots associated with the outboard elevator servo and the Küssner dynamics remained unchanged, a result which was not unexpected, since previous tests showed that although these dynamics were stable their corresponding states were not controllable. Thus, any model incorporating either the outboard elevator dynamics or the Küssner dynamics, or both, were found to be not completely state controllable.

With full state variable feedback, (control law, Eq.4.6), substantial reductions of the wing bending moments, of the order of 50% or more were easily achieved (Figure 4.7), although at a cost of a small increase, (of about 12%), in torsional moments sustained at the wing root (Figure 4.8). However by adjusting the weighting matrices in the performance index of the optimal control problem, it was always possible to effect simultaneous reductions in the bending and torsional moments sustained by the wing in response to some command or disturbance. Figures 4.10-4.12 show one such set of results for control law of Eq.4.15, where, for the wing root, for example, when a reduction in bending moment of 40% was achieved, a reduction in torsional moment of about 5% could be achieved simultaneously using this control law.

Because of the obvious practical difficulty of implementing FSVF, a number of simulation tests on the aircraft was carried out employing reduced-order control. Tests made on reduced-order feedback control demonstrated how it was possible to reduce the number of variables being fed back from 24 to 5, while still maintaining an acceptable level of alleviation of the

effects of the airloads.

It turned out that the five variables were relatively easy to measure being vertical velocity, w, pitch rate, q, aileron deflection, δ_A, inboard elevator deflection, δ_{E_i} and outboard elevator deflection, δ_{E_o}. It was however necessary to investigate the effects of any further loss of feedback and this led to a systematic scheme of tests made on the model CLEMENTI with various combinations of the gains associated with 5-SVF in the feedback loop. By means of eigenvalue analysis, it was possible to establish the condition that both pitch rate, q, and aileron deflection, δ_A, must always be available as feedback signals to guarantee the stability of the closed-loop SLACS. However, in all subsequent tests in the research, it was assumed that all five variables would be available for feedback and consequently 5-SVF was referred to as the 'safety law'.

It was found that the handling qualities of the aircraft were essentially unimpaired by the use of different control laws, although, with the 'safety law' operational, oscillations in the bending moments on the wing of the aircraft occurred (Figure 4.13) which, it was considered, could result in the accumulation of fatigue of the wing structure.

Since the research was primarily concerned with the reduction of structural loads on the wing of the aircraft, and since in all tests carried out, each SLACS was judged principally by the steady-state level of load reduction it provided, a method was developed, (reported in Section 4.4.3c), for quickly evaluating the steady-state load levels from a knowledge

of the aircraft dynamics and the command vector being applied. The results of tests using the method showed (Table 4.7), that in almost every case where reduced-order control (down to five motion variables) was employed, some reduction in bending and torsional loads on the wing was possible. However, with the 'safety law' operational, it was only possible to achieve a bending moment reduction of about 25% at the wing root. From this result it was concluded that reduced state feedback, which may result because enough sensors cannot be provided, or, when present, cannot provide accurate measurement, or may have failed in their operation, may be expressed in terms of the increased level of bending moments which will result. In addition, there can be some oscillation in the bending responses. With higher orders of feedback, the reduction was in the region of 40%. Such a result also served to confirm the previous remark that much of the aeroelastic energy appears to be contained in the first bending mode.

Eigenvalue analysis indicated that the response time of the inboard elevator servo was required to be reduced by some 400 times (a requirement which cannot be met in practice: see Wood and Lewis (1978)), in order to achieve the required structural load alleviation. However, in none of the artificial test situations used in the research were the observed actuator rates so high as to be unachievable by currently available servo-actuators. It was concluded that such a high rate will only be required for a step change, for example in angle of attack. In normal in-flight manoeuvres or even in atmospheric turbulence, th corresponding rate required may be well within the capability of present-day servoactuators.

Simulation tests involving atmospheric turbulence confirmed the result obtained from the deterministic tests, namely that the FSVF law, derived on the basis of the model CLEMENTI, was most effective in causing substantial reductions in bending moments at all five different wing stations, including the wing root, (see Figures 4.19 and 4.20).

A separate method was employed (due to Swaim et al (1977)), for predicting the r.m.s levels of bending moment at each wing station when the aircraft was 'flying' in simulated atmospheric turbulence. The tests showed that reductions in bending moment of between 80%-95% were achievable (Table 4.8). Even at the wing tip, where the ailerons are located, the reduction was greater than 80% when using FSVF control. With only the 'safety law' operational, a 25% reduction was still achievable at the wing tip, and better than 25% at the other wing stations.

The synthesis of any SLACS ought to employ the highest order of feedback feasible, consistent with economic and practical hardware constraints such as weight, cost and volume. Although FSVF resulted in the greatest reductions in bending and torsional moments on the wing of the aircraft, it was evident that it would not be possible to synthesise such control laws for two principal reasons, viz.,

(a) a few of the state variables, such as those associated with the Küssner dynamics, were only used for analytical convenience and do not in themselves have any explicit physical significance;

and (b) even if it were possible to provide such a large

number of sensors, this would be very costly, especially when it is considered that triplex or even quadruplex systems will be required.

It is also important that not too great a dependence should be placed upon the availability of a large number of measurements, since, as demonstrated earlier in this report, sudden loss of such measurements results in an increased level of bending and torsional loads sustained in the wing, a situation which, if unaccounted for, could cause disastrous results.

For the reasons mentioned above, a number of studies were made to improve possible flight integrity, while at the same time attempting to secure maximum load reductions, by the use of state estimators, or Luenberger observers, to reconstruct any missing signals. Both full and reduced-order observers, driven by the available outputs and controls of the system, were investigated.

In Chapter 5, a simple algorithm based upon optimal control methods was developed and used to derive all the parameters required for implementing a full-order observer. The performance criterion employed in this case was a weighting of the error between the actual state and the estimated state. Minimisation of the associated performance index resulted in the solution of the 'gain matrix' of the observer. All work with the full-order observer was carried out using the model FAURÉ because this model differed from CLEMENTI only in the absence of the Küssner dynamics and gust dynamics, and it was not proposed to excite these dynamics in the tests.

Initially, the observer performance was assessed by inspecting the eigenvalues of each new design and comparing these eigenvalues with those of the controlled aircraft. One such result (assuming that only vertical velocity, w, was available), was given in Table 5.1 which was produced by a simple choice of observer weighting matrices, i.e Eq.5.37 and Eq.5.38. Some difficulty was experienced regarding the placement of observer poles since the only means by which such placement could be achieved was by empirical selection of Q and R weighting matrices. According to Luenberger (1966), there is little reason to choose observer poles much faster than the poles of the closed-loop system. However, for the observer design, indicated in Table 5.1, the real parts of the eigenvalues of the observer should at least have been greater than those of the eigenvalues of the controlled aircraft (considered in this case to be adequately represented by the model FAURÉ). This observer design was nevertheless tested with the controlled aircraft by means of digital simulation and using the same deterministic test situations employed previously (Table 4.1).

With the initial conditions of the aircraft and the observer perfectly matched, it was possible to achieve the same response as originally determined for the aircraft employing FSVF (see Figures 5.1-5.3). In a number of reports (Newmann (1970), Arimoto and Hino (1974)), it had been suggested that the performance of an observer will deteriorate substantially if the initial conditions on its states are not matched with those of the system being 'observed'. In an attempt to confirm the validity of this proposition, a number of tests were made for the

situation where the initial conditions of the observer did not agree with those of the dynamic model of the aircraft. It was shown that for the particular design studied, the observer was most sensitive to a mismatch of initial conditions on vertical velocity, w; somewhat less sensitive to a mismatch on pitch rate, q; and least sensitive to a mismatch of inboard elevator deflection, δ_{E_i}. The strong sensitivity to a mismatch of initial conditions on vertical velocity was believed to be a result of the original specification of the particular observer design studied, viz., reconstruction of the system state was to be achieved by providing an accurate measurement of vertical velocity. In addition, these results were not wholly unexpected because of the questions raised earlier, about the suitability of this particular observer in respect of the poor placement of its poles.

Further tests (involving only different choices of weighting matrices) showed that it was possible to obtain a desired set of dynamics associated with each observer design although it was not possible to establish any fixed pattern for a suitable choice of weighting matrices. A workable design would therefore only result from carrying out a large number of test computer runs, during which, both the locations of the observer's eigenvalues and the response of the aircraft, with observer incorporated, need to be checked.

A number of further tests were proposed for new observer designs based upon the availability of other measurements, viz., q, δ_A and δ_{E_i}. With only pitch rate, q, assumed to be available, no significant change in the observer performance was recorded

when compared with that of earlier designs based upon the availability of vertical velocity, w. However, further tests showed that, as would be expected, the availability of more measurements had a beneficial effect upon the aircraft's response. With w and q available simultaneously, the bending moments experienced in the wing of the aircraft were initially quite severe although the transients decayed quickly (<1s.,see Figure 5.11). With the presence of all four signals, viz., w, q, δ_A, δ_{E_i} the transient excursions in bending moments were much less than in the previous design but the decay of such transients were not as fast, in some cases lasting up to 4 seconds,(Figure 5.12). Also the observer 'gain matrix' associated with the measurement of four variables contained some elements which were large ($\gg 10^3$). It was considered that in practice it will be inappropriate to use gains $>10^2$ because not only the pure signal will be amplified but also any noise signal present in the feedback path. Consequently the results associated with this test may not be achievable in practice. However, it is possible that further numerical experiment with different weighting values in the $\hat{Q}$ and $\hat{R}$ matrices may produce a workable design with the type of performance indicated in Figure 5.12.

The full-order observers reported upon in Chapter 5 were regarded as being sub-optimal. The chief reason for this was that an attempt was made to minimise the error between the reconstructed state and the actual state of the system without taking account of what amount of controlling action will be required. Secondly, these observers were used to reconstruct those signals associated with the 'safety law': for the implementa-

tion of a SLACS, it is expected that the presence of those motion variables connected with the 'safety law', i.e., w, q, δ_A, δ_{E_i} and δ_{E_o} will always be guaranteed by using a suitable hardware redundancy scheme. Thus it was considered that if an observer were to be used to provide some measure of reliability, (in software) to the SLACS by reconstructing any missing feedback signals, then it would be wasteful of computer storage and time to reconstruct signals which were, in any case, already being measured. Thirdly, the full-order observers considered were all extremely sensitive to mismatching of initial conditions between the state vector of the aircraft and those of the observer model.

For these reasons, an optimal minimal-order observer design, proposed by Miller (1973), was considered and reported upon in Chapter 6. In this case, the design parameters were chosen to minimise the expectation of the regulator cost functional, and not the state estimation error. Further, the initial stat of the aircraft was not required to be known, but only the mean values and the covariances of the initial conditions were required. In the study the mean value of the initial state vector, $\underline{m}$, was taken to be zero and the covariance matrix, Σ_o, was taken as the solution of the degenerate Riccati equation given as (3.76), (see previous work reported in Section 3.3 on the solution of the covariance matrix). The observer matrices, when solved, were fixed as a result of the choice of $\underline{m}$ and Σ_o and these matrices were used in all tests reported upon in Chapter 6. Also, regardless of the initial conditions of the aircraft, the initial conditions required to be set on the observer states were

also fixed and had to be evaluated for each new test situation by means of Eq.6.89. The test situations employed previously were again used to allow comparison of results obtained. Since it was found from previous tests (in Chapter 5), that the presence of four measurements , viz., w, q, δ_A and δ_{E_i} gave the best results in terms of the transient behaviour of a proposed observer design, the permanent and assured availability of these measurements was again assumed in all studies using the reduced-order observer.

Dynamic response tests indicated that the observer design considered was, in particular, less sensitive to imperfect matching of initial conditions. In the case A test situation, the response of the aircraft (with the observer incorporated) was identical to those responses obtained when FSVF design were considered (Figure 6.1). However, when more severe manoeuvre demands were made on the system, it was noticed that the observer dynamics could be sufficiently pronounced to affect the wing bending and torsional moments (Figures 6.2 and 6.3). These fluctuations in bending and torsional moments were nevertheless insubstantial and certainly were not as great as those obtained when full-order observers were employed. In all cases, the observer transients settled within 2 seconds.

In general then, the observer tests showed that, even with only a few measurements, it was possible to reconstruct fairly accurate estimates of the state vector which, in turn, allowed full state feedback control, together with its attendant advantages, to be made possible. The tests have also served to demonstrate that part of the flight integrity requirements for imple-

menting the SLACS may be met by employing software reliability. In general a hardware redundancy scheme will still be required for the servo-actuators and particularly those motion sensors from which the 'safety law' is derived.

With the advent of small dedicated microprocessor units (MPU's), it has become possible to consider the practical problem of synthesising complex control systems such as those which will be required for providing structural load alleviation. Such systems may, for instance, be used to enhance the safety and reliability of operation of the SLACS considered by providing:

(a) Flight controller monitoring
(b) State-estimation
(c) Sensor signal monitoring
and (d) Self-checking.

The final exercise of the research investigation (reported upon in Chapter 7), was concerned with how (a) may be achieved. A Bell and Howell PMS-500 Micro-computer System (MCS) was used to detect a simulated failure of a linear feedback controller. Once the failure in the feedback signal was detected by the MCS, a surrogate gain (stored in ROM) was employed, which restored the feedback signal to its proper value. When used in this way, the MCS was referred to as a self-repairing controller (SRC). The available MCS did not have sufficient core space to allow any of (b), (c) or (d) to be adequately demonstrated, although, a possible scheme was described in Section 7.4. Also, in the course of the development work on the SRC, it was established that the need to use floating-point software techniques was a

serious performance limitation in respect of the sampling rate which could be achieved.

For the simulation of failures, a test unit, referred to as a self-repairing controller test unit (SRCTU) was designed. Because the D-A converter on the PMS-500 MCS was limited to 4 output channels, the SRCTU was designed to continuously process a maximum of 4 signals at a time. A failed signal was produced, in the SRCTU, by periodically grounding the pure signal (v_i), in a pseudo-random fashion, (Figure 7.7). In addition, this signal was scaled by means of an analogue multiplier unit, by using an appropriate gain value (k_i). Thus, one of the output signals of the SRCTU was related to its corresponding input signal, by,

$$v_o = k_i v_i \qquad \ldots (8.1)$$

The signals v_o and v_i were then sampled by the PMS-500 MCS. Using a surrogate gain ($\hat{k}_i$), the PMS-500 MCS was programmed to produce an estimate of the output signal, i.e., $\hat{v}_o$, based upon the sample of the pure signal, v_i, i.e.,

$$\hat{v}_o = \hat{k}_i v_i \qquad \ldots (8.2)$$

In the MCS, the two signals v_o and $\hat{v}_o$ were compared to within a prescribed tolerance and by this means it was possible to arrange that only the correct signal level was output through the D-A converter (Figure 7.8).

All the tests reported upon in Chapter 7 were based upon simultaneous processing of 4 sets of signals. To determine the maximum rate of processing, it was arranged that one of these signals was a pure sine wave whose frequency could be varied.

The results showed that with the PMS-500 MCS programmed to process 4 independent signals in sequence, a sampling rate of 100 samples/s. could be achieved. However it was found that 50Hz should be regarded as a limiting frequency above which the PMS-500 MCS could not be relied upon to give an adequate reconstruction of the input signals (Figure 7.10).

In order to assess the performance of the SRC in a more realistic situation having typical aircraft sensor signals, the mathematical model, HANDEL, was simulated on an EAI TR-48 analogue computer. The model was continuously driven by means of a 'gust' signal derived as the output from a Butterworth filter. The signals w, q, δ_A and δ_{E_i} were connected to the SRCTU where they were failed before being sampled by the PMS-500 MCS (Figure 7.12). From the results obtained, (Figure 7.13), it was evident that the system used was adequate in providing a reasonable amount of self-repair to distorted feedback signals. A number of areas of study however remained to be considered and these are treated in the remaining section of this Chapter.

8.2 Recommendations for further work

1. There remains a clear need for further investigation of the suitability of the mathematical models employed in this research for the design of structural load alleviation control systems. Because of computational problems, the most complete model of the aircraft (model,ARNE), was not employed for the assessment of SLACS schemes. Those less complete models used were a result of a number of structural dynamic approximations and, in particular, the model CLEMENTI was a result of a residualisation carried out on ARNE. Schwanz (1972) warns against the a priori selection of an inappropriate formulation since such selection can lead to large errors in the design of the flight control system. Any such investigation should also include a study of more accurate representations of the Küssner and Wagner functions and of the actuator dynamics.

2. The assessment of the SLACS schemes may be enhanced by incorporating the effects of changes in flight conditions, of aircraft mass changes, and of any coupling effects, whether structural or aerodynamic, produced as a result of lateral motion.

3. There remains a need for a continued investigation regarding the selection of suitable weighting matrices. The method proposed by Harvey and Stein (1978), should be extended to include application of weighting values on an output vector of any dimension. In addition,

there still exists a need for determining some possible explicit relationship between the selected weighting matrices and the desired output response of the aircraft.

4. An attempt should be made to test the validity of the proposition made in Section 3.2.1.2 that the incorporation of a Kalman-Bucy filter into the feedback loop will not substantially improve the performance of the SLACS. However, particular note should be made of the fact that such a filter will only be required to be driven by those measurements which are easily available such as the signals associated with the 'safety law'. Thus, with such a filter, it may be possible to recoup some of the bending moment reductions lost as a result of using only the 'safety law'.

5. Because reduced-order Luenberger observers are simpler to synthesise, when compared with either a Kalman-Bucy filter, or a full-order Luenberger observer, further checks should be made on the design considered to investigate the degradation in performance of the observer, in the presence of noise such as atmospheric turbulence or measurement noise. Some degradation in performance is expected since the observer design did not take explicit account of the presence of noise.

6. The practicability of synthesising the SLACS designs considered should be further investigated by the use of microprocessor oriented computer systems (MCS's). Such systems will be required to be fast with cycle times of 200ns., or less, since they will be required to work in

real time. The storage requirements of such systems must also be high: for the reduced-order observer design studied, about 10k of ROM will be required to implement 17-SVF. An MCS must also be capable of at least 16-bit word working in order to maintain the numerical accuracy required, (for example when an observer algorithm is being implemented), in the manipulation of large matrices.

7. An attempt should be made to confirm some of the findings of this research investigation by carrying out tests on the C-5A aircraft. The variables associated with the 'safety law' will be easy to derive from appropriately positioned measurement sensors. Bending moments in the wing structure could be evaluated from computations on readings taken from a number of strain gauges. Such tests may however require modifications to be made to the actuation system incorporating the ailerons and inboard sections of the elevator: since these surfaces will be continuously active, some strengthening of the areas surrounding the surfaces may be required; also, it may not be possible with the hydraulic actuators employed on the aircraft, to derive the actuation rates required for load alleviation especially in atmospheric turbulence.

REFERENCES

ARIMOTO S AND H.HINO
Performance Deterioration of Optimal Regulators Incorporating State Estimators
Int J.Control,Vol 19,1133-1142,Jun,1974

ATHANS M.
The Matrix Minimum Principle.
J. of Information & Control,Vol.11,pp.592-606,1968.

ATHANS M.
The Role and Use of the Stochastic Linear Quadratic Gaussian Problem in Control System Design.
IEEE Tr.Vol.AC-16,No.6,1971,pp.529-552.

ATHANS M AND P.L.FALB
OPTIMAL CONTROL THEORY
McGraw Hill Book Co.,NY.,1966

ATHANS M. AND F.C.SCHWEPPE
Gradient Matrices and Matrix Calculations.
Technical Note #53,MIT,Lincoln Labs,Lexington,Mass., 1965.

ATTWOOD J.L.,R.H.CANNON.,J.M.JOHNSON AND G.M.ANDREW
Gust Alleviation Systems.
US Patent 2,985,409,1961.

BISPLINGHOFF R.L.,H.ASHLEY AND R.L.HALFMAN
AEROELASTICITY
Addison-Wesley Publishing Co.,Inc.,1955

BONGIORNO Jr.J.J. AND D.C.YOULA
On Observers in Multi-Variable Control Systems
Int.J.Cont.,Vol 8,No 3,1968,pp221-243

BRAINERD C.H. AND D.L.KOHLMAN
A Simulator Evaluation of the Use of Spoilers on a Light Aircraft.
NASA-CR-2121,1972.

BROCKETT R.W
FINITE DIMENSIONAL LINEAR SYSTEMS

John Wiley, 1970.

BRYSON Jr.A.E. AND Y.C.HO
APPLIED OPTIMAL CONTROL:
OPTIMIZATION,ESTIMATION AND CONTROL.
Ginn and Co.,1969.

BURNS R.J. AND K.S.P.KUMAR
Sensitivity Considerations in Specific Optimum Controls
Int.J.Control,Vol.5,p.289,1967.

BURRIS P.M. AND M.A.BENDER
Aircraft Load Alleviation and Mode Stabilisation

AFFDL-TR-68-161,1969,WPAFB,USA.

CHALK C.R. et al.
Background Information and User's Guide for MIL-F-8785B(ASG): Military Specification - Flying Qualities of Piloted Aircraft.
AFFDL-TR-69-72, Aug.,1969.

COUPRY G.
Pilotage Automatique D'Un Avion Volant En Atmosphere Turbulente
Agard,Oct.,1971,Paris.

DAVIS H.M. AND R.L.SWAIM
Controlling Dynamic Response in Rough Air.

AIAA Paper No.66-997,Dec.,1966.

DeRUSSO P.M.,R.J.ROY AND C.M.CLOSE
STATE VARIABLES FOR ENGINEERS

John Wiley & Sons,3rd Ed.,Jun.,1967.

DOWELL E.H.,H.C.CURTISS,R.H.SCANLAN AND F.SISTO
A MODERN COURSE IN AEROELASTICITY

Sijthoff & Noordhoff,Holland,1978.

EISENBERG B.R. AND A.P.SAGE
Closed Loop Optimisation
of Fixed Configuration Systems
Int. J.Control,Vol.3,p.183,1966.

FINK D.E.
Pan American Using New Equipment.

Av.Week & Space Tech.,May 19,1980,pp.34-36.

FULLER A.T.
Performance Criteria for Control Systems.

J.Elec.& Cont.,Vol.7,1959,pp.456-462.

FUNG Y.C.
AN INTRODUCTION TO THE THEORY OF AEROELASTICITY

John Wiley & Sons Inc.,1955.

GOLUB G.H.,S.NASH AND C.VAN.LOAN
A Hessenberg-Schur Method for the Problem AX+XB=C.

TRANS. IEEE,Vol.AC-24,6,1979,pp909-913.

GUNDRY J.
The Effectiveness and Sophistication of Motion
Cues Provided in Flight Simulations.
Proc.Inst.M.C.Conf. on Human Operators and
Simulation,1977,Loughborough,35-41.

HARPUR N.F.
Effect of Active Control Systems on
Structural Design Criteria.
Agard 37th Meeting of Struct. and Materials
Panel,Oct.,1973.

HARVEY C.A. AND R.E.POPE
Study of Synthesis Techniques for
Insensitive Aircraft Control Systems.
NASA CR-2803,Apr.,1977.

HARVEY C.A. AND G.STEIN
Quadratic Weights for Asymptotic Regulator Properties.

Trans IEEE.,Vol.AC-23,3,pp378-387,1979.

HAWK J.,R.J.CONNER AND C.LEVY
Dynamic Analysis of the C-47
Gust Load Alleviation System.
Douglas Report SM14456,Douglas Aircraft,
Santa Monica,Calif.,July,1952.

HINSDALE A.J.
Lateral Ride Quality of the B-1 Aircraft Subjected to
a Reduction of Lateral Static Stability.
NASA CR-148206,April,1976.

HIRSCH R.
Etudes et Essais d'un Avion Absorbeur de Rafales.

D.O.C.(USA) Aero No.42,Jan.,1957,pp13-28.

HOBLIT F.M.
Effect of Yaw Damper on Lateral Gust Loads
in Design of the L-1011 Transport.
Agard,37th Meeting of Structures
and Materials Panel,1973.

HUNSAKER J.C. AND E.B.WILSON
Report on Behaviour of Aeroplanes in Gust Turbulence.

NACA TR-1(MIT),Oct.,1915.

HUNTER P.A. AND O.C.KRAFT
A Flight Investigation of an Automatic Gust Alleviation
System in a Transport Aircraft.
NASA TND-532,Jan.,1961.

KALMAN R.E.
Contributions to the Theory of Optimal Control.

Bol.Soc.Mat.Mex.,Vol.5,pp102-119,1960.

KALMAN R.E. AND R.BUCY
New Results in Linear Filtering and Prediction.

Trans ASME,Vol.83D,1961,p.95.

KRAFT C.C.
Initial Results of a Flight Investigation
of a Gust Alleviation System.
NASA TM-3612,1956.

KUO B.C.
AUTOMATIC CONTROL SYSTEMS.

Prentice Hall Inc..1975.

KÜSSNER H.G.
Züsammenfassender Bericht über Den
Instationären Auftrieb von Flügeln.
Luftfahrtforsch..B.D.13,NR.12,Dec..1936.

KWAKERNAAK H. AND R.SIVAN.
LINEAR OPTIMAL CONTROL SYSTEMS

Wiley Interscience,1972.

LANCZOS
APPLIED ANALYSIS

Pitman,London,1957,pp.139-140.

LANGE R.H. et al.
Application of Active Controls Technology
to the NASA Jetstar Aircraft.
NASA CR-2561,June 1975.

LARSON R.E. AND R.M.DRESSLER
Optimal Control of a Class of Partially
Controlled Systems.
Proc.Hawaii Int.Conf.of System Sciences,Jan.,1968.

LAUB A.J.
A Schur Method for Solving Algebraic Riccati Equations.

Trans. IEEE.,Vol.AC-24,No.6,1979,pp913-914.

LUENBERGER D.G.
Canonical Forms for Linear Multivariable Systems

IEEE Tr. Vol.AC-12,Jun.,1967,pp290.

LUENBERGER D.G.
An Introduction to Observers.

IEEE Tr.Vol.AC-16,No.6,1971.

LUENBERGER D.G.
Observers for Multivariable Systems.

IEEE Tr.Vol.AC-11,No.2,Apr.1966.

MAEDA H AND H.HINO
Design of Optimal Observers for Linear Time-Invariant Systems

Int.J.of Control,Vol.19,No.5,1974,pp993-1004.

MARSHALL S.A. AND H.NICHOLSON
Optimal Control of Linear Multivariable
Systems with Quadratic Performance Criteria.
Proc.IEE,Vol.117,No.8,1970,pp.1705-1713.

McLEAN D.
Gust Load Alleviation Control Systems:
A Feasibility Study.
Transport Technology Report No.TT-7606,1976.
The University,Loughborough,Leics.,LE11 3TU.

McLEAN D.
Gust Alleviation Control Systems for Aircraft.

Proc.IEE,Vol.125,No.7,1978,pp.675-685.

McLEAN D. AND R.A.PRASAD
A Structural Load Alleviation System
For a Large Aircraft.
Trans.Inst M.C.,1980A(to appear).

McLEAN D. AND R.A.PRASAD
A Structural Load Alleviation Control System
for a Large Aircraft.
Transport Technology Report No.tt-8002,1980B,
The University,Loughborough,Leics.,LE11 3TU.

McLEAN D. AND R.A.PRASAD
Use of a Microprocessor in a
Proposed Flight Control System.
IFAC Conference: Application of Microprocessors in
Devices for Instrumentation and Control,21-23 Nov.,1980C

MILLER R.A.
Specific Optimal Control of the Linear Regulator Using a Minimal Order Observer.
Int.J.of Control,Vol.18 ,No. 1 ,1973,pp.139-159.

MILNE R.
Dynamics of the Deformable Aeroplane.
A.R.C R&M 3345,1964.

NEWMANN M.M.
Optimal and Sub-Optimal Control Using an Observer When Some of the State Variables are not Measurable.
Int.J.of Control,Vol.9,No.3,1969,pp.281-290.

NEWMANN M.M.
Specific Optimal Control of the Linear Regulator Using a Dynamic Controller based on the Minimal Order Luenberger Observer.
Int.J.of Control,Vol.12,No.1,1970,pp.33-48.

OSTGAARD M.A.
Active Control Technology.
AFFDL FGT WPAFB, Ohio 45433,1976.

PHILLIPS W.H. AND C.C.KRAFT
Theoretical Study of Some Methods for Increasing the Smoothness of Flight through Rough Air.
NASA TN2416,1951.

PONTRYAGIN L.S..V.BOLTYANSKII..R.GAMKRELIDZE AND E.MISHCHENKO
THE MATHEMATICAL THEORY OF OPTIMAL PROCESSES
Interscience Publisher Inc.,N.Y..1962.

PORTER B. AND M.A.WOODHEAD.
Performance of Optimal Control Systems When Some of the State Variables are not Measurable.
Int.J.of Control,Vol.8,No.2,1968,pp.191-195.

POTTER J.E.
Matrix Quadratic Solutions.
SIAM J.App.Maths.,Vol.14,No.3,1966,pp.496-501.

PRASAD R.A.,S.L.A.SAULLIS AND L.TSITSILONIS
The Role of Simulation in Automatic
Flight Control Systems Research.
The Aeronautical Journal,R.Aero.Soc.,Aug,1980,p.238.

RICHARDS R.J.
AN INTRODUCTION TO THE DYNAMICS OF CONTROL.
Longman 1979,pp.270-272.

ROESCH P. AND R.B.HARLAN
A Passive Gust Load Alleviation System For Light Aircraft
AIAA Paper No.74-773,1974.

SARMA V.V.S. AND B.J.DEEKSHATULU
Optimum Control when some of the
State Variables are not Measurable.
Int.J.Control,Vol.7,pp.251,1968.

SCHWANZ R.C.
Formulations of the Equations of Motion of an Aeroelastic
Aircraft for Stability and Control and Flight Control
Applications
AFFDL/FGC-TM-72-14,Aug.,1972.

SCHWENDLER R. AND R.MacNEAL
Optimum Structural Representation
in Aeroelastic Analysis.
ASD-TR-61-680,March,1962.

SEARS W.R.
Operational Methods in the Theory
of Airfoils in Non-Uniform Motion.
Journal of the Franklin Institute,
Vol.230,pp.95-111,1940.

SIMS C.S. AND J.L.MELSA
Sensitivity Reduction in Specific Optimal
Control by the Use of a Dynamic Controller.
Int.J.Control,Vol.8,p.491,1968.

SMITH R.E. AND E.L.S.LUM
Linear Optimal Control Theory and Angular Acceleration
Sensing Applied to Active Structural Bending
Control on the XB-70.
AFFDL-TR-66-68,WPAFB,Dayton,Ohio,1966.

SMITH R.E. AND E.L.S.LUM
Linear Optimal Theory Applied to
Active Structual Bending Control.
AIAA Paper No.69-970,Dec.,1966.

SMITH R.E.,E.L.S.LUM AND T.G.YAMAMOTO
Application of Linear Optimal Theory to
Control the Flexible Aircraft Ride Qualities.
AFFDL-TR-67-136,Jan.,1968.

SPRATER A.
Stabilising Device for Flying Machines.

US Patent 1,119234,1914.

STEINHAUSER R.
Investigations for the Calculation of Robust Control Systems.

ESA-TT-488,Jun.1978,pp.1-30.

STEWART E.C.
Discussion of an Aeromechanical Gust Alleviation
System to Improve Ride Comfort of Light Airplanes.
SAE Paper No.750544,1975.

STOCKDALE C.R. AND R.D.POYNEER
Control Configured Vehicle Ride Control System.

AFFDL-TR-73-83,July,1973.

STONE C.R. et.al.
Studies of the Compatibility of Relaxed Static Stability
and Manoeuvre Load Control to C-5A type Aircraft.
AFFDL-TR-72-38,Vol.II,Jun.,1972.

SWAIM R.L.,D.SCHMIDT.,P.A.ROBERTS AND A.J.HINSDALE.
An Analytical Method for Ride Quality of Flexible Airplanes.

AIAA Journal,Vol.15,No.1,Jan.,1977,pp.4-7.

TAYLOR G.S.
Statistical Theory of Turbulence.

Jour.of Aerosp.Sci.,Vol.4,No.8,Jun.,1937,pp.311-315.

TOBAK M.
On the Minimisation of Airplane Responses to Random Gusts.
NASA-TN-3290,1957.

TRUXAL J.G.
AUTOMATIC FEEDBACK CONTROL SYSTEM SYNTHESIS.
McGraw Hill NY,1955.

VAN DIERENDONCK A.J.,C.R.STONE AND M.D.WARD
'Application of Practical Optimal Control to the C-5A LICS'.
Proc.AIAA Guidance Control Conf.,Aug 20-22,1973.

VON KARMAN T.
Fundamentals of the Statistical Theory of Turbulence.
J.Aero.Sci.,Vol.4,No.2,1937,pp.31-138.

WAGNER H.
Über Die Entstehung des Dynamischen Auftriebes von Tragflügeln.
Z.Agnew.Math.Mech.,B.D.5,Heft 1,Feb.,1925.

WOOD N.E. AND R.A.LEWIS.
Electromechanical Actuation Development.
AFFDL-TR-78-150,Dec.,1978.

WYKES J.H. AND A.S.MORI
An Analysis of Flexible Aircraft Structural Mode Control Pt.1 - Unclassified Data.
AFFDL-TR-65-190,June,1966.

ZBROZEK J.K.
Theoretical Analysis of a Gust Alleviator Used on a Lancaster Aircraft, and Comparison with Experiment.
RAE.TN.Aero 2645,Jan.,1961.

ZBROZEK J.K.,W.SMITH AND D.WHITE
Preliminary Investigation on a Gust Alleviation Investigation on a Lancaster Aircraft.
ARC R&M 2972,Aug.,1957.

APPENDIX 1

COMPOSITION OF THE STATE AND OUTPUT VECTORS OF EACH MATHEMATICAL MODEL CONSIDERED.

1. ARNE

a. State Vector		
Variable	Symbol	Vector Element
Vertical Velocity	w	x_1
Normalised Pitch Rate	q/n_2	x_2
Rate of Change of Bending Displacement	$\dot{\lambda}_i$	x_3-x_{17}
Bending Displacement (i= 1,2 ...15)	λ_i	x_{18}-x_{32}
Aileron Deflection	δ_A	x_{33}
Inboard Elevator Deflection	δ_{e_i}	x_{34}
Outboard Elevator Deflection	δ_{e_o}	x_{35}
Küssner Dynamics	-	x_{36}-x_{41}
Vertical Gust Velocity	w_g	x_{42}
Wagner Dynamics	-	x_{43}-x_{79}

b. Output Vector

Variable	Symbol	Vector Element
Bending moments at Wing Stations 1-5	-	y_i i=1,3,5,7,9
Torsional Moments at Wing Stations 1-5	-	y_j j=2,4,6,8,10
Rates of change of B.M. at WS 1-5	-	y_k k=11,13,15, 17,19
Rates of change of T.M. at WS 1-5	-	y_l l=12,14,16, 18,20
Rates of change of Bending Displacement	$\dot{\lambda}_i$	y_{21}-y_{35}
Bending Displacement (i=1.2 ..15)	λ_i	y_{36}-y_{50}
Aileron Rate	$\dot{\delta}_A$	y_{51}
Inboard Elevator Rate	$\dot{\delta}_{e_i}$	y_{52}
Aileron Deflection	δ_A	y_{53}
Inboard Elevator Deflection	δ_{e_i}	y_{54}
Vertical Velocity	w	y_{55}
Normalised Pitch Rate	q/n_2	y56

2 BACH

a. State Vector

x_1 - x_{42} identical to x_1 - x_{42} of ARNE

No Wagner Dynamics included.

b. Output Vector

Identical to that of ARNE.

3. CLEMENTI

a. State Vector.

Variable	Symbol	Vector Element
Vertical Velocity	w	x_1
Normalised Pitch Rate	q/n_2	x_2
Bending Rate	$\dot{\lambda}_i$	$x_3 - x_8$
Bending Displacement (i=1,2,3.4.5.6.)	λ_i	$x_9 - x_{14}$
Aileron Deflection	δ_A	x_{15}
Inboard Elevator Deflection	δ_{e_i}	x_{16}
Outboard " "	δ_{e_o}	x_{17}
Küssner Dynamics	-	$x_{18} - x_{23}$
Vertical Gust Velocity	w_g	x_{24}

b Output Vector.

Variable	Symbol	Vector Element
Bending Moments (BM) at WS 1-5	-	y_i; i=1,3,5,7,9
Torsion Moments (TM) at WS 1-5	-	y_j; j=2,4,6,8,10
BM Rates at WS 1-5	-	y_k; k=11,13,15,17,19
TM Rates at WS 1-5	-	y_l; l=12,14,16,18,20
~~Bending~~ Mode Rates ~~at WS 1-5~~ $\dot{\lambda}_i$	$\dot{\lambda}_i$	$y_{21} - y_{26}$
~~Bending~~ Mode Displacement ~~at WS 1-5~~ λ_i	λ_i	$y_{27} - y_{32}$
Aileron Rate	$\dot{\delta}_A$	y_{33}
Inboard Elevator Rate	$\dot{\delta}_{e_i}$	y_{34}
Aileron Deflection	δ_A	y_{35}
Inboard Elevator Deflection	δ_{e_i}	y_{36}
Vertical Velocity	w	y_{37}
Normalised Pitch Rate.	q/n_2	y_{38}

4. FAURÉ

a. State Vector

$x_1 - x_{17}$ identical to $x_1 - x_{17}$ of CLEMENTI

No Küssner Dynamics.

No vertical gust.

b. Output Vector.

Identical to that of CLEMENTI.

5. GERSHWIN

a. State Vector

Variables	Symbols	Vector Elements
Vertical Velocity	w	x_1
Normalised Pitch Rate	q/n_2	x_2
First Bending Mode Rate	$\dot{\lambda}_i$	x_3
First Bending Mode Displacement	λ_i	x_4
Aileron Deflection	δ_A	x_5
Inboard Elevator Deflection	δ_{e_i}	x_6
Outboard Elevator Deflection	δ_{e_o}	x_7
Küssner Dynamics	-	x_8-x_{13}
Vertical Gust Velocity	w_g	x_{14}

b. Output Vector

Identical to that of CLEMENTI.

6. HANDEL

a. State Vector

Variable	Symbols	Vector Elements
Vertical Velocity	w	x_1
Normalised Pitch Rate	q/n_2	x_2
Aileron Deflection	δ_A	x_3
Inboard Elevator Deflection	δ_{e_i}	x_4
Outboard Elevator Deflection	δ_{e_o}	x_5

b. Output Vector.

Identical to that of CLEMENTI.

APPENDIX II

Expressing the Transfer Function of the Dryden Filter in Terms of a State Variable Representation

Equation (2.29) gives:

$$G_{w_g}(s) = \sigma_w \sqrt{\frac{L_w}{U_o}} \frac{\left[1 + \sqrt{3}\left(\frac{L_w}{U_o}\right)s\right]}{\left[1 + \left[\frac{L_w}{U_o}\right]s\right]} \qquad \ldots \text{(II.1)}$$

The vertical gust velocity is the given by:

$$w_g(s) = \sigma_w \sqrt{\frac{L_w}{U_o}} \frac{\left[1 + \sqrt{3}\left[\frac{L_w}{U_o}\right]s\right]}{\left[1 + \left[\frac{L_w}{U_o}\right]s\right]^2}\eta(s) \qquad \ldots \text{(II.2)}$$

$$\therefore \frac{L_w^2}{U_o^2}\ddot{w}_g + 2\frac{L_w}{U_o}\dot{w}_g + w_g = \sigma_w\sqrt{\frac{L_w}{U_o}}\,\eta(t) + \sigma_w\sqrt{3}\left[\frac{L_w}{U_o}\right]^{\frac{1}{2}}\dot{\eta}(t) \quad \ldots \text{(II.3)}$$

$$\therefore \ddot{w}_g = -2\frac{U_o}{L_w}\dot{w}_g - \frac{U_o^2}{L_w^2}w_g + \sigma_w\sqrt{\frac{U_o^3}{L_w^3}}\,\eta(t) + \sigma_w\sqrt{\frac{3U_o}{L_w}}\,\dot{\eta}(t) \quad \ldots \text{(II.4)}$$

Let,

$$x_p \triangleq w_g \qquad \ldots \text{(II.5)}$$

$$x_{p-1} \triangleq \dot{w}_g - \sigma_w\sqrt{\frac{3U_o}{L_w}}\cdot\eta(t) \qquad \ldots \text{(II.6)}$$

(II.6) was so defined in order that terms in $\dot{\eta}(t)$, such as is found in (II.4) be avoided from the final expressions.

$$\therefore \dot{x}_{p-1} = \ddot{w}_g - \sigma_w\sqrt{\frac{3U_o}{L_w}}\,\dot{\eta}(t)$$

$$= -2\frac{U_o}{L_w}\dot{w}_g - \frac{U_o^2}{L_w^2}w_g + \sigma_w\sqrt{\frac{U_o^3}{L_w^3}}\,\eta(t) \quad \ldots \text{(II.7)}$$

$$\therefore \dot{x}_{p-1} = -2\frac{U_o}{L_w} x_{p-1} - 2\frac{U_o}{L_w}\sigma_w\sqrt{\frac{3U_o}{L_w}}\,\eta(t) \ldots$$

$$- \frac{U_o^2}{L_w^2} x_p + \sigma_w\sqrt{\frac{U_o^3}{L_w^3}}\,\eta(t)$$

$$= -2\frac{U_o}{L_w} x_{p-1} - \frac{U_o^2}{L_w^2} x_p + \sigma_w\sqrt{\frac{U_o^3}{L_w^3}}\,(1-2\sqrt{3})\,\eta(t)$$

... (II.8)

Also,

$$\dot{x}_p = x_{p-1} + \sigma_w\sqrt{\frac{3U_o}{L_w}}\,\eta(t) \qquad \ldots \text{(II.9)}$$

(II.2) has now been rendered into state variable form given by (II.8) and (II.9).

Thus,

$$\begin{bmatrix} \dot{x}_{p-1} \\ \dot{x}_p \end{bmatrix} = \begin{bmatrix} -2\frac{U_o}{L_w} & -\frac{U_o^2}{L_w^2} \\ 1 & 0 \end{bmatrix} \begin{bmatrix} x_{p-1} \\ x_p \end{bmatrix} + \begin{bmatrix} \sigma_w\sqrt{\frac{U_o^3}{L_w^3}}\,(1-2\sqrt{3}) \\ \sigma_w\sqrt{\frac{3U_o}{L_w}} \end{bmatrix} \eta(t) \qquad \ldots \text{(II.10)}$$

(II.10) is of the form of (2.4), where:

$$\underline{z}_g = \begin{bmatrix} x_{p-1} \\ x_p \end{bmatrix} \qquad \ldots \text{(II.11)}$$

$$D_g = \begin{bmatrix} -2\frac{U_o}{L_w} & -\frac{U_o^2}{L_w} \\ 1 & 0 \end{bmatrix} \qquad \ldots \text{(II.12)}$$

$$\underline{G}_g = \begin{bmatrix} \sigma_w\sqrt{\frac{U_o^3}{L_w^3}}\,(1-2\sqrt{3}) \\ \sigma_w\sqrt{\frac{3U_o}{L_w}} \end{bmatrix} \qquad \ldots \text{(II.13)}$$

APPENDIX III

III.1 Solution of the State Equation with Stochastic Inputs by the Transition Matrix Method

The state equation given in (2.4) is:

$$\dot{\underline{x}} = A\underline{x} + B\underline{u} + G\eta \qquad \ldots \text{(III.1)}$$

Let a solution of $\underline{x}$ be given by

$$\underline{x}(t) = \Phi(t-t_o).C_1(t) \; ; \; \Phi(t_o)=I \qquad \ldots \text{(III.2)}$$

where,

$$\frac{d\Phi(t-t_o)}{dt} \triangleq A\Phi(t-t_o) \qquad \ldots \text{(III.3)}$$

Differentiating (III.2) and using (III.3) gives:

$$\dot{\underline{x}}(t) = A\underline{x}(t) + \Phi(t-t_o).\dot{C}_1(t) \qquad \ldots \text{(III.4)}$$

Comparing (III.1) and (III.4),

$$\Phi(t-t_o).\dot{C}_1(t) = B\underline{u} + G\eta \qquad \ldots \text{(III.5)}$$

$$C_1(t) = \int_{t_o}^{t} [\Phi^{-1}(\tau-t_o)(B\underline{u} + G\eta)]d\tau + C_2 \qquad \ldots \text{(III.6)}$$

Using (III.2) and (III.6), at $t = t_o$

$$C_1(t_o) = \underline{x}(t_o) = C_2 \qquad \ldots \text{(III.7)}$$

Substituting for C_2 of equation (III.7) into (III.6) and then substituting for C_1 in equation (III.2) gives:

$$\underline{x}(t) = \Phi(t-t_o)\underline{x}(t_o) + \int_{t_o}^{t} \{\Phi(t-t_o)\Phi^{-1}(\tau-t_o)[Bu(\tau)+B_g\eta(\tau)]\}d\tau \qquad \ldots \text{(III.8)}$$

Using two well known properties of the transition matrix (Brockett (1970)), given by:

$$\Phi^{-1}(\tau) = \Phi(-\tau) \qquad \ldots \text{(III.9)}$$

$$\Phi(t_2-t_o) = \Phi(t_2-t_1)\Phi(t_1-t_o) \qquad \ldots \text{(III.10)}$$

equation (III.8) can be rewritten in the form:

$$\underline{x}(t) = \underbrace{\Phi(t-t_o)\underline{x}(t_o) + \int_{t_o}^{t} \Phi(t-\tau)B\underline{u}(\tau)d\tau}_{\text{Deterministic Solution}} + \int_{t_o}^{t} \Phi(t-\tau)G\eta(\tau)d\tau \qquad \ldots \text{(III.11)}$$

The terms on the right hand side of (III.11) correspond with those on the r.h.s of (III.1). Since the system is linear, the superposition theorem applies. Thus it turns out that the inclusion of atmospheric turbulence (represented by $G\eta$, in (III.1)), simply results in an extra additive term to the deterministic solution.

III.2 Computer Algorithm for Solution of the State Equation

For numerical solution of (III.11), it is usual to assume the control $\underline{u}$ and the input noise, η, to be piecewise constant over the interval T. The interval, T, can be made as small as desired.

Let

$$\Delta_Z(T) \triangleq \int_0^T \Phi(T-\tau).Z.d\tau \qquad \ldots \text{(III.12)}$$

where Z is a general driving matrix. If the system is regarded as being discrete, (III.11) may be re-expressed as:

$$\underline{x}[(r+1)T] = \Phi[T].\underline{x}[rT] + \Delta_b[T].\underline{u}[rT] + \Delta_g[T]\eta[rT] \qquad \ldots \text{(III.13)}$$

In this research, the Dryden filter*, driven by white noise, η, was used to introduce simulated atmospheric turbulence into the model. If the model was to be subjected to disturbances, then the matrix G, in (III.1), was set to the appropriate coefficient values specified according to equation (II.10) of Appendix II, using the relationship given by (2.8). In a deterministic study, G would be set to zero.

The transition matrix, Φ, may be expressed as a series expansion which converges if A is a stability matrix. To ensure convergence of that series in a limited number of terms, it is usual to determine Φ, over a very small step size δT, where:

$$\Phi(\delta T) = I + A\delta T + \frac{A^2(\delta T)^2}{2!} + \frac{A^3(\delta T)^3}{3!} + \ldots \quad \ldots\ldots (III.14)$$

The series is truncated by using a stopping criterion based upon the magnitude of the relative difference between elements of the i^{th} term and the $i+1^{th}$ term, (Nicholson (1966)). Repeated squaring of $\Phi(\delta T)$ results in $\Phi(T)$ using a property of the transition matrix that:

$$\begin{aligned} \Phi(2\delta T) &= \Phi^2(\delta T) \\ \Phi(4\delta T) &= \Phi^2(2\delta T) \\ &\vdots \qquad\qquad \vdots \\ \Phi(n\delta T) &= \Phi^2\left(\frac{n\delta T}{2}\right) = \Phi(T) \end{aligned} \quad \ldots (III.15)$$

Thus for a discrete interval (T) of 0.1 seconds, δT may be chosen to be 0.78125E-3 and $\Phi(T)$ may then be obtained in 7 iterations.

---

* See Appendix II.

From (III.12), if A is non-singular,

$$\Delta_z(T) = A^{-1}[\Phi(T)-I].Z \quad \ldots \text{(III.16)}$$

or,

$$\Delta_z(T) = \left\{IT + \frac{AT^2}{2!} + \frac{A^2T^3}{3!} + \ldots\right\}.Z \quad \ldots \text{(III.17)}$$

$$\Delta_z(\delta T) = \left\{I\delta T + \frac{A(\delta T)^2}{2!} + \frac{A^2(\delta T)^3}{3!} + \ldots\right\}.Z \quad \ldots \text{(III.18)}$$

From (III.16),

$$\begin{aligned}\Delta_z(\delta T) &= A^{-1}[\Phi(\delta T)-I].Z \\ \Delta_z(2\delta T) &= A^{-1}[\Phi(2\delta T)-I].Z \\ &= [I + \Phi(\delta T)].\Delta_z(\delta T) \\ \Delta_z(n\delta T) &= [I + (\tfrac{n\delta T}{2})].\Delta_z(\tfrac{n\delta T}{2}) = \Delta_z(T)\end{aligned} \quad \ldots \text{(III.19)}$$

In the computer program RESPON, (Appendix IV), the stopping criterion used was to truncate (III.18), if the error between all corresponding elements of the i^{th} term and the $i+1^{th}$ term was less than 0.001. Thus for a prespecified value of δT, $\Phi(\delta T)$ and $\Delta_z(\delta T)$ were evaluated using (III.14) and (III.18) respectively. These calculations then allowed $\Phi(T)$ and $\Delta(T)$ to be determined using (III.15) and (III.19) respectively. The appropriate matrices were then substituted in (III.13) and a recursive routine used to determine the state vector at each interval of time, typically every 0.1 seconds. The output vector was determined using the relationship:

$$\underline{y}[(r+1)T] = C\underline{x}[(r+1)T] + E\underline{u}[(r+1)T] \quad \ldots \text{(III.20)}$$

APPENDIX IV

COMPUTER PROGRAMS

Digital programming was used extensively throughout the period of this research. The bulk of the initial work relating to determination of the feedback control laws and the obtaining of time responses of the aircraft was carried out using an ICL 1904S computer at Loughborough University of Technology (LUT). In the particular case of determining feedback control laws for the model BACH, the computer program, OUTREG, had to be split into a two-pass one and program runs carried out on a CDC 7600 computer at the University of Manchester. This computer has a greater storage capacity and is somewhat faster than the ICL 1904S machine at LUT. All the programs run on these computers were written in ALGOL 60*. During the latter stages of this research study, Loughborough University Computer Centre acquired a PRIME 400 computer which became available on a semi-interactive basis. All the studies relating to the application of observers were accomplished on the PRIME facility. As an ALGOL 60 compiler is not available on this machine, some of the computer programs+ written in ALGOL 60 were rewritten in FORTRAN primarily to facilitate speedier testing of the observer performance on a single computer, but also to improve the efficiency in terms of core and run-time requirements of the original programs. All the computer programs used are available in the Department of Transport Technology at Loughborough University and are described briefly in Table IV.1.

---

* Originally written by Dr. D.McLean, Department of Transport Technology, Loughborough University, Loughborough, Leics.,LE11 3

\+ See Table IV.1.

Table IV.1 Description of Computer Programs used.

PRIME 400 COMPUTER PROGRAM	ALGOL 60 EQUIVALENT	DESCRIPTION.
CONOBS	OBSERVTROL	Determination of Controllability and/or Observability
RESPON	STATRAN	Transition Matrix Solution of the state Equations.
OUTREG	OUTREG	Solution of the Feedback Gain Matrix
COVRNC	COVAR	Determines r.m.s. values of the output vector of the aircraft in response to simulated Atmospheric Turbulence.
MILEST		Uses Miller's Algorithm to determine all the relevant matrices of an optimal reduced-order observer.
RAPEST		Determines all relevant matrices for a Full-Order Observer design.

APPENDIX V

MICRO-COMPUTER PROGRAM

Prog. Page	Addr. Line	Instr. No.	Instruction	pROM 8-bit code
	0	217	Load 1/10	11011001
	1	074	Divide by 2	01001010
	2	192	Square A	11000000
	3	042	Load A to RAM 10	00101010
	4	147	Stat. MXA 0011	10010011
	5	162	Comp OCL 1	10100010
	6	113	Jmp. to PPG.1	01110001
0	7			
	8			
	9			
	10			
	11			
	12			
	13			
	14			
	15			
	0	114	Jmp. to PPG.2	01110010
	1	130	Jmp. to LN.2	10000010
	2	114	Jmp. to PPG.2	01110010
	3			
	4			
	5			
	6	128	Jmp. to LN.0	10000000
1	7			
	8			
	9			
	10			
	11			
	12			
	13			
	14			
	15			

Prog. Page	Addr. Line	Instr. No.	Instruction	pROM 8-bit code
	0	160	Comp. MT	10100000
	1	168	Comp. SDT	10101000
	2	147	Stat. MXA 0011	10010011
	3	162	Comp. OCL 1	10100010
	4	162	Comp. OCL 1	10100010
	5	159	Stat. MXA 1111	10011111
	6	162	Comp. OCL 1	10100010
2	7	156	Stat. MXA 1100	10011100
	8	160	Comp. MT	10100000
	9	160	Comp. MT	10100000
	10	145	Stat. MXA 0001	10010001
	11	162	Comp. OCL 1	10100010
	12	144	Stat. MXA 0000	10010000
	13	162	Comp. OCL 1	10100010
	14	145	Stat. MXA 0001	10010001
	15	162	Comp. OCL 1	10100010
	0	160	Comp. MT	10100000
	1	144	Inp. via Ch.0	10010000
	2	160	Comp. MT	10100000
	3	049	Load A to RAM 9	00101001
	4	144	Stat. MXA 0000	10010000
	5	162	Comp. OCL 1	10100010
	6	160	Comp. MT	10100000
3	7	144	Inp. via Ch.0	10010000
	8	160	Comp. MT	10100000
	9	040	Load A to RAM 8	00101000
	10	066	B - A	01000010
	11	177	Abs A	10110001
	12	010	Input to A (RAM 10)	00001010
	13	072	Compare	01001000
	14	008	Input to A (RAM 8)	00001000
	15	170	Skp. if 1 in P Flag	10101010

Prog. Page	Addr. Line	Instr. No.	Instruction	pROM 8 bit code
	0	009	Load A to RAM 9	00001001
	1	208	A to 8 Level Stack	11010000
	2	088	Ext State to P Flag	01011000
	3	171	Skp if 0 in P Flag	10101011
	4	117	Jmp to PPG 5	01110101
	5	146	Stat MXA 0010	10010010
	6	162	Comp. OCL 1	10100010
4	7	162	comp. OCL 1	10100010
	8	160	Comp. MT	10100000
	9	163	Comp. OCL 2	10100011
	10	160	Comp.MT	10100000
	11	142	Jmp. to LN 14	10001110
	12			
	13			
	14	144	Stat MXA 0000	10010000
	15	114	Jmp. to PPG 2	01110010
	0			
	1			
	2			
	3			
	4	158	Stat. MXA 1110	10011110
	5	162	Comp OCL 1	10100010
	6	027	Input to A (RAM 27)	00011011
5	7	077	Multiply by 2	01001101
	8	070	Comp MSD	01000110
	9	208	A to 8 Level Stack	11010000
	10	156	Stat. MXA 1100	10011100
	11	103	A to Data Output	01100111
	12	163	Comp. OCL 2	10100011
	13	027	Read RAM 27	00011011
	14	077	Multiply by 2	01001101
	15	070	Comp. MSD	01000110

Prog. Page	Addr. Line	Instr. No.	Instruction	pROM 8-bit code
	0	208	A to 8 Level Stack	11010000
	1	157	Stat MXA 1101	10011101
	2	103	A to Data Output	01100111
	3	163	Comp. OCL 2	10100011
	4	027	Input to A (RAM 27)	00011011
	5	077	Multiply by 2	01001101
	6	070	Comp. MSD	01000110
6	7	208	A to 8 Level Stack	11010000
	8	158	Stat MXA 1110	10011110
	9	103	A to Data Output	01100111
	10	163	Comp. OCL 2	10100011
	11	027	Input to A (RAM 27)	00011011
	12	077	Multiply by 2	01001101
	13	070	Comp. MSD	01000110
	14	208	A to 8 Level Stack	11010000
	15	159	Stat. MXA1111	10011111
	0	103	A to Data Output	01100111
	1	163	Comp. OCL 2	10100011
	2	114	Jmp. to PPG 2	01110010
	3			
	4			
	5			
	6			
7	7			
	8			
	9			
	10			
	11			
	12			
	13			
	14			
	15			

APPENDIX VI

COEFFICIENT MATRIX DATA : MODEL CLEMENTI

The state equation representing the dynamics of the subject aircraft is given in (2.6) as

$$\dot{\underline{x}} = A\underline{x} + B\underline{u} + G\eta \qquad \text{(VI.1)}$$

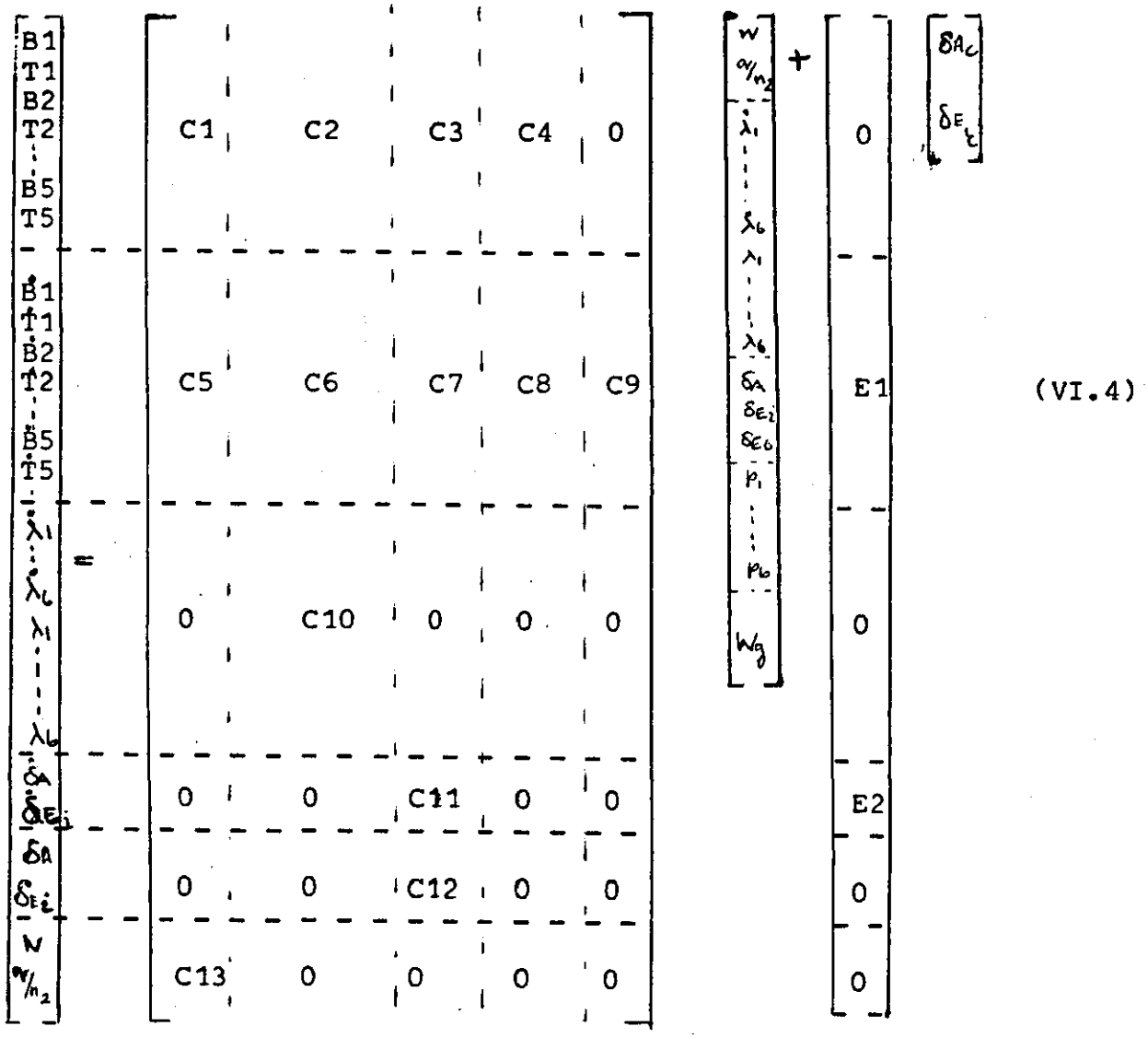
The appropriate output equation is given in (2.11) as

$$\underline{y} = C\underline{x} + E\underline{u} \qquad \text{(VI.2)}$$

For the majority of cases studied, the aircraft was considered to be adequately represented by the model CLEMENTI and only data relating to this model is included in this Appendix. A more extensive data set can be obtained in Harvey and Pope (1975).

In Section 3 of Appendix I is shown a table of the composition of the state and output vectors of CLEMENTI. These vectors can be conveniently divided into subvectors by partitioning matrices A, B, G, C and E of (VI.1) and (VI.2) thus separating the rigid body dynamics, structural flexibility effects, actuator dynamics, Küssner dynamics and gust dynamics, viz.,

$$\begin{bmatrix} \dot{w} \\ \dot{q}/n_2 \\ \dot{\lambda}_1 \\ \vdots \\ \dot{\lambda}_6 \\ \dot{\delta}_A \\ \dot{\delta}_{E_1} \\ \dot{\delta}_{E_0} \\ \dot{p}_1 \\ \vdots \\ \dot{p}_6 \\ \dot{w}_g \end{bmatrix} = \left[\begin{array}{ccccc} A1 & A2 & A3 & A4 & 0 \\ A5 & A6 & A7 & A8 & 0 \\ 0 & 0 & A9 & 0 & 0 \\ 0 & 0 & 0 & A10 & A11 \\ 0 & 0 & 0 & 0 & A12 \end{array}\right] \begin{bmatrix} w \\ q/n_2 \\ \lambda_1 \\ \vdots \\ \lambda_6 \\ \delta_A \\ \delta_{E_1} \\ \delta_{E_0} \\ p_1 \\ \vdots \\ p_6 \\ w_g \end{bmatrix} + \begin{bmatrix} 0 \\ 0 \\ B1 \\ 0 \\ 0 \end{bmatrix} \begin{bmatrix} \delta_{A_c} \\ \delta_{E_{1_c}} \end{bmatrix} + \begin{bmatrix} 0 \\ 0 \\ 0 \\ 0 \\ G1 \end{bmatrix} \eta \qquad \text{(VI.3)}$$



(VI.4)

A1 and A3 are the coefficient submatrices describing the rigid body dynamics, viz.,

$$A1 = \begin{bmatrix} -0.68E0 & -0.328E1 \\ -0.55E0 & -0.117E1 \end{bmatrix} \qquad \text{(VI.5)}$$

$$A3 = \begin{bmatrix} -0.23E3 & -0.190E3 & -0.301E2 \\ -0.576E3 & -0.250E4 & -0.440E3 \end{bmatrix} \qquad \text{(VI.6)}$$

A2 contains the coupling terms due to the structural flexibility effects on the rigid body motion, viz.,

$$A2 = \begin{bmatrix} 3 & 4 & 5 & 6 \\ -0.400E-01 & -0.100E-01 & -0.200E-01 & 0.200E-01 \\ 0.400E-01 & -0.400E-01 & -0.330E\ 00 & -0.320E\ 00 \\ 7 & 8 & 9 & 10 \\ -0.200E-01 & 0.500E-01 & -0.640E\ 00 & -0.650E\ 00 \\ -0.120E\ 00 & 0.250E\ 00 & -0.110E\ 00 & -0.168E\ 01 \\ 11 & 12 & 13 & 14 \\ -0.171E\ 01 & 0.450E\ 01 & 1\ -0.136E\ 01 & 0.185E\ 01 \\ -0.103/\ 02 & -0.570E\ 01 & 2\ -0.494E\ 01 & 0.911E\ 01 \end{bmatrix} \qquad \text{(VI.7)}$$

A4 contains the coupling terms due to the Küssner dynamics, viz.,

A4 =

18	19	20	21	22
-0.480E 00	-0.705E 01	-0.920E 00	0.000E 00	0.000E 00
0.271E 01	-0.105E 01	-0.119E 02	0.000E 00	0.000E 00

(VI.8)

A5 contains the coupling terms due to the effects of the rigid body dynamics upon the structural flexibility effects, viz.,

A5 =

3	-0.149E 01	0.110E 00
4	0.500E-01	-0.900E-01
5	0.500E-01	-0.850E 00
6	-0.111E 01	-0.990E 00
7	-0.200E 00	-0.240E 00
8	0.460E 00	0.420E 00
9	0.000E 00	0.000E 00
10	0.000E 00	0.000E 00
11	0.000E 00	0.000E 00
12	0.000E 00	0.000E 00
13	0.000E 00	0.000E 00
14	0.000E 00	0.000E 00

(VI.9)

A6 represents the coefficient sub-matrix of the structural flexibility effects.

A6 =

-0.990E 00	-0.200E-01	-0.150E 00	0.510E 00	0.200E-01	-0.260E 00
0.100E-01	-0.470E 00	-0.700E-01	-0.600E-01	-0.100E-01	0.000E 00
0.500E-01	-0.700E-01	-0.129E 01	-0.410E 00	-0.300E-01	-0.600E-01
0.800E-01	-0.400E-01	-0.270E 00	-0.109E 01	-0.180E 00	0.440E 00
0.600E-01	-0.200E-01	-0.500E-01	-0.110E 00	-0.860E 00	0.120E 00
-0.110E 00	0.200E-01	0.400E-01	0.180E 00	0.100E 00	-0.115E 01
0.100E 01	0.000E 00	0.000E 00	0.000E 00	0.000E 00	0.000E 00
0.000E 00	0.000E 00	0.100E 01	0.000E 00	0.000E 00	0.000E 00
0.000E 00	0.000E 00	0.000E 00	0.100E 01	0.000E 00	0.000E 00
0.000E 00	0.000E 00	0.000E 00	0.000E 00	0.100E 01	0.000E 00
0.000E 00	0.000E 00	0.000E 00	0.000E 00	0.000E 00	0.100E 01
-0.299E 02	-0.409E 01	-0.166E 02	-0.406E 02	-0.584E 01	-0.669E 01
0.270E 00	-0.124E 03	-0.870E 00	-0.158E 01	-0.160E 00	0.151E 01
0.140E 01	-0.650E 00	-0.193E 03	-0.154E 02	-0.980E 00	-0.315E 01
-0.200E 00	-0.680E 00	-0.937E 01	-0.243E 03	-0.718E 01	0.170E 02
0.230E 00	-0.750E 00	-0.130E 01	-0.323E 01	-0.306E 03	0.608E 01
-0.120E 00	0.201E 01	0.150E 01	0.451E 01	0.477E 01	0.352E 03
0.000E 00	0.000E 00	0.000E 00	0.000E 00	0.000E 00	0.000E 00
0.000E 00	0.000E 00	0.000E 00	0.000E 00	0.000E 00	0.000E 00
0.000E 00	0.000E 00	0.000E 00	0.000E 00	0.000E 00	0.000E 00
0.000E 00	0.000E 00	0.000E 00	0.000E 00	0.000E 00	0.000E 00
0.000E 00	0.000E 00	0.000E 00	0.000E 00	0.000E 00	0.000E 00
0.000E 00	0.000E 00	0.000E 00	0.000E 00	0.000E 00	0.000E 00

A7 is the sub-matrix representing the effects of control surface deflections upon structural flexibility, viz.,

$$A7 = \begin{bmatrix} -0.340E\,04 & 0.142E\,04 & 0.260E\,03 \\ -0.133E\,03 & -0.292E\,03 & -0.639E\,02 \\ -0.142E\,04 & -0.257E\,04 & -0.582E\,03 \\ 0.804E\,03 & -0.253E\,04 & -0.625E\,03 \\ -0.131E\,02 & -0.653E\,03 & -0.179E\,03 \\ -0.411E\,03 & 0.112E\,04 & 0.323E\,03 \\ 0.000E\,00 & 0.000E\,00 & 0.000E\,00 \\ 0.000E\,00 & 0.000E\,00 & 0.000E\,00 \\ 0.000E\,00 & 0.000E\,00 & 0.000E\,00 \\ 0.000E\,00 & 0.000E\,00 & 0.000E\,00 \\ 0.000E\,00 & 0.000E\,00 & 0.000E\,00 \\ 0.000E\,00 & 0.000E\,00 & 0.000E\,00 \end{bmatrix} \qquad \text{(VI.11)}$$

A8 is the sub-matrix representing the effects of the Küssner dynamics on structural flexibility, viz.,

$$A8 = \begin{bmatrix} 0.630E\,00 & -0.231E\,02 & 0.668E\,01 & 0.000E\,00 & 0.000E\,00 \\ -0.210E\,00 & 0.168E\,01 & -0.133E\,01 & 0.000E\,00 & 0.000E\,00 \\ -0.230E\,01 & 0.112E\,02 & -0.119E\,02 & 0.000E\,00 & 0.000E\,00 \\ -0.101E\,01 & -0.426E\,01 & -0.115E\,02 & 0.000E\,00 & 0.000E\,00 \\ -0.330E\,00 & -0.400E-01 & -0.295E\,01 & 0.000E\,00 & 0.000E\,00 \\ 0.440E\,00 & 0.163E\,01 & 0.503E\,01 & 0.000E\,00 & 0.000E\,00 \\ 0.000E\,00 & 0.000E\,00 & 0.000E\,00 & 0.000E\,00 & 0.000E\,00 \\ 0.000E\,00 & 0.000E\,00 & 0.000E\,00 & 0.000E\,00 & 0.000E\,00 \\ 0.000E\,00 & 0.000E\,00 & 0.000E\,00 & 0.000E\,00 & 0.000E\,00 \\ 0.000E\,00 & 0.000E\,00 & 0.000E\,00 & 0.000E\,00 & 0.000E\,00 \\ 0.000E\,00 & 0.000E\,00 & 0.000E\,00 & 0.000E\,00 & 0.000E\,00 \\ 0.000E\,00 & 0.000E\,00 & 0.000E\,00 & 0.000E\,00 & 0.000E\,00 \end{bmatrix}$$

(VI.12)

A9 and B1 are the sub-matrices associated with the model of the actuator dynamics, viz.,

$$A9 = \begin{bmatrix} -0.600E\,01 & -0.000E\,00 & 0.000E\,00 \\ 0.000E\,00 & -0.750E\,01 & 0.000E\,00 \\ 0.000E\,00 & 00.000E\,00 & -0.750E\,01 \end{bmatrix} \qquad \text{(VI.13)}$$

$$B1 = \begin{bmatrix} 15 & 0.600E\,01 & 0.000E\,00 \\ 16 & 0.000E\,00 & 0.750E\,01 \\ 17 & 0.000E\,00 & 0.000E\,00 \end{bmatrix} \qquad \text{(VI.14)}$$

A10 is the sub-matrix representing the Küssner dynamics, viz.,

A10 =

$$\begin{bmatrix} -0.222E\,02 & 0.000E\,00 & 0.000E\,00 & 0.000E\,00 & 0.000E\,00 \\ 0.000E\,00 & -0.855E\,01 & 0.000E\,00 & 0.000E\,00 & 0.855E\,01 \\ -0.510E\,01 & 0.000E\,00 & 0.000E\,00 & 0.100E\,01 & 0.000E\,00 \\ 0.909E\,02 & 0.000E\,00 & -0.390E\,02 & -0.102E\,02 & 0.000E\,00 \\ 0.000E\,00 & 0.000E\,00 & 0.000E\,00 & 0.000E\,00 & -0.110E\,02 \end{bmatrix} \qquad \text{(VI.15)}$$

A11 is the sub-matrix representing the effects of vertical gusts upon the Küssner dynamics, viz.,

$$A11 = \begin{bmatrix} 0.000E\,00 & 0.222E\,02 \\ 0.000E\,00 & 0.000E\,00 \\ 0.000E\,00 & 0.000E\,00 \\ 0.000E\,00 & 0.000E\,00 \\ 0.000E\,00 & 0.110E\,02 \end{bmatrix} \qquad \text{(VI.16)}$$

A12 and G1 are scalar values representing the appropriate coefficients of the Dryden model of the gust, viz.,

$$A12 = \begin{bmatrix} -0.5E0 & -0.6E-1 \\ 0.1E1 & 0.0 \end{bmatrix} \qquad \text{(VI.17)}$$

$$G1 = \begin{bmatrix} -0.93E-1 \\ 0.26\ E0 \end{bmatrix} \qquad \text{(VI.18)}$$

The sub-matrices of C and E (VI.4) are defined as follows:

C1 =

	1	2
1	-0.114E 05	-0.210E 04
2	-0.168E 05	-0.176E 04
3	0.216E 04	0.945E 03
4	-0.869E 04	-0.123E 04
5	0.325E 04	0.869E 03
6	-0.457E 04	-0.457E 03
7	-0.202E 04	-0.370E 03
8	-0.637E 04	-0.110E 04
9	-0.176E 04	-0.513E 03
10	-0.364E 04	-0.702E 03

(VI.19)

C2 =

3	4	5	6	7	8
0.119E 05	-0.112E 04	-0.105E 05	0.596E 04	0.378E 04	-0.960E 04
-0.137E 04	-0.102E 04	-0.171E 04	0.621E 04	-0.894E 03	-0.302E 04
0.877E 04	-0.406E 03	-0.437E 04	0.402E 04	0.263E 04	-0.528E 04
-0.173E 04	-0.107E 04	-0.204E 04	0.548E 04	-0.104E 04	0.326E 04
0.540E 04	0.579E 02	0.106E 04	0.909E 03	-0.103E 04	-0.758E 03
-0.193E 04	-0.104E 04	-0.174E 04	0.398E 04	-0.164E 04	0.878E 03
0.284E 04	0.172E 03	0.302E 04	-0.107E 04	-0.146E 03	-0.194E 04
-0.179E 04	-0.216E 03	-0.657E 03	0.132E 04	-0.340E 03	0.216E 03
0.136E 04	0.996E 02	0.202E 04	-0.778E 03	-0.339E 03	0.211E 04
-0.133E 04	-0.154E 03	-0.820E 03	0.858E 03	-0.678E 02	-0.424E 03

(VI.20)

C2 =

9	10	11	12	13	14
0.127E 07	-0.274E 06	-0.335E 07	0.196E 07	0.165E 07	-0.433E 07
-0.796E 05	-0.270E 06	-0.570E 06	0.163E 07	-0.402E 06	0.156E 07
0.100E 07	-0.104E 06	-0.147E 07	0.144E 07	0.114E 07	-0.246E 07
-0.781E 05	-0.276E 06	-0.607E 06	0.160E 07	-0.388E 06	0.150E 07
0.647E 06	0.172E 05	0.358E 06	0.321E 06	-0.436E 06	-0.332E 06
-0.706E 05	-0.264E 06	-0.451E 06	0.116E 07	-0.648E 06	0.524E 06
0.384E 06	0.469E 05	0.103E 07	-0.509E 06	-0.497E 05	0.862E 06
-0.264E 05	-0.412E 05	-0.980E 05	0.253E 06	-0.743E 05	0.498E 05
0.181E 06	0.327E 05	0.782E 06	-0.393E 06	-0.150E 06	0.111E 07
-0.177E 05	-0.250E 05	-0.775E 05	0.145E 06	-0.281E 05	-0.301E 05

(VI.20)

C3 =

15	16	17
-0.492E 07	-0.427E 07	-0.327E 06
0.355E 05	0.232E 06	0.142E 06
-0.986E 06	0.156E 07	0.103E 07
0.732E 05	0.496E 06	0.186E 06
0.162E 07	0.164E 07	0.602E 06
0.185E 07	0.155E 07	0.465E 06
0.542E 06	0.146E 06	-0.557E 05
0.541E 07	0.466E 06	0.152E 06
-0.781E 06	-0.632E 06	-0.326E 06
0.531E 07	0.294E 06	0.101E 06

(VI.21)

C4 =

18	19	20	21	22
0.746E 04	-0.132E 06	-0.183E 05	0.000E 00	0.000E 00
0.878E 04	-0.211E 06	0.112E 04	0.000E 00	0.000E 00
-0.279E 04	0.240E 05	0.683E 04	0.000E 00	0.000E 00
0.629E 04	-0.112E 06	0.229E 04	0.000E 00	0.000E 00
-0.181E 04	0.359E 05	0.710E 04	0.000E 00	0.000E 00
0.139E 04	-0.610E 05	0.696E 04	0.000E 00	0.000E 00
0.151E 04	-0.262E 05	0.639E 03	0.000E 00	0.000E 00
0.523E 03	-0.783E 05	0.205E 04	0.000E 00	0.000E 00
0.194E 04	-0.212E 05	-0.271E 04	0.000E 00	0.000E 00
0.172E 03	-0.448E 05	0.129E 04	0.000E 00	0.000E 00

(VI.22)

C5 =

11	0.181E 06	0.447E 06
12	0.354E 04	-0.808E 03
13	0.106E 06	0.273E 06
14	0.585E 03	0.811E 04
15	0.502E 05	0.130E 06
16	-0.442E 04	-0.488E 04
17	0.268E 05	0.590E 05
18	-0.260E 03	-0.124E 04
19	0.110E 05	0.250E 05
20	-0.278E 03	-0.197E 03

(VI.23)

C6 =

$$
\begin{bmatrix}
0.124E\,07 & -0.259E\,06 & -0.322E\,07 & 0.204E\,07 & 0.173E\,07 & -0.451E\,07 \\
-0.520E\,05 & -0.246E\,00 & -0.521E\,06 & 0.152E\,07 & -0.387E\,06 & 0.158E\,07 \\
0.982E\,06 & -0.995E\,05 & -0.139E\,07 & 0.150E\,07 & 0.117E\,07 & -0.254E\,07 \\
-0.554E\,05 & -0.252E\,06 & -0.556E\,06 & 0.150E\,07 & -0.374E\,06 & 0.151E\,07 \\
0.638E\,06 & 0.187E\,05 & 0.339E\,06 & 0.348E\,06 & -0.425E\,06 & -0.355E\,06 \\
-0.524E\,05 & -0.247E\,06 & -0.404E\,06 & 0.107E\,07 & -0.640E\,06 & 0.552E\,06 \\
0.384E\,06 & 0.531E\,05 & 0.106E\,07 & -0.515E\,06 & -0.398E\,05 & 0.861E\,06 \\
-0.770E\,04 & -0.270E\,05 & -0.454E\,05 & 0.149E\,06 & -0.553E\,05 & 0.573E\,05 \\
0.182E\,06 & 0.382E\,05 & 0.792E\,06 & -0.398E\,06 & -0.142E\,06 & 0.110E\,07 \\
-0.747E\,04 & -0.166E\,05 & -0.450E\,05 & 0.794E\,05 & -0.158E\,05 & -0.294E\,05
\end{bmatrix}
$$

$$
\begin{bmatrix}
-0.312E\,06 & 0.706E\,06 & 0.568E\,07 & 0.139E\,07 & 0.572E\,06 & -0.130E\,06 \\
-0.124E\,05 & 0.136E\,06 & 0.262E\,06 & -0.105E\,07 & 0.268E\,06 & -0.124E\,07 \\
-0.237E\,06 & 0.391E\,06 & 0.307E\,07 & 0.710E\,06 & 0.247E\,06 & -0.197E\,06 \\
-0.206E\,04 & 0.136E\,06 & 0.302E\,06 & -0.906E\,06 & 0.299E\,06 & -0.129E\,07 \\
-0.153E\,06 & 0.155E\,06 & 0.857E\,06 & 0.600E\,06 & 0.811E\,06 & -0.705E\,06 \\
0.435E\,04 & 0.111E\,06 & 0.132E\,06 & -0.684E\,06 & 0.459E\,06 & -0.460E\,06 \\
-0.877E\,05 & 0.562E\,05 & -0.108E\,06 & 0.717E\,06 & 0.311E\,06 & -0.126E\,07 \\
0.368E\,04 & 0.123E\,05 & -0.142E\,05 & -0.891E\,05 & 0.604E\,05 & -0.147E\,06 \\
-0.444E\,05 & 0.132E\,05 & -0.254E\,06 & 0.426E\,06 & 0.204E\,06 & -0.105E\,07 \\
0.770E\,04 & 0.101E\,05 & 0.751E\,05 & -0.704E\,05 & -0.790E\,04 & 0.116E\,06
\end{bmatrix}
$$

(VI.24)

C7 =

$$
\begin{bmatrix}
0.208E\,09 & 0.979E\,09 & 0.173E\,09 \\
0.154E\,08 & 0.218E\,08 & 0.372E\,07 \\
0.116E\,09 & 0.590E\,09 & 0.103E\,09 \\
0.128E\,08 & 0.141E\,08 & 0.261E\,07 \\
0.435E\,08 & 0.280E\,09 & 0.484E\,08 \\
0.424E\,07 & -0.131E\,08 & -0.244E\,07 \\
0.128E\,08 & 0.134E\,09 & 0.239E\,08 \\
0.977E\,06 & -0.219E\,07 & -0.478E\,06 \\
0.147E\,07 & 0.531E\,08 & 0.965E\,07 \\
-0.287E\,07 & -0.122E\,07 & -0.303E\,06
\end{bmatrix}
$$

(VI.25)

C8 =

$$
\begin{bmatrix}
-0.101E\,07 & 0.442E\,06 & 0.459E\,07 & -0.443E\,04 & -0.461E\,06 \\
-0.688E\,05 & 0.894E\,06 & 0.103E\,06 & -0.470E\,03 & -0.898E\,06 \\
-0.626E\,06 & -0.850E\,05 & 0.276E\,07 & 0.184E\,04 & 0.425E\,05 \\
-0.220E\,05 & 0.827E\,05 & 0.679E\,05 & 0.480E\,03 & -0.107E\,06 \\
-0.305E\,06 & -0.123E\,06 & 0.131E\,07 & 0.500E\,03 & 0.107E\,06 \\
0.163E\,05 & -0.163E\,05 & -0.607E\,05 & 0.317E\,03 & -0.678E\,04 \\
-0.132E\,06 & 0.142E\,06 & 0.627E\,06 & -0.153E\,04 & -0.115E\,06 \\
0.386E\,04 & 0.168E\,05 & -0.104E\,05 & 0.394E\,03 & -0.144E\,05 \\
-0.537E\,05 & -0.410E\,05 & 0.294E\,06 & -0.918E\,02 & 0.567E\,05 \\
0.380E\,04 & -0.240E\,05 & -0.579E\,04 & 0.159E\,03 & 0.234E\,05
\end{bmatrix}
$$

(VI.26)

C9 =

$$\begin{bmatrix} 0.000E\ 00 & 0.236E\ 05 \\ 0.000E\ 00 & 0.454E\ 05 \\ 0.000E\ 00 & 0.685E\ 03 \\ 0.000E\ 00 & 0.308E\ 04 \\ 0.000E\ 00 & 0.759E\ 04 \\ 0.000E\ 00 & -0.550E\ 04 \\ 0.000E\ 00 & -0.341E\ 04 \\ 0.000E\ 00 & -0.415E\ 04 \\ 0.000E\ 00 & -0.287E\ 04 \\ 0.000E\ 00 & -0.343E\ 04 \end{bmatrix} \qquad \text{(VI.27)}$$

C10 = $[I_{12}]$ (VI.28)

C11 =

$$\begin{bmatrix} -0.600E\ 01 & 0.000E\ 00 & 0.000E\ 00 \\ 0.000E\ 00 & -0.750E\ 01 & 0.000E\ 00 \end{bmatrix} \qquad \text{(VI.29)}$$

C12 =

$$\begin{bmatrix} 0.100E\ 01 & 0.000E\ 00 & 0.000E\ 00 \\ 0.000E\ 00 & 0.100E\ 01 & 0.000E\ 00 \end{bmatrix} \qquad \text{(VI.30)}$$

C13 = $[I_2]$ (VI.31)

E_1 =

$$\begin{bmatrix} 11 & -0.849E\ 07 & 0.318E\ 07 \\ 12 & -0.127E\ 08 & 0.247E\ 06 \\ 13 & -0.617E\ 06 & 0.756E\ 06 \\ 14 & -0.104E\ 08 & 0.820E\ 06 \\ 15 & 0.870E\ 06 & -0.879E\ 06 \\ 16 & -0.555E\ 07 & 0.112E\ 06 \\ 17 & -0.608E\ 06 & -0.441E\ 06 \\ 18 & -0.175E\ 07 & -0.518E\ 05 \\ 19 & -0.123E\ 07 & 0.115E\ 06 \\ 20 & 0.902E\ 07 & -0.489E\ 05 \end{bmatrix} \qquad \text{(VI.32)}$$

E_2

$$\begin{bmatrix} 33 & 0.600E\ 01 & 0.000E\ 00 \\ 34 & 0.000E\ 00 & 0.750E\ 01 \end{bmatrix} \qquad \text{(VI.33)}$$